

Prepared in cooperation with Santa Barbara County Department of Public Works Water Agency

Hydrologic Models and Analysis of Water Availability in Cuyama Valley, California



Scientific Investigations Report 2014–5150
Version 1.1, May 2015

Cover. Looking northwest from the south side of Cuyama Valley to the Caliente Range. Photograph taken by Randall T. Hanson, U.S. Geological Survey, September 19, 2009.

Hydrologic Models and Analysis of Water Availability in Cuyama Valley, California

By R.T. Hanson, Lorraine E. Flint, Claudia C. Faunt, Dennis R. Gibbs, and Wolfgang Schmid

In cooperation with Santa Barbara County Department of Public Works Water Agency

Scientific Investigations Report 2014–5150
Version 1.1, May 2015

U.S. Department of the Interior
U.S. Geological Survey

U.S. Department of the Interior
SALLY JEWELL, Secretary

U.S. Geological Survey
Suzette M. Kimball, Acting Director

U.S. Geological Survey, Reston, Virginia: 2015
First release: 2014
Revised: May 2015 (ver 1.1)

For more information on the USGS—the Federal source for science about the Earth, its natural and living resources, natural hazards, and the environment, visit <http://www.usgs.gov> or call 1–888–ASK–USGS.

For an overview of USGS information products, including maps, imagery, and publications, visit <http://www.usgs.gov/pubprod>

To order this and other USGS information products, visit <http://store.usgs.gov>

Any use of trade, firm, or product names is for descriptive purposes only and does not imply endorsement by the U.S. Government.

Although this information product, for the most part, is in the public domain, it also may contain copyrighted materials as noted in the text. Permission to reproduce copyrighted items must be secured from the copyright owner.

Suggested citation:

Hanson, R.T., Flint, L.E., Faunt, C.C., Gibbs, D.R., and Schmid, W., 2015, Hydrologic models and analysis of water availability in Cuyama Valley, California (ver. 1.1, May 2015): U.S Geological Survey Scientific Investigations Report 2014–5150, 150 p., <http://dx.doi.org/10.3133/sir20145150>.

Contents

Abstract.....	1
Introduction.....	2
Purpose and Scope	2
Approach.....	2
Description of the Study Area	2
Hydrologic and Water-Balance Subregions	3
Geologic Framework	3
Hydrogeologic Units.....	3
Faults and the Groundwater Flow System.....	4
Hydrogeologic Framework.....	4
Three-Dimensional Model of Grain-Size Distribution.....	5
Hydrologic System.....	6
Climate	6
Effects of Water Use on the Landscape	6
Surface Water	7
Groundwater.....	7
Model Development.....	7
Water-Balance Model.....	8
Estimation of Recharge and Runoff	8
Calibration and Comparison With Measured Streamflows.....	8
Development of BCM Results for CUVHM model.....	9
Integrated Hydrologic Model—CUVHM	9
Discretization	10
Spatial Discretization and Layering	10
Temporal discretization	10
Initial Conditions and Recent Conditions	11
Boundary Conditions	11
No-Flow Boundaries	11
General-Head Boundaries	11
Surface-Water Inflows and Outflows	11
Groundwater Pumpage	12
Agricultural Supply.....	12
Water Supply	13
Landscape Use and Movement of Water	13
Delivery Requirement.....	14
Soils	14
Land Use.....	14

Contents—Continued

Land-Use maps	15
Crop-Type Data.....	16
Climate Data	17
Precipitation	17
Reference Evapotranspiration (ET_r)	18
Groundwater Agricultural Supply	18
Net Recharge	18
Aquifer Characteristics.....	18
Textural Analysis.....	19
Hydraulic properties.....	19
Hydraulic Conductivity of Lithologic End Members.....	20
Storage Properties	21
Hydrogeologic Structures	22
Initial Conditions	22
Model Calibration and Sensitivity	23
Observations Used In Model Calibration.....	24
Groundwater Observations.....	24
Water-Level Maps	26
Land-Subsidence Observations	26
Pumpage Observations.....	26
Model Parameters	26
Farm Process Parameters.....	27
Hydraulic Parameters	27
Streamflow Properties.....	28
Multi-Aquifer Well Parameters	28
General-Head Boundary Parameters.....	28
Horizontal Flow Barrier Parameters	28
Subsidence Parameters	28
Sensitivity Analysis.....	28
Model Uncertainty, Limitations, and Potential Improvements	29
Hydrologic Budget and Flow Analysis	31
Projection of Potential Water Availability.....	32
Suggestions for Future Work	34
Summary and Conclusions.....	34
References Cited	36
Figures	41
Tables	126

Figures

1. Maps showing <i>A</i> , Cuyama Valley watershed and groundwater basin, and <i>B</i> , detailed location map with the active hydrologic model grid, groundwater basin, and major rivers, Cuyama Valley, California	42
2. Maps showing <i>A</i> , groundwater hydrologic subregions and related geologic structures; <i>B</i> , simplified Cuyama major groundwater regions; and <i>C</i> , groups of landscape water-balance subregions for 1943–2010 in Cuyama Valley, California	44
3. Map showing generalized <i>A</i> , outcrops of geologic units and major faults within model grid; <i>B</i> , axial hydrogeologic cross-section (A–A’); and <i>C</i> , transverse hydrogeologic cross-section (B–B’) of Cuyama Valley, California.....	48
4. Maps showing extent and percentage of coarse-grained deposits for the <i>A</i> , Recent Alluvial aquifer; <i>B</i> , Older Alluvial aquifer; and <i>C</i> , Morales Formation aquifer of Cuyama Valley, California.....	51
5. Graph showing cumulative departure of precipitation along with wet-dry periods, land-use map periods, periods of application for land-use, land-ownership and related farm wells, and selected crop attributes for Cuyama Valley, California.....	54
6. Maps showing average annual <i>A</i> , precipitation, and <i>B</i> , potential evapotranspiration for the simulation period for Cuyama Valley, California	55
7. <i>A</i> , Timeline showing history of water and land-use development through time, and <i>B</i> , graph showing population growth for Cuyama Valley, California	57
8. Map showing distribution of streams with streamflow routing cells and segments, and location of inflows, Cuyama Valley, California.....	58
9. Map showing distribution of agricultural, urban-supply, and domestic wells, Cuyama Valley, California	59
10. Graph showing estimated groundwater pumpage from municipal and domestic wells, Cuyama Valley, California	60
11. Map showing the generalized distribution of bedrock, subwatersheds and related inflow points used with the Basin Characterization Model recharge-runoff estimates for Cuyama Valley.....	61
12. Graph showing comparison of Basic Characteristics Model simulated potential evapotranspiration using the Priestley-Taylor approach with measured reference evapotranspiration from California Irrigation Management Information System station in Cuyama Valley, California	62
13. Graphs showing comparisons of basin discharge, estimated by using the Basin Characterization Model, with measured streamflow for gaged basins in the Cuyama Valley model domain.....	63
14. Graphs showing annual streamflow for all Streamflow Routing inflows in Cuyama Valley, California, <i>A</i> , for 1939–2009, and <i>B</i> , in comparison to precipitation.....	64
15. Maps showing <i>A</i> , drawdown contours for 1947–66; and groundwater-level contours for <i>B</i> , summer 1966; <i>C</i> , spring 2010; and <i>D</i> , summer 2010 for Cuyama Valley, California	65

Figures—Continued

16.	Map showing distribution of model cells representing no-flow, groundwater underflow, springs, streams, and horizontal groundwater flow barrier boundaries in the Cuyama Valley, California	69
17.	Map showing agricultural soils for the Cuyama Valley simplified from Soil Survey Geographic Database.....	70
18.	Maps showing early periods of land-use groups discretized to the model grid, and pie chart of percentages of total land use over the modeled area for <i>A</i> , 1952; <i>B</i> , 1959; <i>C</i> , 1966; and <i>D</i> , 1977 for Cuyama Valley, California	71
19.	Maps showing land-use groups discretized to the model grid, and pie chart of percentages of total land use over the modeled area for <i>A</i> , 1984; <i>B</i> , 2000; and <i>C</i> , 2002 for Cuyama Valley, California	75
20.	Maps showing 2004–06 periods of land-use groups discretized to the model grid, and pie chart of percentages of total land use over the modeled area for <i>A</i> , 2004; <i>B</i> , 2005; and <i>C</i> , 2006 for Cuyama Valley, California	78
21.	Maps showing 2007–09 periods of land-use groups discretized to the model grid, and pie chart of percentages of total land use over the modeled area for <i>A</i> , 2007; <i>B</i> , 2008; and <i>C</i> , 2009 for Cuyama Valley, California	81
22.	Maps showing <i>A</i> , actual major categories of land-use for 2010; <i>B</i> , equivalent land-use groups discretized to the model grid, and pie chart of percentage of total land use over the entire model area; and <i>C</i> , changes in percentages of selected land use through time, Cuyama Valley, California	84
23.	Graphs showing monthly crop coefficients for <i>A</i> , orchards; <i>B</i> , grains and hay; <i>C</i> , vegetables; <i>D</i> , general land use; and <i>E</i> , native vegetation in the Cuyama Valley, California	87
24.	Maps showing <i>A</i> , locations of wells with pumping tests, and the distribution of parameter zones used for model calibration of hydraulic properties for <i>B</i> , model layer 1; <i>C</i> , model layer 2; and <i>D</i> , model layer 3 in the Cuyama Valley, California	88
25.	Map showing calibration data sites of wells for groundwater levels and water-level differences for the Cuyama Valley Hydrologic Model, Cuyama Valley, California	92
26.	Graphs showing simulated and measured hydrographs for selected wells in <i>A</i> , Main-zone; <i>B</i> , Ventucopa Upland; and <i>C</i> , Sierra Madre Foothills subregions, Cuyama Valley, California	93
27.	Graphs showing <i>A</i> , histogram of distribution of water-level residuals for the Cuyama Valley hydrologic model model, <i>B</i> , correlation graph by subregions of measured versus simulated water levels, and <i>C</i> , correlation between simulated and measured vertical water-level differences for selected wells, Cuyama Valley, California	102

Figures—Continued

- | | | |
|-----|---|-----|
| 28. | Maps showing comparison of the contoured measured water levels with simulated water levels <i>A</i> , for fall 1966; <i>B</i> , for spring 2010; and <i>C</i> , for fall 2010, Cuyama Valley, California | 105 |
| 29. | Graphs showing historical subsidence as <i>A</i> , map of seasonal InSAR with graphs of simulated and measured time series for selected locations of relative land-surface deformation from Plate-Boundary Observation sites and Point InSAR targets, and <i>B</i> , simulated total subsidence 1950–2010 for the calibrated hydrologic flow model, Cuyama Valley, California | 108 |
| 30. | Graph showing reported and simulated agricultural pumpage for Cuyama Valley, California | 110 |
| 31. | Graph showing relative composite sensitivity of computed observations at calibration points to changes in selected parameters from analysis with PEST | 111 |
| 32. | Stacked bar charts showing hydrologic budget for the landscape with <i>A</i> , the temporal distribution of total landscape inflows and outflows; and <i>B</i> , pie chart showing average annual components of farm budget of the simulated landscape flow system within the Cuyama Valley Hydrologic Model, Cuyama Valley, California | 112 |
| 33. | Graphs showing <i>A</i> , the simulated net flow of groundwater in the hydrologic cycle; <i>B</i> , pie chart showing average annual components of simulated groundwater flow; <i>C</i> , the cumulative change in storage; and <i>D</i> , changes in groundwater storage, Cuyama Valley, California | 114 |
| 34. | Chart showing the percentage of simulated groundwater pumpage for the water years 1950–2010 for all three model layers, Cuyama Valley, California | 118 |
| 35. | Stacked bar charts showing <i>A</i> , percentage of total recharge by aquifer model layers; and <i>B</i> , Net downward flow between model layers, Cuyama Valley, California | 119 |
| 36. | Maps showing <i>A</i> , projected simulated water levels; and <i>B</i> , the difference in water levels between projection of simulated water levels in fall 2071 and simulated water levels in fall 2010 for the hydrologic flow model of Cuyama Valley, California | 121 |
| 37. | Three projected scenarios showing projected <i>A</i> , cumulative change in net groundwater storage, <i>B</i> , potential groundwater levels at CVKR and CVBR monitoring sites, and <i>C</i> , potential land subsidence near Cuyama, Cuyama Valley, California | 123 |

Tables

1. Summary of groundwater regional zones and subregions for the Cuyama Valley Hydrologic Model, Cuyama Valley, California	127
2. Summary of climate periods for the Cuyama Valley Hydrologic Model, Cuyama Valley, California	128
3. Scaling coefficients for estimation of streamflow for MODFLOW Streamflow Routing from recharge and runoff maps developed by the Basin Characterization Model for ungaged basins in three geologic types in Cuyama Valley.....	129
4. Streamgages used for Basin Characterization Model calibration with calibration statistics for Cuyama Valley, California	130
5. Summary of One-Water Hydrologic Flow Model Packages and processes used with the hydrologic flow model of Cuyama Valley, California	131
6. Coordinates of the hydrologic flow model of Cuyama Valley, California.....	132
7. Percentage of different virtual crop categories in Cuyama Valley Hydrologic Model for selected land-use periods	133
8. Summary of Cuyama Valley Farm process virtual-crop crop category, crop-index number, and select properties for the Cuyama Valley Hydrologic Model, Cuyama Valley, California	134
9. Summary of fractions of transpiration and evaporation by month, for Cuyama Valley crop categories	135
10. Irrigation efficiency, by month, for each crop of the Cuyama Valley, California.....	138
11. Summary of reference evapotranspiration comparisons between Penman-Montieth from California Irrigation Management Information System stations and Priestley-Taylor estimates from regional climate data, Cuyama Valley, California	139
12. Summary of hydraulic properties estimated from the Cuyama Valley hydrologic model calibration	140
13. Summary of parameter zones and related property parameter names used to calibrate horizontal hydraulic conductivity, vertical hydraulic conductivity, and aquifer specific storage and specific yield in the Cuyama Valley hydrologic model, Cuyama Valley, California	141
14. Summary of selected parameter values estimated for the Cuyama Valley hydrologic model, Cuyama Valley, California	142
15. Summary of streambed conductivity parameters and current values, Cuyama Valley, California	147
16. Summary of groundwater-flow budgets for selected periods, Cuyama Valley, California	149

Conversion Factors

Inch/Pound to SI

Multiply	By	To obtain
Length		
inch (in.)	2.54	centimeter (cm)
inch (in.)	25.4	millimeter (mm)
foot (ft)	0.3048	meter (m)
mile (mi)	1.609	kilometer (km)
Area		
Acre	4,047	square meter (m ²)
Acre	0.4047	hectare (ha)
Acre	0.4047	square hectometer (hm ²)
Acre	0.004047	square kilometer (km ²)
square foot (ft ²)	929.0	square centimeter (cm ²)
square foot (ft ²)	0.09290	square meter (m ²)
section (640 acres or 1 square mile)	259.0	square hectometer (hm ²)
Volume		
acre-foot (acre-ft)	1,233	cubic meter (m ³)
acre-foot (acre-ft)	0.001233	cubic hectometer (hm ³)
Flow rate		
acre-foot per day (acre-ft/d)	0.01427	cubic meter per second (m ³ /s)
acre-foot per year (acre-ft/yr)	1,233	cubic meter per year (m ³ /yr)
acre-foot per year (acre-ft/yr)	0.001233	cubic hectometer per year (hm ³ /yr)
Hydraulic conductivity		
foot per day (ft/d)	0.3048	meter per day (m/d)

Abbreviations

BCM	Basin Characteristics Model
CADWR	California Department of Water Resources
CIR	Consumptive irrigation requirement
CUVHM	Cuyama Valley Hydrologic Model
SBDPWWA	Santa Barbara Department of Public Works Water Agency
ENSO	El Nino-Southern Oscillation
ET_{hr} , ET_o	Reference evapotranspiration
ET_{act}	Actual evapotranspiration
K_c	Crop coefficient
K_h	Horizontal hydraulic conductivity
K_v	Vertical hydraulic conductivity
MF2K5	MODFLOW-2005
OWHM	One Water Hydrologic Flow Model
NAMS/PE	North American Monsoon-Pineapple Express
PDO	Pacific Decadal Oscillation
PEST	Parameter Estimation Program
SOSWR	Sum of squared weighted residual
TFDR	Total farm delivery requirement
USGS	U.S. Geological Survey
WBS	Water-balance subregions

Acknowledgments

The authors acknowledge Alan Flint, Chris Harich, Donald Martin, Sarah Falk, and Katherine Paybins, who contributed to the technical content of this study. The authors also thank Larry Schneider of the U.S. Geological Survey for completion of the technical illustrations in this document.

This page intentionally left blank.

Hydrologic Models and Analysis of Water Availability in Cuyama Valley, California

By R.T. Hanson, Lorraine Flint, Claudia C. Faunt, Dennis Gibbs, and Wolfgang Schmid

Abstract

Changes in population, agricultural development practices (including shifts to more water-intensive crops), and climate variability are placing increasingly larger demands on available water resources, particularly groundwater, in the Cuyama Valley, one of the most productive agricultural regions in Santa Barbara County. The goal of this study was to produce a model capable of being accurate at scales relevant to water management decisions that could be considered in the evaluation of the sustainable water supply. The Cuyama Valley Hydrologic Model (CUVHM) was designed to simulate the most important natural and human components of the hydrologic system, including components dependent on variations in climate, thereby providing a reliable assessment of groundwater conditions and processes that can inform water users and help to improve planning for future conditions. Model development included a revision of the conceptual model of the flow system, construction of a precipitation-runoff model using the Basin Characterization Model (BCM), and construction of an integrated hydrologic flow model with MODFLOW-One-Water Hydrologic Flow Model (MF-OWHM). The hydrologic models were calibrated to historical conditions of water and land use and, then, used to assess the use and movement of water throughout the Valley. These tools provide a means to understand the evolution of water use in the Valley, its availability, and the limits of sustainability.

The conceptual model identified inflows and outflows that include the movement and use of water in both natural and anthropogenic systems. The groundwater flow system is characterized by a layered geologic sedimentary sequence that—in combination with the effects of groundwater pumping, natural recharge, and the application of irrigation water at the land surface—displays vertical hydraulic-head gradients. Overall, most of the agricultural demand for water in the Cuyama Valley in the initial part of the growing season is supplied by groundwater, which is augmented by precipitation during wet winter and spring seasons. In addition, the amount of groundwater used for irrigation varies from year to year in response to climate variation and can increase dramatically in dry years. Model simulation results, however, also indicated that irrigation may have been less

efficient during wet years. Agricultural pumpage is a major component to simulated outflow that is often poorly recorded. Therefore, an integrated, coupled farm-process model is used to estimate historical pumpage for water-balance subregions that evolved with the development of groundwater in the Valley from 1949 through 2010. The integrated hydrologic model includes these water-balance subregions and delineates natural, municipal, and agricultural land use; streamflow networks; and groundwater flow systems. The redefinition of the geohydrologic framework (including the internal architecture of the sedimentary units) and incorporation of these units into the simulation of the regional groundwater flow system indicated that faults have compartmentalized the alluvial deposits into subregions, which have responded differently to regional groundwater flow, locations of recharge, and the effects of development. The Cuyama Valley comprises nine subregions grouped into three regional zones, the Main, Ventucopa Uplands, and Sierra Madre Foothills, which are fault bounded, represent different proportions of the three alluvial aquifers, and have different water quality.

The CUVHM uses MF-OWHM to simulate and assess the use and movement of water, including the evolution of land use and related water-balance regions. The model is capable of being accurate at annual to interannual time frames and at subregional to valley-wide spatial scales, which allows for analysis of the groundwater hydrologic budget for the water years 1950–2010, as well as potential assessment of the sustainable use of groundwater.

Simulated changes in storage over time showed that significant withdrawals from storage generally occurred not only during drought years (1976–77 and 1988–92) but also during the early stages of industrial agriculture, which was initially dominated by alfalfa production. Since the 1990s, agriculture has shifted to more water-intensive crops. Measured and simulated groundwater levels indicated substantial declines in selected subregions, mining of groundwater that is thousands to tens of thousands of years old, increased groundwater storage depletion, and land subsidence. Most of the recharge occurs in the upland regions of Ventucopa and Sierra Madre Foothills, and the largest fractions of pumpage and storage depletion occur in the Main subregion. The long-term imbalance between inflows and outflows resulted in simulated overdraft (groundwater

withdrawals in excess of natural recharge) of the groundwater basin over the 61-year period of 1949–2010. Changes in storage varied considerably from year to year, depending on land use, pumpage, and climate conditions. Climatically driven factors can greatly affect inflows, outflows, and water use by more than a factor of two between wet and dry years. Although precipitation during inter-decadal wet years previously replenished the basin, the water use and storage depletion have lessened the effects of these major recharge events. Simulated and measured water-level altitudes indicated the presence of large areas where depressed water levels have resulted in large desaturated zones in the younger and Older Alluvium layers in the Main-zone subregions. The results of modeled projection of the base-case scenario 61 years into the future indicated that current supply-and-demand are unsustainable and will result in additional groundwater-level declines and related storage depletion and land subsidence. The reduced-supply and reduced-demand projections reduced groundwater storage depletion but may not allow for sustainable agriculture under current demands, agricultural practices, and land use.

Introduction

Cuyama Valley is north of Sierra Madre Mountains in south-central California (fig. 1) and is one of the most productive agricultural regions in Santa Barbara County. Increases in population in the Valley and transitions to crops that consume additional water have increased the demand for water within Cuyama Valley groundwater basin (CUVGB). Although a small amount of urban supply is provided by groundwater, irrigated agriculture is solely supplied by groundwater pumpage. The aquifers in the Valley have been subject to overdraft (groundwater withdrawals in excess of natural recharge) since the 1950s (Singer and Swarzenski, 1970), and more recently, land subsidence related to increased and sustained groundwater pumpage has occurred (Everett and others, 2013). The water levels throughout most of the central parts of Cuyama Valley have not substantially recovered since the onset of industrial agriculture in the 1970s. As a part of a resource assessment process, the U.S. Geological Survey (USGS) undertook the study described in this report in cooperation with the Santa Barbara Department of Public Works Water Agency (SBDPWWA) to better understand the hydrologic budget and limits of availability and sustainability.

The purpose of the study was to quantify the water availability of the Cuyama Groundwater Basin under varying cultural and climatic scenarios to inform regional stakeholders' potential constraints of water-supply availability options for the aquifer system, which is the sole source of water supply for the basin. A regional hydrologic flow model capable of being accurate at scales relevant to water management decisions was developed with the SBDPWWA for the Cuyama Valley, California.

Purpose and Scope

This report documents (1) an analysis of the conceptual model of the hydrologic system of the Cuyama Valley, (2) the description of the hydrologic features used in the hydrologic flow models of the Valley groundwater system, (3) development and calibration of a three-dimensional (3D) regional flow model, and (4) an analysis of water availability with respect to current water and land use and potential climate variability and change. Because the regional hydrologic model incorporates time-varying inflows and outflows, the model can be used to evaluate the basin-scale effects of temporal changes in groundwater recharge and pumping. Overall, the development of the geohydrologic and hydrologic models, data networks, and hydrologic analyses provide a basis for assessing water availability and formulating and assessing water-resource management strategies.

Approach

The creation of the first set of hydrologic models of Cuyama Valley for this study required the updating of the conceptual model, the geohydrologic framework, and the estimation of the components of the hydrologic cycle. The conceptual model was realigned with recent information about the framework of recharge, land use, and streamflow infiltration (Everett and others, 2013; Sweetkind and others, 2013). Refinement of the geohydrologic framework required the remapping of geologic surfaces and reconciliation of recent geologic information available from wells and investigations (Sweetkind and others, 2013).

The Cuyama Valley Hydrologic Model (CUVHM) was constructed on the basis of the new conceptual and geohydrologic models to simulate the flow and use of water for the period September 1949 through December 2010. This model includes new layering, inflows and outflows, and more detailed representation of the current land cover/land use and vegetation. The new valley-wide model (fig. 1B) includes estimates of runoff from the surrounding watersheds simulated by using the Basin Characterization Model (BCM) (Flint and Flint, 2012), a regional-scale precipitation-runoff model (fig. 1A).

Description of the Study Area

Cuyama Valley is a high desert watershed with a surface-water drainage area of about 690 square miles (mi²) and an underlying main alluvial basin covering about 230 mi² that straddles the northeastern part of Santa Barbara County and parts of San Luis Obispo, Ventura, and Kern Counties (the Cuyama River forms part of the county boundary) within the CUVGB (figs. 1A, 1B). This high desert watershed trends northwesterly from the Sierra Madre Mountains on the south

to the Caliente Range on the north (fig. 1A). Land-surface elevations in the watershed range from 800 feet (ft) above NAVD88 near Twitchell Reservoir to greater than 8,000 ft at Mt. Pinos, and land surface elevations within the groundwater basin proper range from about 1,950 ft to 3,600 ft above NAVD88. The valley is drained by the Cuyama River and its tributaries, of which Santa Barbara Creek is the largest (fig. 1B). The valley has been developed predominantly for oil production since the 1950s and for agriculture since the 1930s but also contains the towns of Cuyama and New Cuyama and other small towns (fig. 1B). The CUVGB encompasses about 230 mi², of which about 30 percent is used for agriculture, about 69 percent is natural vegetation, and one percent is urban land as of 2010. The residents of the valley rely almost exclusively on groundwater for their drinking-water supply and for irrigation (Gibbs, 2010). As a result, the aquifer is susceptible to overdraft (groundwater pumpage in excess of recharge) and related secondary effects such as land subsidence and poor water quality when outflows (including pumpage) exceed inflows for an extended period of time.

Hydrologic and Water-Balance Subregions

The assessment and analysis of groundwater availability relative to the components of the hydrologic cycle required the division of Cuyama Valley into subregions that can be analyzed individually with respect to supply-and-demand components. This study also required a more precise delineation of the groundwater basin. The delineation described by the California Department of Water Resources (2003) includes several extraneous regions that are not part of the main regional aquifer systems within Cuyama Valley. Thus, the extent of the groundwater basin was redefined as a part of this study (fig. 1B). The basin was further divided into nine groundwater hydrologic subregions (fig. 2A, table 1). These subregions separate the aquifers into regions that: are fault bounded; represent different proportions of the three alluvial aquifer systems; have different water-quality characteristics; and where the response to the use, movement, and consumption of water is similar in specific parts of the aquifers but differ from the responses in the other subregions. In this context, these subregions of Cuyama Valley may be considered a collection of subbasins that are partially hydraulically connected, but have different hydrologic features or hydraulic properties and consequently respond differently to natural and anthropogenic stresses. To facilitate regional water-availability analysis, these nine subregions were grouped into three simplified major regional zones that represent the Main zone, Ventucopa Uplands, and Sierra Madre Foothills (fig. 2B).

The valley also was divided into multiple water-accounting units called water-balance subregions (WBS), to create the associations between demand for water for irrigation and supply from wells that link the supply-and-demand components driven by changing land use and land ownership

(fig. 2C). These subregions comprise a combination of private and public lands from which data can be used to estimate the water-balance components of land use, streamflow, and groundwater flow relative to the use and movement of water at the land surface. The increase in the number—from 2 in 1949 to 83 in 2010—reflect the historical development of the valley across the landscape. The changing number of WBS generally represents changes in land ownership and use that occurred during 10 different periods within the 61 years of simulation. Superimposed on these WBS are cell-by-cell distributions of changes in land use that include different natural vegetation, urban, and agricultural uses throughout the valley (described later in the “Model Development” section). The most recent WBS are based on land-use parcels of 2010 and were sequentially changed for earlier periods to provide a logical progression of land-use and ownership changes over the 61-year simulation period (1949–2010). These WBS are also combined with the nine groundwater subregions for the purposes of water-supply analysis and are generally coincident with those subregions (fig. 2A).

Geologic Framework

The Cuyama Valley is a down-faulted block or graben that is bordered on the north by the Morales and Whiterock Faults and on the south by the South Cuyama and Ozena Faults (fig. 3A). The eastern part of the valley is underlain by the Cuyama syncline, with a strike parallel to the elongation of the valley, which plunges toward the northwest. The north limb of this fold is truncated against the Morales Fault (Singer and Swarzenski, 1970).

Hydrogeologic Units

The hydrogeologic framework of Cuyama Valley was developed through a reevaluation and synthesis of geologic information from previous studies, which resulted in a simplified grouping of geologic units into hydrogeologic units (Sweetkind and others, 2013). Geologic units within the Cuyama Valley groundwater basin include unconsolidated Pleistocene and Holocene alluvial deposits and fluvial deposits of the Cuyama River drainage, and the underlying, partly consolidated nonmarine Morales Formation of Pliocene to Pleistocene age (Upson and Worts, 1951; Singer and Swarzenski, 1970). These deposits unconformably overlie a late Cretaceous to middle Cenozoic succession of consolidated marine and nonmarine sedimentary rocks, which themselves overlie crystalline granitic and gneissic rocks (Hill and others, 1958; Dibblee, 1982; Lagoe, 1987; Bazeley, 1988; fig. 3A). Previous USGS studies of Cuyama Valley (Upson and Worts, 1951; Singer and Swarzenski, 1970) delineated aquifers in the saturated parts of the Recent and Older Alluvium, units that historically have yielded most of the water pumped in the study area. Since these studies were completed, water levels

4 Hydrologic Models and Analysis of Water Availability in Cuyama Valley, California

have declined in some areas into the deeper units such as the Morales Formation. The hydrogeologic framework that was used to represent the three discrete hydrologic model layers as determined by Sweetkind and others (2013) is illustrated in figure 3A:

1. Recent Alluvium aquifer—one layer of the younger alluvial deposits representing an alluvial deposit layer.
2. Older Alluvium aquifer—one layer of the older alluvial deposits.
3. Morales Formation aquifer—one layer representing the uppermost units of the Morales Formation.

Collectively, these aquifers are variable in areal extent and range in thickness from a few feet up to thousands of feet. The outcrops and extent of these units are superimposed onto the BCM and the CUVHM active model grids (fig. 3A).

Faults and the Groundwater Flow System

Faults of hydrologic significance occur at the basin margins, where fault offset juxtaposes basin-fill sediments against older consolidated rocks, and within the basin, where basin-fill units of differing water-transmitting ability are juxtaposed. Faults within the basin fill have been recognized previously as being associated with historical surface springs or lateral changes in groundwater elevations (Singer and Swarzenski, 1970). Sweetkind and others (2013) identified three faults within the basin that offset the basin-filling deposits and are associated with known water-level changes (Upson and Worts, 1951; Singer and Swarzenski, 1970): the thrust faults that bound Turkey Trap Ridge and Graveyard Ridge, the Santa Barbara Canyon Fault, and the Rehoboth Fault (fig. 3A). Upson and Worts (1951) reported the presence of springs and seeps along the base of Turkey Trap and Graveyard Ridges in 1946. Singer and Swarzenski (1970) reported water-level drawdowns of 80 to 100 feet in the area near these ridges and indicated that water removed by pumping from this region is slow to replenish because faults restrict movement of water. The impediment to flow might be related to the hydraulic properties of the fault itself or fault juxtaposition of older, slightly less permeable material. A fault (or fault zone), here called the Santa Barbara Canyon Fault (SBCF; fig. 3A), was suggested by Singer and Swarzenski (1970) as the cause of a steep hydraulic gradient in the southeastern part of Cuyama Valley, where water levels in the vicinity of Ventucopa are at least 100 ft higher than water levels a couple miles to the northwest. The relatively small amount of vertical offset on the Santa Barbara Canyon Fault indicates that changes in water levels across this fault documented in previous studies are caused by distinct fault-zone properties, rather than juxtaposition of units of differing water-transmitting ability. Another fault, here called the

Rehoboth Fault (fig. 3A), is inferred from lateral water-level changes in the west-central part of the valley. The other major faults in Cuyama Valley (figs. 2A, 3A), such as the Russell, Morales, South Cuyama, Ozena, and Whiterock Faults, are represented as no-flow groundwater boundaries along the outer edge of the alluvial basin.

Hydrogeologic Framework

A digital 3D hydrogeologic framework model of the alluvial basin was developed and is described in detail by Sweetkind and others (2013). The framework model uses information from a variety of datasets, including existing lithologic and electrical geophysical logs from oil and gas wells and water wells, cross sections, and geologic maps, to delineate the volumes of the aquifer system bounded by faults and relevant depositional or formational boundaries. The model is the digital representation of the interpreted geometry and thickness of subsurface geologic units and the geometry of folds and faults that bound the basin and lie within it. Specifically, the model was constructed to represent the subsurface geometry of the Recent Alluvial aquifer, the Older Alluvial aquifer, the Morales Formation aquifer, and a composite pre-Morales Formation bedrock unit. This model provides the fundamental hydrogeologic framework for the subsequent development of a transient numerical model of groundwater flow in the study area.

The framework model may be explored and visualized by slicing the model volume at any chosen location (for example, figs 3B, C). Two sections were cut from the framework model along the same two section lines as published by Singer and Swarzenski (1970). One section (A–A', fig. 3B) is aligned roughly east-west, parallel to the trace of the interbasin thrust faults that bound the Turkey Trap Ridge and Graveyard Ridge, and a second (B–B', fig. 3C) is a roughly north-south section transverse to the major structural grain of the basin. Together with the map, the sections show the extent and thickness of the aquifers. The sections show the thickness of Recent Alluvial aquifer in the axis of the valley, underlain by Older Alluvial aquifer. The Older Alluvial aquifer dominates the southern part of the valley, beneath its outcrop exposures, with the Morales Formation aquifer underlying it. The Morales Formation aquifer predominates in the Cuyama Badlands area, where it is virtually the only permeable stratigraphic unit except for thin Recent Alluvium along the trace of the Cuyama River channel. The Morales Formation aquifer is also exposed at the ground surface in the western part of the valley, where it is locally overlain by thin deposits of alluvium in the channel of the Cuyama River. The effect of fault offset is not obvious at the scale of figure 3A, except for the appearance of Older Alluvial aquifer at land surface at Graveyard Ridge and Turkey Trap Ridge.

Three-Dimensional Model of Grain-Size Distribution

An analysis of variability of lithology and grain size was conducted for the three principal basin-filling units, the Recent Alluvial aquifer, Older Alluvial aquifer, and Morales Formation aquifer. The details of this analysis are documented by Sweetkind and others (2013). Textural variability in the basin-filling units is ultimately a function of the sedimentary facies, environment of deposition, and depositional history of the basin. Textural data such as grain size, sorting, and bedding characteristics form the geologic basis for estimating the hydraulic properties within the numerical hydrologic-flow model.

The spatial distribution and the characteristics of the sediments forming the three aquifers are related to the Pliocene and Pleistocene tectonic evolution and uplift of the basin, the progressive narrowing of the valley, and the gradually increasing channelization of the Cuyama River drainage. The Morales Formation is a widespread unit that was deposited prior to the constriction of the basin by encroaching thrust faults. As a result of tectonic uplift, the previously deposited Morales Formation was exposed and eroded. Streams deposited and reworked sediment from the Morales Formation into a narrower basin that resulted in the deposition of the Older Alluvial aquifer. The Recent Alluvial aquifer is confined to the center of Cuyama Valley and alluvial channels tributary to the Cuyama River. Textural variations in the Recent Alluvial aquifer appear to be primarily climate-driven and reflect regional rainfall variations that control stream incision and aggradation.

Sediment grain size, a textural parameter commonly reported in oil-well and water-well data as well as in outcrop observations, was analyzed and modeled. Boulders, gravels and sands are considered coarse-grained, whereas silts and clays are considered fine-grained. As part of a statistical and geostatistical analysis, the percentage of coarse-grained sediment was calculated for the entire thickness of each aquifer for all 218 available wells. Percent coarse-grained sediment was calculated as the total thickness of coarse-grained intervals divided by the total thickness of the aquifer. The global mean percentage of coarse-grained texture is 34 percent, with the Recent Alluvial aquifer being significantly more coarse-grained than the Older Alluvial aquifer or the Morales Formation aquifer.

Initially, the interpreted grain-size and bedding-frequency parameters derived from data from the oil and gas exploration boreholes were used to construct a 3D model of textural variations within the basin by extrapolating data away from boreholes using a nearest-neighbor 3D-gridding process for a cell size of 500 meters (m) horizontally and 10 m vertically (Sweetkind and others, 2013). Using geostatistical methods, this model was refined to a higher resolution 250-meter

grid for producing a series of plan-view estimates of texture variation of grain-size variability for each aquifer that is coincident with the gridding of the hydrologic model (fig. 4). The two-dimensional (2D) kriged estimates of percentage of coarse-grained texture highlight textural distributions within and between the aquifers.

The spatial patterns of the percentage of coarse-grained texture for each aquifer show significant heterogeneity in the texture of the sediments, which reflects the depositional environment and the geomorphic evolution of the region since Pliocene time. The texture model of the Recent Alluvial aquifer has the highest percentage of coarse-grained deposits (fig. 4A). It is coarsest in the eastern part of the valley, becomes finer grained with distance downstream to the west, and, although not evident at the scale of these maps, is also coarsest in the vicinity of the active Cuyama River channel. The coarse-grained nature of the Recent Alluvial aquifer reflects a number of factors, including the short distances between the sediment sources in the surrounding uplands and the sites of sediment deposition as well as the high-energy nature of Cuyama River and tributary creeks that transport sediments during winter storms and summer monsoonal rains. The spatial structure of the kriged textural model for the Recent Alluvial aquifer can be attributed to the alignment of the active drainages, whereas the textural models of the older aquifers are less correlated to modern topography.

The texture model for the Older Alluvial aquifer differs in spatial structure from the Recent Alluvial aquifer in being overall much finer grained and generally unrelated to the modern active drainages (fig. 4B). The Older Alluvial aquifer is moderately coarse-grained in the eastern half of Cuyama Valley, but transitions to fine-grained at the western end of the valley. Much of (the) Older Alluvial aquifer is derived from erosional reworking of uplifted parts of the Morales Formation. The Older Alluvial aquifer is generally coarser than the Morales Formation aquifer and has more numerous medium- and coarse-grained lenses that probably represent alluvial channel deposits.

The Morales Formation aquifer is much finer-grained than the overlying units (fig. 4C). This aquifer has relatively few coarse-grained intervals and is characterized by relatively fine-grained material, particularly in the axis of the valley, where Older Alluvial aquifer contains some of the coarsest intervals. The Morales Formation aquifer is particularly fine grained in the western half of Cuyama Valley, where surface geologic mapping identifies a lacustrine facies in this unit (Upson and Worts, 1951; Dibblee and Minch, 2005; DeLong and others, 2008). However, the Morales Formation aquifer becomes more coarse-grained along the southern flank of the valley and to the southeast, perhaps reflecting available sediment supply from uplifting areas outside the valley at the time of deposition.

Hydrologic System

The conceptual model for the hydrologic cycle starts with inflows from precipitation and streamflow. Streamflow enters Cuyama Valley through the Cuyama River and as runoff from the side slopes and local stream networks that drain the surrounding mountains. Infiltration of runoff along with percolation of some precipitation and irrigation below the root zone contribute to groundwater recharge. Additional underflow of groundwater occurs along the Cuyama River channel as inflows at the eastern and outflows at the western boundaries of the valley in all three aquifers (fig. 2A). Outflow also occurs as evapotranspiration from natural vegetation, urban landscapes, and irrigated agriculture. Additional outflow occurs as groundwater pumpage for agricultural, urban, and domestic uses. These natural and man-made inflows and outflows represent the supply-and-demand components of water use within the hydrologic cycle in Cuyama Valley. Since the 1990s, the developed hydrologic system now also includes the pumpage of water in one groundwater subregion that is exported to adjacent subregions for irrigation use.

Climate

The climate of the Cuyama Valley is arid, with hot summers and cool winters. The record of cumulative departure from the mean of precipitation for the late 1940s or 1950s (depending on when records were available) to 2010 shows that major and minor wet periods and dry periods are typical of the climate variability for Cuyama Valley (figs. 5, 6A). The map of average annual precipitation indicates that higher precipitation occurs within the large mountain-front inland regions (fig. 6A).

On figure 5, 16 wet and dry periods are shown, and 15 major wet and dry periods are coincident with the period of simulation and related stress periods from October 1949 through December 2010 (fig. 5; table 2). Average rainfall ranges from about 7 inches per year on the valley floor to about 15 inches per year in the eastern part of Cuyama Valley (Gibbs, 2010; fig. 6A).

Time-series analysis of the residuals from the cumulative departure of precipitation from the Santa Barbara Canyon (Reyes Ranch) long-term hydrologic time series from Cuyama Valley suggest a significant influence in climate variability. The estimated periodicities include 6 percent of the oscillations coincident with the El Niño-Southern Oscillation (ENSO, 2–6 years), 0 percent of cycles from the North American Monsoon-Pineapple Express (NAMS/PE, 7–10 years), and 94 percent of the variation from the Pacific Decadal Oscillation (PDO, 10–30 years) (Hanson and others, 2006; Dickinson and others, 2014). This long-term record shows periods of 27 years (55 percent of the variation), 22 years (36 percent of the variation), 13.5 years (3 percent

of the variation) (PDO), and 2–6 years (ENSO) that explain variation in precipitation (fig. 5). Thus, almost all of the variation in precipitation and streamflow occurs in the longer climate cycles. No records of streamflow or groundwater levels are long enough for estimation of climate cycles. The longer cycles will be important periods for the evaluation of interdecadal sustainability of the water resources.

The average annual reference evapotranspiration (ET_h) values show the orographic effects similar to those in the precipitation values. The ET_h in the Cuyama Valley transitions from values of about 55 to 56 inches per year (in/yr) at the base of the Caliente Mountains to lower values of about 45 to 53 in/yr toward the south end of the Cuyama Valley near Ventucopa (fig. 6B). Values of ET_h in the inland areas of Cuyama Valley consistently range from 53 to 55 in/yr with very little variation (fig. 6B). Variations in ET_h are higher in the southeastern part of Valley, where they range from 45 to 57 in/yr due to shading effects from the rugged terrain.

Effects of Water Use on the Landscape

An integral part of the hydrologic system is the use and movement of water across the landscape, which in this study includes the shallow subsurface defined by the root zone. This includes the evolution of the development and use of land in Cuyama Valley, from the tracts of the Spanish land grants to modern agriculture, urbanization, and industry. Several major periods of development occurred in Cuyama Valley, including the transformation of the land grants into cattle ranches with the eventual need for alfalfa, the introduction of the petroleum industry and founding of the town of Cuyama by the Atlantic Richfield Company (ARCO), and the introduction of large-scale agriculture with orchards, vineyards, and organic farming (fig. 7). Also farming has evolved from the planting of predominantly potatoes and alfalfa during the 1940s–1970s to a doubling of the acreage of grain crops and a tripling of the acreage in carrot crops by the mid-1980s (fig. 7A). Carrot and grains represent more than half of the crops grown in the Cuyama Valley in recent decades (fig. 7A).

Population growth in Cuyama Valley was estimated from census tract data (U.S. Census Bureau, 2014a, b) and showed a steady increase from just over 1,000 inhabitants to more than 8,600 inhabitants from 1950 through 2010 (fig. 7). The town of Cuyama was established along with the discovery and development of petroleum resources (fig. 7). Cuyama, along with New Cuyama and the smaller town of Ventucopa, represent the three clusters of housing in the valley. These urban clusters represent less than 1 percent of the land on the valley floor. The towns of Cuyama and New Cuyama are served water from the Cuyama Community Service District supply wells, while the schools and other residents are served water by their own local wells.

The evolution of the landscape occurred as a combination of changes in land use and related land ownership in Cuyama Valley. For the purpose of modeling the hydrologic system, temporal changes in the land ownership were represented by using a sequence of 10 different periods over the 61 years of historical simulation 1949–2010 (figs. 2C, 5). These periods were first defined for 2010 on the basis of current land use and ownership and then discretized from recent years to past years to represent the multi-year periods of 1943–50, 1951–59, 1960–69, 1970–79, 1980–85, 1986–92, 1993–95, 1996–2000, 2001–09, and 2010 (fig. 5). The changing water-balance subregions (WBS; fig. 2C) reflect the evolution of land ownership and land-use that required groundwater pumpage, as well as regions of native vegetation using precipitation only, and urban and domestic areas served by separate specified sources of groundwater pumpage. The more detailed land-use changes that cover 14 periods (fig. 5) are described later in the “Land Use” section.

Surface Water

Streamflow infiltration together with deep percolation of precipitation, is a major source of natural recharge in Cuyama Valley. Streamflow within the valley occurs primarily from runoff that originates from rainfall and snowmelt in upstream tributary drainages, entering the valley through the Cuyama River and Reyes Creek and other ungaged tributaries. During occasional large storms that can result in flood flows, runoff is also generated within Cuyama Valley and flows through the tributaries to the Cuyama River (fig. 8). Streamflow is currently measured at two gages that record the flow into Cuyama Valley: the Cuyama River near Ventucopa (11136500, 1937–58; 11136501, 2002–10); and, Santa Barbara Canyon Creek near Ventucopa (11136600, 2002–10; fig. 8). There is no downstream gage to measure outflow prior to the streamgage at Buckhorn and inflow to Twitchell Reservoir (fig. 1), which include flows from other large tributary watersheds downstream of Cuyama Valley. The remainder of the tributary canyons and outflow from the Valley along the Cuyama River remain ungaged with the exception of occasional flood-flow measurements.

Groundwater

Under predevelopment conditions, groundwater flowed from the foothills of the surrounding mountains of the Cuyama Valley toward the Pacific Ocean. Under developed conditions, pumpage in excess of recharge has occurred for decades, altering the predevelopment flows in response to groundwater storage depletion and regional cones of depression (or drawdown) in groundwater levels in the center of the valley. Groundwater levels in these persistent depressions show additional seasonal declines that are driven by a combination

of agricultural and water-supply pumpage. Groundwater inflows include recharge from infiltration of precipitation, streamflow (figs. 6A, 8), and applied water from irrigation. Additional inflow occurs as underflow across the southeastern boundary of the valley, beneath the stream channel of the Cuyama River and Reyes Creek. Outflow from groundwater includes pumpage, base flow or rejected recharge along streams, evapotranspiration, and subsurface underflow to the west from the aquifer systems (fig. 9).

Development of groundwater in the Cuyama Valley has resulted in the construction and pumpage of several hundred wells between 1949 and 2010. This includes about 120 domestic wells, two municipal-supply wells, and more than 100 agricultural irrigation wells (fig. 9). Total pumpage for water supply grew from less than 50 acre-feet (acre-ft) prior to 1982 to more than 150 acre-ft from 1983 to 2010, with an increase around 1982, which was coincident with the increase in population in the valley (fig. 10). The domestic pumpage was estimated on the basis of population growth and an assumed consumption of about 0.54 acre-ft per year per land parcel for each “domestic” (household) well. A minor amount of the increase can also be attributed to the increase in rural residential (domestic) pumpage between 2000 and 2010 (fig. 10). Most of the drinking-water supply is pumped by the Cuyama Valley Community Service District. For the period 1949–2010, the overall distribution of pumpage for drinking-water supply is estimated to be about 88 percent urban, and 12 percent domestic. Temperature difference logs indicated that all three aquifers are contributing to groundwater flow and pumpage in various parts of the valley (Everett and others, 2013).

Model Development

Two hydrologic models were developed for the Cuyama Valley watershed. One is a water-balance model representing the watersheds in the mountains surrounding the valley that was developed by using the Basin Characterization Model (BCM) (Flint and Flint, 2012; Flint and others, 2012; Thorne and others, 2012). Simulations made with this model provided runoff estimates for all of the ungaged ephemeral streams and arroyos that form a drainage network that carries mountain-front recharge from streamflow infiltration of flood flows along the boundary of the alluvial groundwater basin. The second model, referred to herein as the Cuyama Valley Hydrologic Model (CUVHM), is an integrated hydrologic model that was developed using an integrated hydrologic flow model with MODFLOW-One-Water Hydrologic Flow Model (MF-OWHM) (Schmid and others, 2006a, b; Schmid and Hanson, 2009, 2013; Hanson and others, 2010, 2014) to simulate the use and movement of water throughout the groundwater basin.

Water-Balance Model

Estimation of Recharge and Runoff

Rainfall-runoff models require streamflow data for calibration and, then, can be used to simulate flow at gaged and ungaged locations. Rainfall-runoff models do not provide an estimate of spatially distributed recharge to complement runoff estimates, but do provide a more complete picture of the hydrologic processes in data-sparse basins. The Basin Characterization Model (BCM) is a grid-based, regional water-balance model that can provide process-based estimates of recharge and runoff for ungaged locations. BCM was used in this study to provide flow boundary conditions for the CUVHM. The BCM model domain includes the 144 subwatersheds that surround and drain into the alluvial/structural valley (fig. 11).

BCM is a distributed parameter water-balance model that performs a multi-year simulation of surface and shallow subsurface hydrologic processes. The water balance calculations are performed at a monthly time step and independently at an evenly distributed 270 square meters (m^2) grid cell spacing. The model inputs include (1) topography, soil properties, and geology datasets, which are virtually static with time; (2) monthly gridded precipitation and temperature datasets (Parameter–Elevation Regressions on Independent Slopes Model, PRISM; Daly and others, 2008; 800-m transient dataset); and (3) monthly gridded potential evapotranspiration (PET). The monthly gridded PET is simulated using an hourly energy-balance calculation that is based on solar radiation, air temperature, and the Priestley–Taylor equation (Flint and Childs, 1987) to calculate potential evapotranspiration (Flint and Childs, 1991). Clear sky PET is calculated using a solar radiation model that incorporates seasonal atmospheric transmissivity parameters and site-specific parameters of slope, aspect, and topographic shading. Hourly PET is averaged to a monthly rate and cloudiness corrections are made using cloudiness data from National Renewable Energy (2014). Modeled PET for the southwestern United States was calibrated to the measured PET rates from California Irrigation Management Information System (CIMIS) (California Department of Water Resources, 2007) and Arizona Meteorological Network (University of Arizona, 2012) stations, and is comparable to the estimates from Cuyama Valley CIMIS station No. 88 (figs. 6B, 12). No error analysis was made for the PET. There is a bias in the comparison to CIMIS measured ET_0 on the valley floor equivalent of approximately –10 percent (BCM estimates are lower than measured at the CIMIS station), or approximately –0.8 inches per month for the months with the highest PET, and less than –0.1 inches per month for low PET months (fig. 12).

For the Cuyama Valley, the precipitation, air temperature, and monthly PET maps were combined with maps of elevation, bedrock permeability (estimated on the basis of geology (Jennings, 1977) and iteratively modified in the model calibration process), and soil-water storage from the SSURGO

soil databases (U.S. Department of Agriculture Natural Resources Conservation Service, 2006). Once available monthly water is calculated, if available water exceeds total soil storage, this excess water becomes runoff, and the amount of water between total soil storage and field capacity storage becomes potential recharge. If available water is less than total soil storage but greater than field capacity, the water exceeding field capacity becomes potential recharge. If potential recharge is greater than bedrock permeability (K), then recharge equals K and potential recharge that exceeds K becomes runoff, or else it will recharge at K until it reaches field capacity. Any water less than field capacity will be lost to actual evapotranspiration at the rate of PET for that month until it reaches wilting point. Additional details of model operation and input and output datasets can be found in Thorne and others (2012).

Calibration and Comparison With Measured Streamflows

The BCM is calibrated to partition excess water into recharge and runoff by comparing simulation results for runoff with measured surface-water flow and iteratively changing K until a reasonable match is achieved. This was done for seven basins (fig. 11) with varying amounts of impairment (regulated flow) and representing three main geologic units, sandstone, conglomerate, and alluvium (fig. 11, table 3). Finally, basin discharge was calculated from recharge and runoff accumulated from grid cells upstream of “pour points,” to more accurately reflect stream channel losses and gains between stream gages and to create surface-water flow recession and baseflow that can extend throughout the dry season (Flint and others, 2012). The “pour points” represent locations where outflow from each of the surrounding watersheds flows into the valley. The portions of the recharge and runoff estimated by BCM simulations then become the inflow at 144 pour-point locations within the streamflow network that is simulated by MF-OWHM in the CUVHM model (fig. 8). The fractions of recharge and runoff that are ultimately used within CUVHM were adjusted for the two largest inflows along the Cuyama River and Santa Barbara Creek during BCM calibration.

The BCM was calibrated against selected monthly streamflows at seven USGS streamgages (fig. 13, table 4). Comparisons of BCM-estimated basin discharge and measured streamflow indicate a relatively good match with BCM results. By adjusting the parameter controlling baseflow, the total measured streamflow volume for the period of record for each streamgage was matched exactly by BCM estimates. Calibration statistics indicate relatively good goodness-of-fit on the basis of the Nash-Sutcliffe Efficiency (NSE) statistic, and monthly and annual r^2 values (table 4). The majority of the runoff is derived from the watersheds that drain the Cuyama River and Santa Barbara Canyon, with lesser amounts of storm flows from other ungaged creeks such as Aliso, Apache, Quatal, Berringer, and Reyes Creeks.

Development of BCM Results for CUVHM model

The average annual areal recharge for 1980–2009 ranges from 0 to 11.8 in/yr. The relative proportions of (1) shallow subsurface flow from recharge that becomes baseflow, (2) runoff that becomes streamflow, and (3) runoff that become deep recharge to the mountain-block or alluvial-basin areas were calculated and are indicated in table 4. These were used to develop scaling factors for 144 ungaged basins surrounding the fault-defined valley in two main geologic types, and 13 pour points within the alluvial valley. The first two columns in table 3 indicate the scaling coefficients used to distribute the total potential stream inflow estimates for the MF-OWHM SFR Package that were the initial estimates of inflow used for model calibration. The third column is an estimate of the recharge upstream of each basin's pour point that becomes mountain block recharge. It was assumed that no mountain block recharge would cross the fault boundaries that surround most of the valley and would discharge upgradient of the fault. Therefore only the scaling factors for the SFR recharge and SFR runoff were used and selectively adjusted to estimate the fractions of runoff and rejected recharge that become inflow along the mountain fronts during the CUVHM model calibration for the largest contributing drainages, the Cuyama River and Santa Barbara Canyon Creek. The scaling factor for each column of table 3 was multiplied by the accumulated recharge or runoff for each subwatershed for each geologic type and summed to provide the SFR boundary condition for each of the 144 basins as a monthly recharge and a runoff flow. Average annual streamflow applied to SFR boundaries is approximately 1,500 acre-ft, ranging from 0 to 120,000 acre-feet per year (acre-ft/yr) (fig. 14A). Annual streamflow exceeds 10 acre-ft in only 14 of 144 basins for any of the last 40 years, and with the exception of the two largest basins in the southeastern conglomerates, all are on the southern side of the valley, an area dominated by sandstones. These 14 basins contribute more than 60 percent of the total streamflow.

The Cuyama Valley is classified as semiarid, which means that average annual precipitation is between 20 and 50 percent of potential evapotranspiration, indicating little potential for runoff or recharge. However, recharge in a semiarid basin does not occur on the basis of average annual conditions. In certain areas of a basin, such as at higher elevations on the southern slopes of Cuyama Valley, precipitation in some months can exceed potential evapotranspiration and soil storage, and runoff and (or) recharge can occur. Note that there is commonly little streamflow in the Cuyama Valley (fig. 14A), and significant streamflow (greater than 10,000 acre-ft/yr) occurs in only 23 of 71 years (1939–2010), or about 32 percent of the time. The relation of streamflow and especially recharge to precipitation is nonlinear in arid and semiarid environments (Flint and others, 2012), which is confirmed in Cuyama Valley (fig. 14B).

For application to the CUVHM, the monthly streamflows developed through simulations with the BCM for the 144 pour points are used as inflow rates for the monthly periods and provide the intermittent inflows along the outer boundary of the active CUVHM model area. The overall estimate of gaged and ungaged inflow for the period 1950–2010 averaged 29,500 acre-ft/yr, with about 19,100 acre-ft/yr as runoff (65 percent) and 10,400 acre-ft/yr as recharge (35 percent) for the watersheds surrounding and draining into the valley. Recharge occurring as underflow (mountain-block recharge) was considered negligible, because faults bound most of the valley and the age of many groundwater samples from wells along the mountain-fronts are thousands to tens of thousands of years old (Everett and others, 2013). Consequently, the BCM recharge as groundwater underflow into the valley (mountain-block recharge) was considered to discharge locally through ET or additional baseflow as rejected mountain-front recharge. The reader is referred to BCM documentation for more details on limitations associated with monthly stress periods (Flint and Flint, 2012; Flint and others, 2012; Thorne and others, 2012).

Integrated Hydrologic Model—CUVHM

The Cuyama Valley Hydrologic Model, or CUVHM, was developed to (1) characterize the historical conditions for the analysis of the use and movement of water throughout the valley, and (2) provide a tool for stakeholders to address water availability and water-use issues in the valley. In order to maintain the usefulness of the CUVHM, periodic updates will be required as changing conditions in the actual hydrologic system continue to respond to the stresses imposed upon it, and as new information on the surface-water and groundwater systems become available. The CUVHM is a numerical hydrologic flow model developed with the finite-difference hydrologic modeling software One Water Hydrologic Flow Model (MF-OWHM) (Hanson and Schmid, 2013; Hanson and others, 2014a, b) that includes MODFLOW-2005 (MF2K5) (Harbaugh and others, 2000; Hill and others, 2000; Harbaugh, 2005) and incorporates an updated version of the Farm Process (FMP3) (Hanson and others, 2014b). The MF-OWHM is the newest version of MODFLOW-2005 with the Farm Process (Schmid and others, 2006a, b; Schmid and Hanson, 2009) that incorporates a dynamically integrated water supply-and-demand accounting within agricultural areas and areas of native vegetation. The MF-OWHM enables a more-detailed and realistic simulation of hydrologic systems than do earlier versions of MODFLOW. The MF-OWHM code incorporates the simulation of conjunctive use with linkages of supply-constrained and demand-driven use and movement of water across the landscape, surface-water, and groundwater flow systems throughout the Cuyama Valley (Hanson and others, 2010, 2014b; Hanson and Schmid, 2013).

The CUVHM was constructed in three major phases. The first phase was the collection of new data and compilation of existing data (Everett and others, 2013). The geohydrologic framework model was then developed on the basis of work in previous studies and analysis of new data (Sweetkind and others, 2013). This framework was further modified to include the inflow and outflows of the updated conceptual model, geohydrologic model development to determine the distribution of hydraulic properties, and finally, development of the hydrologic models. These components of model development were completed iteratively during the development and calibration of the model. The final components of MF-OWHM (processes and packages) used for the CUVHM are summarized in table 5.

Input parameters to the CUVHM were adjusted during implementation of these model development phases. Input parameters to the CUVHM were adjusted, with the aid of trial-and-error and automated parameter estimation calibration. The parameter estimation codes UCODE-2005 (Poeter and others, 2005) and PEST (Doherty, 2004, 2010a, b, c; Doherty and Hunt, 2010) were used to help with the calculation of sensitivities and parameter estimation. The model was calibrated to heads (groundwater levels), head differences, head changes with time, and land subsidence. During construction and calibration of the model, it became evident that several updates and enhancements were needed within MF2K5, the FMP, and some post-processing software. These updates and enhancements are summarized in the documentation of MF-OWHM (Hanson and others, 2014a, b). The CUVHM model components can be grouped in terms of the discretization and boundaries, land-use, streamflow, aquifer characteristics, initial conditions, and water budgets. The next few sections of the report describe the model components within these groups.

Discretization

The CUVHM domain includes the major alluvial deposits of the entire Cuyama Valley. The valley extends from east of Ventucopa and the confluence of Reyes Creek with Cuyama River to the narrows along Cuyama River northwest of New Cuyama, to the headlands of the foothills of the Sierra Madre Mountains on the southwest and west, and is bounded on the northeast by Caliente Range and Cuyama badlands (fig. 2A). The finite-difference model grid used to represent the land surface and subsurface alluvial deposits consists of a series of orthogonal square model cells. Spatial and temporal discretizations are held to uniform increments throughout space and time.

Spatial Discretization and Layering

The total active modeled area is 164 mi² on a finite-difference grid consisting of 135 rows, 300 columns (40,500 cells), and 3 layers having a varying number of active cells per layer, for a total of 15,577 active model cells (figs. 1B, 3A). In the horizontal dimension, about 17 percent of the cells (6,813 cells) are used to define the active part of the hydrologic model grid. The model has a uniform horizontal discretization of 15.4 acres per cell (820.2 ft by 820.2 ft equal to 250 m by 250 m) and is oriented subparallel to the tectonic structure of the Cuyama Valley and to the Cuyama River, 33 degrees west of due north (fig. 1B). This cell size was chosen to be comparable to the typical land parcel size and to facilitate the future linkage of the CUVHM model with remotely sensed land-use data for potential updates of land use and other landscape properties. The bounding coordinates for the total model grid are summarized in table 6.

The model includes three layers that are aligned with the hydrostratigraphic units described previously (Sweetkind and others, 2013). The top of the model is represented by the altitude of the land surface and is a composite of model layers 1, 2, and 3. The uppermost, Recent Alluvial aquifer model layer (layer 1) ranges in thickness from an assumed minimum of 16 ft (5 m) to an estimated maximum of about 633 ft (193 m). The second layer is coincident with the Older Alluvial aquifer system and ranges in thickness from an assumed minimum of 16 ft (5 m) to an estimated maximum of about 1,350 ft (411 m). The third layer is coincident with the extent of the upper portion of the Morales Formation and ranges in thickness from an assumed minimum of 16 ft (5 m) to an estimated maximum of about 4,710 ft (1,436 m).

Temporal Discretization

In order to adequately represent the dynamics of changing precipitation and streamflow, as well as the dynamics of the growing season, including the irrigation supply and demand components, the CUVHM is discretized into monthly stress periods and bimonthly time steps. Periods of user-specified (or BCM simulated) model inflows and outflows and boundary heads are referred to as stress periods. A model stress period is an interval of time in which the user-specified inflows and outflows are held constant. Variations in stresses are simulated by changing inflows and outflows and boundary heads from one stress period to the next. These inflows, outflows and boundary heads that include pumping, precipitation, reference evapotranspiration (ET_h), stream inflows, irrigation, and underflow beneath the Cuyama River are assumed to be constant within each stress period. Stress periods are further divided into bimonthly (approximately 15-day) time steps, which are units of time for which water levels and flows are calculated throughout all model cells. The total simulation period was 61.25 years (or 735 monthly stress periods) from October 1949 through December 2010.

Initial Conditions and Recent Conditions

Initial conditions are the distribution of water levels at every active cell within each of the three model layers estimated for 1947 and assumed to apply to October 1949. Data for 1947–66 drawdowns (fig. 15A) were used because more data were available for 1947 than for 1949, and any water-level changes during those 2 years early in development are assumed to have been negligible. Also, because very little data are available for the late 1940s, water-level data for years 1938–1955 were used to create the 1947 composite water-level contour map. The spring 1966 water-level contour map from Singer and Swarzenski (1970; fig. 15B) was used to help identify spatial trends in water levels on the 1947 map. A map of drawdown between 1947 and 1966 was developed by Singer and Swarzenski (1970). In order to check the accuracy of the 1947 map having more limited data, the contour maps were converted to raster grids, and the spring 1966 water-level and the 1947–66 drawdown raster grids were differenced. A good match was found with the Singer and Swarzenski (1970) water-level change map. In this study, all model layers were simulated as confined yet still represent the drawdown and evolution of the large cones of depression in the water table in the central subregions of the Cuyama Valley. For the parts of model layers that represent areas of the aquifers that are actually unconfined, the saturated thickness is held constant during declining or rising water levels. Though all layers are treated as confined in the model during the simulation, only parts of model layers 2 and 3 actually remain confined while other parts remain unconfined. Storage properties in the outcrop subregions (fig. 3A) of the uppermost layers (1, 2, or 3) are represented by specific yield and are coincident with the unconfined portion of the system (see “Storage Properties” section). The regions of large water-level declines and related large unsaturated zones in the central zones of the valley are illustrated by the water-level maps from summer 1966 (fig. 15B), and from spring and summer of 2010 (fig. 15C, D). The geologic cross sections indicate that, after sustained groundwater-level declines between 1966 and 2008, portions or all of the shallower zones of these aquifers were drained (figs. 3B, C).

Boundary Conditions

Boundary conditions are applied at some model cells to simulate the inflows and outflows from the active model region as groundwater underflow (both inflows and outflows) and aquifer interaction along intermittent streams, as well as interaction with landscape processes (figs. 8 and 16). Two general types of boundary conditions are used in the model: no-flow and general-head. Inflows and outflows simulated across the hydrologic boundaries include recharge to and discharge from the groundwater system as well as interdependent flows between the groundwater, streams, and landscape processes such as ET and irrigation. The intermittent stream-aquifer interaction and landscape process interactions are discussed in later sections.

No-Flow Boundaries

No-flow boundaries were used for the bottom of the model and the lateral boundaries that are coincident with faults. The lower boundary was limited to the bottom of the Morales Formation or a total thickness for the formation of 300 m (980 ft), which is deeper than the deepest supply wells. Lateral no-flow boundaries represent the contact between the low-permeability rocks and thrust faults that bound the foothills and the unconsolidated alluvial sediments of Cuyama Valley (figs. 3A, 16).

General-Head Boundaries

The upstream northern and downstream regions of the Cuyama River are lateral hydrologic boundaries of the groundwater flow system that are simulated as head-dependent flow boundaries (figs. 3A, 16). These regions were simulated by using the General Head Boundary Package (GHB) of MODFLOW (Harbaugh, 2005). General-head boundaries were specified for model cells in layers 1 through 3 for the inflow region with spatially and temporally constant boundary heads and cell-specific hydraulic conductance. The hydraulic conductances of the lateral boundary cells were initially based on the texture-derived hydraulic conductivity of the aquifer sediments (described in the section “Aquifer Characteristics”). Hydraulic conductances were adjusted during model calibration.

Surface-Water Inflows and Outflows

Surface-water inflows and outflows were simulated with a streamflow routing network comprising 708 individual stream segments that represent the Cuyama River and its major and minor tributaries. This network was used to simulate the inflows from 144 major and minor drainages from the surrounding mountains, streamflow infiltration, and occasional outflows along the Cuyama River network (fig. 8). Additional stream inflow also was specified from the discharge of the waste-water treatment plant for the period 1938–2010. These features were simulated by using the Streamflow Routing Package (SFR2) (Prudic and others, 2004; Niswonger and Prudic, 2005); the head-dependent boundary condition used in SFR2 allows for streamflow routing, the capture and conveyance of overland runoff, streamflow infiltration into the aquifer (losing stream reaches), and any potential base flow as groundwater discharge to streams (gaining stream reaches). Runoff estimated by FMP is redirected to the streamflow networks and provides a substantial component of groundwater recharge and streamflow during the wettest months. Each of the major and minor drainages is represented by a collection of stream cells (referred to as reaches). The cells or reaches are combined between tributary points to form a collection of cells or reaches known as a segment. The stage-discharge relations were assumed to be constant for each segment in the SFR stream network. The details on how the

relation is specified are given in the SFR manual (Niswonger and Prudic, 2005). The streambed elevations for the beginning and end of each segment are specified, along with the stream channel width, streambed thickness, and the vertical hydraulic conductivity of reaches within each segment (fig. 8).

In addition to intermittent and ephemeral streamflows, and about 9 springs and groups of seeps historically discharged shallow groundwater in Cuyama Valley prior to the 1970s (Singer and Swarzenski, 1970). Prior to groundwater development, these springs flowed at rates from 0.01 cubic feet per second (ft³/sec) (5 gallons per minute, gpm) to as much as 1.9 ft³/sec (860 gpm) along the outcrop boundaries that are aligned with the Turkey Trap and Graveyard Ridge Faults in the center of the valley along the northwestern segments of the Cuyama River channel (fig. 16). These springs and seeps are no longer flowing since the 1970s.

Groundwater Pumpage

Groundwater pumpage is a major component of the hydrologic budget of Cuyama Valley, and is grouped into two categories of pumpage for this study: agricultural and water supply. Agricultural pumpage includes water withdrawn from all farm wells used to supply water for irrigation, and water supply includes groundwater withdrawn for municipal, domestic/rural residential and industrial uses. Farm wells were simulated as a combination of single-aquifer wells (Schmid and others, 2006a) and multi-aquifer wells. Farm wells that are single-aquifer wells are simulated in a similar manner as used in the WEL Package (Harbaugh and others, 2000), while multi-aquifer wells are simulated by the multi-node well (MNW) Package (Halford and Hanson, 2002). The total pumpage for each WBS (that is, virtual farm) is distributed among each of the farm wells (both single-aquifer wells and multi-aquifer wells) that collectively supply groundwater to that WBS needed for irrigation for each monthly stress period (fig. 2C). The distribution of pumpage between wells is based on the average pumping rate up to the maximum yield of each well (Schmid and others, 2006a). Agricultural pumpage is estimated within FMP of the MF-OWHM model. Pumpage from wells used for municipal and domestic supply is specified on the basis of reported and estimated values. A select number of farm wells and municipal wells are simulated as multi-aquifer (MNW) wells that derive water from up to three aquifer model layers. Because some wells in the valley were not located in the DWR well-permit database, additional “virtual wells” or “other agricultural wells” (fig. 9) were simulated to satisfy simulated delivery of groundwater to selected WBSs. In this report, a virtual well is one for which there is no specific information available for the existing well.

Agricultural Supply

Because pumpage from agricultural wells has never been metered in the Cuyama Valley, those values must be indirectly estimated for simulating and analyzing water use. The two most common methods of indirectly estimating pumpage

are through analysis of data for power consumption by well pumps and data for consumptive use of water. Because many wells are driven by either electric or diesel power sources, and because of the inherent complexity of accounting for additional uses for electricity on a farm by farm basis, the use of electric power records is considered unreliable for estimating agricultural pumpage here. Consumptive-use estimates are also considered unreliable because this method does not account for the combined consumption of precipitation and water applied for irrigation and does not capture the variability in consumption with changing climate. The estimation of agricultural pumpage through application of FMP provides physically-based, dynamic, and linked pumpage estimates as an alternative to these other indirect methods (Hanson and others, 2014b; Schmid and Hanson, 2009).

Pumpage for agricultural supply is estimated as a combination of crop irrigation requirement and inefficient losses required to satisfy the total farm delivery requirement for all wells that deliver water to a particular WBS. Inefficient losses include those from in-farm conveyance of irrigation water, as well as potential losses from runoff and deep percolation below the root zone during irrigation. The crop irrigation requirement in this context refers to all evaporation and transpiration of water by a particular crop within a model cell, and is a part of the total consumptive use. Total consumptive use is the water consumed by evaporation and transpiration from all sources of water. Groundwater pumpage needed to satisfy the total farm delivery requirement can be estimated by taking into account any potential surface-water supply, the efficiency of irrigation, additional effective precipitation, fractions of transpiration and evaporation within each model cell, and the fractions of inefficient losses to runoff and deep percolation. Because all irrigation in Cuyama Valley is supplied by groundwater pumpage, surface-water supplies are not simulated. Unmetered pumpage is estimated through consumptive use by the FMP on the basis of a suite of land-use estimates applied to selected periods of the entire simulation period (table 2). Data from as many as 94 actual farm wells (fig. 9) were used for simulating pumpage for irrigation and the number of active wells for any given month varies through time on the basis of reported drill dates and destruction dates. There is no known reported agricultural pumpage data for Cuyama Valley that can be used as corroborative observations for calibration of simulated pumpage.

Pumpage for each well was allocated to the model layers on the basis of the construction information available. The open-screen interval was used to identify the model layers from which water was withdrawn, with the model assuming full penetration of each layer. If no construction information was available for “real” wells, or virtual wells were needed for irrigation, top and bottom model layer for each well were assigned on the basis of data from other wells in the area. The FMP allocated pumpage on a well-by-well basis, using the average fraction of total required pumpage within a particular WBS up to the pumping capacity of each well’s screened interval that supplies water. The capacity of the farm wells ranges from several hundred to several thousand gallons per

minute, and the casing diameters range from 6 to 16 inches. However, during model calibration pumping capacities were set to a larger value to insure that supply would meet demand. In addition, the deficit irrigation scenario was used with FMP to reduce demand to available supply, and virtual wells were used for farms with simulated demand that did not have a known well a priori.

Water Supply

Pumpage information for municipal and industrial (M and I) uses and for domestic water supply was based on available reported monthly to annual pumpage on a well-by-well basis. As many as 17 wells, including the 2 Cuyama Community Service District (CCSD) production wells, were used to represent M and I wells at various periods during the 61-year simulation. The actual locations of municipal-supply wells were used in the model. The MNW Package is used to simulate municipal-supply groundwater pumpage. The open-screen interval or total depth was used to identify the model layers from which pumping occurred.

For domestic wells, either actual locations were used, or, if the actual locations were unknown for a select land parcel, the parcel was assigned a single virtual well (fig. 9). The well package was used to simulate the domestic pumpage from single aquifer model layers. The number of the domestic wells varies for each stress period. Drilling and destruction dates were used when available, or otherwise, wells were assumed to be present for the entire period of simulation. Total domestic pumpage was estimated to range from about 8 to 37 acre-ft/yr from as many as 95 domestic wells (figs. 9 and 10). Domestic pumpage was estimated on the basis of an assumed consumption rate of 0.25 to 0.94 acre-ft/yr and averaged about 0.54 acre-ft/yr per well (fig. 10). Overall, the combined M and I and domestic pumpage is minor compared to agricultural pumpage, but is important locally. For example, the CCSD wells supplied between 165 and 206 acre-ft/yr for the period 1998 to 2007 (U.S. Wilson, Cuyama Community Service District, written commun., 2008).

Landscape Use and Movement of Water

The FMP provides coupled simulation of the groundwater and surface-water components of the hydrologic cycle for irrigated and non-irrigated areas. A dynamic allocation of groundwater recharge and groundwater pumping is simulated on the basis of residual crop-water demand after surface-water deliveries and root uptake from shallow groundwater. The estimation of irrigation pumpage in FMP is dependent on contributions of water from precipitation and variable irrigation efficiencies and is also connected to irrigation inefficiency losses as return flows (deep percolation and runoff combined). The FMP not only estimates supply and demand, movement, and consumption of agricultural irrigation water, but also estimates these components for natural vegetation and for landscape irrigation in urban areas. Thus, the use of FMP in MF-OWHM represents the simulation of fully coupled flow

of water through surface-water, land-use, and groundwater processes and is also dependent on atmospheric conditions through precipitation and reference evapotranspiration (Schmid and others, 2006b; Schmid and Hanson, 2009; Hanson and others, 2014b). MF-OWHM simulates the demand components representing crop irrigation requirements that are subject to crop and farm-specific inefficiency losses, and the supply components representing precipitation, direct uptake from groundwater, and irrigation from pumped groundwater. Soil moisture is not considered a significant source or storage component of the water budget in well managed, irrigated agriculture. The FMP also simulates additional head-dependent inflows and outflows from the landscape, such as a monthly approximation of surface runoff from precipitation and surface-water return flows to the streamflow network, and groundwater recharge by way of deep percolation of water in excess of actual evapotranspiration (ET_{act}) and runoff (Schmid and others, 2006a, b; Schmid and Hanson, 2009).

Inflows and outflows throughout the WBSs on the landscape are simulated by FMP as mass balances within each WBS and are calculated and balanced for each simulation time step. The following summarizes how FMP accounts for inflows and outflows for each WBS; more details can be found in the FMP and MF-OWHM documentation step (Schmid and others, 2006a, b; Schmid and Hanson, 2009; Hanson and others, 2014). The FMP dynamically integrates irrigation water demand from evapotranspiration with water supply and inefficiency losses. FMP allocates water, simulates processes, and computes the surface-water and groundwater inflows and outflows for each WBS in the active model domain induced by irrigated and non-irrigated agriculture and natural vegetation. On the basis of cell-by-cell estimations for each WBS, the FMP first calculates water demand as the transpiration from plant-water consumption and the related evaporation. The FMP then determines a residual water demand that cannot be satisfied by precipitation and (or) by root uptake from shallow groundwater near the root zone. Next, the FMP equates this residual water demand with the irrigation requirement for the cells with irrigated crops (that is, exclusive of any natural vegetation), which is called the crop irrigation requirement (CIR).

The CIR is then adjusted (increased) by accounting for evaporative losses from irrigation and other inefficiency losses to yield a final total farm delivery requirement (TFDR). For Cuyama Valley, where groundwater is the sole source of water used for irrigation, FMP attempts to satisfy the TFDR using only pumped groundwater. The amount of excess water from irrigation and (or) precipitation that is not effectively used for crop growth or is otherwise “lost” as described above then becomes either overland runoff to nearby streams or groundwater recharge as deep percolation below the root zone. Thus, the FMP dynamically links the demand, supply, and related change in aquifer storage. All of the supply and demand components are then tabulated into WBS landscape budgets that complement the groundwater-flow and streamflow budgets that collectively represent the hydrologic cycle within Cuyama Valley.

In order to estimate the inflows and outflows, the FMP integrates various components of supply and demand data that can be specified over time or held constant for the entire simulation. The FMP requires soil, crop, and climate data to compute consumptive use and the groundwater pumping capacity of all wells that serve a WBS.

The FMP dynamically simulates these supply and demand components for a WBS within MF-OWHM by integrating the following computational components specific to Cuyama Valley's hydrologic setting:

1. TFDR, which is largely dependent on the CIR but also depends on efficiency, changing climate (ET and precipitation), and variable aquifer head.
2. Supplemental groundwater pumpage, which is estimated as the TFDR, but is limited by a specified maximum WBS well-pumping capacity on a well-by-well basis.
3. Net recharge (deep percolation) to groundwater, which is taken to be the sum of excess irrigation and precipitation minus the sum of surface-water runoff and ET from groundwater (Schmid and others, 2006a, p. 20). (Groundwater discharge to streams is accounted for by SFR2).

The MF-OWHM code maintains a mass balance of the landscape for each WBS, for the streamflow network, and for the groundwater-flow system. Flows between these budgets are accommodated by head- and flow-dependent inflows and outflows, such as the actual ET, runoff and infiltration, or transpiration from groundwater. Quantities of interest, such as TFDR, surface-water and groundwater supply, and excess applied irrigation water depend on these head-dependent inflows and outflows.

For the CUVHM, the processes of evaporation, transpiration, runoff, deep percolation to groundwater, and groundwater pumpage were estimated using MF-OWHM. The simulated deliveries and groundwater pumpage reflect climatic differences, differences in agricultural practices among defined WBSs, changes in the water-delivery system, and changes in the distribution of the WBSs that reflect changing land use and water usage during the 1939–2010 simulation period. The CUVHM model provides a detailed transient analysis of changes in groundwater availability in relation to climatic variability, urbanization, land use, WBS, and changes in irrigated agriculture.

Delivery Requirement

The TFDR is determined as the sum of consumptive use of all WBS cells for irrigated crops and inefficient losses of applied irrigation water with respect to plant consumption. In order to calculate the components of the water budget, the FMP also requires estimates of both the irrigation and groundwater components and ET as a whole. Consumption of water by individual crops in each WBS is simulated with steady-state transpiration, varying with changing water level, which is approximated in FMP by an analytical solution. Thus, the amount of evaporation and transpiration from the water

table are both a function of soil type, water-table altitude, the root depth of each crop type, and the user-specified anoxia and wilting point of each crop. As mentioned previously, soil moisture is not accounted for directly other than by a capillary fringe based on soil type. Therefore, the TFDR requires soil, land use (specifically distribution of crop types), and climate data to compute consumptive use on a cell-by-cell basis.

Soils

The CUVHM soils were simplified into four categories—sand, sandy loam, silty clay, and silt—on the basis of data from the Soil Survey Geographic Database (SSURGO; U.S. Department of Agriculture Natural Resources Conservation Service, 2005, 2006; fig. 17). The capillary fringe was also estimated for each soil type, and ranges from 4 to 6 feet thick. These soil attributes are used for the entire simulation period and the cell-by-cell distribution is independent of the crop and WBS. The FMP associates the distributed soil types with the specified capillary fringes and internal coefficients that allow individual analytical solutions for the calculation of ET (Schmid and others, 2006a).

Land Use

The FMP can be used to estimate components of consumptive water use for a wide variety of land-uses, including vegetation in irrigated or non-irrigated agriculture, fallow fields, riparian or natural vegetation, and urban landscape settings. FMP also can be used to simulate an assortment of irrigation settings that span the spectrum from flooded fields such as rice and cotton, to drip irrigation of truck crops, vineyards, and orchards. Applications with zero transpiration, such as artificial recharge systems (including Aquifer Storage and Recovery, or ASR, systems) also can be simulated with FMP (Hanson and others, 2010, 2014a).

For the Cuyama Valley, the land-use attributes are defined on a cell-by-cell basis and include urban and agricultural areas, as well as areas of natural vegetation. The land use that covered the largest fraction of each cell was used as the use representative of that cell. The CUVHM model employs a standardized land-use category system that combines the classification systems for agricultural and native vegetation as well as generalized land uses from historical maps. This system combines the USGS National Land Cover Database (NLCD) (Anderson and others, 1976; Homer and others, 2012), the USDA National Vegetation Classification System (NVCS) (Brohman and Bryant, 2005; Federal Geographic Data Committee, 2008), and the U.S. Forest Service CALVEG (“Classification and Assessment with Landsat of Visible Ecological Groupings”) system (U.S. Department of Agriculture, 2007). The CUVHM has 41 land-use categories that represent 41 agricultural, urban vegetation, native vegetation, general, and non-vegetation land uses. This includes a split in crop attributes for the period prior to 1993 and for 1993–2010. Crops that are represented at various land-use periods include 8 hay and grain crops, 8 vegetable

crops, 10 orchard crops, 4 natural vegetation types, 4 non-vegetation land uses, and 5 generalized land-use categories (table 7). Constructing maps of land use, including crops, is problematic because of the complex pattern that is subject to rapid change in the dynamic environment of modern agriculture. Despite the uncertainty and complexity, land-use maps were developed for 14 different periods during the entire period of simulation. Most of the more recent maps (2007–10) were based on interpreted high-altitude aerial photography that is supplemented with published land-use maps and CropScape images (Mueller and others, 2011; U.S. Department of Agriculture, 2012) and confirmed with the NAIP photo imagery. Land-use changes may occur gradually or rapidly in response to changes in climate, urbanization, zoning, or farming practices. This required making decisions as to how and when to assign land-use changes to the modeled domain. For this simulation, the seven land-use patterns were generally aligned with the wet-dry climate cycle for which they were compiled (table 2, fig. 5).

From 13 to 34 percent of the valley floor is developed land that is not native trees or shrub land (table 7). Most of this land is agricultural land that was further subdivided into agricultural classifications. The agricultural categories were augmented with more general classes for earlier years, when the delineation of land use was less detailed. In general, the class-1 categories represent groups of vegetation that have similar amounts of water consumption and similar growth cycles that drive their consumption of water. Because of the interest by water managers in water use by vegetables and by orchard and field crops, selected varieties that are grown in Cuyama Valley were simulated individually when their distribution was available from the land-use maps. These land-use categories were then defined on the basis of land-use maps and these groups of similar crops are herein referred to as “virtual crops” (table 7, figs. 5, 18–22). For the entire simulation period, these virtual crops were used to drive the use and demand for water for each WBS. Each of the virtual crops was represented by an index number in the FMP (table 7). Many of the virtual crops were amalgamations of the multiple crop types (table 7, grouping of other classes). For example, virtual crops such as “Irrigated Row and Vegetables Crop” or “Field Crops” were amalgamations of other more detailed virtual crops. Because the virtual crop maps for the earlier periods were more generalized, some of the more permanent or more established land cover, such as “native vegetation” and orchard crops, which were mapped more recently, were assumed to be active earlier and were embedded in the earlier land-use maps on the basis of the most recent land-use period (2010). The land-use periods simulated are the multi-year periods of 1949–55, 1955–62, 1962–76, 1976–79, 1980–84; biannually for 1985–86, 1987–88, 1989–90, 1991–92, 1993–94, 1995–96, 1997–98, 1999–2000, 2001–02, 2003–04; and annually from 2005–10 (fig. 5).

Land-Use Maps

For the period 1945–79, land use was based on the Anderson level II classifications (Anderson and others, 1976) for the 1977 land-use map (fig. 18), and stored in the Geographic Information Retrieval and Analysis System (GIRAS) (U.S. Geological Survey, 1990). Data were compiled by geographic quadrangle from the mid-1970s to the early 1980s. The original 1977 land-use map includes 22 vegetation classes that matched 8 of the CUVHM virtual crops (fig. 18). Five of these classes are different types of native vegetation, and six classes represent developed land uses. Because of this generalized classification, the agricultural virtual crop classes were replaced with the virtual crop of identical extent from the 2000 virtual-crop map. For example, where only “cropland” was specified in 1977, the virtual crops interpreted on the 2000 virtual crop map were embedded. This assumes the farmer would be growing the same type of crop in a given area through the period of the hydrologic simulation. For some crops, such as for orchards, this is generally a good assumption; for other crop types, however, the type of crop may have changed several times. Despite the general nature of the map, it shows that approximately 66 percent of the valley was covered by native vegetation, 34 percent was agricultural land and less than 1 percent was urban land use (fig. 18D; table 7). Because earlier land-use maps were not available, land-ownership parcels were used to define the evolution from native vegetation to agricultural land use (fig. 18A–C).

For the period 1980–94, land use was based on the NLCD land-use map (fig. 19A). The NLCD classification, is a 21-class hierarchical, modified, Anderson Land Cover Classification (U.S. Geological Survey, 1999). The NLCD data are derived from images acquired by Landsat’s Thematic Mapper (TM) sensor, and several ancillary data sources. The NLCD is based on imagery acquired throughout the 1980s (U.S. Geological Survey, 1999). It is the first national land-cover dataset produced since the early 1970s, effectively replacing the GIRAS datasets. Despite the availability of more recent datasets, however, many of the land-use categories were more general than those in the original 1977 land-use map. Therefore, the general land-use categories were replaced with the more detailed classifications from the 1977 land-use map (fig. 18A).

For the period 1995 through 2000, land use was assigned on the basis of land-use data for 2000 (fig. 19B), which were obtained in digital format from the California Department of Water Resources (2000). The county land-use survey data were developed by CADWR, through its Division of Planning and Local Assistance, from aerial photography and extensive field surveys. The land uses that were compiled were detailed agricultural uses and less detailed urban and native vegetation land uses. The agricultural classifications can be correlated to the 12 CADWR class-1 categories (California Department of Water Resources, 2000). Such level of spatial detail is ideal for this study, because the crop types are aggregated into classes that have similar water-use characteristics. The

CADWR prepares these detailed county maps of agricultural land use every 6–7 years. Because the virtual-crop map for 2000 represents a composite map of land use from the late 1990s, this type of map also lacks the temporal detail needed to accurately reflect the dynamics of changing agriculture or urbanization. Although the data are suitable for representing regional spatial patterns of land use and crop patterns, there are some discrepancies across county boundaries. The agricultural classes were used instead of the more detailed crops that were identified. The land use was grouped into 14 classes, and the crop that covers the majority of each model cell was identified as the virtual crop for that cell. Upland areas omitted from the CADWR maps were classified as native vegetation. For the period 2001–2002, land-use parcels were used to define the change in agricultural land use (fig. 19C). For all these maps, approximately 65 percent of the valley was covered by native vegetation, 34 percent was agricultural land, and less than 1 percent was urban land (fig. 19; table 7).

For the period of 2004–09, land use was assigned on the basis of the use in 2000 (California Department of Water Resources, 2000; figs. 20, 21). As in prior years, land-use parcels were used to define the change in agricultural land use. The spatial distribution is similar to that in 2000, with only small local changes. Approximately 65 percent of the valley was covered by native vegetation, 34 percent was agricultural land, and less than 1 percent was urban land (figs. 20, 21; table 7).

For 2010, land-use data were obtained in digital format from the CropScape (U.S. Department of Agriculture, 2012; fig. 22). These data were based on parcel maps and show more detailed crop distributions than the CADWR land-use maps (California Department of Water Resources, 2000). These data, however, do not cover the entire valley and were supplemented and modified with the CADWR land-use maps (California Department of Water Resources, 2000) in areas where the data were missing. The spatial distribution of different land use is similar to that of 1997 and 2000, with only small local changes. Approximately 65 percent of the valley was covered by native vegetation, 35 percent was agricultural land, and less than 1 percent was urban land (fig. 22). The actual land use (fig. 22A) and the model discretized land use (fig. 22B) are shown for this most detailed land-use cover to demonstrate the alignment of actual and modeled land use over the active model area. Overall, the changes in total land use include a small decrease in natural vegetation, a small increase in total percentage of agricultural land use, but multiple changes in the types of crops grown on that agricultural land.

Crop-Type Data

The virtual crops provide a basis for estimating the consumptive use of water at the land surface, a key component of the TFDR (Schmid and others, 2006a). The TFDR is largely determined by the consumptive irrigation requirement (CIR). The CIR is determined from the product

of a reference ET (ET_h) and an area-weighted crop coefficient (K_c) on a cell-by-cell basis; these products are summed over all cells within each WBS. Because so many factors affect ET (including weather conditions, soil properties, and plant characteristics), it is difficult to formulate an equation that can produce estimates of ET under different sets of conditions (California Department of Water Resources, 2013). Therefore, the reference crop ET was developed (California Department of Water Resources, 2013). The reference ET from a uniform (evenly mowed) grass surface is commonly denoted as ET_o or ET_h from the CIMIS station 88 (fig. 6B).

Specified root depths, suction pressures for the unsaturated root zone, K_{cs} , and fractions of transpiration and evaporation affect the consumption and movement of water for each crop category (Schmid and Hanson, 2009). For the CUVHM, the root depths and root uptake pressures were held constant for the entire simulation and are based on values from the literature (table 8). Pressure heads for suction pressures in the root zone are a range of negative (unsaturated) pressures for agriculture and native vegetation such as grasses, shrubs, and trees.

Direct transpiration (T) and evaporation (E) from groundwater occur at a rising water table when the top of the capillary fringe above the water table reaches the bottom of the root zone of plants or when the top of the capillary fringe above the water table reaches the land surface, respectively. For changing water tables, the direct T and E from groundwater are eliminated when the top of the capillary fringe above the water table reaches the land surface or when the top of the capillary fringe above the water table falls below the land surface (Schmid and others, 2006a).

Crop water demand, which is the product of the K_c values and a crop stress coefficient, can be related to crop growth stages. The K_c values used in this study were based on an unstressed crop growth curve. This growth curve was divided into twelve monthly stages spanning the initial growth stage, the rapid growth stage, the mid-season stage, the late-season stage, and a period of no planting (fig. 23). Although the specific growth dates for each virtual crop vary depending on the planting date and climatic zone, growth dates are assumed to be spatially uniform throughout the valley. The only change in K_c value at a given location is based on a change in virtual-crop type with land-use changes and with changes in the crop stress coefficient for different wet- and dry-year seasons.

The K_c values were derived from several sources (figs. 23A, B, C, D, E). When available, published K_c values for similar coastal areas were used (Brouwer and others, 1985; Brouwer and Heibloem, 1986; Snyder and others, 1987a, b; Allen and others, 1998). If no published K_c values were available for similar coastal areas, published K_c values for the western San Joaquin Valley compiled by Brush and others (2004), for turf grass (Gibeault and others, 1989), and for various Central coast field and vegetable crops (Snyder and Schullbach, 1992) were used. In many cases, multiple crops were area-weighted to produce a composite virtual K_c value. The K_c values were divided into two periods of agriculture,

representing an early period of more traditional seasonal agriculture in the Cuyama Valley (1949–92) and a more recent period of more intensified agriculture (1993–2010). The transition between these periods of agriculture was placed at the end of the last multi-year drought (1984–92). Finally, the K_c values were multiplied by a crop-stress coefficient (Schmid and Hanson, 2009), the values of which depended on climatic conditions and other factors. The climatic stress on irrigated agriculture can vary by more than 20 percent between wet and dry seasons (Hanson and others, 2010). Eight stress coefficients were used to represent the wet- and dry-year seasons. These stress coefficients were adjusted during model calibration.

Other WBS and crop-related properties that were specified include the fraction of transpiration (F_{tr}), fraction of evaporation from precipitation (F_{ep}), and fraction of evaporation from irrigation (F_{ei}), and the irrigation efficiencies. These fractions (F_{tr} , F_{ep} , and F_{ei}) vary linearly with the respective area occupied by crops and the area open to soil-evaporation (Schmid and others, 2006a). Because the cropped area and the exposed wetted area amount to the entire area, F_{tr} plus F_{ep} equals one. In addition, F_{ei} must be less than or equal to F_{ep} . The F_{tr} is assumed to be independent of whether the transpiratory consumptive use is satisfied by irrigation, precipitation, or groundwater uptake. The fraction of the consumptive use that is transpiratory (F_{tr}) or evaporative (F_{ep} and F_{ei}) depends highly on type of crop and growth stage. When the vegetation cover reaches nearly 100 percent, then $F_{tr} = 1$, with F_{ep} and $F_{ei} = 0$. As a result, the fractions of transpiration and evaporation vary by virtual crop for different months of the year (table 9).

Irrigation efficiency is defined as the fraction of applied water actually consumed. The applied water that is not consumed, as a result of excess irrigation and excess precipitation, becomes losses to runoff and deep percolation (Schmid and others, 2006a). In the CUVHM, the irrigation efficiencies are specified as a matrix of efficiencies for each WBS and each crop for each of the monthly stress periods (Schmid and Hanson, 2009). In this way, the efficiencies differ from crop to crop for different WBSs and can change through time. The range in irrigation efficiency for each crop or crop group is tabulated in table 10. Irrigation efficiencies are assumed to have varied in time, reflecting improvements in irrigation application technologies and changes in the cost and availability of water (Brush and others, 2004). In general, the efficiencies have improved through time with technological advances in irrigation systems, changes in cropping patterns, and better leveling of the fields (California Department of Water Resources, 1994). The increase in efficiency is taken into account during calibration by applying fractional irrigation efficiencies that were estimated to increase through time.

In general, irrigation efficiencies are poorly known (California Department of Water Resources, 1994; and Brush and others, 2004). The CUVHM efficiencies specified in the FMP are typically quite variable, with lower values in wet seasons and in early years with less efficient means of

irrigation and higher values in dry seasons and in more recent years with improved irrigation methods. However, irrigation efficiencies also can vary between seasons, and this variability can differ between wet-year and dry-year periods. Thus, irrigation efficiencies were also scaled on the basis of wet- and dry-year seasons. These scale factors were adjusted during model calibration.

Climate Data

The consumptive use of water, specifically the TFDR, is directly related to the climate. Although several of the properties specified previously take into account yearly or monthly variations, and some have a climatic component, the main climatic contributors to the FMP are precipitation and potential or reference evapotranspiration (ET_h). In constructing the CUVHM, climate data were developed for precipitation and potential evapotranspiration and distributed spatially and temporally for all months and active model cells (Hanson and others, 2012; Flint and Flint, 2012).

Precipitation

Precipitation for the CUVHM is specified through the FMP at the uppermost active cells across the entire active model grid. For each month of the entire period of simulation the total monthly precipitation is specified at an equivalent average daily rate. Gridded regional estimates of precipitation and temperature are obtained at a 800-m spatial resolution from the Parameter-elevation Regression on Independent Slopes Model (PRISM, www.prism.oregonstate.edu) (Daly and others, 2008), transient monthly dataset, downscaled to a 270-m grid resolution (Flint and Flint, 2012). PRISM uses instrumental observations and a digital elevation model, making adjustments for features such as elevation, aspect, slope, and rain shadows. Flint and Flint (2012) downscaled the PRISM precipitation estimates from 800-m to 270-m using a gradient-inverse-distance-squared approach that incorporates northing, easting, and elevation. A monthly precipitation rate was bilinearly interpolated from the 270-meter monthly raster estimates to the center of each 15-acre model cell of the rotated model grid, and varies month to month with the general distribution reflected by the long-term average (fig. 6A).

Portions of the precipitation are simulated as consumption through evaporation and transpiration from the WBS on a cell-by-cell basis. If precipitation in excess of ET occurs, a portion of this precipitation becomes runoff and the remaining portion becomes deep percolation as natural groundwater recharge from precipitation or artificial groundwater recharge from excess irrigation. The portions of runoff from precipitation vary by land-use type specified through the estimation of virtual-crop properties (table 8). Certain types of crops have additional runoff, such as some pistachio orchards on which a plastic mulch is applied. Larger fractions of runoff for irrigation and precipitation were specified for these types of agricultural practices.

Reference Evapotranspiration (ET_h)

Estimates of ET_h can be derived by using either complex parameter-based equations or simpler empirical equations. The main difficulty encountered in the use of parameter-based equations is the lack of accurate or complete data with a sufficient spatial and temporal distribution for the parameters and the general requirement to make estimates on a daily basis. In addition, the detailed climatological data required for the parameter-based equations (such as the Penman-Monteith equation) are not available for many sites in California, especially prior to the operation of the California Irrigation Management Information System (CIMIS) stations started in 1987. For the CUVHM, ET_h was developed on the basis of an hourly energy-balance calculation that is based on solar radiation, air temperature, and the Priestley–Taylor equation (Flint and Childs, 1987) to calculate potential evapotranspiration (ET_h ; Flint and Childs, 1991). Clear-sky ET_h is calculated using a solar radiation model that incorporates seasonal atmospheric transmissivity parameters and site parameters of slope, aspect, and topographic shading (to define the percentage of sky exposing every grid cell) (Flint and Flint, 2007). Hourly ET_h is aggregated to a monthly rate and cloudiness corrections are made using cloudiness data from NREL (National Renewable Energy Lab, 2014). Modeled ET_h for the southwestern United States was then calibrated to the measured ET_h rates from CIMIS and Arizona Meteorological Network (AZMET) stations (Flint and Flint, 2007).

One CIMIS station has been operated in Cuyama Valley since 1989 (Cuyama Station No. 88; fig. 6B). The Cuyama Valley station has an average annual ET_h of 60.8 inches. The comparison with simulated potential ET (ET_h) is shown for CIMIS Station No. 88 (fig. 12). Simulated ET_h has an average annual value of 60.0 inches and underestimates measured ET_h for all months, with a standard error of the regression of 0.37 inches/month for the entire year. Monthly differences between measured ET_h and simulated ET_h range from 2 percent to 14 percent, with the highest differences in the summer months (table 11). When forced through zero, the regression equation has a slope of 1.1097, indicating an underestimation of the evapotranspiration in general relative to the CIMIS data.

Groundwater Agricultural Supply

The groundwater supplied to each WBS is simulated by a series of single-model-layer “farm wells” or through multi-aquifer wells simulated with the MNW1 Package (Halford and Hanson, 2002). The multi-aquifer farm wells that are simulated by MNW1 were reduced to a single priority well in each cell when more than one multi-aquifer well occurred in same cell. The priority for the multi-aquifer farm wells was given to wells with more than 10 percent screened interval in more than one layer, largest capacity, and longest history of potential pumpage. All remaining wells were simulated as

single-aquifer farm wells through the farms-wells feature in the FMP. In addition, any multi-aquifer farm wells that did not include more than about 10 percent of the second model-layer thickness were also treated as single-aquifer farm wells. This resulted in as many as 103 single-aquifer farm wells and 29 multi-aquifer farms wells.

Agricultural groundwater pumpage requirements are estimated by the FMP after water supplied by precipitation is subtracted from the total actual ET on a cell-by-cell basis. The remainder of the water needed for agricultural land-use is the crop irrigation requirement that is summed on a cell-by-cell basis within each WBS as the TFDR which is the CIR combined with other potential losses from inefficient irrigation. The TFDR that is required from groundwater pumpage is estimated from this sole-source aquifer. This allows a way to simulate an estimate of historical unmetered pumpage for the period 1949–2010.

Net Recharge

The net recharge in a WBS is defined as losses after consumption due to excess irrigation and excess precipitation, reduced by losses to surface-water runoff and ET from groundwater (Schmid and others, 2006a). The fraction of losses to surface-water runoff depends on whether the runoff is related to irrigation or to precipitation. Losses based on irrigation depend on different irrigation methods, which, in turn, depend on the virtual crop type and related fractions of runoff from precipitation and irrigation (table 8) as well as other factors such as soil type and irrigation efficiency. The ET from groundwater is subtracted from the potential net downward flux to the uppermost aquifer. Hence, net recharge to groundwater can be affected by both user-specified and head-dependent parameters. This definition of net recharge requires the following assumptions: deep percolation below the active root zone is equal to groundwater recharge, ET from groundwater equals an instantaneous outflow from aquifer storage within any time step, and the net change in soil moisture storage for well managed (irrigated) agricultural areas for periods of weeks to months is negligible (Schmid and others, 2006a). The net recharge to the aquifers is applied to each uppermost active model cell in each WBS.

Aquifer Characteristics

The unconsolidated alluvial deposits and the Morales Formation form a three-layered aquifer system within the regional aquifer system defined by the three hydrogeologic units in the Cuyama Valley. Each aquifer can be characterized by variations in hydraulic properties, which are based on the textural distribution of coarse and fine-grained sediments and zones representing subregions in which the sediments accumulated in particular depositional environments. The hydraulic properties represent the ability for the aquifer to transmit water and to store or release water and are functions

of depositional environment and lithology. Variations in depositional environments and lithology cause differences in grain size, grain shape, grain orientation, and the degree of sorting. This causes considerable spatial variation in the hydraulic properties of the deposits. Thus, variable lithology and depositional environments determine spatial variation in the hydraulic properties of the deposits. The hydraulic water-transmitting properties of the aquifer sediments are represented by horizontal (K_h) and vertical (K_v) hydraulic conductivity and hydraulic storage properties of the hydrogeologic units that constitute the aquifer system are represented by hydraulic conductivity and the storativity, respectively. The relation between hydrogeologic units in the aquifer system, lithology, and hydraulic properties has been developed in many previous studies that include both the properties of the aquifers and those of any fine-grained interbeds or confining units (Hanson and others, 1990, 2003, 2004, 2014a, b; Laudon and Belitz, 1991; Phillips and Belitz, 1991; Hanson and Benedict, 1993; Leighton and others, 1994; Fio and Leighton, 1995; Belitz and Phillips, 1995; Burow and others, 2004, Phillips and others, 2007; and Faunt and others, 2009a, b).

Textural Analysis

Lateral and vertical variations in sediment texture affect the direction and rate of groundwater flow as well as the magnitude and distribution of aquifer-system storativity. The textural distribution was used to define the vertical and lateral hydraulic conductivity and storage property distributions for the hydrologic model (Sweetkind and others, 2013). As in many of the previous studies identified above, the textural distribution was based on drillers' and geophysical logs. The primary variable selected for the textural analysis was the percentage of coarse-grained sediment, with the complement being the percentage of fine-grained sediment.

Based on the distribution of texture in the Cuyama Valley and the reanalysis of the hydrogeology (Sweetkind and others, 2013) the groundwater system was split into three aquifers. Within each hydrogeologic model layer, the fraction of coarse- and fine-grained sediments within the thickness of each layer was estimated on a cell-by-cell basis. Texture was estimated at the model-cell centers of the model grid for each of the model layers that are coincident with the hydrogeologic units. The fraction of coarse- and fine-grained sediments within the thickness of each layer was estimated on a cell-by-cell basis.

Hydraulic Properties

Estimates of textural-based hydraulic properties were segregated into three hydrogeologic units that were delineated on the basis of the distribution of sediment texture derived from drillers' logs, geologic logs, and geophysical logs. The hydraulic properties of an aquifer are its transmission and storage properties. The transmission properties of the Cuyama

Valley aquifer are represented by the hydraulic conductivity (K) in this study. Equivalent horizontal and vertical hydraulic conductivities are assumed to be correlated to sediment texture (the fraction of coarse-grained and fine-grained sediment). The method uses the estimated binary sediment texture for each model cell and horizontal and vertical hydraulic conductivity estimates for each textural end member.

Faunt and others (2009a) identify the power mean as useful for defining hydraulic conductivity values. In addition, their work also includes a review of the literature that describes the use of power mean for estimating hydraulic conductivity. A power mean is a mean of the following form:

$$M^p(x) = \left(\frac{1}{n} \sum_{k=1}^n x_k^p \right)^{1/p} \quad (1)$$

where

- p is the averaging power-mean exponent,
- n is the number of elements being averaged, and
- X_k is the k^{th} element in the list.

The horizontal hydraulic conductivity ($K_{h,i}$) was calculated as the weighted arithmetic mean (also equivalent to the power mean to the zero power) of the hydraulic conductivities of the coarse-grained (K_c) and fine-grained (K_f) lithologic end members and the distribution of sediment texture for each (i^{th}) model cell:

$$K_{h,i} = [K_c F_{c,i} + K_f F_{f,i}] \quad (2)$$

where

- $F_{c,i}$ is the fraction of coarse-grained sediment in a cell, estimated from sediment texture data, as described in the previous section, and
- $F_{f,i}$ is the fraction of fine-grained sediment in a cell ($1 - F_{c,i}$).

Because K_f is much smaller than K_c , the arithmetic mean heavily weights the coarse-grained end member for horizontal hydraulic conductivity.

Vertical hydraulic conductivity between model layers ($K_{v,k+1/2}$) was calculated as the p^{th} weighted power mean of the hydraulic conductivities of the coarse- and fine-grained lithologic end members, and k is the model-layer number (Faunt and others, 2009b):

$$K_{v,k+1/2} = \left[F_{c,k+1/2} K_c^p + F_{f,k+1/2} K_f^p \right]^{1/p} \quad (3)$$

where

- $F_{c,k+1/2}$ is the fraction of coarse-grained sediment between layer midpoints, and
- $F_{f,k+1/2}$ is the fraction of fine-grained sediment between layer midpoints of k^{th} element in the list.

The harmonic mean is a weighted power mean with the exponent $p = -1.0$ in eqn. 3 and results in increased vertical anisotropy. The geometric mean is a weighted power mean with $p = 0.0$ in eqn. 3 and results in decreased vertical anisotropy. Phillips and Belitz (1991) determined that vertical conductivities could be calculated using either weighted harmonic or weighted geometric means. Belitz and others (1993) represented the vertical conductivities with the weighted harmonic mean. The vertical conductivities can be represented as power means in which p varied between -1.0 (the harmonic mean) and 0.0 (the geometric mean) (Faunt and others, 2009b; Hanson and others, 2014a). The relation between hydraulic conductivity and percentage of coarse-grained deposits based on hydraulic conductivity end members and exponent of the power mean is nonlinear. The resulting value is a function of the power mean and as a result is sensitive to the power used (averaging method). Both the harmonic and geometric means weight the fine-grained end members more heavily, and as a result, the vertical hydraulic conductivities are much lower than the horizontal. Dimitrakopoulos and Desbarats (1993) determined that the value of p depended to some extent on the size and thickness of the grid blocks used to discretize the model domain; smaller grid cells resulted in smaller values of p . The exponent p was specified for each model layer and adjusted during model calibration. The resulting K_f values of the exponent, p were -0.9 for the Recent Alluvium aquifer (layer 1), -0.5 for the Older Alluvium aquifer (layer 2), and -0.7 for the Morales Formation aquifer (layer 3).

Data from aquifer tests in the Cuyama Valley that generally represent short-term pump tests that were compiled and used to provide selected transmissivity and hydraulic conductivity values (Everett and others, 2013; fig 24A). The estimated hydraulic conductivity values from these tests ranged from 0.3 to 39 feet per day (ft/d) from an estimated transmissivity derived from Jacob's method (Jacob, 1946). Additional estimates of hydraulic conductivity for the three aquifers include slug tests from the three multiple-well monitoring sites and range between 1.6 and 28 ft/d (Everett and others, 2011, 2013). These estimates were used as additional observations during model calibration to constrain the hydraulic conductivity of the model layers in select regions (table 12).

Hydraulic Conductivity of Lithologic End Members

Parameter estimation, in combination with the texture model developed for the region on the basis of the known stratigraphic units and kriged subsurface texture based on reported lithology, was used to estimate K_c and K_f , the end-member hydraulic conductivities (Sweetkind and others, 2013). These end members were used to estimate the horizontal and vertical K for each cell in the model, which are then related to zonal subareas (table 13; figs. 24B–D) that are used to estimate final values derived from model calibration. The Layer Property Flow Package (LPF) is used to simulate the hydraulic properties and groundwater flow

process for the application of MF-OWHM to Cuyama Valley's aquifer systems. The final parameters from model calibration representing hydraulic properties and related scale factors are included in the summary of parameter values in table 14 discussed in the section "Model Calibration."

The hydrostratigraphic layers of the aquifer system in Cuyama Valley formed in somewhat different depositional environments and have textural compositions that affect the end-member K values. In the model, each of these layers was further subdivided into subareas that helped facilitate model calibration and better represent subareas that are different depositional environments (table 12; fig. 24). These also were used to define the subareas distribution of vertical hydraulic conductivity (fig. 24). In subareas where the Older Alluvium (layer 2) was estimated to be missing between the Recent Alluvium and Morales Formation, the hydraulic properties are represented by assumed values that allow communication between the Recent Alluvium and the Morales Formation model layers.

Because the hydraulic properties differ for each of the hydrostratigraphic units, they were estimated separately. The parameters used to control these subareas within each model layer represent unconfined aquifers in the outcrop areas as well as subareas of confined aquifers where the Older Alluvium or Morales Formation underlie the other aquifers. In addition, the subareas where the Older Alluvium aquifer is missing is also treated separately and represent subareas where the hydraulic properties allow the surrounding units to communicate. Therefore, the hydraulic properties of each of these subareas were estimated with separate model parameters during model calibration (table 13). The estimated values of K_f range from 3.9×10^{-03} ft/d for the alluvial aquifer layer to 2.9×10^{-03} ft/d for the Morales Formation; K_c range from 20.3 ft/d for the alluvial aquifers to 0.8 ft/d for the sediments of the Morales Formation layer. For each unit, the distributions of horizontal and vertical K 's vary with the distribution of sediment texture within each zone of each layer (figs. 4, 24). During calibration, a multiplier was used for each zone, and the final range in vertical and horizontal hydraulic conductivities was calculated based on this formulation (fig. 24; tables 12, 13, 14).

Unlike previous analysis of the valley in which the hydraulic conductivity was not differentiated for the various aquifers, the recent and Older Alluvium were delineated as separate units with separate estimates and zonation of the coarse- and fine-grained end-member values of the hydraulic conductivity. Hydraulic conductivities generally decrease with depth and with increasing distances from the original source of the sediments (eroded and (or) transported from the adjacent mountain ranges and river channels), which is consistent with the fining down and fining toward the center sequences observed in the aquifer sediments and textural model (Sweetkind and others, 2013). In several subregions, however, smaller values of hydraulic conductivity have been estimated at depth because of fine-grained textures and secondary alteration such as cementation (Everett and other, 2013; Sweetkind and others, 2013). Coarser grained sediments

were simulated near stream channels in the alluvium in the outcrop parts of all three layers. The hydraulic property zones used in CUVHM also were aligned with the textural zones and with the internal fault boundaries.

Storage Properties

The hydraulic properties used to simulate the changes in storage of water within the saturated parts of the aquifer system consist of three components (Hanson, 1988):

1. Specific yield.
2. Elastic specific storage.
3. Inelastic specific storage.

The first two components, specific yield and the elastic specific storage, represent and govern the reversible uptake and release of water to and from storage. Specific yield is unconfined storage and represents gravity-driven draining or filling (resaturation) of sediments with changes of the water table. The elastic storage coefficient represents the component of confined storage because of the compressibility of water and the reversible compressibility of the matrix or the skeletal framework of the aquifer system (Jacob, 1940; Hanson, 1988). The inelastic storage coefficient governs the irreversible release of water from the inelastic compaction of the fine-grained deposits or permanent reduction of pore space, which can also lead to land subsidence. Changes in inelastic storage in fine-grained beds is beginning to occur. Because this is potentially a significant source of water, as a result of the relatively large water-level declines in the Main-zone subregions in the Cuyama Valley, the estimation of water derived from inelastic compaction was included as a feature in this hydrologic model. Given the fine-grained nature of parts of the three aquifers in the Cuyama Valley, the elastic components of storage for the coarse and fine-grained sediments were simulated separately with the Subsidence Package (SUB) in MF-OWHM. Thus, separate values of elastic storage for coarse and fine-grained sediments were used to simulate elastic specific storage for the aquifers and fine-grained interbeds that were applied to all layers. Specific yield typically is orders of magnitude larger than specific storage and is volumetrically the dominant storage parameter for the outcrop regions of all three aquifers.

The Layer Property Flow Package (LPF) and SUB were collectively used to define storage properties in each of the aquifers represented in the model. The LPF and multiplier (MULT) Packages were used to calculate and specify the aquifer-storage components, which included the compressibility of water for all model layers and the specific yield for the portions of the uppermost active layers (layers 1, 2, 3; fig. 3A). The SUB Package was used to specify the specific storage related to the skeletal elastic compressibility of the coarse and fine-grained portions of the aquifers and the inelastic compressibility of the fine-grained portions of the aquifers. The resulting equation for the composite storage is represented (Hanson and others, 2014) as follows:

$$S^* = S + S' + S_y \quad (4)$$

where

- S^* is the total storage of the aquifer layer,
- S is the elastic storage of the coarse-grained component,
- S' is the elastic and inelastic storage of the fine-grained component, and
- S_y is the specific yield from the water table drainage for the unconfined portions of an aquifer.

Both S and S' can be further represented by its respective components:

$$S = b * S_s = \rho g (\alpha + n\beta) * b \quad (5)$$

where

- ρg is the weight of water,
- α is the compressibility of the coarse- or fine-grained matrix material,
- n is the total porosity of the coarse- or fine-grained material,
- b is the fractional thickness of the total model-layer thickness of the coarse- or fine-grained material, and
- β is the compressibility of water.

The aquifer-system specific storage for each model layer on a cell-by-cell basis can be further subdivided into its components for coarse- and fine-grained material, resulting in a complete equation of storage based on textural fractions of total porosity and the matrix compressibility:

$$S_s = S_{sFc} + S_{sFf} = \rho g [(\alpha_{Fc} + n_{Fc}\beta) * F_{cI} + (\alpha_{Ff} + n_{Ff}\beta) * F_{fI}] \quad (6)$$

where

- total porosity, $n_T = n_{Fc} + n_{Ff}$, is the sum of the coarse and fine-grained fractions of porosity, with $n_{Fc} = n_{Fc} \times F_{cI}$ and $n_{Ff} = n_{Ff} \times F_{fI}$
- α_{Fc} and α_{Ff} are the compressibility of the coarse or fine-grained matrix material, respectively;
- F_{cI} is the fraction of coarse-grained sediment in cell (I,J); and
- F_{fI} is the fraction of fine-grained sediment in the i^{th} model cell $(1 - F_{cI})$.

Although all model layers are simulated as convertible from confined to unconfined, portions of uppermost active model layer represent unconfined conditions, and are therefore assigned a specific yield. Specific yield, which is a function of sediment porosity and moisture-retention characteristics, cannot exceed sediment porosity. The zones used to specify the subareas of the storage properties are similar to the layers used for the other hydraulic properties (tables 13, 14; fig. 24) except for the unconfined subareas of the uppermost layers.

The compressibility of water as well as the compressibility of the aquifer skeleton is dependent on the specified porosities for the coarse- and fine-grained fractions of each hydrostratigraphic unit (model layer). The estimated total porosities from selected core samples from alluvial sediments in nearby Santa Clara Valley ranged from 23 to 43 percent, and the effective porosity ranged from 22 to 40 percent on the basis of laboratory tests of selected cores (Newhouse and others, 2004). For this model, porosity values range from 20 percent for the coarse-grained sediments of the Recent Alluvium to 29 percent for fine-grained sediments within the Morales Formation aquifer sediments (table 14). The products of these average porosity and the respective cell-by-cell average coarse- and fine-grained fractional aggregate thicknesses are summed and multiplied by the compressibility of water ($1.4 \times 10^{-6} \text{ ft}^{-1}$) to yield one part of the composite aquifer specific storage value for each active cell of every layer.

Specific yield was specified for all active cells of each layer where those model cells represent the uppermost model cell and unconfined conditions. Specific yield was calculated by using a linear relationship between the fraction of coarse grained deposits, between 0 and 1, and an upper maximum estimated specific yield value ranging from 0.14 for the alluvial to 0.25 for the Morales Formation (table 14). During calibration, a multiplier was used for each zone and to determine the final range in specific yield (fig. 24; tables 12, 13, 14).

Hydrogeologic Structures

The subregions of the Main zone are bounded by faults. The faults along the edges of these zones delineate the no-flow boundaries of the active flow region. The Morales, Graveyard, Turkey Track, Santa Barbara Canyon, and Rehoboth Faults subdivide and compartmentalize the Main-zone subregions from the bounding subregions of the Sierra Madre Foothills and Ventucopa zones (Sweetkind and others, 2013; fig. 2A). These interior faults separate the Cuyama Valley into a set of subregions that respond differently to climate and water-resource development. The Horizontal Flow Barrier Package (Hsieh and Freckelton, 1993) was used to simulate resistance to flow across these structures. The effectiveness of these faults as partial flow barriers was then estimated by a parameter representing the conductance of the vertical model cell faces aligned with the fault trace (table 14). All faults were essentially barriers to groundwater flow, although some leakage occurs across the Rehoboth Fault (fig. 3A).

Initial Conditions

For transient models, initial conditions define the system state at the beginning of the simulation. There is a long history of groundwater development and irrigation in the study area. Despite the fact that the system has been under stress since the 1940s, historical water levels and other data sufficient

for estimating stresses are not available until about the 1960s (figs. 25, 26). The combined effects of groundwater pumping for irrigation and water supply have greatly depressed the groundwater levels in the Main zone. The pumpage has also increased the vertical head differences in some parts of the Main zone; however, the vertical head difference remains small in other regions, such as Ventucopa. In addition, head differences vary seasonally, ranging from about 40 ft in a downward gradient direction during the pumping season to about 8 ft of upward gradient during the nonpumping winter months at the multiple-well monitoring site (CVKR) in the Main-zone subregions. There are almost no head differences less than 5 ft away from the main regions of pumping (CVFR; fig. 26A; Everett and others, 2011, 2013). While the effects of climate variability may preclude the occurrence of true steady-state conditions for this hydrologic system, prior to development that started in the 1940s the basin was virtually full and in a quasi-steady-state condition, responding to changes driven by the natural cycles of climate variability. Initially, groundwater levels may have been shallow in many parts of the basin, as evidenced by the presence of cottonwood riparian areas along some reaches of the Cuyama River and the discharge of springs along the Graveyard and Turkey Track Faults that separate the Main zone subregions near the Cuyama River (fig. 2A). As a result of these subsurface conditions combined with the exceptionally wet climatic conditions for the initial years (1939–45), which reflect regional climate variability in the years prior to the simulation, the initial conditions used in the model do not represent steady-state conditions but rather estimates of hydrologic conditions in 1949. These initial conditions were derived from a combination of land-surface data and model-derived initial water levels. The groundwater flow simulation starts in October 1949, for which there are no data to map the undifferentiated groundwater levels throughout the regional aquifer system. Thus, initial heads were further refined by periodically using the simulated heads from the end of the first year (October 1950) of simulation as initial heads during calibration. This substitution was made in concert with scaling parameters of the overall elevation of initial water levels that helped refine the initial heads for all three model layers during parameter estimation.

The range in water levels over which elastic and inelastic compaction occur is controlled by the previous maximum stresses imposed on the aquifer system from the history of geologic loading and water-level declines (Terzaghi and Peck, 1948; Riley, 1969), as well as secondary effects such as cementation. The previous maximum stress can be expressed as a critical head—the previous minimum head—so that head changes in the stress range above the critical head (elastic stress range) that result in elastic deformation (reversible compaction and expansion) of the aquifer system, and head declines in the stress range below the critical head (inelastic stress range) result in inelastic compaction (largely irreversible) of the system. A head decline below the previous critical head establishes a new critical head so that any

subsequent head increase results in elastic expansion of the aquifer system. The specification of the critical heads that control the transition from elastic to inelastic compaction within the fine-grained deposits of the aquifers is initially unknown for each aquifer. This threshold in pressure can typically vary from 50 to more than 200 feet below predevelopment water levels for alluvial basins and usually represents sediments that are overconsolidated because of geologic and hydrologic stresses and secondary lithification (Holzer, 1981; Hanson and others, 1990, 2003; Hanson and Benedict, 1993). Because these are initially unknown, the critical heads were specified as a constant depth below land surface and were modified during model calibration with respect to recent land subsidence observations.

When the simulation is started, the simulated heads and flows change in response to the initially specified and ongoing inflows and outflows. Because the irrigation and pumping stresses on the system change rapidly, the inconsistencies between the initially specified conditions and the simulated initial processes and properties generally are not problematic because the next stress regime soon dominates the solution (Hill and Tiedeman, 2007). As a result, comparing observed and simulated values becomes meaningful after a relatively short simulation time. This study and previous studies (Belitz and Phillips, 1995; Faunt and others, 2009a) show that the time frame for the stabilization is typically less than several months to years of the simulation.

Model Calibration and Sensitivity

The CUHM was calibrated through a combination of trial-and-error and an automated process of minimizing differences between “real-world” observations and model output. The hydrologic framework and definitions of water balance zones were modified as part of this process. Simulation with the CUVHM requires specification of several hundred parameters that vary spatially and temporally, making it a challenge to develop an optimized set of calibrated parameter values. As a result, a parameterization procedure was employed to allow a limited number of parameter values to control the temporal and spatial variability of a much larger number of model inputs. The parameterization procedure followed that of Hill and Tiedeman (2007) in defining the term “parameters” to mean model inputs of hydraulic and hydrologic properties but also included landscape and crop-related properties from FMP and fractions of BCM-simulated surface inflow from runoff and recharge of surrounding watersheds. As mentioned earlier, all inflow to the model domain is combined in the SFR2 inflows. Calibration consisted of a systematic application of the parameter estimation method to limit the range of possible solutions.

Even though some parameters demonstrated significant correlations, those parameters selected for model calibration were assumed to be independent. Parameter estimation software packages (UCODE, Poeter and others, 2005; PEST, Doherty, 2010a, b, c; Doherty and Hunt, 2010) were used directly for all sensitivity analyses and parameter estimation. Initially, UCODE was used to estimate parameters. In order to use some of the extended capabilities in PEST, a combination of PEST and manual adjustments were used to conduct the final parameter estimation and sensitivity analyses.

Calibration of transient-state conditions was dependent on the components of the use and movement of water across the landscape and their interplay with the streamflow network and groundwater flow system. Calibration started with adjustments of all parameters from the landscape, such as fractions of transpiration, irrigation efficiencies, stress factors for K_c s, and fractions of runoff, as well as aquifer properties, including fault conductances across fault planes or zones. Then, adjustments were made to other factors related to movement of water on the land surface, such as the hydraulic conductivity of the streambeds in the upstream portions of the streamflow network, and the recharge areas of the groundwater flow system. The calibration of the groundwater flow simulations involved adjustment of parameters that control the inflows and outflows to the groundwater flow system. The dominant sources of inflow to the groundwater system are streamflow infiltration and recharge from landscape processes. Therefore, parameters controlling inflow included vertical hydraulic conductivity of the streambed and runoff parameters. Parameters controlling outflow include pumpage and evapotranspiration. Some of the water-budget components are specified values of inflows and outflows that were not adjusted during calibration; these include the runoff component from the BCM model of stream inflows, urban and domestic pumpage, monthly precipitation and reference evapotranspiration, and water-balance area and crop properties (table 14). The remaining water-budget components that are calculated by the model include streamflow gains/losses, outflow through the stream network, actual evaporation and transpiration, groundwater pumpage from agricultural uses, runoff from irrigation and from precipitation, farm-net recharge, wellbore flow through MNW wells, and changes in groundwater storage. The implementation of the multi-node well package maintained the net pumpage but redistributed groundwater flow vertically and related vertical head differences between model layers, by intra-wellbore flow. This wellbore flow occurs not only during periods of pumpage and for undestroyed and unused wells but also in wells that are only used periodically for water supply or during the irrigation season. A total of 200 parameters were initially created to facilitate model calibration, but this number was reduced to 65 parameters after initial global sensitivity and calibration analysis (table 14).

Observations Used In Model Calibration

The ability of the transient hydrologic flow model to simulate the hydrologic system was evaluated on the basis of comparisons with select hydrologic observations, hydrologic time series, and groundwater-level maps. These comparisons were used to assess the capacity of the model to predict the effects of changing inflows and outflows on the hydrologic system, based on reasonable estimates of hydraulic, river, and landscape properties used to estimate pumpage, recharge, and changes in groundwater storage. Model calibration was based primarily on comparisons of spatially and temporally distributed groundwater and subsidence components. Simulated changes in water levels and water-level differences were compared to those measured in long-term, long-screened supply wells used as part of the new valley-wide monitoring network and from recent depth-specific multiple-well monitoring sites (Everett and others, 2013). Recent land subsidence observations from GPS and InSAR satellite images (Everett and others, 2013) were also used for calibration. Some limited estimates of hydraulic properties from aquifer tests and slug tests were also used (Everett and others, 2013) to help constrain parameters adjusted during calibration. Calibration adjustments were based on the combined fit of simulated values to these observations (figs. 26 and 27). The simulated values were compared to all observed values and provided a measure of model performance through various historical time intervals and subregions of the valley. The resulting error distributions constrain the model parameters, and the comparison between simulated and observed values provided a basis for sensitivity analysis of selected parameters. In addition, groundwater-level maps were used for qualitative comparisons. However, these maps were considered less reliable than time-series data because the composite water-level measurements and manually drawn contour lines represent averaged conditions. In many areas there are vertical-head differences within some parts of the aquifer systems. These differences are not well represented by composite water-level measurements and the manual contour lines. An overall estimate of model fit was made using all available groundwater level data.

Although the CUVHM was calibrated to available observations, model uncertainty exists because of the large number of variables that were adjusted as part of the calibration procedure. In addition, limitations are inherent in the necessary simplifications and assumptions needed to represent a complex hydrologic system with a numerical model. These uncertainties and model limitations are discussed later in this report in the section “Model Uncertainty, Limitations, and Potential Improvements.”

Groundwater Observations

The largest set of observed values used for calibration consisted of the groundwater levels and changes in groundwater levels over time. SBDPWWA maintains a database of key wells in the Cuyama Valley that are regularly measured as part of their monitoring network for their annual summary of the valley. These data were combined to form a database of available water levels throughout the Cuyama Valley from 1949 to 2010. About 4,465 water-level measurements (herein referred to as observations) from 258 single and multiple-aquifer wells and the recently installed multi-well monitoring sites were used for model calibration (fig. 25). Despite the number of wells, the lack of wells in southern and southeastern part of the basin means that the model calibration has greater uncertainty in these areas. The well data included 258 initial head observations and 4,207 drawdown observations. Hydrographs for 36 observation wells were developed and used to represent the Main-zone, Ventucopa Upland, and Sierra Madre Foothills subregions of the Cuyama Valley (fig. 26).

In order to represent the overall trends in heads throughout the region and to minimize the potential effects of initial conditions, a set of observations were made for each well based on the overall change in head relative to the first observation for the time span of measurements from each well. In addition to changes in water levels, 45 water-level differences were estimated between 17 pairs of observation wells completed in vertically adjacent aquifers (fig. 25). These observations were used to help with the calibration of vertical hydraulic conductivity and distribution of pumpage during parameter estimation.

Hydrographs that show both simulated and measured heads for select wells help to illustrate the match of water levels throughout the upper and lower parts of the system (fig. 26). The minimum period over which model simulations can accurately reproduce fluctuations in the groundwater flow system (the response time of the model) varies with the depth to water, hydrologic setting, hydraulic properties, climate, and land use. The amplitude of monthly fluctuations in simulated heads are generally less than fluctuations in measured heads, are smallest at the water table, and increase with depth below the land surface, because of the varying pumping rates during monthly stress periods, applications of irrigation water, transition between unconfined and confined conditions, and depth of unsaturated zone.

The overall model fit for water-level comparisons is generally good when the simulated head values are compared with the measured water levels over the combined 1,200 ft range of measured levels. About 37 percent of the residuals were between -20 and $+20$ ft, and 49 percent were between -30 and $+30$ ft. (fig. 27A). Simulated water levels generally match measured water levels, as indicated by an average

residual of 15.6 ft and a sum of squared weighted residual (SOSWR) of 1.02 ft; the residuals ranged from -198 to 371 ft and the standard deviation was 52 ft. The residuals calculated from results of the CUVHM simulations are generally within 30 ft of the measured values, which represents about 2.5 percent of the total elevation range of the aquifers. The simulated water levels tend to underestimate water levels (positive residuals), which is considered a conservative bias. The total change in measured water levels in wells ranged from -345 ft (rise) to 142 ft (decline) and the total simulated change in water levels at these well locations range from -475 to 136 feet. The larger range in observed changes may reflect some values that are instantaneous water-levels affected by nearby pumping. The crossplot of simulated versus measured water levels (herein referred to as correlation diagrams) also indicate a generally good fit across the wide range of altitudes in the valley (fig. 27B). Most of the outliers are a result of underestimation of measured water-level changes in the southern Ventucopa subregion, where large interannual fluctuations in wells near the Cuyama River are related to climate cycles. Overall, the time series of simulated and measured water levels across the valley indicates the model is fairly accurate in the Main-zone and Ventucopa subregions, but does not replicate the elevated water levels of wells in parts of the Sierra Madre Foothill subregions (fig. 26C). The water levels fit better in recent times (the last 10 years of the simulation, 2000–10), when the land use and related crop information is better defined.

The hydrographs for the Main-zone subregions generally indicate a reasonable fit of rates of water-level decline, and in some regions show similar water-level altitudes. For example, in the northern Main zone, water levels match for the early years but are underestimated for some wells in the more recent decades, which could reflect incomplete land-use data for the 1980s through 2010. Similarly, for the Western Main-zone subregion, the rates of decline are similar to those in historical records but some of the temporal changes are missing, which also could be a function of incomplete land-use data. In the Southern Main-zone subregion, the simulated rates of decline show variable matches with observed rates and may overestimate some declines for select subregions, which also could be a result of incomplete land-use data. The hydrographs in the Ventucopa subregions are similar to those constructed from historical records but do not capture the interannual fluctuations for some of the wells near the Cuyama River. This could be a function of the delay in runoff from surrounding watersheds as has been observed in similar settings, such as the Santa Clara–Calleguas basin, where there is multi-year recession of wet-year baseflow (Hanson and others, 2003). Although the simulated trend is similar to that of the historical record for most wells, some of the annual fluctuations were not captured by the simulated water levels. This again is probably a function of incomplete land-use data used to drive

the demand for irrigation and related groundwater pumpage. The hydrographs in the Sierra Madre Foothills are more variable, matching trends in parts of the northern and central subregions for some wells, and over- or underestimating trends for other wells. The number of water-level observations and the land-use data precluded a better match in this region. Additional refinements of the model combined with more detailed land-use and well data likely will allow for a better match with subsequent updates of the model.

Variations in matches of individual hydrographs indicate that simulation results generally provide a reasonable fit, given the general lack of information on the use and movement of water in the valley. The monthly to interannual fluctuations indicate the influence of climate, streamflow infiltration, and annual changes in land use. The goal of the model calibration was to try to match individual groups of hydrographs, and to minimize the sum of squared weighted residuals (SOSWR) for all simulated heads. As mentioned previously, there are large areas for which no water-level data are available (fig. 25). The use of WBSs that represent multiple farms, estimated pumpage rates, spatially and temporally coarse (multi-year) land-use and crop distributions for the periods prior to the last two decades, and assumptions made in spatially distributing pumpage may limit the ability of the model to accurately simulate water levels for the periods before detailed land-use data became available (about 1999). The spatial distribution of the residuals and water-level matches is discussed in more detail in the “Groundwater Levels Map” section. Much of the error, and the primary source of the average error, could be associated with the lack of spatial and temporal detail in land-use estimates in the valley that ultimately drives ET consumption through irrigation and pumping.

Vertical water-level differences range between -54 ft (upward gradient) and 49 ft (downward gradient; fig. 27C). Residuals between observed and simulated vertical water-level differences generally ranged from -14.1 to 1.1 ft and were largest between the upper and lower alluvium in the Main-zone subregions of the model. The water-level differences have a median residual of -0.8 ft, and the model fit is best for the shallower layers, such as in the 10N26W region of the Southern Main-zone subregion (fig. 26). About 58 percent of the simulated vertical head differences are within 5 ft of the measured head differences. Overall, the simulated and observed vertical water-level differences are similar in magnitude and sign and for many sites improve in later (more recent) years with improved information on land use that drives agricultural consumption and related pumpage. Despite the matches, there are areas in which agreement between observed and simulated values could be improved. For example, measured vertical head differences range about 100 ft, whereas simulated differences range only 15 ft, indicating that the simulated vertical hydraulic conductivity may be too large in some areas.

Water-Level Maps

The spatial comparison of the CUVHM-simulated data to observed data allow compilation of water-level maps for the Cuyama Valley aquifer system for September 1966 (fig. 28A), and Spring and Fall of 2010 (figs. 28B, C). The simulated groundwater levels (fig. 28) are in general agreement with the water-level maps for these periods. The thematic pixels from the simulated water levels are a thickness weighted average of composite water levels. The thickness weighted average was used because this is consistent with the observation process in MF-OWHM and is more consistent with the composite water levels derived from wells that were used to create the hand-contoured water level maps and the composite simulated water levels derived from the HOB Package (Hill and others, 2000; Harbaugh, 2005). The water-level maps were useful during the model calibration by providing additional information on the effects of internal flow boundaries along faults and the adjustments to select model hydraulic properties such as vertical hydraulic conductivities.

The sequence of simulated and measured water-level maps both indicate regions in the center of Cuyama Valley where water levels continue to decline and that the declines are concentrated in the Main-zone subregions (fig. 28). Changes in measured and simulated groundwater levels from spring to fall in 2010 range between -3 (rise) and 90 ft (fig. 28B, C). By the fall of 2010, water levels below 1,900 ft persisted in the Main-zone subregions, a pattern replicated by output of the CUVHM (fig. 28C). However, simulated water levels underestimate the hand-drawn contours in northeastern parts of the model (northeast of Ventucopa) where additional refinement of aquifer properties, land use, or recharge may be required (fig. 28).

Land-Subsidence Observations

Measurements of land subsidence were made at two continuous GPS sites and five reference point InSAR sites (fig. 29A). A total of 308 monthly observations were derived from the GPS and InSAR data. These observations show from little to no subsidence to a maximum of about 0.2 feet between 2000 and 2010 when measurements were available. The CUVHM model matches the relative deformation in the Main zone and Ventucopa Upland subregions based on both observed data types. Overall, the CUVHM underestimates the relative vertical displacements but the rates are comparable in the Southern Main-zone subregion at the Cuyama High School Plate Boundary Observation (PBO) site (fig. 29A). The simulated subsidence is generally restricted to the fault-bounded regions of the Main-zone subregions for the period 1950–2010 with 0.1–1.6 ft of simulated subsidence in this region (fig. 29B). Although these magnitudes and rates are currently relatively small compared to the 30 feet of subsidence at rates approaching 1 foot per year at times in the Central Valley (Faunt and others, 2009a), if water-levels in the Cuyama Valley continue to decline there will be more subsidence. Despite the small magnitude, much of this

subsidence is inelastic, resulting in a small permanent loss of storage in the aquifer system. The simulated subsidence indicates the initiation of inelastic subsidence in the late 1970s. Because the amounts of subsidence were so small and the number of observations is sparse, no estimation of residual errors was calculated on this limited set of data.

Pumpage Observations

Observations of agricultural pumpage included previous estimates based on land-use and power records reported for the period 1947–66 by Singer and Swarzenski (table 1, 1970). These annual pumpage estimates were used to guide the final adjustments of landscape properties and irrigation efficiencies but were not used in the formal parameter estimation. The CUVHM model matches the annual agricultural pumpage within 14 percent of the reported values for any particular year and underestimates average annual agricultural pumpages by 1.6 percent for the early dry years (1949–58) and by 2.0 percent for early wet years (such as 1959, 1964, and 1969). Reported pumpage for the early years can vary by as much as 20 percent and is aligned with climate variability to some degree, but indicates persistent pumpage even during the wet years. Overall, the agricultural pumpage increases with changes in land use in more recent years and shows considerable variability that is aligned with changes in climate conditions, with simulated pumpage from 1967 to 2010 ranging from about 42,000 to 88,000 acre-ft/yr (fig. 30). For example, simulated pumpage increases rapidly in 1977, which is coincident with increased agricultural land use, such as alfalfa production, with pumpage for irrigation estimated to have increased to about 76,000 acre-ft/yr. (fig. 7A).

Model Parameters

Although many parameters were originally defined in the model (tables 14 and 15), only about 69 parameters were determined to be relatively sensitive and were subsequently considered and included in the automated calibration process. These parameters included landscape and crop-related properties, hydraulic parameters of the aquifers and multi-node wells, fault conductances (table 14), streamflow vertical conductivities, and fractions of BCM-simulated combined runoff and recharge inflowing along the Cuyama River and Santa Barbara Creek into the SFR2 Package (table 15). Hydraulic properties were initially assigned values based on published values and earlier modeling studies, then adjusted during model calibration. Model parameters were adjusted within ranges of reasonable values to best-fit historical hydrologic conditions measured in the aquifer, the stream network, and the landscape.

Calibration started with the landscape processes, followed by adjustment of hydraulic properties, streambed properties, multi-aquifer well properties, general-head boundary conductances, and fault conductances. Because many of these properties are head dependent or were correlated through

their exchange of water, these properties were adjusted recursively through automated and trial-and-error analysis. The calibration process also required modifications to the parameter framework. For example, calibration also required additional partitions of hydraulic-property-zone parameters and observations for the alluvium. By using the sensitivities calculated as a function of the observations, only those parameters that were determined to be sensitive were adjusted during automated calibration.

Farm Process Parameters

Farm Process parameters that were adjusted during calibration included selected crop properties. Some parameters were fixed, some were adjusted manually, and some were adjusted using PEST. Tables 13–15 indicate which parameters were estimated at some point during the calibration. These included scale factors for seasonal K_c s, percent runoff from inefficient losses from precipitation and irrigation for select crops and natural vegetation, and seasonal scale factors for irrigation efficiencies. The scale factors for seasonal K_c s are used to represent the stress factors (Allen and others, 1998) that amplify or reduce the K_c s, which were estimated under unstressed conditions. Because published K_c s are estimated under unstressed conditions (K_c less than or equal to 1), the K_c s used in this study required reductions for wet winters, summers, and falls of 19–44 percent for the early years and increases of 2–15 percent for later years. Stress factors for K_c s for wet springs were reduced for early and late years by 20 and 13 percent, respectively. Similarly, stress factors for dry-year seasons were increased by 65 percent for dry, late-year summers and 20–24 percent for early- and late-year dry winters (table 14) to align estimated agricultural pumpage with water-level declines. Part of this adjustment could be related to antecedent soil moisture not being accounted for by the FMP, but this would represent a relatively small amount of water. The scale factors for K_c s were adjusted to reach somewhat subjective matches to observations of ET and agricultural pumpage estimates for 1950 and 1966 (Singer and Swarzenski, 1970). Irrigation efficiencies for the early decades were adjusted for dry-year seasons, with spring values increased by 10 percent, fall values reduced by 7 percent, and summer values reduced by 2 percent during calibration. For the greater efficiencies of the recent decades, irrigation efficiencies for all seasons were increased by 10 percent except for dry springs. Irrigation efficiencies for early-year wet-year seasons were increased by 8–11 percent. Irrigation efficiencies for later years were increased relative to the initial estimates by 10–20 percent for winters, springs, and summers (table 14) and reduced relative to initial estimates by 20 percent for wet-year springs. This could indicate that irrigation is less efficient during wetter periods or could include pre-wetting of soils for vegetable crops. Runoff from selected crops and native vegetation is a direct control on the water available for deep percolation or for overland runoff to the streamflow network. The fractions of inefficient losses to runoff were initially adjusted for truck and vegetable crops,

orchards, field, pasture, and grain-and-hay crops, but were finally held constant at 97 percent excess water to runoff after ET consumption of irrigation and precipitation for final calibration. Similarly, fractions of runoff from precipitation were increased to about 92 percent to control the deep percolation and additional runoff from the native vegetation, which is the largest component of the land use in Cuyama Valley. The multiple caliche layers that are common in many parts of the Main-zone subregions of the valley may also enhance runoff and further impede deep percolation from precipitation and irrigation.

Hydraulic Parameters

The model was used to determine the values of 15 hydraulic properties within each model layer during calibration. The values of K_c and K_f for each model layer were adjusted to produce simulated heads representing the long-term trends in the aquifer and to produce heads that best matched the measured heads and estimated streamflow losses. Because of the differences in depositional environments within the various zones of each layer, the hydraulic properties were also adjusted subregionally by using 72 related parameter scale factors for the parameter subregions that are multipliers for horizontal and vertical hydraulic conductivity and storage properties (fig. 24B–D). The hydraulic properties that were adjusted included coarse- and fine-grained values for hydraulic conductivity, porosities, specific yields, and skeletal specific storage for coarse- and fine-grained end-members, and the exponent of the vertical hydraulic conductivity (eqn. 4). Specifying a single exponent value of p of -0.9 for the vertical hydraulic conductivity was replaced with individual values for each model layer of -0.9 , -0.5 , and -0.7 for model layers 1–3, respectively. This resulted in values of K_c (coarse-grained) and K_f (fine-grained) which are relatively close to the harmonic mean of vertical hydraulic conductivity (eqns. 2 and 4) for the Recent Alluvium and Morales Formation aquifer layers and closer to the geometric mean for the Older Alluvium model layer. The compressibility of water was specified as a component of the storage properties proportional to the coarse- and fine-grained porosities and was held constant.

The calibration of hydraulic properties required the adjustment and rescaling of these intrinsic properties based on water-level hydrographs (fig. 26). The most sensitive parameters were vertical hydraulic conductivities (represented by the hydraulic conductivity of the fine-grained fraction) that, in part, controlled the seasonal amplitudes and vertical water-level differences between aquifer layers. Scaled reductions in vertical hydraulic conductivity and storage properties were required for select confined zones and scaled increases in these properties were required for unconfined zones. Horizontal hydraulic conductivities (represented by the hydraulic conductivity of the coarse-grained fraction) were increased during model calibration in many of the aquifer layers (table 13). Because the model was relatively less sensitive to values of porosity and specific yield, these were not included in automated parameter estimation.

Streamflow Properties

The model also required calibration of the streambed vertical hydraulic conductivity parameters. Groups of stream segments where stream channels are similar were represented by 30 parameters of streambed vertical hydraulic conductivity (figs. 8; table 15). The groupings and calibrated vertical hydraulic conductivity values range from 0.2 ft/d in tributaries crossing the alluvium of the western Main-zone subregion to as much as 49 ft/d in the Cuyama River and select tributaries crossing the Recent Alluvium of the southern Ventucopa Uplands (table 15). Because there are no downstream gages, no downstream streamflows or differences between gages as gains and losses on rivers or tributaries were available for calibration of streambed conductivities. The final distribution of streambed vertical hydraulic conductivities for each of the 577 segments is summarized in figure 8 and table 15.

Multi-Aquifer Well Parameters

The skin factors in the MNW Package define the friction losses to water flowing from the aquifer into the well due to the screen and to formation damage. They affect the interlayer flow and related water-level difference between model layers. Three skin factors were used as parameters to control the retardation of wellbore flow within each layer for the multi-aquifer wells (table 14). Skin factors were relatively high to maintain the observed vertical head differences and to control wellbore flow between layers. The final calibrated skin factors ranged between 395 square feet per day (ft²/d) for the Recent Alluvium layer and 1,625 ft²/d for the Morales Formation (table 14).

General-Head Boundary Parameters

The conductance factors in the GHB Package for the groundwater underflow were constant model values. These conductances controlled the small inflows beneath Reyes Creek and the Cuyama River and outflows beneath the Cuyama River at its western groundwater outflow from the valley. The final conductances that controlled lateral outflow were set relatively large in comparison to typical hydraulic conductances to promote underflow from the western boundaries, ranging from 5.4×10^6 to 8.6×10^6 ft²/d. The conductances for the inflows were held small, ranging from 1.1 to 0.1 ft²/d for the alluvium and Morales Formation layers, respectively (table 14). This small conductance restricts flow from the adjacent watersheds through the very narrow alluvial channel in the upper layer. The majority of the inflow from the adjacent watersheds is relatively small and is incorporated into the inflows of the SFR2 Package based on the BCM data.

Horizontal Flow Barrier Parameters

The conductance factors in the HFB Package affected the subsurface flow of water between the groundwater subregions that collectively represent Cuyama Valley. In turn, these flows not only affected water levels but also indirectly affect the propagation of storage depletion and subsurface recharge from underflow. Six parameters were used for the interior faults—Morales, Graveyard, Turkey Track Hill, Rehoboth, and Santa Barbara Faults—as delineated by Sweetkind and others (2013). The Santa Barbara Fault was split into two modeled flow barriers with one representing the fault within the Older Alluvium and Morales Formation and a second representing the flow barrier in the Recent Alluvium. Fault conductances were initially model-estimated parameters but ultimately specified at low values and were held constant for final calibration. These low conductances are consistent with the discontinuities in the water levels mapped by Singer and Swarzenski (1970) and the concept of subregions with limited groundwater flow between them. For example, the Santa Barbara Fault appears to separate the southern Ventucopa Uplands subregion from the Southern Main-zone subregion. The Morales, Graveyard and Turkey Track Hill Faults separate the Southern Main zone from the Western and Northern Main-zone subregions, and the Rehoboth Fault impedes underflow along the Sierra Madre Foothills region in the Older Alluvium and Morales Formation that would potentially replenish the Southern and Western Main-zone subregions. The final calibrated conductances for the faults are summarized in table 14.

Subsidence Parameters

The simulation of land subsidence and related changes in groundwater storage were controlled by nine model parameters that scaled the critical head, elastic skeletal storage, and inelastic skeletal storage for each model layer (table 14). Specified critical heads represent initial conditions in 1949 of overconsolidation and were estimated with PEST during calibration using scaling factors. The majority of the aquifer and interbed confined storage resides in the skeletal elastic storage values used with the SUB Package. These values were estimated using PEST during model calibration with scale factors of initial estimates; the final values were reduced to 42 percent for the Older Alluvium and increased to 34 and 50 percent for the Recent Alluvium and Morales Formation, respectively.

Sensitivity Analysis

The simulated equivalents of the suite of observations in CUVHM were most sensitive to scaling factors for initial heads in layers 1 and 2, secondarily to changes in select climate and landscape properties, and to a lesser extent to selected scaling factors for hydraulic properties for the

aquifers, streambed vertical hydraulic conductivities, and horizontal hydraulic conductivities. Systematic parameter-estimation techniques were primarily used to estimate select model parameters and related sensitivities that are based on perturbation approaches with limited guidance from trial-and-error analysis. Although the sensitivity to initial conditions might be partially solved by simulating a longer initialization period, because groundwater levels adjust relatively slowly, it would take many decades with little information on stresses to arrive at a potentially more uncertain set of initial conditions.

The sensitivity process in PEST identifies the sensitivity of computed values at the locations of measurements to changes in model parameters, and was used to identify which parameters to include and to adjust during calibration (Hill and others, 2000; Doherty and Hunt, 2010). Results of the sensitivity analysis indicated that the model was most sensitive to scaling factors for adjusting the initial heads within the Recent and Older Alluvium aquifer layers. Parameter sensitivities for an additional 29 parameters related to hydraulic properties, stress coefficients of K_c , and scale factors for the runoff from precipitation for native vegetation are shown in declining order of sensitivity on figure 31. The model is next most sensitive to runoff from precipitation over native vegetation, which not only controls a major contribution to recharge through deep percolation but also intermittent unaged runoff contributions to streamflow and stream channel infiltration. Included within the 20 most sensitive parameters are spring and summer scale factors for K_c and irrigation efficiencies. The most sensitive streamflow parameters were the vertical hydraulic conductivity related to sections of Cuyama River channel (wvc_qyacc), various creeks in the unconfined Recent Alluvium in the Ventucopa Uplands subregion (vc_qyauc), the Western Main-zone subregion Cuyama River channel (wmz_qyacc), and northern tributary reaches of the Sierra Madre Foothills (wsmfh_qoan) subregion.

Model Uncertainty, Limitations, and Potential Improvements

The CUVHM is a simplification of the real flow system, and, as such, has some inherent limitations. The accuracy of simulation results is related strongly to the quality and resolution (both spatial and temporal) of input data and of measurements of the system (such as precipitation, water levels, streamflow, and pumpage) used to constrain the calibration. The inflows and outflows in the model were a combination of measured values, adjustments to parameters to represent conceptualizations of the system, estimated inflows provided by the BCM model, and values specified through the use of the model code, MF-OWHM. Differences between simulated and actual hydrologic conditions arise from a number of sources and are collectively known as model error.

While the CUVHM was designed with the capability to be accurate everywhere, the conceptual and numerical models were developed on the basis of assumptions and simplifications that may restrict the use of the model to regional and subregional levels of spatial analysis within seasonal to interannual temporal scales. Potential future refinements and enhancements will continue to improve the level of resolution and model accuracy. In general, proper design and calibration of flow models, along with better estimates of inflows and outflows and changing spatial data such as climate and land use, can minimize some of the inherent model limitations. Limitations of the modeling software, assumptions made during model development, and results of model calibration and sensitivity analysis all are factors that may constrain the appropriate use of this model and can be used to identify where potential future improvements in the simulation of specific processes are needed or where new data are needed to constrain simulations.

Model discretization in space and time can be a potential source of error and uncertainty. Models represent a hydrologic system as a series of discrete spatial units, through which intrinsic properties and flows are assumed to be uniform. The use of a discretized model to represent a hydrologic system introduces limitations for features that occur at scales smaller than the discretization. Transient models are further discretized into a series of discrete units of time, during which specified hydrologic inflows and outflows are held constant. The use of monthly stress periods and two time steps per month in the CUVHM assumes that the variations of inflows and outflows and changes in water levels are piecewise linear changes. Changes at smaller time scales are not simulated, and are not discernable in the model results, which may contribute to some additional temporal uncertainty. For example, the distribution of daily precipitation and soil moisture within each monthly period used by the BCM and CUVHM can result in large variations in simulated recharge and runoff (for example, precipitation occurring as a large one-day storm rather than as a series of smaller storms), and this cannot be accounted for with the existing model. The temporal scale used in the CUVHM was expressly designed to separate the supply and demand components of water use and movement for agriculture.

Differences between simulated and measured hydrologic features also can arise from the numerical solution that attempts to provide a cell-by-cell mass balance of inflows and outflows. Mass-balance errors are minimized by ensuring the model solution reaches a reasonable state of mass balance within each biweekly period. The twice a month time steps were used to remain consistent with the assumptions of the current version of the FMP process. The cumulative mass balance of the model was within 1 percent of the total flow over the 61 years of simulation.

An additional component of model error arises as a consequence of how well model-input values represent the actual hydrologic system. The accuracy of the calibrated model is contingent on the accuracy of the specified inflows and of the specified observed flows used for model comparison. Model calibration provides a means to use comparisons to indirectly constrain the differences between the real-world and simulated mass flows. Thus, the degree to which a simulated condition provides a reasonable representation of the hydrologic system can be evaluated through comparing simulated hydrologic conditions with those observed in the field, which in turn provides a mass-constrained calibration. The performance and accuracy of CUVHM are constrained primarily by groundwater levels, and to a lesser degree by recent land subsidence and vertical groundwater-level differences. The model is used for developing a conceptual understanding of the flow system by quantifying the regional inflows and outflows and their relative proportions. Because the Cuyama Valley flow system is inherently complex, like all models, simplifying assumptions were made in developing and applying the numerical code, MF-OWHM. The model solves for average conditions within each 15-acre cell for each two-week period, with the parameters interpolated or extrapolated from measurements, and (or) estimated during calibration. Modeling the regional aquifer system without the delayed recharge of unconfined conditions also may affect the timing and magnitude of groundwater recharge and can be a potential source of error and uncertainty. Thus, results from the model should be interpreted at the sub-regional to regional scale and multi-year periods for comparative analysis and generalized estimates of flows.

Several elements of the revised model remain uncertain and will require additional investigation to help further improve the accuracy of the simulation of the groundwater and surface-water flow, the simulation of regional storage changes, and the simulation of the use and movement of water across the landscape. For example, some of the crop, soil, and landscape features that are inputs to the Farm Process and are used to calculate water use remain uncertain. Thus, model features such as pumpage and recharge are sensitive to some of these parameters such as K_c s, irrigation efficiencies, multiple cropping, or monthly land use. In particular, the distribution and change in land-use patterns needs to be improved to annual or even monthly scales to significantly increase accuracy of the simulation. Many of the stresses that are driven by these land uses varied throughout the simulation period at higher frequencies than the multi-year estimates of most of the historical land use. This is evident by the improved simulation since 2000, when land use estimates used in the model were more frequent. These variations also are driven by climatic conditions as well as growing periods. Hence, the changes appear seasonally and by climate-driven events that can be yearly or multi-year in length. Because the land use was based on generalized classification for the early

years and select crop categories, some of the agricultural composite crop classes were replaced with the composite crop of identical extent from the 2000 land-use map. For example, where only generalized categories of land use were specified, the composite crops interpreted on the 2000 land-use map were embedded. This assumes the farmer would be growing the same type of crop in a given area over the time frame of the hydrologic simulation when that land-use map was used (figs. 18–22). In some cases, such as orchards, this is generally a good assumption; in other cases, the crops being grown may have changed several times during the years represented by the land-use map. Estimates of ET_0 and growing periods are uncertain and should be better delineated, especially in terms of their relation to climate changes. Finally, the natural vegetation represents between about 87 percent (historically) to 65 percent (recently) of the land use and, as such, is an important control for runoff and recharge in the upland regions of Cuyama Valley. Another potential future refinement to the model could include separation of the natural vegetation into several separate land-use subregions in different parts of the valley. This may improve simulated recharge and runoff in these areas. Though some additional uncertainties may be associated with estimating runoff as a fraction of precipitation and irrigation by crop type that does not consider the effect of soil properties on runoff, improving this feature would require prohibitively small time steps and longer simulation run times. Because the desert caliche layers and not the soils probably control much of the runoff and deep percolation, additional mapping of these layers may be needed to improve the simulation of runoff for these biweekly time intervals.

Some inflows and outflows, such as outflow along the Cuyama River, remain relatively uncertain, and the accuracy of the model could benefit from additional observations of streamflow from other major ungaged drainages such as Reyes Creek, especially if more constraints are needed to improve the overall hydrologic budget and estimates of local recharge and runoff. Continued monitoring of the inflows from the Cuyama River and Santa Barbara Creek will also be useful in maintaining an inventory of the major components of runoff from surrounding mountains.

The CUVHM may benefit from refinement of the location of the trace of the Santa Barbara and Rehoboth Faults, which may change the locations and extents of the flow barriers and potentially segregate the subregions of the valley into subbasins. The accuracy of the model could also be improved if the input values of selected hydraulic properties, such as horizontal and vertical hydraulic conductivities and storages, could be adjusted on the basis of additional field estimates. Additional estimates of horizontal hydraulic conductivity to further constrain the model properties could be obtained from aquifer tests at select supply well sites or well specific-capacity tests at single-aquifer supply wells. In addition, uncertainty in the data used to distribute the textural data is both more sparse and larger with increasing depth. The difference between simulated and measured heads generally

increases with depth below the land surface. This may reflect decreasing accuracy with depth within the texture distribution used to estimate the hydraulic conductivities. Uncertainty in the values for the hydraulic properties of the Morales Formation may be especially large even though many wells currently produce water from this unit in the Cuyama Valley. Thus, textural-data uncertainty is smaller for the younger and Older Alluvium and larger for parts of the Morales Formation.

Several of the processes within the model could also potentially allow for refined simulation of selected flow features. Improved simulation of multi-aquifer wells to account for partial penetration and better estimates of actual pumping capacities of all wells could increase the accuracy of simulated pumpage. Some WBS required virtual wells, so the additional location of wells or water conveyances that are used to service these properties requires additional investigation. Similarly, the simulation of runoff within the Farm Process could be enhanced to better simulate the intensity of wet-year winter precipitation events that would facilitate better estimates of runoff within the valley. Also, the simulation of unconfined conditions and the lowering of the water table in the Main-zone subregions could be improved by the use of the Unsaturated Zone Package (Niswonger and others, 2006) and related Newton-Raphson Solver (Niswonger and others, 2011). However, this upgrade could result in significant increases in total run time of the historical and future simulations.

In summary, some potential components that could improve the accuracy and reduce uncertainty of the simulation could include but are not limited to the following:

1. Improved temporal estimates of land use from annual to seasonal or monthly.
2. Improved estimation and application of crop and irrigation properties.
3. Improved segregation of natural vegetation into multiple classes in different parts of the valley.
4. Improved estimates of unaged stream inflows and outflows through additional streamflow gaging (either used directly or to improve the calibration of BCM).
5. Refined location and extents of the trace of the Santa Barbara and Rehoboth Faults.
6. Improved estimates of hydraulic properties through additional field tests.
7. Improved texture estimates at depth and refined zonation of the Morales Formation.
8. Improved simulation of multi-aquifer wells to account for partial penetration and farm well pumping capacities and additional location of potential wells.
9. Improved groundwater, streamflow, land subsidence, and land cover observations for better model evaluation and calibration.

Despite all of these potential limitations, the CUVHM represents a realistic, reasonably accurate, and reliable means for understanding many aspects of the Cuyama Valley groundwater basin that are needed for planning and evaluating alternatives for managing water resources. Additional observed hydrologic and land-use data could also be used to improve the model calibration. When used correctly, CUVHM can help to continue developing understanding as more data and more capabilities are added. Additional observed hydrologic and land-use data could also be used to improve the model calibration.

Hydrologic Budget and Flow Analysis

The CUVHM simulation of the conjunctive use and movement of water in Cuyama Valley indicates that, overall, the storage depletion and onset of land subsidence are driven by sustained and increased agriculture and related demand for water, thus resulting in a condition of overdraft. While periodic events of recharge occur from natural climate cycles, the current and historical sustained demand for water exceeds the long-term replenishment rate from these quasi-periodic events. The CUVHM confirms that the overdraft conditions have persisted since the onset of increased development in the 1970s up through 2010. The CUVHM indicates a level of pumpage that is consistent with estimates from the early years of reported pumpage and an increase in water demand with increased agricultural development. The overdraft is predominantly the result of cycles of storage depletion in the Main-zone subregions, which are also climatically driven over seasonal to interdecadal periods.

As with groundwater storage depletion and replenishment, the temporal distribution of inflows and outflows to the landscape and surface-water systems also indicates a strong climatic influence. The total inflows to the landscape range from about 100,000 to more than 250,000 acre-ft/yr (fig. 32A), which includes inflows, that are, on average, 53 percent precipitation, 44 percent irrigation from groundwater pumpage, and 3 percent direct uptake of groundwater through ET (fig. 32B). Similarly, the average total outflow from the landscape consists of 25 percent runoff, 8 percent deep percolation to groundwater recharge, 36 percent ET from precipitation, 29 percent ET from irrigation, and less than 3 percent ET directly from uptake of groundwater (fig. 32B). Thus, about half the inflow of water to the landscape comes from precipitation and half from irrigation, and about a third of the outflows occur as each of ET from irrigation, runoff and recharge, and ET from precipitation and groundwater. ET from groundwater is a minor component of inflow to the landscape, and runoff, predominantly from precipitation, is a major outflow from the landscape. Deep percolation from precipitation and irrigation persists for all years but generally is larger during wet years.

In 50 of the 60 years (fig. 33A), the total demand for water on the landscape for agriculture is much greater than the natural inflows in this high desert valley, with irrigation from groundwater supplementing the water needed for agriculture. Groundwater recharge from precipitation and irrigation is about half the groundwater pumpage in the wettest years (for example, in 1998 and 2005) and typically is 10 to 25 percent of groundwater pumpage for most years, resulting in sustained groundwater storage depletion and overdraft. Estimated agricultural pumpage during wetter years is sometimes comparable to that in dry years, which may reflect lower irrigation efficiencies during wet years.

The components of the net annual groundwater budget (fig. 33) are similar to inflows and outflows for the landscape, and vary with climate and changes in land use (fig. 33A). The average hydrologic budget overall and for the most recent decade (2000–10) indicates that streamflow infiltration and recharge from precipitation and irrigation are the largest inflows, and pumpage is the largest component of outflow, as summarized for select periods (fig. 33B; table 16). The percentages of these groundwater inflow and outflow components are summarized in a pie diagram (fig. 33C). Except for the occasional wet years, the major outflow is agricultural pumpage, and most of this outflow is supplied by a decrease in groundwater storage. The net groundwater budget averages about 70,000 acre-ft/yr (in and out of the groundwater system) but changes in groundwater storage can vary widely as shown by the large replenishment of about 80,900 acre-ft that can occur in wet years such as 2005 or additional depletion of about 45,000 acre-ft in dry years such as 2009 (table 16). On average and valley wide, water released from storage contributes 68 percent to the total groundwater outflow, along with a contribution of 25 percent stream leakage and 6 percent farm-net recharge. About 38 percent of the groundwater outflow flows back into aquifer storage, for a net storage depletion of about 30 percent of groundwater flow (fig. 33C). The largest component (44 percent) of groundwater outflow is pumpage, (wells, farm wells, and multi-node wells), which is combined with 9 percent outflow to streams, 5 percent farm-net recharge (groundwater recharge minus ET from groundwater), and 4 percent as groundwater underflow (general head boundary) and spring discharges (drains; fig. 33C). Though some storage replenishment occurs during wet years, which offsets some of the storage depletion in dry years, the overall temporal distribution of net flows shows an increase in storage depletion (inflow of water from net storage; fig. 33D). This is largely focused in the Main-zone subregions, with small amounts of depletion in the Ventucopa Uplands subregions and a small accretion in storage in the Sierra Madre Foothills subregions. The total simulated storage depletion is about 2.1 million acre-ft for the period 1950–2010. The average storage depletion represents about half of the average agricultural pumpage (65,400 acre-ft/yr) per year. The estimates of recharge and underflow are about 30 percent larger than the flows estimated for the earliest years of development (1947–66) by Singer and Swarzenski (1970). About 72 percent of the average storage depletion and

87 percent of the agricultural pumpage occurs in the Main-zone subregion and the remaining average depletion and 11 percent of the agricultural pumpage occurs in the Sierra Madre Foothills region for the historical period. Conversely, about 57 percent of the total average recharge and 64 percent of the average net streamflow infiltration occurs in the Ventucopa Uplands subregion.

The temporal distribution of groundwater pumpage is dominated by agricultural pumpage. Most of the flow of groundwater to wells is from the Recent Alluvium and ranges from 40 to 93 percent (fig. 34). Additional water is derived from the Morales Formation in the early years (1950–77) and from the Older Alluvium in the subsequent years (1978–2010) with shifts in development and related land use in the valley. The relative reductions in pumpage during the intervening wet periods show the sensitivity of the climate built into FMP calculations. For example, agriculture and related irrigation is very sensitive to climate as irrigation is supplemented by precipitation, a portion of which is consumptively used by crops, as demonstrated by the comparison with estimated pumpage for the early years (fig. 30).

More than 70 percent of the recharge occurs within the Recent Alluvium layer during the years of greatest land-use development prior to the 1980s (fig. 35A). An additional 20 percent enters the groundwater flow system through the Older Alluvium. The fractions of recharge to the Morales Formation could be an artifact of the model's initial conditions. There is some variation with climate in the relative proportions of recharge from year to year (deep percolation, fig. 32), but the overall percentages remain relatively constant valley wide. This exchange of water between aquifers largely occurs across layer boundaries and in relatively small amounts by intraborehole flow through long-screened supply wells that are open to both formations. As indicated from the depth-specific water level histories of the multiple-well monitoring sites (fig. 26A), the vertical head gradients can be downward during the growing season and upward during the non-growing season. Most of the vertical interlayer flow occurs across layer boundaries and is focused in the regions where coarse-grained sediments are more prevalent, such as along the stream channels in the Recent Alluvium. The majority of the vertical flow is to the Older Alluvium or the Morales Formation from the Recent Alluvium, where the majority of the recharge is occurring (fig. 35B).

Projection of Potential Water Availability

Three 61-year projections were made to begin the assessment of the sustainability of the water resources in Cuyama Valley. This assessment included a base-case projection of “business-as usual” land use, a reduced-supply projection, and a reduced-demand projection with cessation of agriculture in the Main-zone subregion. Since there is no basin management plan, these three hypothetical scenarios

are used to assess potential water availability beyond 2010 using existing land- and water-use conditions from 2010. All three projections use information on historical hydrologic conditions (streamflows and related climate data) and 2010 land use, wells, and land ownership distributions, with 2010 crop and irrigation properties, to simulate 61 years of potential future hydrologic conditions under current supply-and-demand conditions. This assumes that there is no additional growth or reductions in demand for water resources or additional development of land for agriculture, urban, or domestic uses. Though downscaled and bias-corrected climate-model projections could have been used to create future climate conditions (Hanson and others, 2012), historical climate data were used for these initial projections to ensure that climate variability and climate cycles were similar to recent historical conditions. This assures that the historical variability in inflows and demand from ET is maintained from the historical wet and dry periods. The monthly climate data and streamflows for each water year are used starting with the most recent year (2010) and working backward in years (but forward in the months of each year) to 1950 to make a projection for the period 2011–71 so that year 2071 uses conditions from 1950.

The second scenario is called a reduced-supply scenario that represents a potential management scenario through reduction in supply in which a target yield of the basin would be determined and some acreage-based reduction would have to be made to bring demand in line with the long-term average recharge of the valley. The long-term average recharge was determined from data for the historical period 1950–2010 because conditions in this period are fairly similar and aligned with the PDO climate cycles (1947–77 dry period, 1978–99 wet period, and 2000–10 partial dry period) that control runoff and resulting recharge. The long-term (61-year) average recharge rate from this historical period is about 33,000 acre-ft/yr and the recharge for 2010 was estimated at about 35,000 acre-ft/yr. The distribution of this recharge is 57 percent in the Ventucopa Uplands, 36 percent in the Main-zone, and 7 percent in the Sierra Madre Foothill subregions. The fraction of total recharge within each of the three groups of subregions was prorated by percentage of area in 2010 over the various WBS that are designated as agriculture within each group of subregions. In addition, the distribution of the portions of long-term recharge were distributed for each WBS based on the monthly fractions of simulated monthly usage for 27 agricultural WBS that are part of the total 83 WBS in 2010.

The third scenario is called a reduced-demand scenario that represents the alternative to a reduced supply, a reduced demand projection, by retiring all agriculture in the Main zone. The difference is a reduced supply or a reduction in the amount of water that would be supplied from groundwater pumpage, while a reduced demand could represent a reduction in the acreages or types of crops grown that drives irrigation demand. This reduced demand scenario was implemented by simulating the return of all WBS agricultural land back to native vegetation without irrigation within the Main-zone subregions.

A reduction in supply may have a different effect in the three major subregions of Cuyama Valley. For example, in the Ventucopa region, where there is a lesser long-term storage depletion, less storage depletion may occur, which may increase stream baseflows during dry years. In wetter years, streamflow could pass farther west past the Santa Barbara Fault and into the Main-zone subregion and flow farther for more days of the year. In contrast, reduced supply in the Main-zone subregion will result in less artificial recharge from irrigation, which results in a reduced replenishment, as well as reduced demand from deficit irrigation or reduced acres of agriculture that can be sustained with reduced supply.

For the first base-case scenario, the projected supply-and-demand indicates the potential for additional water-level declines of more than 350 ft in the Main-zone subregion, with a sustained agricultural pumpage of about 65,000 acre-ft/yr (fig. 36). The projected change in cumulative storage indicates that an additional 2.5 million acre-ft of water would be removed above and beyond any potential recharge (fig. 37A). The projected groundwater levels for the end of the projection period show sustained declines in areas of substantial agricultural demand in the Main zone and Sierra Madre Foothills subregions (figs. 2A, 36, 37B). With these sustained declines also comes additional potential land subsidence of almost two feet near Cuyama (fig. 37C) that is mainly focused in the areas of sustained agricultural demand in the Main-zone subregions. Conversely, the Ventucopa Uplands subregion appears to retain conditions similar to current conditions and there is only modest storage depletion in the Sierra Madre Foothills subregion. The combination of storage depletion with continued drawdowns in the aquifers within the younger and Older Alluvium combined with additional potential land subsidence is probably not a sustainable scenario in the Main-zone subregions.

The second scenario represents reduced supply with the use of groundwater allotments within FMP to limit the pumpage within each WBS to a proportional fraction of long-term recharge. This scenario still shows some small amount of long-term storage depletion of about 500 acre-ft (fig. 37A). There is about a 30- to 70-foot recovery of water levels in parts of the Main-zone; levels in other regions such as the Sierra Madre Foothills region show continued declines with additional storage depletion that may be the result of continued pumping from wells that actually serve the Main zone (fig. 37B). While there is a general cessation of additional land subsidence and some elastic rebound for this scenario (fig. 37C), there is still some potential land subsidence occurring in parts of the Main zone. The overall average rate of storage depletion is greatly reduced with pumpage held close to the average long-term recharge rate (table 16). This scenario indicates that while the storage depletion is largely arrested in the Main zone, there still may not be a sustainable resource after the projection of 61 years because of reduced artificial recharge from irrigation in the Main zone and lack of overall long-term storage recovery. This scenario is comparable to the scenarios that describe the relation between safe yield, sustainability, and the water-budget myth

(Bredehoeft and others, 1982; Bredehoeft, 1997, 2002; Alley and Leake, 2004). The reduced pumpage may not allow the current intensity and extent of agriculture to be sustainable even if irrigation was more efficient, for example, by transition from sprinkler to drip or soaker irrigation, or if mulching, canopy, deficit irrigation, and other practices were used to reduce demand from irrigation (ET).

The third scenario that represents reduced demand with cessation of agriculture in the Main-zone subregions results in widespread recovery of water levels except within the Sierra Madre Foothills subregions. This scenario results in storage accretion averaging about 11,900 acre-ft/yr (fig. 37A), that results in about a 170-ft to a more than 200-ft of recovery in groundwater levels in parts of the Main zone but continued declines in parts of the Sierra Madre Foothills (fig. 37B) and cessation of potential land subsidence with some minor elastic recovery (relative uplift) (fig. 37C). Average recharge is again reduced by reduction in direct infiltration from irrigation supplied by pumpage that is about half the average recharge rate (table 16). This scenario represents a radical change in land use that is probably not realistic, but serves to demonstrate the changes that would need to be made and long time frames needed to not only arrest storage depletion but to only partially recover the basin's aquifers. This scenario may also not be feasible with respect to sustainable agriculture in the valley. The three scenarios indicate that other sources of water, combined with managed aquifer recharge, possibly through redistribution of streamflows further into the Main zone, and a comprehensive basin management plan could be needed to augment the current levels of water demand and reduce the disparity between supply and demand. Wet years alone cannot overcome the sustained deficit between supply and demand based on recent climate, land-use conditions and demand for water for irrigation at twice the long-term average recharge rate.

Additional projection scenarios with CUVHM could be simulated with alternative future climate conditions and adaptation of land-use and agricultural practices such as improved irrigation efficiencies to further assess the mitigation of potential overdraft conditions. Alternatively, simulations could be made to assess potential projects such as new land ordinances or reductions in agricultural acreage, groundwater management projects such as managed aquifer recharge that could redistribute streamflow from the Ventucopa Uplands corridor into the Main-zone subregions, climate-change adaptation that would facilitate capturing and replenishing water through managed aquifer recharge, or new policies regarding water use and reuse. These types of scenarios and analysis require a management structure that could develop and evaluate the feasibility of social, political, and engineering solutions and their costs, before a given management strategy and related policies and projects could be evaluated using the CUVHM model. This analysis could help to form the basis for evaluating a potential water-resource management plan by using alternative policies and projects. Though not simulated in this version of CUVHM, as the water table is lowered with a growing unsaturated zone, recharge can be delayed or reduced when the streamflow becomes hydraulically disconnected from the groundwater water table.

Suggestions for Future Work

Future work could include refinement and temporal updates of the Cuyama Valley Hydrologic Model, through additional calibration, with additional model observations, and development of alternative projection scenarios based on a comprehensive basin management plan. An expanded monitoring network would allow a better understanding of changes in groundwater flow, streamflow, and streamflow infiltration, which are the main sources of recharge in the valley. In particular, the additional monitoring of stream inflow, groundwater pumpage, land subsidence, and groundwater levels throughout the valley would help to better quantify the state of the resources as well as provide valuable comparison to model performance. However, monitoring Cuyama River outflows or inflows from other major tributaries and continued monitoring of the inflows on Cuyama River and Santa Barbara Creek are also needed to refine the hydrologic budget as well as to maintain and improve the accuracy of the CUVHM. The calibration of the model, based predominantly on groundwater levels, could be supplemented with additional calibration that include observations from remote-sensing estimates of ET and with additional streamflow values to help improve model accuracy. Additional verification of the numbers and conditions of wells used for irrigation and cropping practices would also potentially improve the accuracy of the model. Projections of water availability and sustainability of supply could include the analysis of alternative scenarios of land use, crops, and irrigation practices, as well as additional capture of intermittent runoff from wet years for managed aquifer recharge.

Summary and Conclusions

Cuyama Valley is north of Sierra Madre Mountains in south-central California (fig. 1A) and is one of the most productive agricultural regions in Santa Barbara County. However, increases in population and transitions to crops that consume additional water have increased the demand for water within the Cuyama Valley groundwater basin (CUVGB). While a small amount of urban supply is pumped from groundwater, irrigated agriculture is supplied solely by groundwater pumpage. This study provided a refined conceptual model, geohydrologic framework, and an integrated hydrologic model, the Cuyama Valley Hydrologic Model, or CUVHM. The goal of this study was to produce a model capable of being accurate at scales relevant to water-supply analysis needed for the evaluation of water availability and sustainability. The CUVHM is the first hydrologic model of this high desert basin. The Basin Characteristics Model (BCM) and the CUVHM were calibrated to historical conditions of water and land use and were used with the new geohydrologic and conceptual models to assess the use and movement of water throughout the Valley. These tools provide a means to understand the evolution of water use, its availability, and the limits of sustainability.

The conceptual model identified inflows and outflows, which include the movement and use of water from natural and human components. The groundwater flow system is characterized by a layered geologic sedimentary system that results in vertical hydraulic gradients due to the combined effects of the application of irrigation water and natural recharge from streamflow infiltration and direct infiltration at the land surface combined with groundwater pumpage, evapotranspiration (ET), and underflow as outflows. Overall, groundwater supplies most of the agricultural demand in the initial part of the growing season, which is augmented by precipitation during wet winter and spring seasons. In addition, the amount of groundwater used for irrigation varies from year to year in response to climate variation and can increase dramatically in dry years, but the model also indicates that irrigation may have been less efficient during wet years. While agricultural irrigation is not measured, it is the largest demand for water along with transpiration by native vegetation. The integrated hydrologic model, CUVHM, includes new water-balance subregions, delineation of natural, municipal, and agricultural land use, streamflow networks, and groundwater flow systems. The redefinition of the geohydrologic framework (including the internal architecture of the deposits) and incorporation of these units into the simulation of the regional groundwater flow system indicate the importance of faults in compartmentalizing the alluvial deposits into subregions that have responded differently with respect to regional groundwater flow, locations of recharge, and the effects of development. The Cuyama Valley comprises nine subregions that are fault bounded, represent different proportions of the three layers of the valley's aquifer system, and show differences in generally poor-quality water (Everett and others, 2013).

The BCM was used to estimate the monthly runoff and recharge in the 144 subbasin watershed that surround the alluvial basin of Cuyama Valley. The BCM of the surrounding watershed indicates that about 65 percent of water leaving the landscape after ET becomes runoff that flows into Cuyama Valley. Some additional recharge within these surrounding watersheds may also become rejected recharge and contribute to runoff into the valley. The BCM generally fits the limited streamflow data that were available from the region and provides a systematic estimate of runoff and recharge for the largely ungedged watersheds surrounding Cuyama Valley. Average annual streamflow applied to streamflow network boundaries is approximately 1,500 acre-ft/yr (acre-feet per year) and ranges from 0 to 120,000 acre-ft/yr. Only 14 of 144 subbasin watersheds exceed 10 . for any of the last 40 years, and with the exception of the two largest subbasins in the southeastern conglomerates, all are present on the southern side of the valley, an area dominated by sandstones. These 14 subbasins contribute more than 60 percent of the total streamflow.

The Cuyama Valley Hydrologic Model was designed to reproduce the most important natural and human components of the hydrologic system, including components dependent on variations in climate, permitting an accurate assessment of groundwater conditions and processes that can inform water users, and help to improve planning for future conditions. Model development included a revised conceptual model of the flow system, construction of a precipitation-runoff model using the Basin Characterization Model, and construction

of an integrated hydrologic flow model with MODFLOW-One-Water Hydrologic Flow Model (MF-OWHM). The new geohydrologic, conceptual, and hydrologic models were developed, and the hydrologic models were calibrated to historical conditions of water and land use, and then used to assess the use and movement of water throughout the Valley. These tools provide a means to understand the evolution of water use, its availability, and the limits of sustainability.

The CUVHM uses MF-OWHM to simulate and assess the use and movement of water, which includes the evolution of changing land use and related water-balance regions. The model is capable of being accurate at annual to interannual time frames and subregional to valley-wide spatial scales that allow for analysis of the assessment of the groundwater hydrologic budget for water years 1949–2010, as well as potential assessment of the sustainability of groundwater use. Overall, the model provides a good representation of the regional flow system and the movement and use of all water.

Simulated changes in storage over time show that significant withdrawals from storage generally occurred not only during drought years (1976–77 and 1988–92) but also during the early stages of industrial agriculture that was initially dominated by alfalfa production. Since the 1990s, growers in the Cuyama Valley have shifted to more water-intensive organic vegetable crops such as carrots, broccoli, and potatoes that are rotated with field crops such as onions and grains. Combined with an extended growing season and increased irrigated acres, the shift in land use has increased demand on limited groundwater resources in excess of natural and artificial recharge. Measured and simulated groundwater levels indicate substantial declines in selected subregions, mining of groundwater that is thousands to tens of thousands of year old, increased storage depletion, and land subsidence. Simulated groundwater flow indicates that vertical gradients between aquifer layers fluctuate and even reverse in several parts of the basin as recharge and pumpage rates change seasonally and annually. The majority of recharge to the Cuyama Valley occurs from stream loss in the upland regions of Ventucopa and Sierra Madre Foothills, and the largest fractions of pumpage and storage depletion occur in the Main-zone subregions. The long-term imbalance between inflows and outflows results in modeled overdraft of the groundwater basin over the 61-year period 1949–2010. Changes in storage vary considerably from year to year, depending on land use, pumpage, and climate conditions. Climate-driven factors can greatly affect inflows, outflows, and water use by as much as a factor of two between wet and dry years. While inflows during inter-decadal wet years partly replenish water in the basin, the longer-term water use and storage depletion from pumping have restricted the effects of these major recharge events. Maps of simulated and measured water-level altitudes indicate large regions where depressed water levels have resulted in large desaturated zones in the recent and Older Alluvium layers in the Main-zone subregions. The projections of the base-case scenario and 2010 land use 61 years into the future indicates that current supply-and-demand are not sustainable (assuming that the past 61 years are representative of future climate) and will result in the potential for additional groundwater-level declines and related storage depletion and land subsidence.

References Cited

- Allen, R.G., Pereira, L.S., Raes, D., and Smith, M., 1998, Crop evapotranspiration—Guidelines for computing crop water requirements: Food and Agriculture Organization of the United Nations, Irrigation and Drainage Paper 56, 300 p.
- Alley, W.M., and Leake, S.A., 2004, The journey from safe yield to sustainability: *Ground Water*, v. 42, no. 1, p. 12–16.
- Anderson, J.R., Hardy, E.E., Roach, J.T., and Witmer, R.E., 1976, A land use and land cover classification system for use with remote sensor data: U.S. Geological Survey Professional Paper 964, 28 p.
- Bazeley, W.J.M., ed., 1988, Tertiary tectonics and sedimentation in the Cuyama basin, San Luis Obispo, Santa Barbara, and Ventura Counties, California: Society of Economic Paleontologists and Mineralogists, Pacific Section, Book 59, p. 87–98.
- Belitz, Kenneth, and Phillips, S.P., 1995, Alternative to agricultural drains in California's San Joaquin Valley: Results of a regional-scale hydrogeologic approach: *Water Resources Research*, v. 31, no. 8, p. 1845–1862.
- Belitz, Kenneth, Phillips, S.P., and Gronberg, J.M., 1993, Numerical simulation of ground-water flow in the central part of the Western San Joaquin Valley, California: U.S. Geological Survey Water-Supply Paper 2396, 69 p.
- Bredehoeft, J. D., 1997, Safe yield and the water budget myth, *Ground Water*, v. 35, no. 6, p. 929
- Bredehoeft, J. D., 2002, The water budget myth revisited: why hydrogeologists model: *Ground Water*, vol. 40., no. 4, p. 340–345.
- Bredehoeft, J.D., Papadopolous, S.S., and Cooper Jr., H.H., 1982, The water budget myth, *in* Scientific Basis of Water Resources Management: National Academy Press, Washington, D.C., p. 51–57.
- Brohman, R., and Bryant, L. eds., 2005, Existing vegetation classification and mapping technical guide: Gen. Tech. Rep. WO-67, Washington, DC: U.S. Department of Agriculture Forest Service, Ecosystem Management Coordination Staff, 305 p.
- Brouwer, C. and Heibloem, M., 1986, Irrigation water management: training manual no. 3—Irrigation water needs: Food and Agriculture Organization of the United Nations, Land and Water Development Division.
- Brouwer, C., Goffeau, A., and Heibloem, M., 1985, Irrigation water management: Training manual no. 1—Introduction into Irrigation. Food and Agriculture Organization of the United Nations, Land and Water Development Division, 91p.
- Brush, C.F., Belitz, K., and Phillips, S.P., 2004, Estimation of a water budget for 1972–2000 for the Grasslands Area, Central Part of the Western San Joaquin Valley, California: U.S. Geological Survey Scientific Investigations Report 2004–5180, 51p.
- Burow, K.R., Shelton, J.L., Hevesi, J.A., and Weissmann, G.S., 2004, Hydrogeologic characterization of the Modesto area, San Joaquin Valley, California: U.S. Geological Survey Scientific Investigations Report 2004–5232, 54 p.
- California Department of Water Resources, 1994, California water plan update: Bulletin 160-93, California Department of Water Resources, Sacramento, Calif.
- California Department of Water Resources, 2000, Explanations of land use attributes used in database files associated with shape files: Land and Water Use Section, 11 p.
- California Department of Water Resources, 2003, California's Groundwater: Bulletin 118 Update 2003, Chapter 6: Basic Groundwater Concepts: accessed May 1, 2012, http://www.water.ca.gov/pubs/groundwater/bulletin_118/california%27s_groundwater_bulletin_11_-_update_2003_/bulletin118-chapter6.pdf.
- California Department of Water Resources, 2007, California Irrigation Management Information System: <http://www.cimis.water.ca.gov/cimis/welcome.jsp>.
- California Department of Water Resources, 2013, California Irrigation Management Information System: accessed January 20, 2013, <http://www.cimis.water.ca.gov/cimis/welcome.jsp>.
- Daly, C., Halbleib, M., Smith, J. I., Gibson, W. P., Doggett, M. K., Taylor, G. H., Curtis, J., and Pasteris, P. A., 2008, Physiographically sensitive mapping of temperature and precipitation across the conterminous United States: *International Journal of Climatology*, v. 28, no. 15, p. 2031–2064, <http://onlinelibrary.wiley.com/doi/10.1002/joc.1688/abstract>.
- DeLong, S.B., Pelletier, J.D., and Arnold, L.J., 2008, Climate change triggered sedimentation and progressive tectonic uplift in a coupled piedmont-axial system—Cuyama Valley, California, USA: *Earth Surface Processes and Landforms*, v. 33, p. 1033–1046.
- Dibblee, T.W., and Minch, J.A., ed., 2005, Geologic map of the Peak Mountain quadrangle, San Luis Obispo and Santa Barbara Counties, California: Dibblee Geological Foundation Map DF-181, scale 1:24,000.

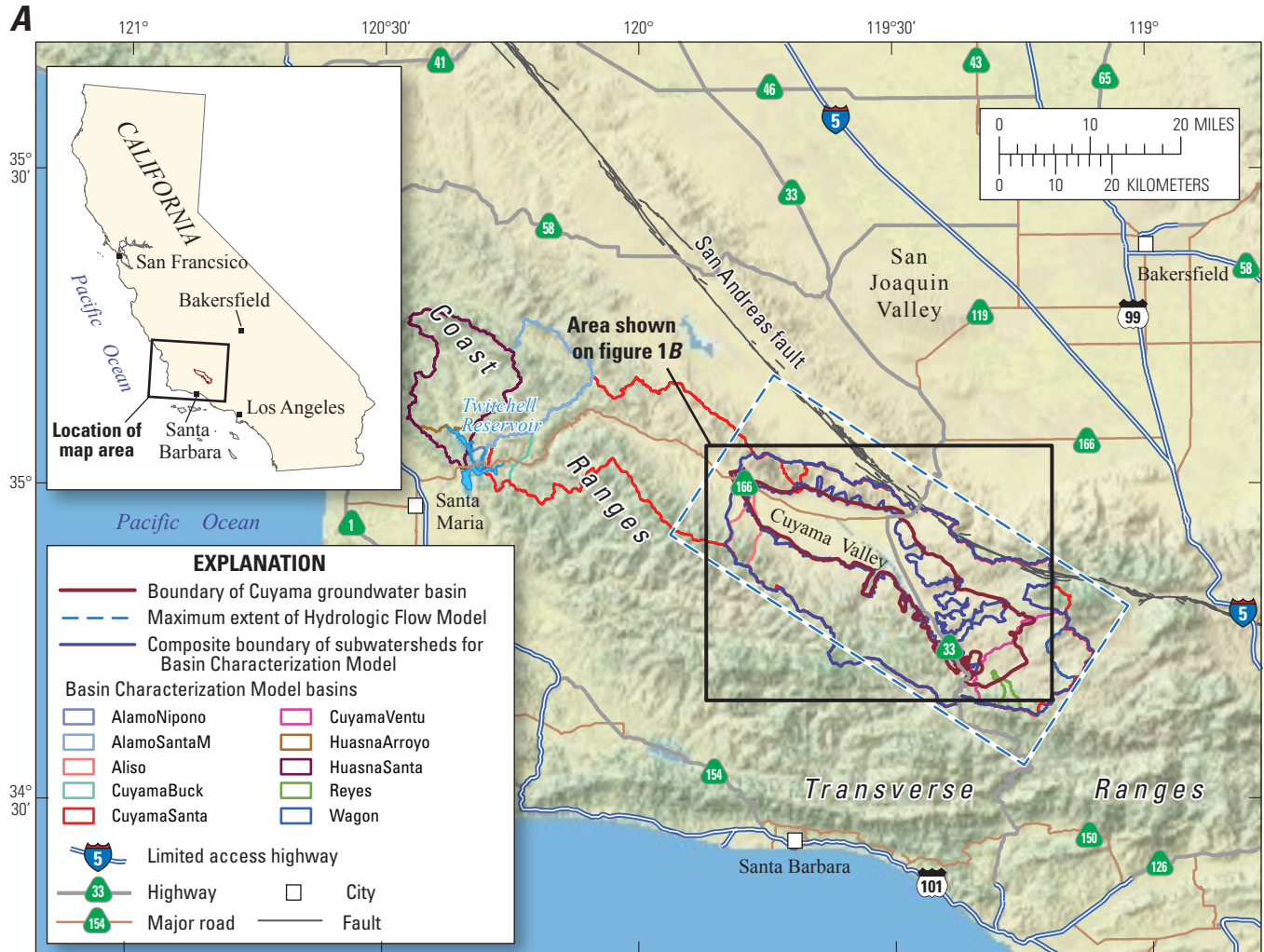
- Dibblee, T.W. Jr., 1982, Geology of the Alamo Mountain, Frazier Mountain, Lockwood Valley, Mount Pinos, and Cuyama Badlands areas, Southern California, *in* Fife, D.L. and Minch, J.A., eds., *Geology and mineral wealth of the California Transverse Ranges: Mason Hill Volume: South Coast Geological Society*, p. 57–77.
- Dickinson, J.E., Hanson, R.T., and Predmore, S.K., 2014, HydroClimATE—Hydrologic and climatic analysis toolkit: U.S. Geological Survey Techniques and Methods 4–A9, 49 p.
- Dimitrakopoulos, Roussos, and Desbarats, A.J., 1993, Geostatistical modeling of grid block permeabilities for 3D reservoir simulators: *Reservoir Engineering*, v. 8, p. 13–18.
- Doherty, J., 2004, PEST Model-independent Parameter Estimation, User Manual: fifth ed. Watermark Numerical Computing Inc.
- Doherty, J., 2010a, PEST, Model-independent parameter estimation—User manual (5th ed., with slight additions): Brisbane, Australia, Watermark Numerical Computing.
- Doherty, J., 2010b, Addendum to the PEST manual: Brisbane, Australia, Watermark Numerical Computing.
- Doherty, J., 2010c, BeoPEST for Windows: Brisbane, Australia, Watermark Numerical Computing.
- Doherty, J.E., and Hunt, R.J., 2010, Approaches to highly parameterized inversion—A guide to using PEST for groundwater-model calibration: U.S. Geological Survey Scientific Investigations Report 2010–5169, 59 p.
- Everett, R.R., Hanson, R.T., and Sweetkind, D.S., 2011, Kirschenmann Road multi-well monitoring site, Cuyama Valley, Santa Barbara County, California: U.S. Geological Survey Open-File Report 2011–1292, 4 p., <http://pubs.usgs.gov/of/2011/1292/>.
- Everett, R.R., Gibbs, D.R., Hanson, R.T., Sweetkind, D.S., Brandt, J.T., Falk, S.E. and Harich, C.R., 2013, Geology, water-quality, hydrology, and geomechanics of the Cuyama Valley groundwater basin, California, 2008–12: U.S. Geological Survey Scientific Investigations Report 2013–5108, 62 p.
- Faunt, C.C., Hanson R.T., Schmid, Wolfgang, Belitz, K., and Predmore, S., 2009a, Documentation of the Ground-water Flow Model, Chap. C *of* Faunt, Claudia, ed., *Ground-Water Availability of California's Central Valley*: U.S. Geological Survey Professional Paper 1766, p. 121–212
- Faunt, C.C., Belitz, K., and Hanson, R.T., 2009b, Texture Model of the Valley Fill Deposits of the Central Valley, California: *Hydrogeology Journal*, DOI 10.1007/s10040-009-0539-7, 25p.
- Federal Geographic Data Committee, 2008, National vegetation classification standard, Ver. 2: FGDC-STD-005-2008, accessed May 5, 2014, <https://www.fgdc.gov/standards/projects/FGDC-standards-projects/vegetation>.
- Fio, J.L., and Leighton, D.A., 1995, Geohydrologic framework, historical development of the ground-water system, and general hydrologic and water-quality conditions in 1990, South San Francisco Bay and Peninsula area, California: U.S. Geological Survey Open-File Report 94–357, 46 p.
- Flint, A.L. and Childs, S.W., 1987, Calculation of solar radiation in mountainous terrain: *Journal of Agricultural and Forest Meteorology*, v. 40, p. 233–249.
- Flint, A.L. and Childs, S.W., 1991, Modification of the Priestley-Taylor equation to estimate evapotranspiration for soil water limited conditions: *Journal of Agricultural and Forest Meteorology*, v. 56, p. 247–260.
- Flint, L.E. and Flint, A.L., 2007, Regional analysis of ground-water recharge, *in* Stonestrom, D. A.; Constantz, J.; Ferré, T. P. A.; and Leake, S.A., eds., *Ground-water recharge in the arid and semiarid southwestern United States*, U.S. Geological Survey Professional Paper 1703, p. 29–59.
- Flint, L.E. and Flint, A.L., 2012, Simulation of climate change in San Francisco Bay Basins, California: Case studies in the Russian River Valley and Santa Cruz Mountains: U.S. Geological Survey Scientific Investigations Report 2012–5132, 55 p.
- Flint, L.E., Flint, A.L., Stolp, B.J., and Danskin, W.R., 2012, A basin-scale approach for assessing water resources in a semiarid environment: San Diego region, California and Mexico, *Hydrology and Earth System Sciences*, v. 16, p. 1–17.
- Gibbs, D., 2010, Cuyama Groundwater Basin: Department of Public Works, Santa Barbara County, 8 p.
- Gibeault, V.A., Cockerham, S., Henry, J.M., and Meyer, J., 1989, California Turfgrass: It's use, water requirement, and irrigation: *California Turfgrass Culture*, University of California Cooperative Extension, v. 39, no. 3–4, 14 p.
- Halford, K.J. and Hanson, R.T., 2002, User guide for the drawdown-limited, multi-node well (MNW) package for the U.S. Geological Survey's modular three-dimensional finite-difference ground-water flow model, versions MODFLOW-96 and MODFLOW-2000: U.S. Geological Survey Open-File Report 02–293, 33 p., <http://water.usgs.gov/pubs/of/2002/ofr02293/>.
- Hanson, R.T., 1988, Aquifer-system compaction, Tucson basin and Avra Valley, Arizona: U.S. Geological Survey Water-Resources Investigation Report 88–4172, 69 p.

- Hanson, R.T., and Benedict, J.F., 1993, Simulation of ground-water flow and potential land subsidence, upper Santa Cruz River Basin, Arizona: U.S. Geological Survey Water-Resources Investigation Report 93-4196, 47 p., <http://pubs.er.usgs.gov/usgspubs/wri/wri934196>.
- Hanson, R.T., and Leake, S.A., 1998, Documentation for HYDMOD, A program for time-series data from the U.S. Geological Survey's modular three-dimensional finite-difference ground-water flow model: U.S. Geological Survey Water-Resources Investigations Report 98-564, 57 p.
- Hanson, R.T., Anderson, S.R., and Pool, D.R., 1990, Simulation of ground-water flow and potential land subsidence, Avra Valley, Arizona: U.S. Geological Survey Water-Resources Investigation Report 90-4178, 41 p., <http://pubs.er.usgs.gov/usgspubs/wri/wri904178>.
- Hanson, R.T., Martin, P., and Koczot, K.M., 2003, Simulation of ground-water/surface-water flow in the Santa Clara-Calleguas Basin, Ventura County, California: U.S. Geological Survey Water-Resources Investigation 02-4136, 214 p.
- Hanson, R.T., Li, Z., and Faunt C., 2004, Documentation of the Santa Clara Valley regional ground-water/surface-water flow model, Santa Clara County, California: Scientific Investigations Report 2004-5231, 75 p., <http://pubs.water.usgs.gov/sir2004-5231/>.
- Hanson, R.T., Dettinger, M.D., and Newhouse, M.W., 2006, Relations between climate variability and hydrologic time series from four alluvial basins across the southwestern United States: *Hydrogeology Journal*, v. 14, no. 7, p. 1122-1146
- Hanson, R.T., Schmid, Wolfgang, Faunt, C.C., and Lockwood, B., 2010, Simulation and Analysis of Conjunctive Use with MODFLOW's Farm Process: *Groundwater*, v. 48, no. 5, p. 674-689, doi: 10.1111/j.1745-6584.2010.00730.x.
- Hanson, R.T., Flint, L.E., Flint, A.L., Dettinger, M.D., Faunt, C.C., Cayan, D., and Schmid, Wolfgang, 2012, A method for physically based model analysis of conjunctive use in response to potential climate changes: *Water Resources Research*, v. 48, 23p., doi:10.1029/2011WR010774
- Hanson, R.T., and Schmid, Wolfgang, 2013, Economic Resilience through "One-Water" Management: U.S. Geological Survey Open-File Report 2013-1175, 2 p.
- Hanson, R.T., Schmid, Wolfgang, Faunt, C. C., Lear, J., and Lockwood, B., 2014a, Integrated Hydrologic Model of Pajaro Valley, Santa Cruz and Monterey Counties, California: U.S. Geological Survey Scientific Investigations Report 2014-5111, 166 p.
- Hanson, R.T., Boyce, S.E., Schmid, Wolfgang, Hughes, J.D., Mehl, S.M., Leake, S.A., Maddock, Thomas, III, and Niswonger, R.G., 2014b, One-Water Hydrologic Flow Model (OWHM): U.S. Geological Survey Techniques and Methods 6-A51, 122 p.
- Harbaugh, A.W., 2005, MODFLOW-2005, the U.S. Geological Survey modular ground-water model—the Ground-Water Flow Process: U.S. Geological Survey Techniques and Methods 6-A16, variously paginated.
- Harbaugh, A.W., Banta, E.R., Hill, M.C., and McDonald, M.G., 2000, MODFLOW-2000: U.S. Geological Survey modular ground-water model—User guide to modularization concepts and the ground-water flow process: U.S. Geological Survey Open-File Report 00-92, 121 p.
- Hill, M.C., 1990, Preconditioned conjugate-gradient 2 (PCG2), a computer program for solving ground-water flow equations: U.S. Geological Survey Water-Resources Investigations Report 90-4048, 43 p.
- Hill, M.C., and Tiedeman, C.R., 2007, Effective groundwater model calibration: with analysis of data, sensitivities, predictions, and uncertainty: New York, Wiley and Sons, 464 p.
- Hill, M.C., Banta, E.R., Harbaugh, A.W., and Anderman, E.R., 2000, MODFLOW-2000, The U.S Geological Survey modular ground-water model—User guide to the observation, sensitivity, and parameter-estimation processes and three post-processing programs: U.S. Geological Survey Open-File Report 00-184, 209 p.
- Hill, M.L., Carlson, S.A., and Dibblee, T.W., Jr., 1958, Stratigraphy of Cuyama Valley-Caliente Range Area, California: *American Association of Petroleum Geologists Bulletin*, v. 42, p. 2973-3000.
- Holzer, T.L., 1981, Preconsolidation stress of aquifer systems in areas of induced land subsidence: *Water Resources Research*, v. 17, no. 3, p. 693-704.
- Homer, C.H., Fry, J.A., and Barnes C.A., 2012, The national land cover database: U.S. Geological Survey Fact Sheet 2012-3020, 4 p.
- Hsieh, P.A., and Freckelton, J.R., 1993, Documentation of a computer program to simulate horizontal-flow barriers using the U.S. Geological Survey's modular three-dimensional finite-difference ground-water-flow model: U.S. Geological Survey Open-File Report 92-477, 32 p.
- Jacob, C. E., 1940, On the flow of water in an elastic artesian aquifer: *Transactions of the American Geophysical Union*, v. 21, no. 2, p. 574-586.

- Jacob, C. E., 1946, Drawdown test to determine effective radius of artesian well: American Society of Civil Engineers Proceedings, v. 72, May.
- Jennings, C. W., 1977, Geologic map of California: California Division of Mines and Geology Geologic Data Map Number 2, scale 1:750,000.
- Lagoe, M.B., 1987, Middle Cenozoic basin development, Cuyama Basin, California, *in* Ingersoll, R.V. and Ernst, W.G., eds., Cenozoic basin development of coastal California, Rubey volume VI : Prentice-Hall, Englewood Cliffs, New Jersey, p. 172–206.
- Lantis, D.W., Steiner, R., Karinen, A.E., 1977, California, Land of Contrast, 3d ed: Kendall/Hunt Publishing Company, Dubuque, Iowa.
- Laudon, Julie, and Belitz, Kenneth, 1991, Texture and depositional history of late pleistocene-holocene alluvium in the central part of the western San Joaquin Valley, California: Bulletin of the Association of Engineering Geologists, v. 28, no. 1, p. 73–88.
- Leighton, D.A., Fio, J.L., and Metzger, L.F., 1994, Database of well and areal data, South San Francisco Bay and Peninsula area, California: U.S. Geological Survey Water-Resources Investigations Report 94–4151, 47 p.
- Mueller, R., Yang, Z., Han, W., and Di, L., 2011, CropScape: A new web based visualization portal for the dissemination of NASS geospatial cropland products: USDA National Agricultural Statistics Service, 33 p, http://www.nass.usda.gov/Education_and_Outreach/Reports,_Presentations_and_Conferences/Presentations/Mueller_WSS11_CropScape.pdf.
- National Renewable Energy Laboratory, 2014, Measurement and instrumentation data center (MODC): U.S. Department of Energy, Golden, Colo., <http://www.nrel.gov/modc/>, last accessed June 15, 2014.
- Newhouse, M.W., Hanson, R.T., Wentworth, C.M., Everett, R., Williams, C. F., Tinsley J., Noce, T. E., and Carkin, B.A., 2004, Geologic, water-chemistry, and hydrologic data from multiple-well monitoring sites and selected water-supply wells in the Santa Clara Valley, California, 1999–2003: U.S. Geological Survey Scientific Investigations Report 2004–5250, 134 p.
- Niswonger, R.G., and Prudic, D.E., 2005, Documentation of the Streamflow-Routing (SFR2) Package to include unsaturated flow beneath streams—A modification to SFR1: U.S. Geological Survey Techniques and Methods 6-A13.
- Niswonger, R.G., Prudic, D.E., and Regan, R.S., 2006, Documentation of the Unsaturated-Zone Flow (UZFI) Package for modeling unsaturated flow between the land surface and the water table with MODFLOW-2005: U.S. Geological Survey Techniques and Methods 6-A19, 62 p.
- Niswonger, R.G., Panday, Sorab, and Ibaraki, Motomu, 2011, MODFLOW-NWT, A Newton formulation for MODFLOW-2005: U.S. Geological Survey Techniques and Methods 6–A37, 44 p.
- Phillips, S.P., and Belitz, Kenneth, 1991, Calibration of a textured-based model of a ground-water flow system, western San Joaquin Valley, California: Groundwater, v. 29, no. 5, p. 702–715.
- Phillips, S.P., Green, C.T., Burow, K.R., Shelton, J.L., and Rewis, D.L., 2007, Simulation of multiscale ground-water flow in part of the northeastern San Joaquin Valley, California: U.S. Geological Survey Scientific Investigations Report 2007–5009, 43 p.
- Poeter, E.P., Hill, M.C., Banta, E.R., Mehl, Steffen, and Christensen, Steen, 2005, UCODE_2005 and six other computer codes for universal sensitivity analysis, calibration, and uncertainty evaluation: U.S. Geological Survey Techniques and Methods 6–A11, 283 p.
- Prudic, D.E., Konikow, L.F., and Banta, E.A., 2004, A new Streamflow-Routing (SFR1) package to simulate stream-aquifer interaction with MODFLOW-2000: U.S. Geological Survey Open-File Report 04–1042, 95 p.
- Riley, F.S., 1969, Analysis of borehole extensometer data from central California, *in* Tison, L.J., ed., Land subsidence: Volume 2: Proceedings of the Tokyo Symposium, September 1969, International Association of Scientific Hydrology Publication 89, p. 423–431, accessed November 23, 2007, <http://www.cig.ensmp.fr/~iahs/redbooks/a088/088047.pdf>.
- Schmid, Wolfgang, and Hanson R.T., 2009, The farm process version 2 (FMP2) for MODFLOW-2005—Modifications and upgrades to FMP1: U.S. Geological Survey Techniques in Water Resources Investigations, Book 6, Chapter A32, 102 p.
- Schmid, Wolfgang, Hanson, R.T., Maddock III, T.M., and Leake, S.A., 2006a, User’s guide for the farm process (FMP) for the U.S. Geological Survey’s modular three-dimensional finite-difference ground-water flow model, MODFLOW-2000: U.S. Geological Survey Techniques and Methods 6-A17, 127 p.

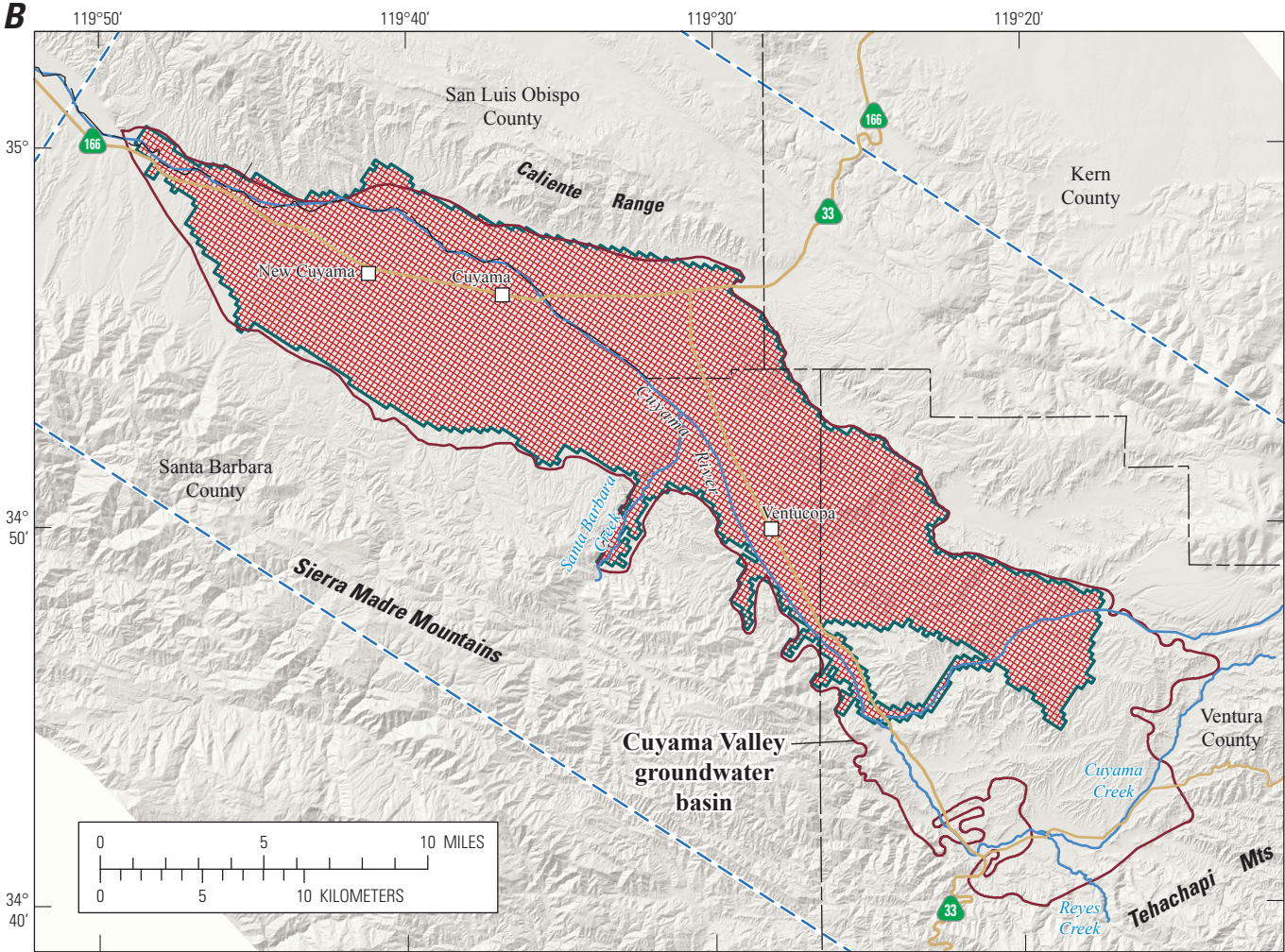
- Schmid, Wolfgang, Hanson, R.T., and Maddock III, Thomas, 2006b, Overview and advances of the farm process for MODFLOW-2000: Managing groundwater systems: Conference Proceedings, International Groundwater Modeling Center, Golden, Colo., May 21–24, 2006, p. 23–27
- Singer, J.A., and Swarzenski, W.V., 1970, Pumpage and ground-water storage depletion in Cuyama Valley California, 1947–66: U.S. Geological Survey Open-File Report 70–304, 24 p.
- Snyder, R.L., and Schullbach, K.F., 1992, Central coast Crop Coefficients for Field and Vegetable Crops: California Department of Water Resources, Water Conservation Office, Drought Tips No. 92-45, 12 p.
- Snyder, R.L., Lamina, B.J., Shaw, D.A., and Pruitt, W.O., 1987a, Using reference evapotranspiration (ET_o) and crop coefficients to estimate crop evapotranspiration (Et_{ch}) for agronomic crops, grasses, and vegetable crops: Leaflet 21427, Cooperative Extension of the University of California Division of Agriculture and Natural Resources, Berkeley, Calif., 12 p.
- Snyder, R.L., Lamina, B.J., Shaw, D.A., and Pruitt, W.O., 1987b, Using reference evapotranspiration (ET_o) and crop coefficients to estimate crop evapotranspiration (Et_{ch}) for trees and vines: Leaflet 21428, Cooperative Extension of the University of California, Division of Agriculture and Natural Resources, Berkeley, Calif., 8 p.
- Sweetkind, D.S., Faunt, C.C., and Hanson, R.T., 2013, Construction of 3-D geologic framework and textural models for Cuyama Valley groundwater basin, California: U.S. Geological Survey Scientific Investigations Report 2013–5127, 46 p.
- Terzaghi, Karl, and Peck, R.B., 1948, Soil mechanics in engineering practice: New York, John Wiley and Sons, Inc. 566 p.
- Thorne, J.H., Flint, L.E., Flint, A.L., Boynton, R., and Thuy- N’goc Le, 2012, Development and application of downscaled hydroclimatic predictor variables for use in climate vulnerability and assessment studies: California Energy Commission, Publication number: CEC-500-2012-010.
- University of Arizona, 2012, The Arizona meteorological network: Arizona Cooperative Extension, College of Agriculture and Life Sciences, accessed May 2013, <http://ag.arizona.edu/azmet/>.
- Upson, J.E., and Worts, G.F., 1951, Ground water in the Cuyama Valley, California: U.S. Geological Survey Water Supply Paper 1110–B, 81 p.
- U.S. Census Bureau, 2014a, , Census data 1950 and 1960: U.S. Census Bureau, accessed March 27, 2014, <http://www.census.gov/population/cencounts/ca190090.txt>.
- U.S. Census Bureau, 2014b, Census data for 2010: U.S. Census Bureau, accessed March 25, 2014, <http://www.census.gov/2010census/popmap/>
- U.S. Department of Agriculture Natural Resources Conservation Service, 2005, Soil survey geographic (SSURGO) database: USDA Natural Resources Conservation Service, accessed September 12, 2005, <http://www.nrcs.usda.gov/products/datasets/ssurgo/>.
- U.S. Department of Agriculture Natural Resources Conservation Service, 2006, State soil survey map (SSURGO): U.S. Department of Agriculture, accessed July 2010, <http://soildatamart.nrcs.usda.gov>.
- U.S. Department of Agriculture, 2007, Existing Vegetation—CALVEG, [ESRI personal geodatabase], McClellan, CA: USDA Forest Service, Pacific Southwest Region, Remote Sensing Laboratory, accessed August 19, 2011, <http://www.fs.usda.gov/detail/r5/landmanagement/resourcemanagement/?cid=stelprdb5347188>.
- U.S. Department of Agriculture, 2012, Cropscape raster data sets: U.S. Department of Agriculture, accessed, January 2013, <http://nassgeodata.gmu.edu/CropScape/>.
- U.S. Geological Survey, 1990, Land use and land cover digital data from 1:250,000- and 1:100,000-scale maps—Data User Guide 4.: U.S. Geological Survey, Reston, Va.
- U.S. Geological Survey, 1999a, National land cover digital data: U.S. Geological Survey, <http://edc.usgs.gov/products/landcover/nlcd.html>.

Figures



Shaded relief base from ESRI ArcGIS Online Map Service
http://services.arcgisonline.com/arcgis/services/ESRI_ShadedRelief_World_2D.
 Roads from Cal-Atlas Geospatial Clearinghouse <http://atlas.ca.gov/download.html>
 Place names sourced from USGS Geographic Names Information System,
 1974-2009. San Andreas fault from Bryant (2005). Albers Projection, NAD83

Figure 1. A, Cuyama Valley watershed and groundwater basin, and B, detailed location map with the active hydrologic model grid, groundwater basin, and major rivers, Cuyama Valley, California.

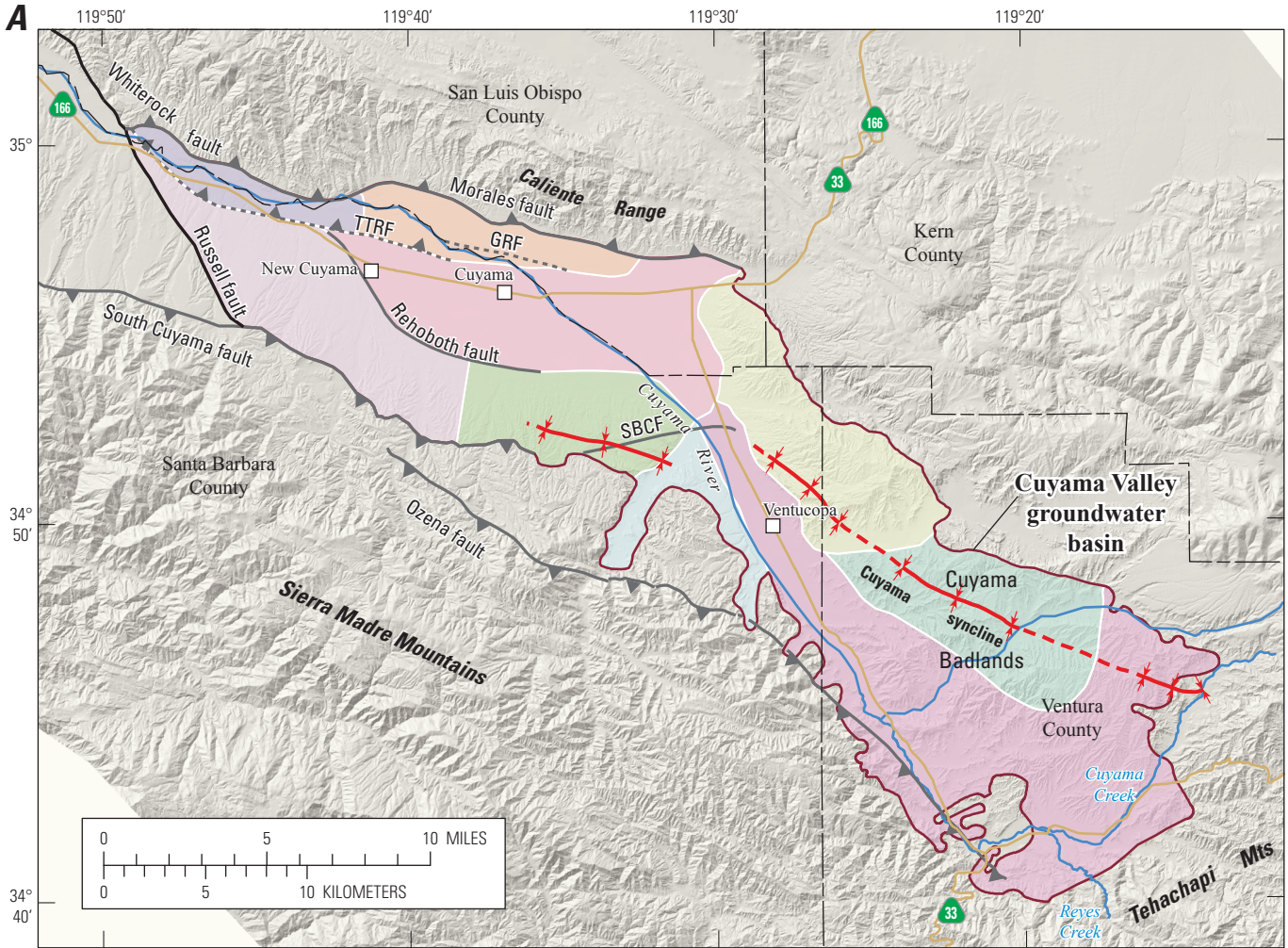


Shaded relief base created from 30-m digital elevation model from USGS National Elevation Dataset (NED); North America Vertical Datum 1983 (NAVD83). Hydrology sourced from 1:24,000-scale National Hydrography Dataset, 1974-2009. Place names sourced from USGS Geographic Names Information System, 1974-2009. Albers Projection, NAD83.

EXPLANATION

-  Active CUVHM model-grid boundary
-  Active model-grid
-  Maximum extent of Hydrologic Flow Model from figure 1A
-  Major river or stream

Figure 1. —Continued



Shaded relief base created from 30-m digital elevation model from USGS National Elevation Dataset (NED); North America Vertical Datum 1983 (NAVD83). Hydrology sourced from 1:24,000-scale National Hydrography Dataset, 1974-2009. Place names sourced from USGS Geographic Names Information System, 1974-2009. Albers Projection, NAD83.

EXPLANATION

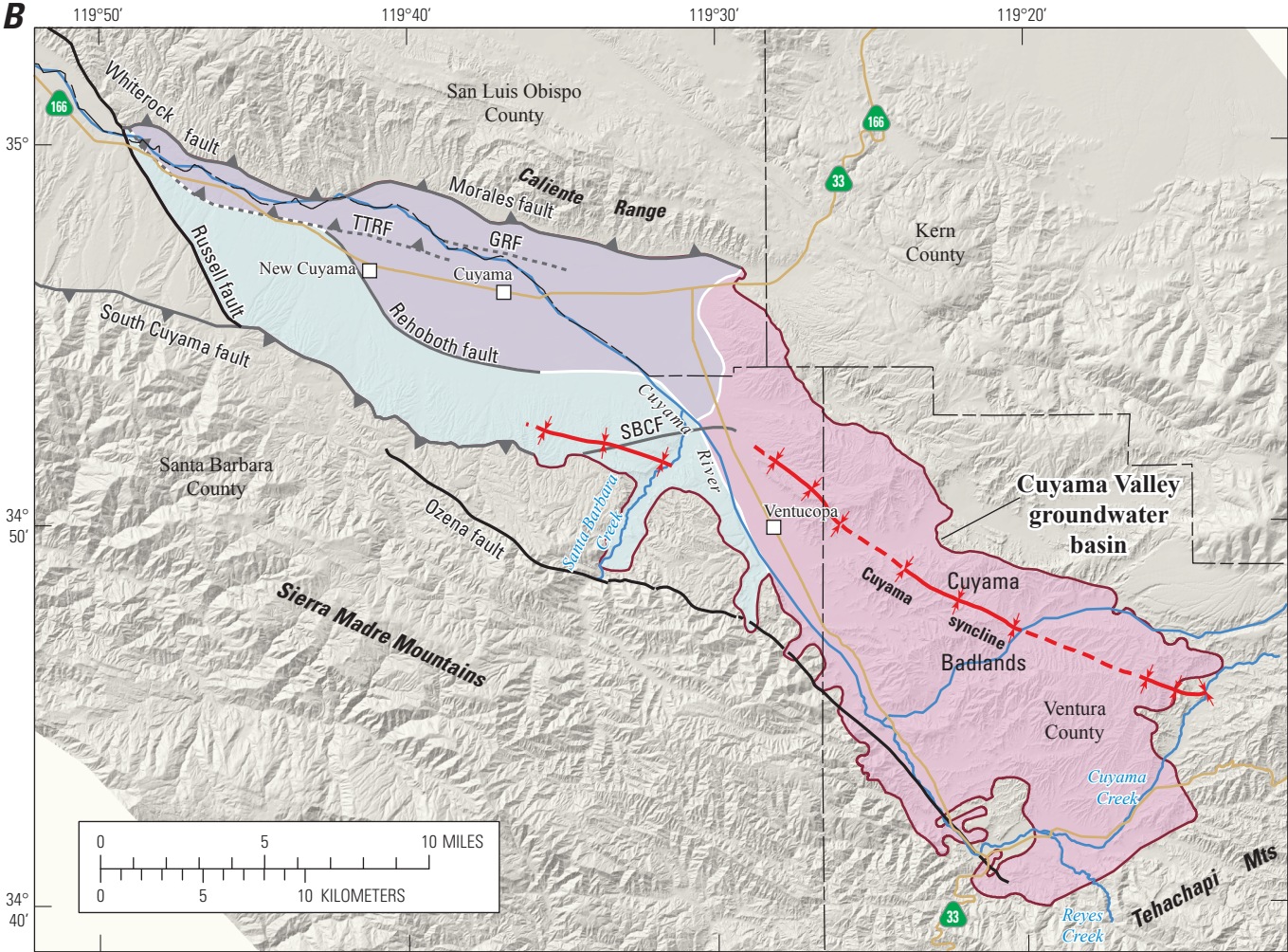
Cuyama groundwater basin subregions (table 1)

- Caliente/Northern-Main (CNMZ)
- Central Sierra Madre Foothills (CSMFH)
- Northeast Ventucopa Uplands (NEVU)
- Northwestern Sierra Madre Foothills (NSMFH)
- Northern Ventucopa Uplands (NVU)
- Southern Sierra Madre Foothills (SSMFH)
- Southern Ventucopa Uplands (SVU)
- Southern-Main (SMZ)
- Western-Main (WMZ)

See table 1 for subregion designation

- Normal fault
- Thrust fault
- Thrust fault, concealed
- Syncline
- Syncline, concealed
- GRF, Graveyard fault;
- SBCF, Santa Barbara Canyon fault;
- TTRF, Turkey Trap Ridge fault

Figure 2. A, Groundwater hydrologic subregions and related geologic structures; B, simplified Cuyama major groundwater regions; and C, groups of landscape water-balance subregions for 1943–2010 in Cuyama Valley, California.



Shaded relief base created from 30-m digital elevation model from USGS National Elevation Dataset (NED); North America Vertical Datum 1983 (NAVD83). Hydrology sourced from 1:24,000-scale National Hydrography Dataset, 1974-2009. Place names sourced from USGS Geographic Names Information System, 1974-2009. Albers Projection, NAD83.

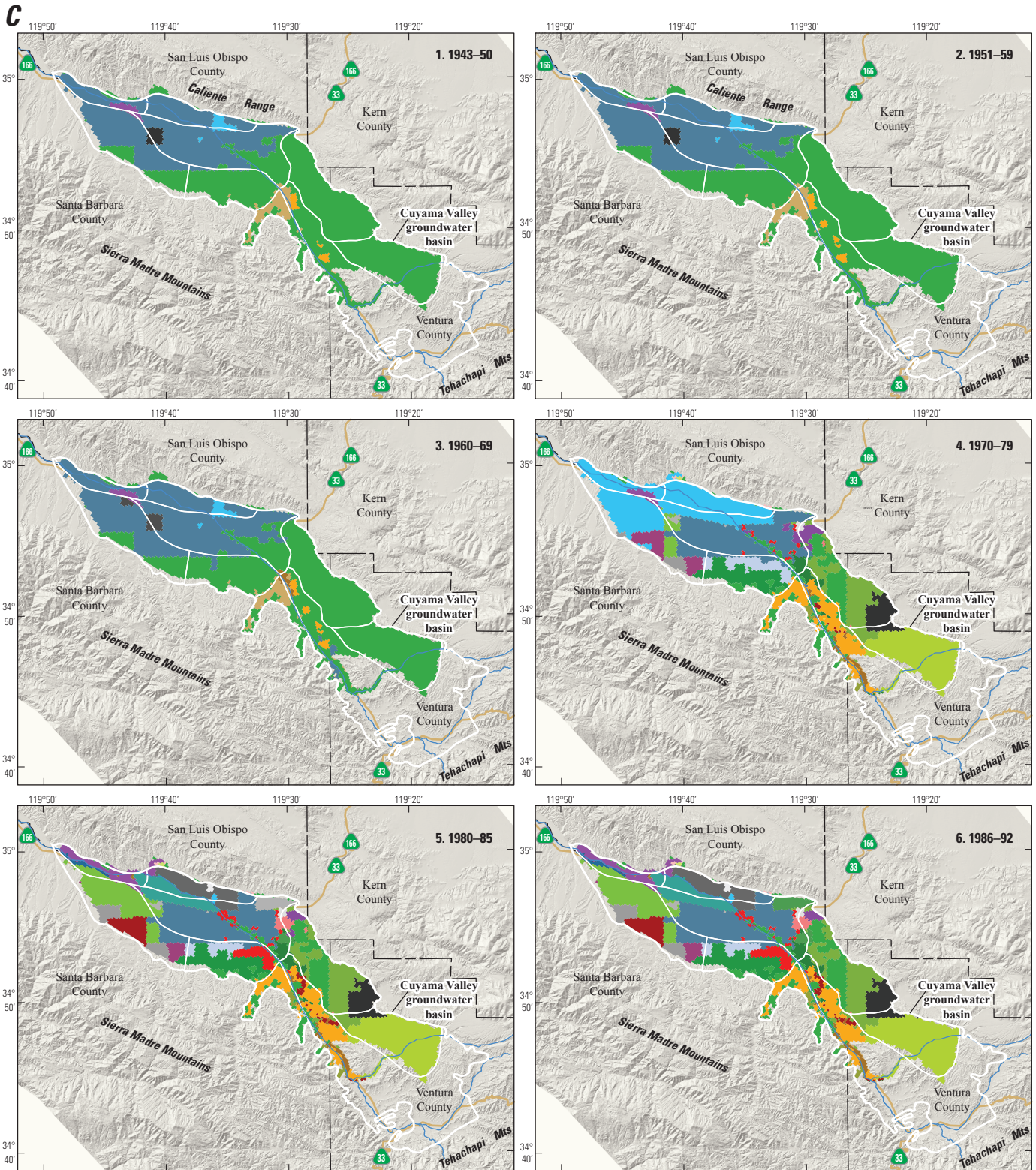
EXPLANATION

Simplified Cuyuma groundwater basin zones

- Main
- Sierra Madre Foothills
- Ventucopa Uplands

- Normal fault
 - ▲ Thrust fault
 - ▲- Thrust fault, concealed
 - ⋈ Syncline
 - - - Syncline, concealed
- GRF, Graveyard fault;
 SBCF, Santa Barbara Canyon fault;
 TTRF, Turkey Trap Ridge fault

Figure 2. —Continued

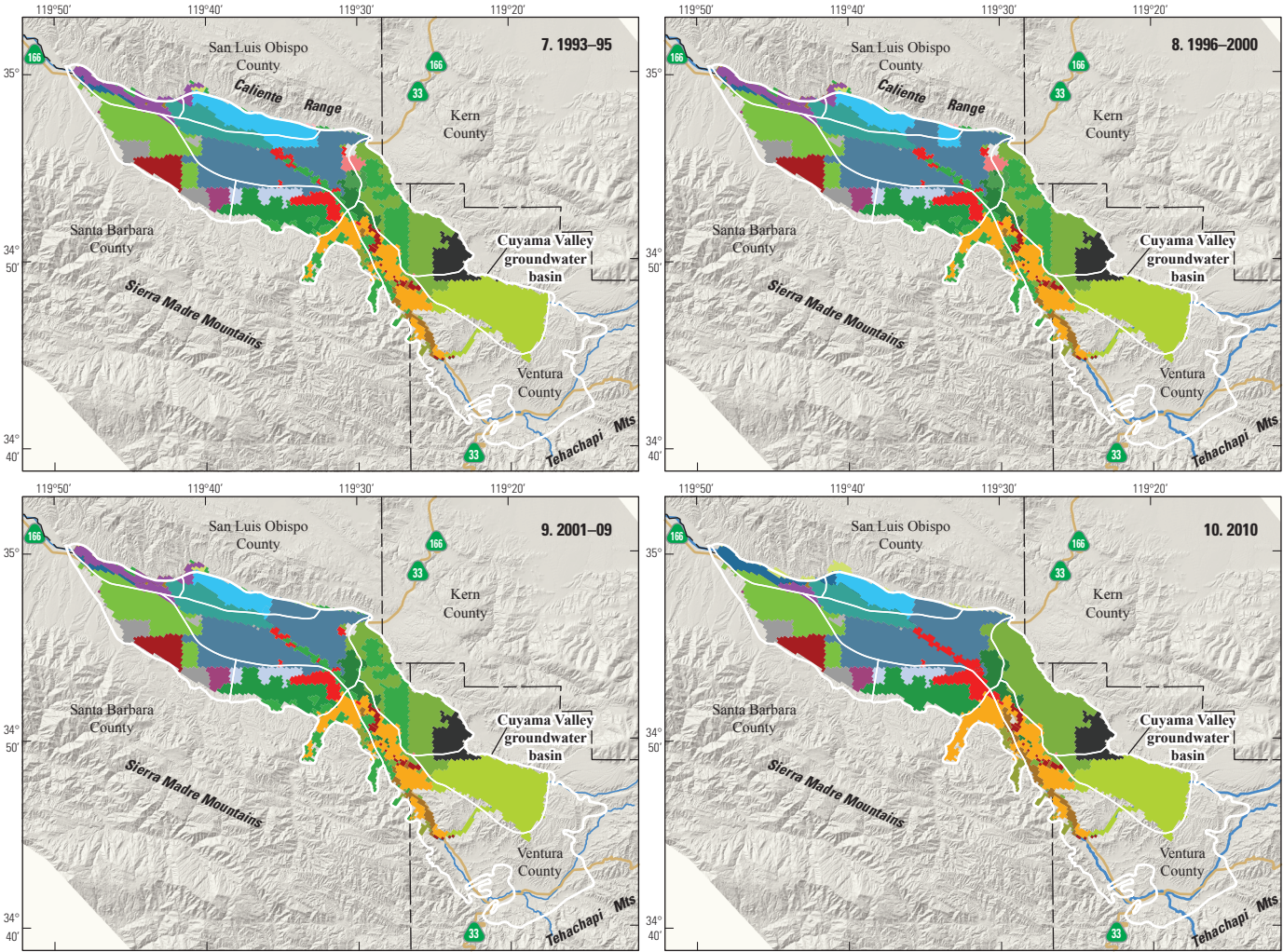


Shaded relief base created from 30-m digital elevation model from USGS National Elevation Dataset (NED); North America Vertical Datum 1983 (NAVD83). Hydrology sourced from 1:24,000-scale National Hydrography Dataset, 1974-2009. Place names sourced from USGS Geographic Names Information System, 1974-2009. Albers Projection, NAD83.



Figure 2. —Continued

C (Continued)



Shaded relief base created from 30-m digital elevation model from USGS National Elevation Dataset (NED); North America Vertical Datum 1983 (NAVD83). Hydrology sourced from 1:24,000-scale National Hydrography Dataset, 1974-2009. Place names sourced from USGS Geographic Names Information System, 1974-2009. Albers Projection, NAD83.



EXPLANATION

Farm groundwater ID for 1943 to 1969

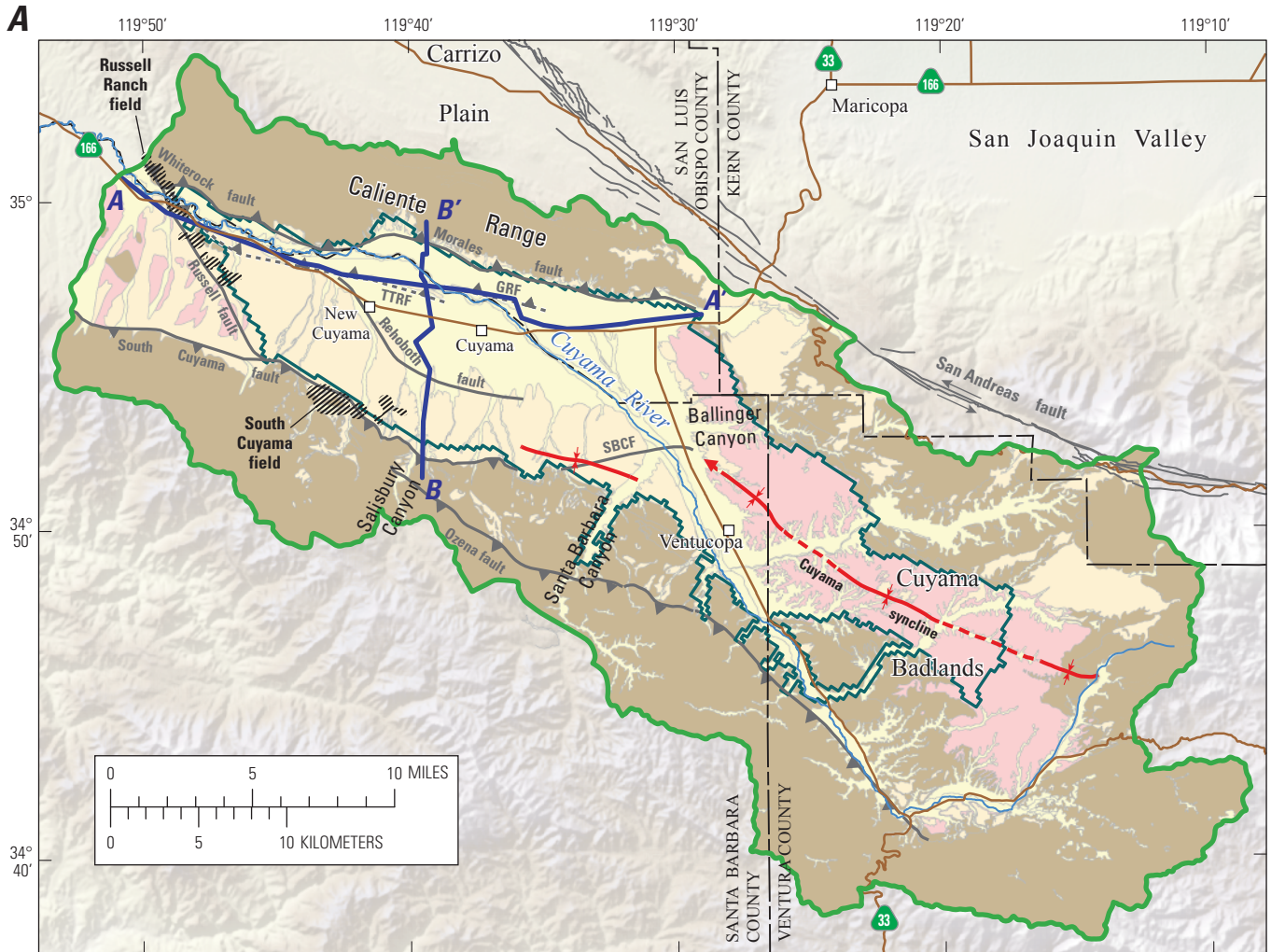
- | | |
|---|---|
| Zone_primary use | |
| ■ CNMZ_Ag | ■ Native |
| ■ SMZ_Ag | |
| ■ SMZ_Dom | |
| ■ SMZ_Ind | |
| ■ SSMFH_Rch | |
| ■ SVU_Ag | |
| ■ SVU_Ind | |
| ■ WMZ_Ag | |

See table 1 and figure 2A for zone designation

Farm groundwater ID for 1970 to 2010

- | | | | | | |
|--|--|--|---|------------------|--|
| Zone_primary use | | Zone_primary use | | Zone_primary use | |
| ■ CNMZ_Ag | ■ NVU_Ag | ■ NSMZ_Nat | ■ Native | | |
| ■ CNMZ_Dom | ■ NVU_Dom | ■ SSMFH_Nat | | | |
| ■ CNMZ_Ind | ■ NVU_Ind | ■ SVU_Ag | | | |
| ■ CNMZ_Nat | ■ NVU_Nat | ■ SVU_Dom | | | |
| ■ CNMZ_Urb | ■ NVU_Urb | ■ SVU_Ind | | | |
| ■ CSMFH_Ag | ■ SMZ_Ag | ■ SVU_Nat | | | |
| ■ CSMFH_Nat | ■ SMZ_Dom | ■ SVU_Rch | | | |
| ■ NEVU_Nat | ■ SMZ_Nat | ■ WMZ_Ag | | | |
| ■ NSMFH_Ag | ■ SMZ_Rch | ■ WMZ_Nat | | | |
| ■ NSMFH_Urb | ■ SMZ_Urb | ■ WMZ_Rch | | | |

Figure 2. —Continued



Shaded relief base created from 30-m digital elevation model from USGS National Elevation Dataset (NED); North American Vertical Datum 1983 (NAVD83). Hydrology sourced from 1:24,000-scale National Hydrography Dataset, 1974-2009. Place names sourced from USGS Geographic Names Information System, 1974-2009. San Andreas fault from Bryan (2005). Albers Projection, NAD83.

Modified from Sweetkind and others, 2013

EXPLANATION

Generalized stratigraphic units

- Recent alluvial aquifer
- Older alluvial aquifer
- Morales Formation aquifer
- Bedrock

- Normal fault
- ▲ Thrust fault
- Thrust fault, concealed
- ↔ Strike-slip fault

GRF, Graveyard Ridge fault;
SBCF, Santa Barbara Canyon fault;
TTRF, Turkey Trap Ridge fault

- ↘ Syncline, showing plunge direction
- Syncline, concealed
- Composite subbasin boundary for Basin Characterization Model
- Active model-grid boundary for CUVHM model
- ▨ Oil field
- A — A' Line of section

Figure 3. Generalized A, outcrops of geologic units and major faults within model grid; B, axial hydrogeologic cross-section (A–A’); and C, transverse hydrogeologic cross-section (B–B’) of Cuyama Valley, California.

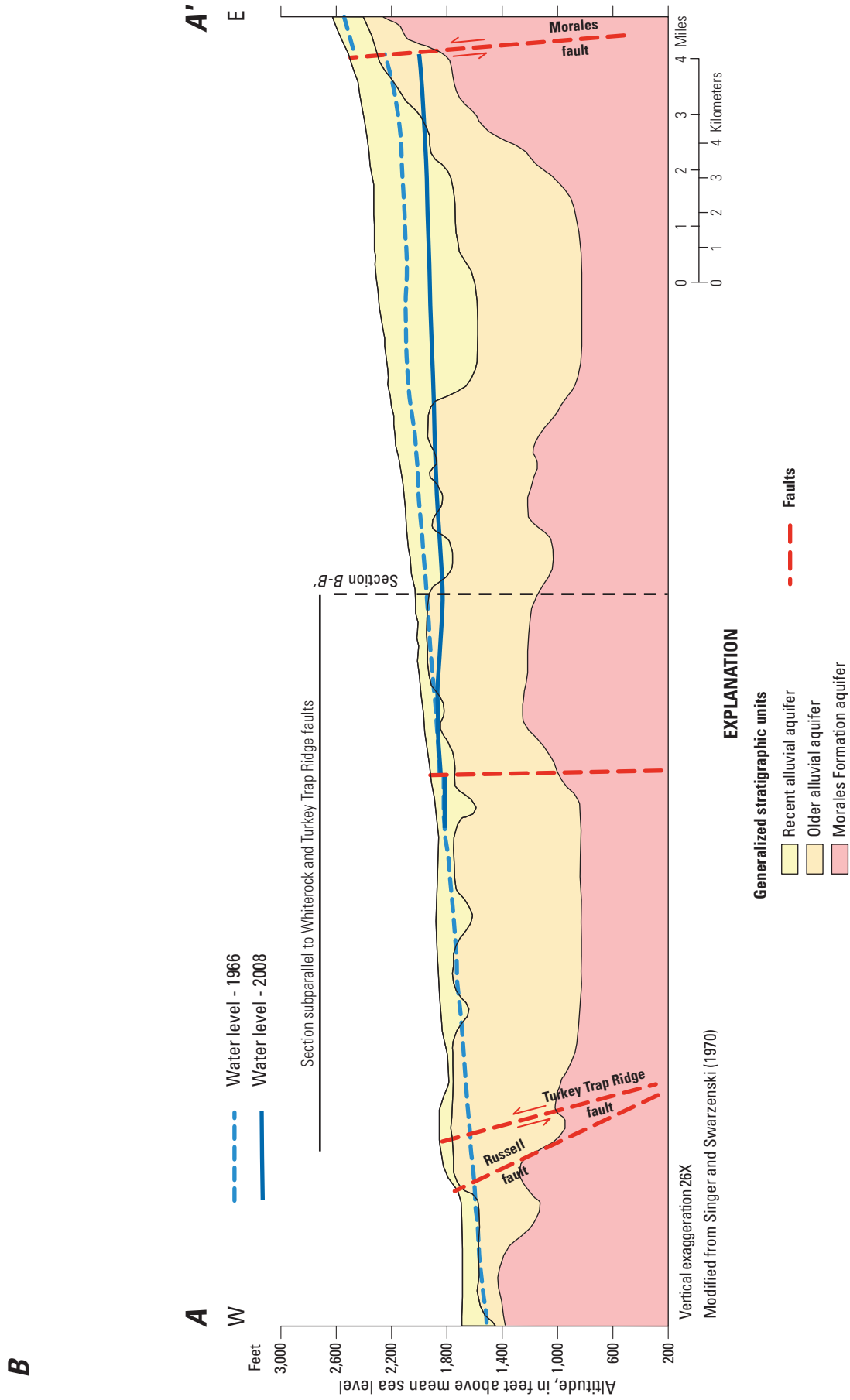


Figure 3. —Continued

C

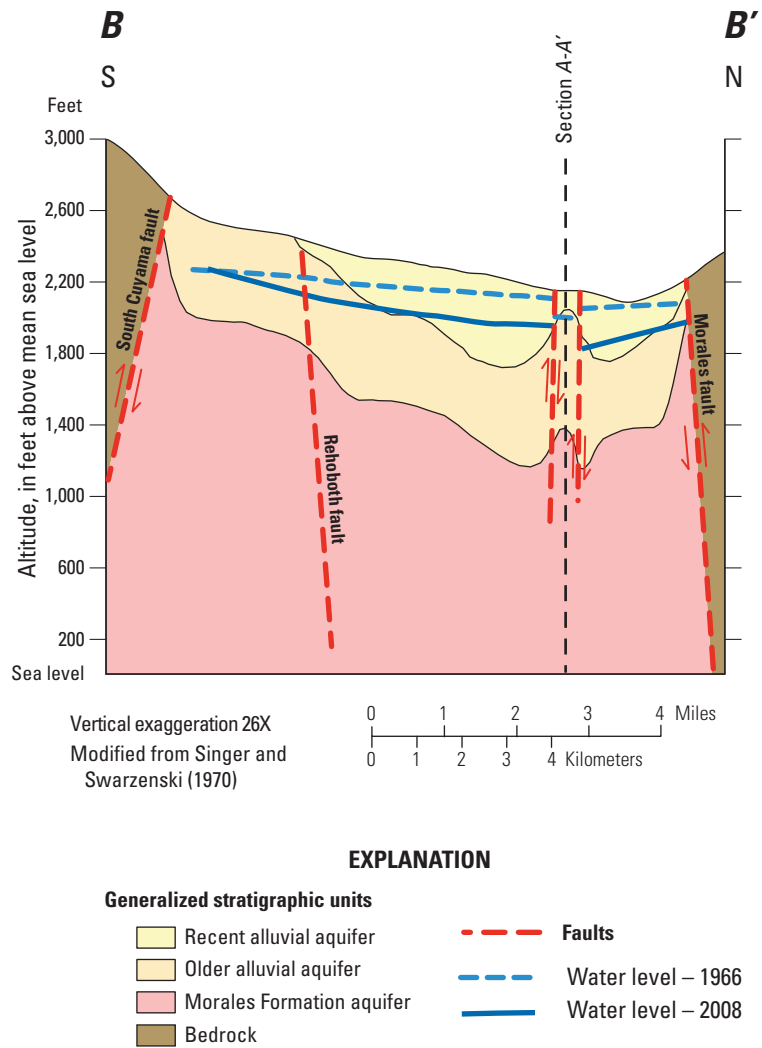
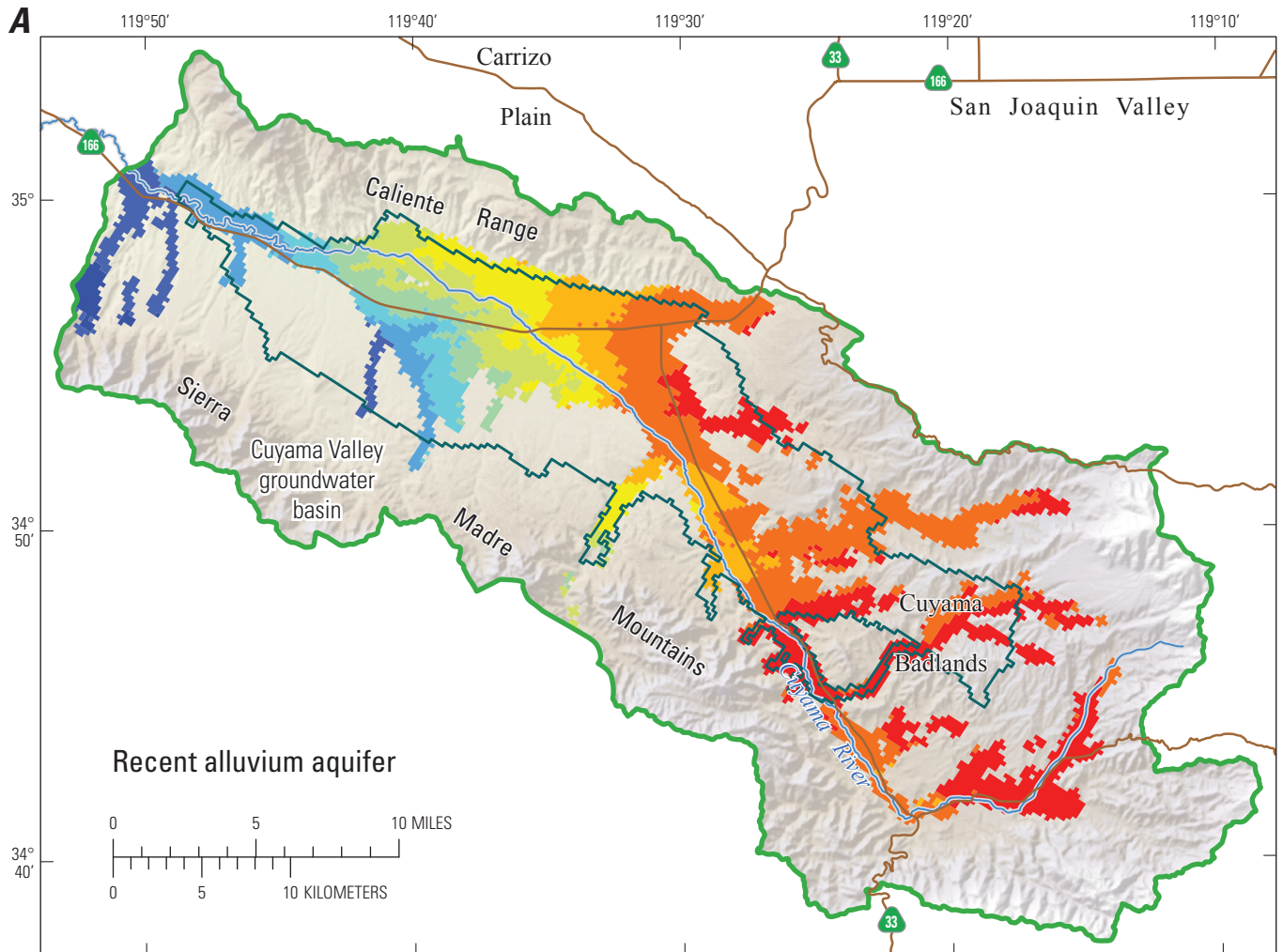


Figure 3. —Continued

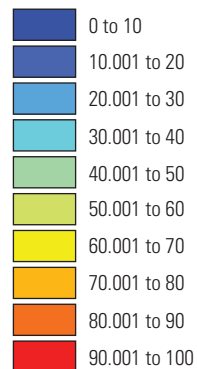


Shaded relief base created from 30-m digital elevation model from USGS National Elevation Dataset (NED); North American Vertical Datum 1983 (NAVD83). Hydrology sourced from 1:24,000-scale National Hydrography Dataset, 1974-2009. Place names sourced from USGS Geographic Names Information System, 1974-2009. Albers Projection, NAD83.

EXPLANATION

Estimated sedimentary texture

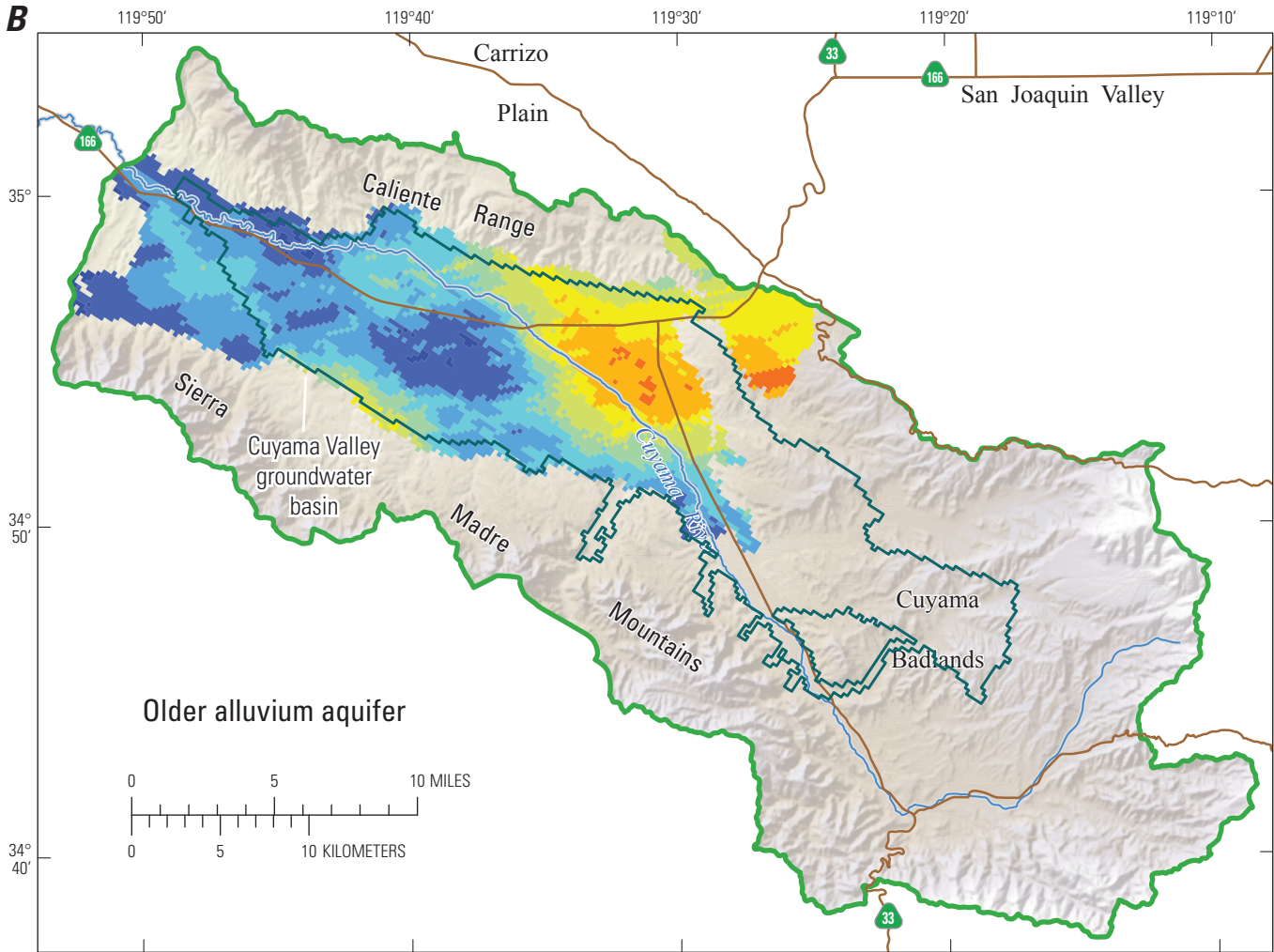
Percentage coarse-grained sediments



— Composite subbasin boundary for Basin Characterization Model

□ Active CUVHM model-grid boundary

Figure 4. Extent and percentage of coarse-grained deposits for the A, Recent Alluvial aquifer; B, Older Alluvial aquifer; and C, Morales Formation aquifer of Cuyama Valley, California.

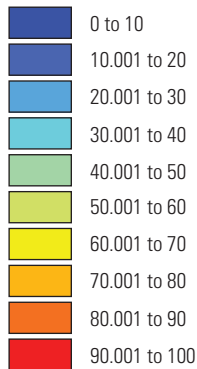


Shaded relief base created from 30-m digital elevation model from USGS National Elevation Dataset (NED); North American Vertical Datum 1983 (NAVD83). Hydrology sourced from 1:24,000-scale National Hydrography Dataset, 1974-2009. Place names sourced from USGS Geographic Names Information System, 1974-2009. Albers Projection, NAD83.

EXPLANATION

Estimated sedimentary texture

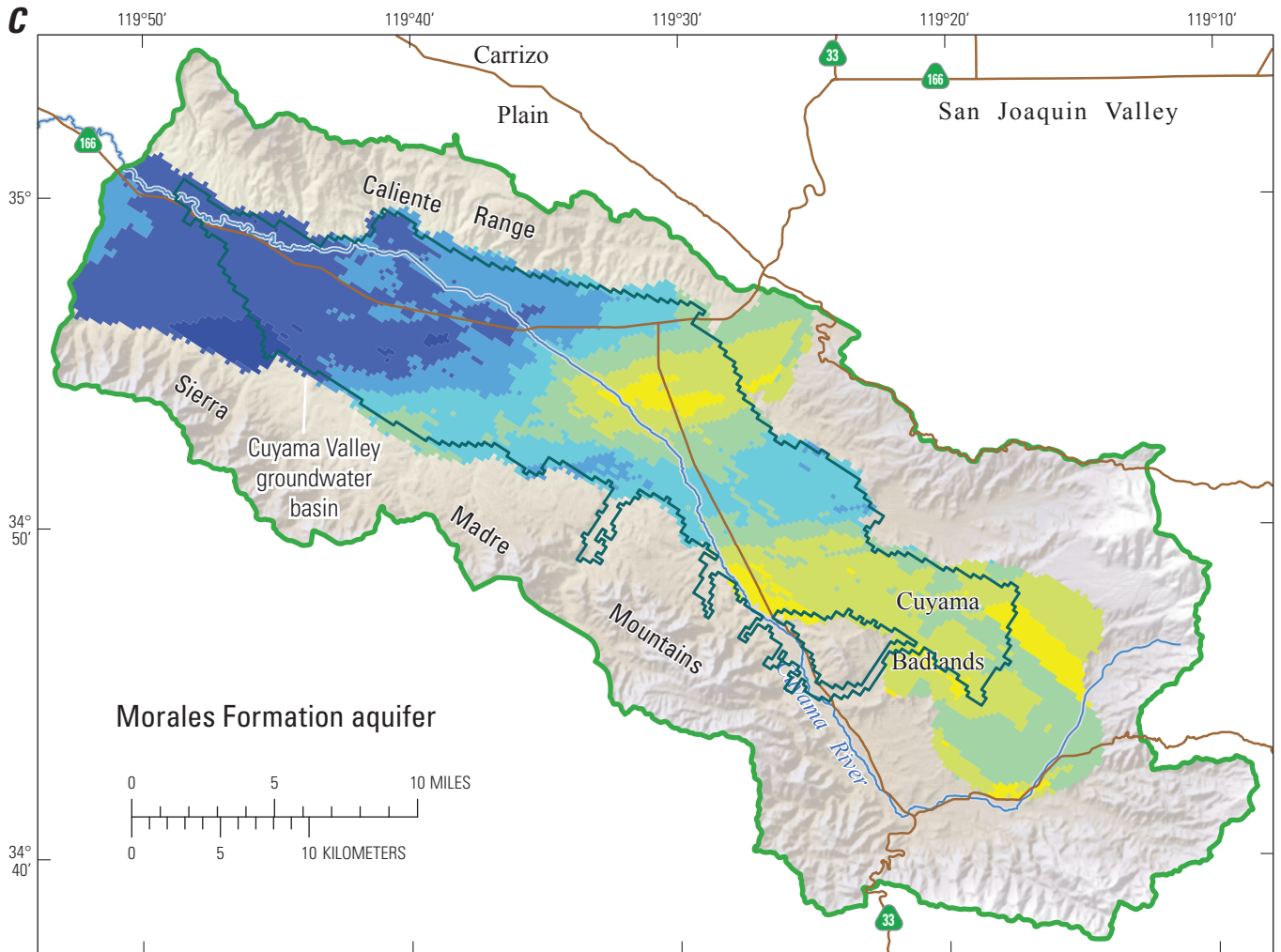
Percentage coarse-grained sediments



Composite subbasin boundary for Basin Characterization Model

Active CUVHM model-grid boundary

Figure 4. —Continued



Shaded relief base created from 30-m digital elevation model from USGS National Elevation Dataset (NED); North American Vertical Datum 1983 (NAVD83). Hydrology sourced from 1:24,000-scale National Hydrography Dataset, 1974-2009. Place names sourced from USGS Geographic Names Information System, 1974-2009. Albers Projection, NAD83.

EXPLANATION

Estimated sedimentary texture

Percentage coarse-grained sediments



— Composite subbasin boundary for Basin Characterization Model

Active CUVHM model-grid boundary

Figure 4. —Continued

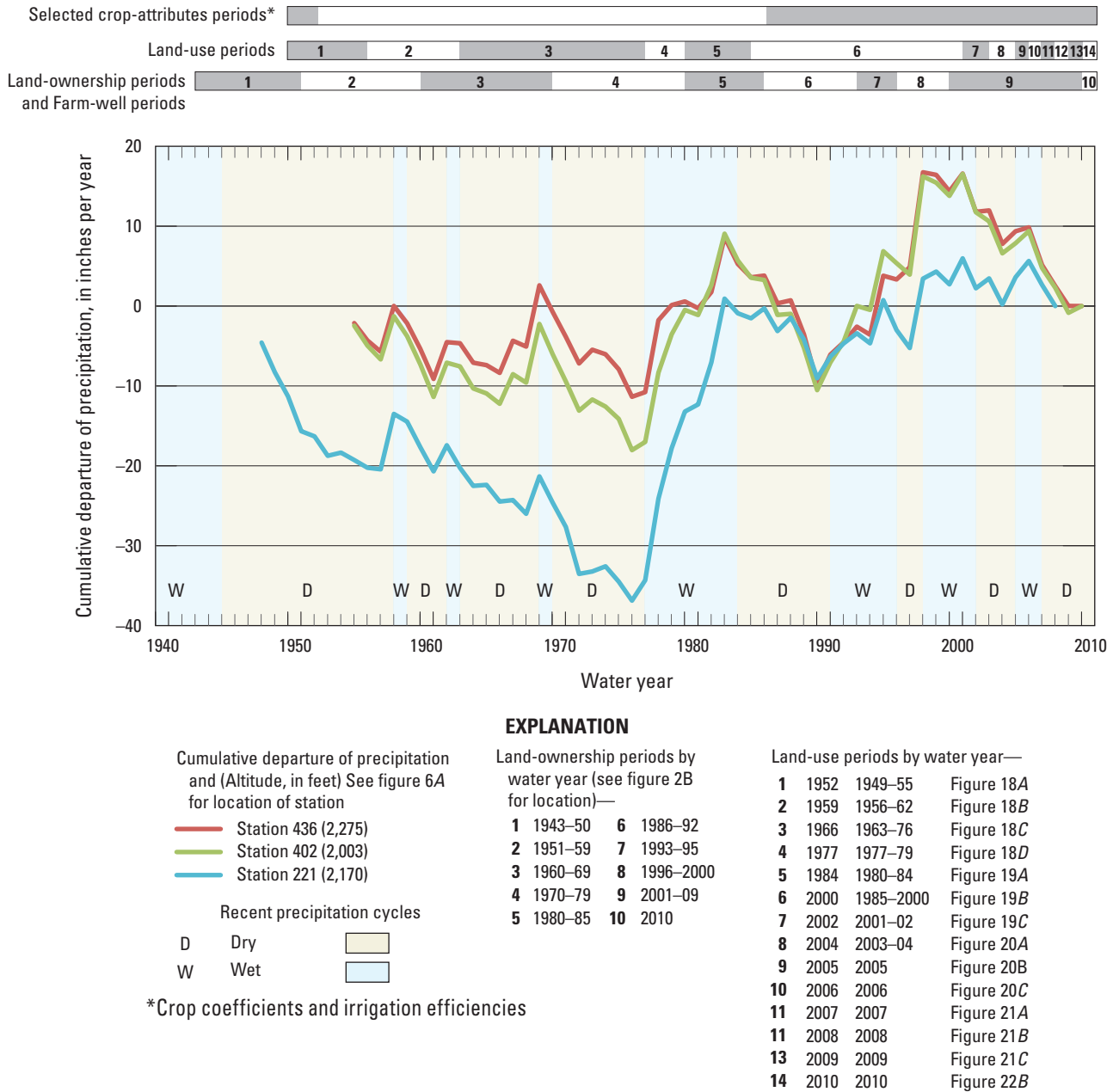
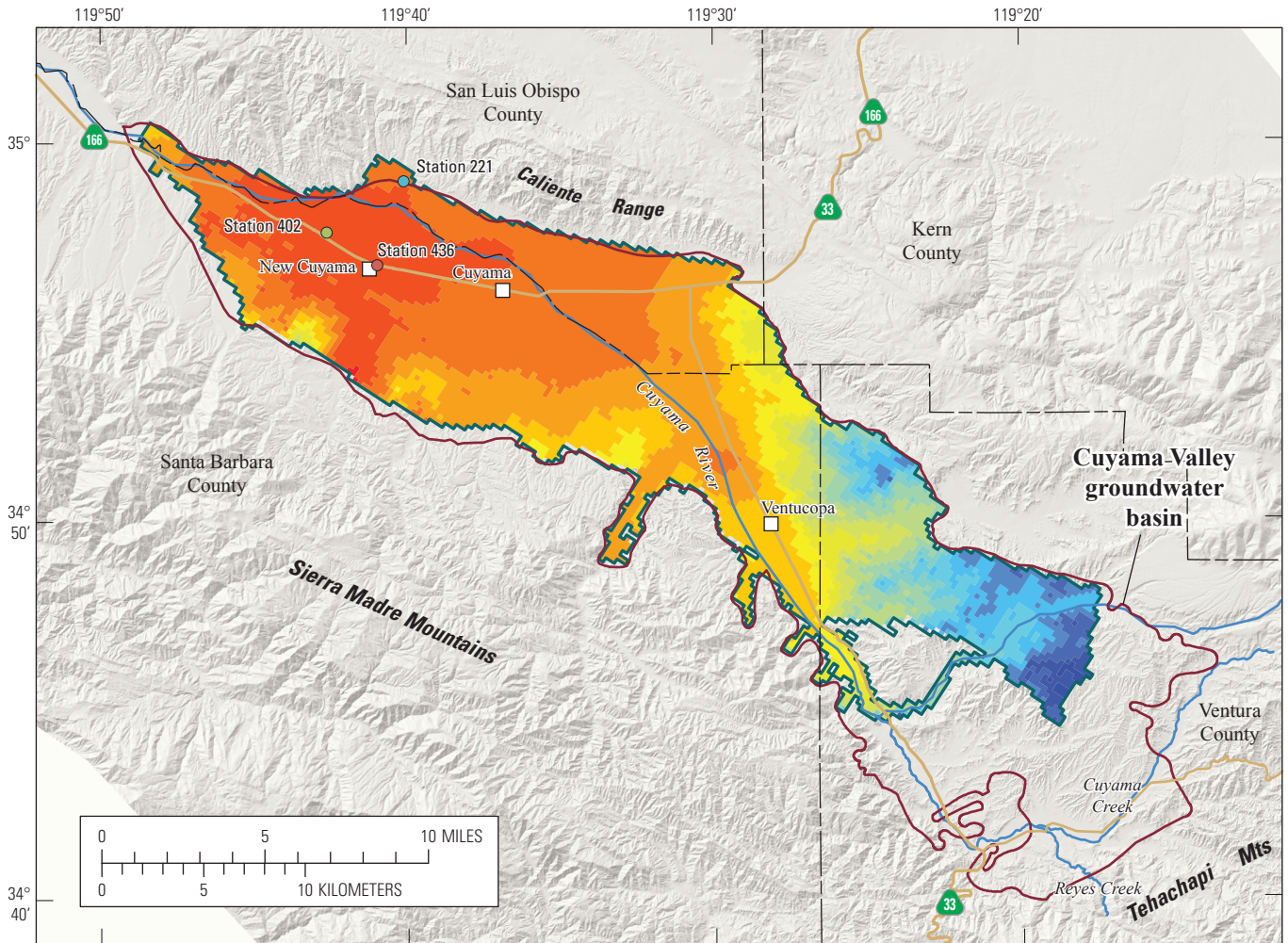


Figure 5. Cumulative departure of precipitation along with wet-dry periods, land-use map periods, periods of application for land-use, land-ownership (WBS) and related farm wells, and selected crop attributes for Cuyama Valley, California.



Shaded relief base created from 30-m digital elevation model from USGS National Elevation Dataset (NED); North America Vertical Datum 1983 (NAVD83). Hydrology sourced from 1:24,000-scale National Hydrography Dataset, 1974-2009. Place names sourced from USGS Geographic Names Information System, 1974-2009. Albers Projection, NAD83.

EXPLANATION

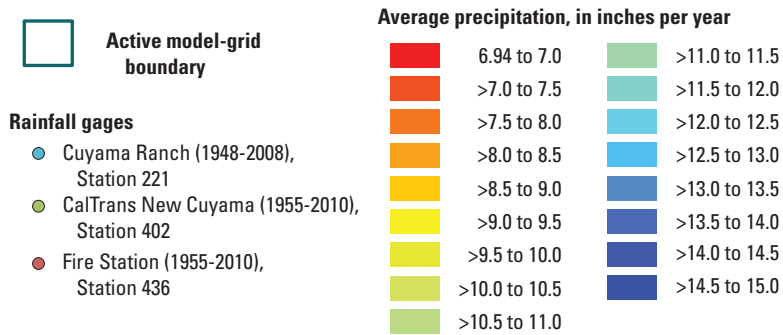
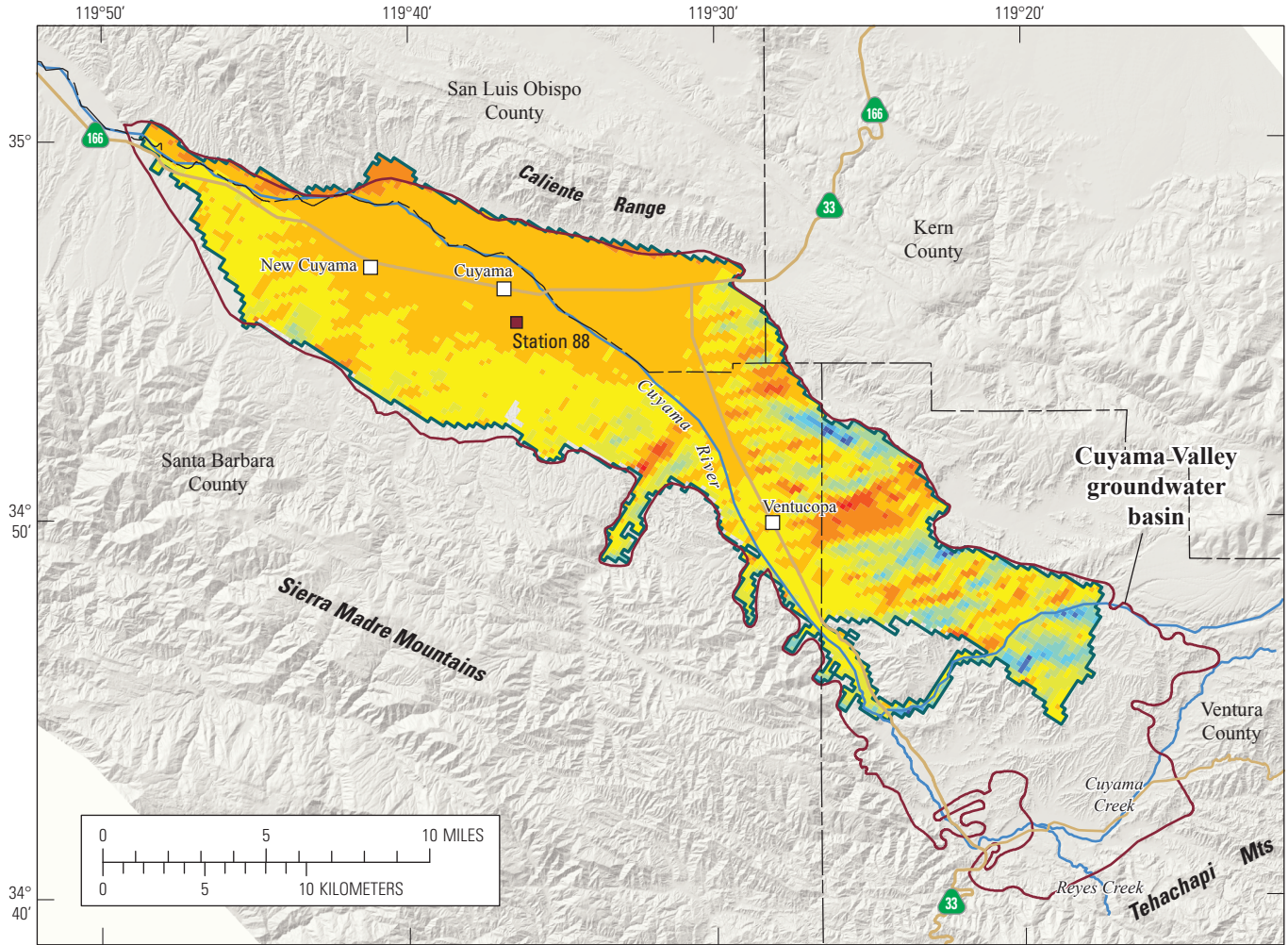


Figure 6. Average annual *A*, precipitation, and *B*, potential evapotranspiration for the simulation period (1949–2010) for Cuyama Valley, California.



Shaded relief base created from 30-m digital elevation model from USGS National Elevation Dataset (NED); North America Vertical Datum 1983 (NAVD83). Hydrology sourced from 1:24,000-scale National Hydrography Dataset, 1974-2009. Place names sourced from USGS Geographic Names Information System, 1974-2009. Albers Projection, NAD83.

EXPLANATION

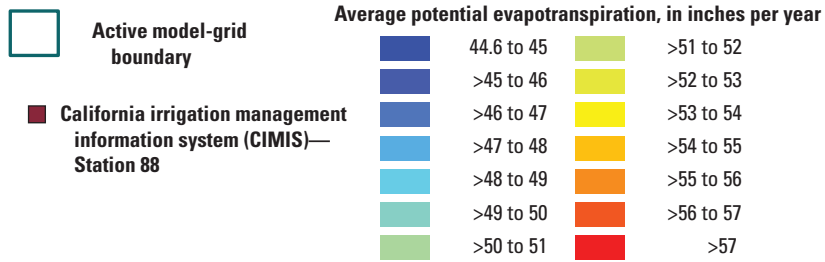
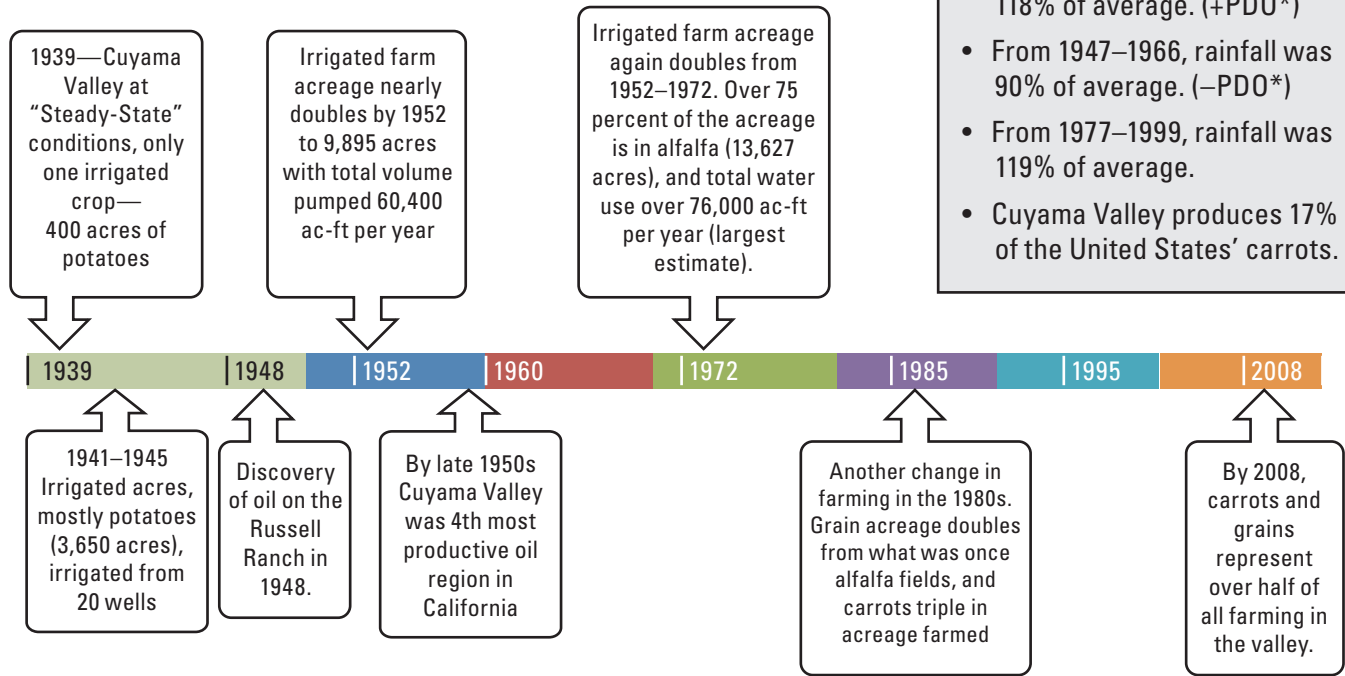


Figure 6. —Continued

A

Cuyama Valley development timeline



Timeline notes
(Singer and Swarzenski, 1970)

- From 1939–1946, rainfall was 118% of average. (+PDO*)
- From 1947–1966, rainfall was 90% of average. (–PDO*)
- From 1977–1999, rainfall was 119% of average.
- Cuyama Valley produces 17% of the United States’ carrots.

*Pacific Decadal Oscillation

B

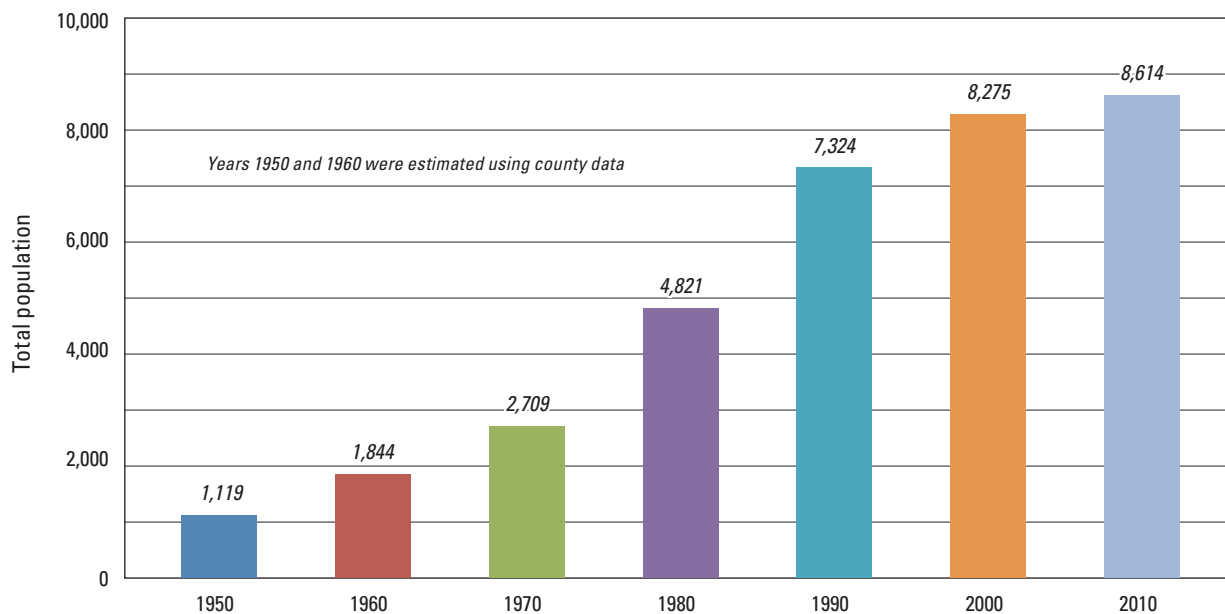
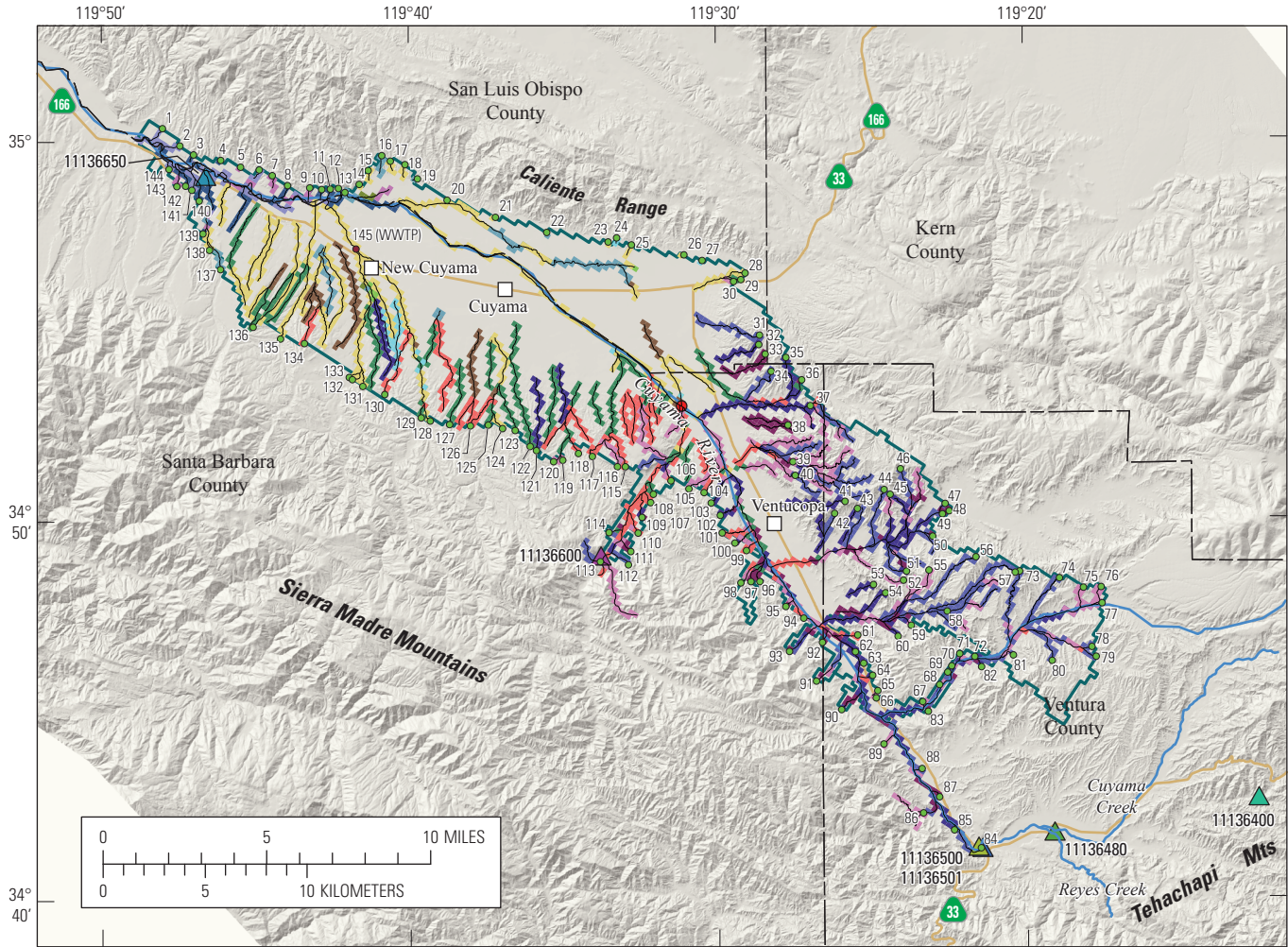


Figure 7. Generalized A, history of water and land-use development through time, and B, population growth for Cuyama Valley, California.

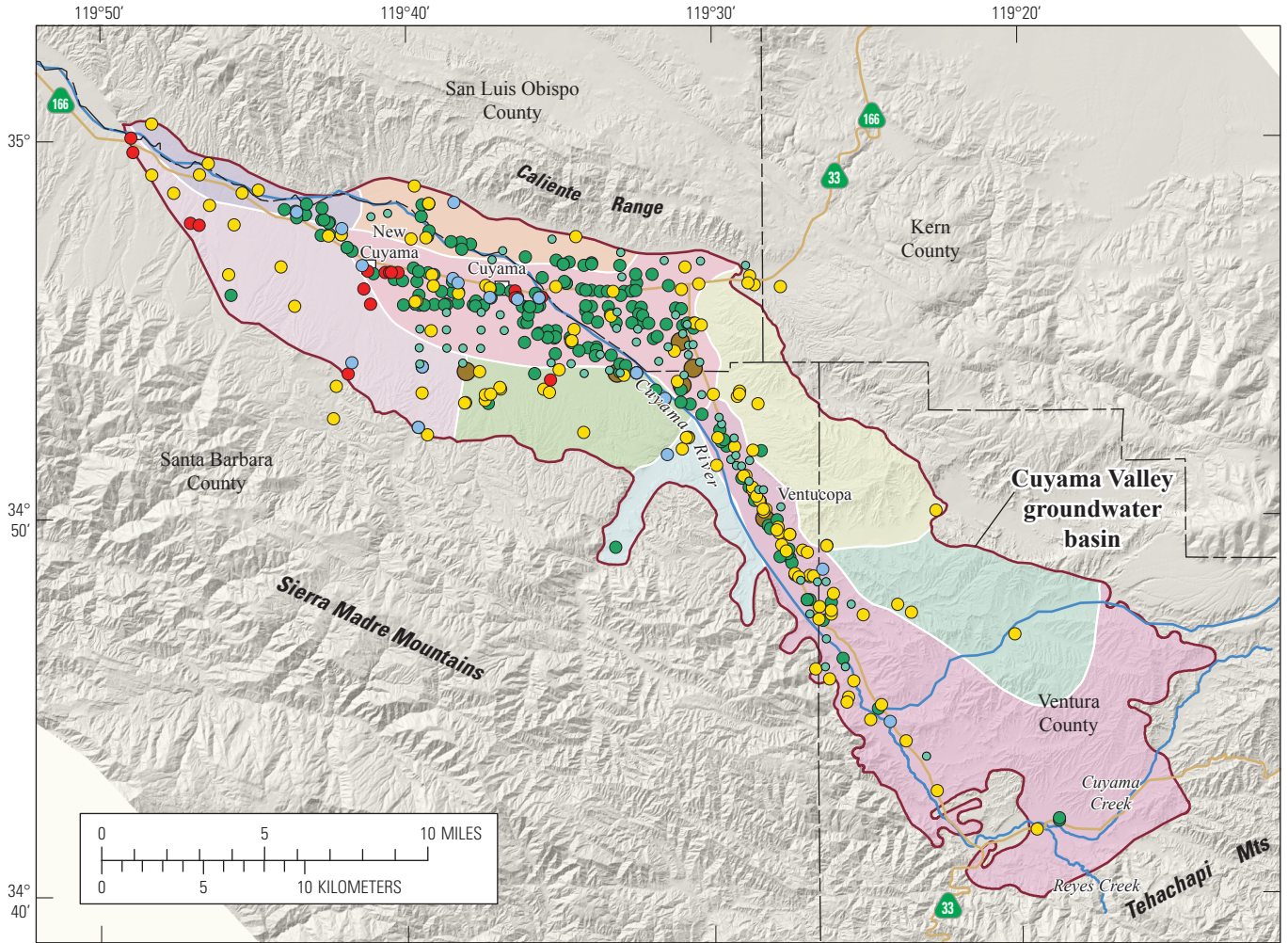


Shaded relief base created from 30-m digital elevation model from USGS National Elevation Dataset (NED); North America Vertical Datum 1983 (NAVD83). Hydrology sourced from 1:24,000-scale National Hydrography Dataset, 1974-2009. Place names sourced from USGS Geographic Names Information System, 1974-2009. Albers Projection, NAD83.

EXPLANATION

 <p>Active CUVHM model-grid boundary</p>	<p>Stream channel parameter names</p> <table border="0"> <tr> <td style="vertical-align: top;"> <p>Western zone</p> <ul style="list-style-type: none">  QYA  QYACC  QOA <p>North Main zone</p> <ul style="list-style-type: none">  QYA  QYACC  QOA <p>South Main zone</p> <ul style="list-style-type: none">  QYA  QYACC </td> <td style="vertical-align: top;"> <p>Sierra Madre Foothills</p> <ul style="list-style-type: none">  QOA-North  QOA-Middle  QOA-South <p>Ventucopa Uplands</p> <ul style="list-style-type: none">  QYAUC  QYACC  QOA  MOCU <p><i>QYA is Quaternary young alluvium</i> <i>QOA is Quaternary older alluvium</i> <i>MOCU is Morales unconfined</i> <i>CC is Cuyama Channel</i> <i>UC is unconfined</i></p> </td> </tr> </table>	<p>Western zone</p> <ul style="list-style-type: none">  QYA  QYACC  QOA <p>North Main zone</p> <ul style="list-style-type: none">  QYA  QYACC  QOA <p>South Main zone</p> <ul style="list-style-type: none">  QYA  QYACC 	<p>Sierra Madre Foothills</p> <ul style="list-style-type: none">  QOA-North  QOA-Middle  QOA-South <p>Ventucopa Uplands</p> <ul style="list-style-type: none">  QYAUC  QYACC  QOA  MOCU <p><i>QYA is Quaternary young alluvium</i> <i>QOA is Quaternary older alluvium</i> <i>MOCU is Morales unconfined</i> <i>CC is Cuyama Channel</i> <i>UC is unconfined</i></p>	<p>USGS stream gage and number</p> <ul style="list-style-type: none">  Aliso Canyon Creek near New Cuyama—11136650  Santa Barbara Canyon Creek near Ventucopa—11136600  Cuyama River near Ventucopa—11136500  Cuyama River near Ventucopa—11136501  Reyes Creek near Ventucopa—11136480  Wagon Road Creek near Stauffer—11136400 <p> Diversion location</p> <p> Inflow points—Numbers represent streamflow identifiers for inflow points for runoff from BCM model and from the Waste-water Treatment Plant (WWTP-145)</p>
<p>Western zone</p> <ul style="list-style-type: none">  QYA  QYACC  QOA <p>North Main zone</p> <ul style="list-style-type: none">  QYA  QYACC  QOA <p>South Main zone</p> <ul style="list-style-type: none">  QYA  QYACC 	<p>Sierra Madre Foothills</p> <ul style="list-style-type: none">  QOA-North  QOA-Middle  QOA-South <p>Ventucopa Uplands</p> <ul style="list-style-type: none">  QYAUC  QYACC  QOA  MOCU <p><i>QYA is Quaternary young alluvium</i> <i>QOA is Quaternary older alluvium</i> <i>MOCU is Morales unconfined</i> <i>CC is Cuyama Channel</i> <i>UC is unconfined</i></p>			

Figure 8. Distribution of streams with streamflow routing cells and segments, and location of inflows, Cuyama Valley, California.



Shaded relief base created from 30-m digital elevation model from USGS National Elevation Dataset (NED); North America Vertical Datum 1983 (NAVD83). Hydrology sourced from 1:24,000-scale National Hydrography Dataset, 1974-2009. Place names sourced from USGS Geographic Names Information System, 1974-2009. Albers Projection, NAD83.

EXPLANATION

Cuyama groundwater basin subregion

- Caliente Northern-Main
- Central Sierra Madre Foothills
- Northeast Ventucopa Uplands
- Northwestern Sierra Madre Foothills
- Northern Ventucopa Uplands
- Southern Sierra Madre Foothills
- Southern Ventucopa Uplands
- Southern-Main
- Western Basin

Well and type

- Agriculture
- Other agriculture
- Domestic
- Municipal and industrial
- Observation
- Virtual

Figure 9. Distribution of agricultural, urban-supply, and domestic wells, Cuyama Valley, California.

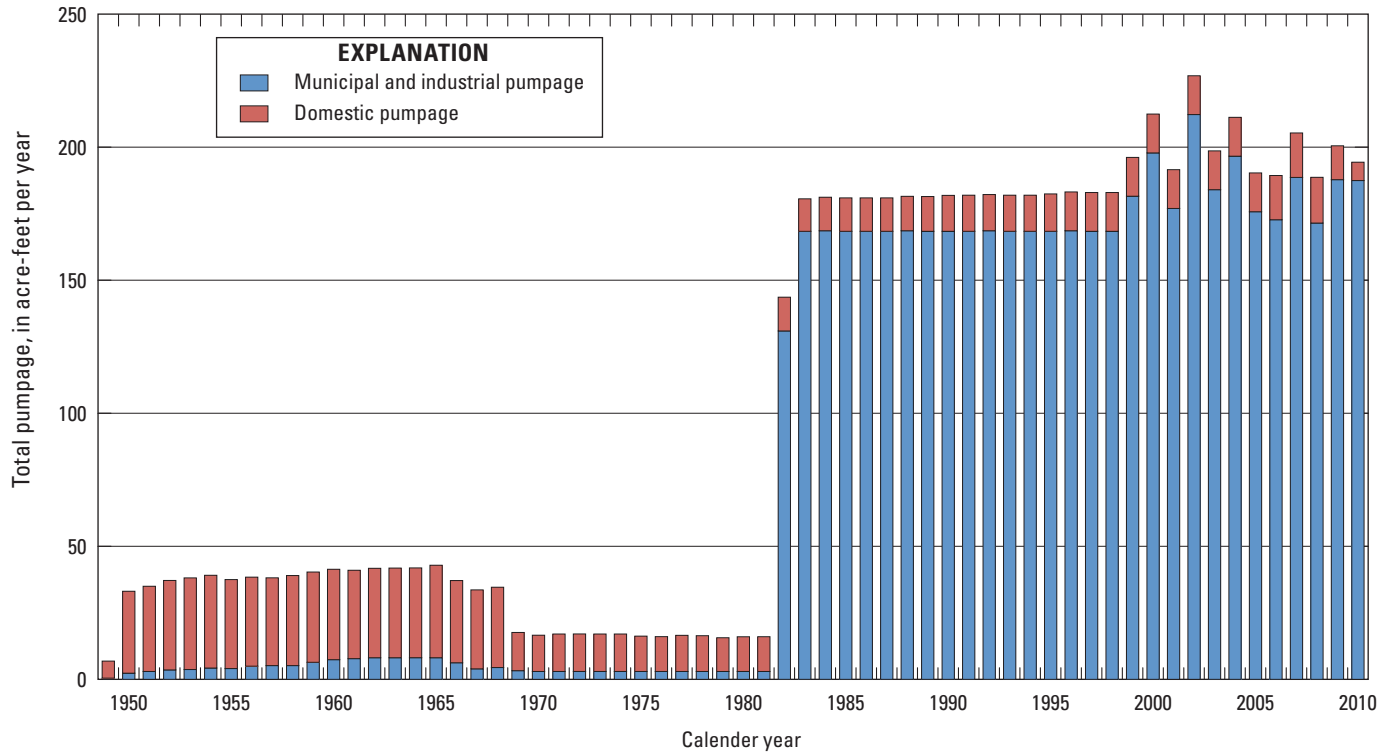
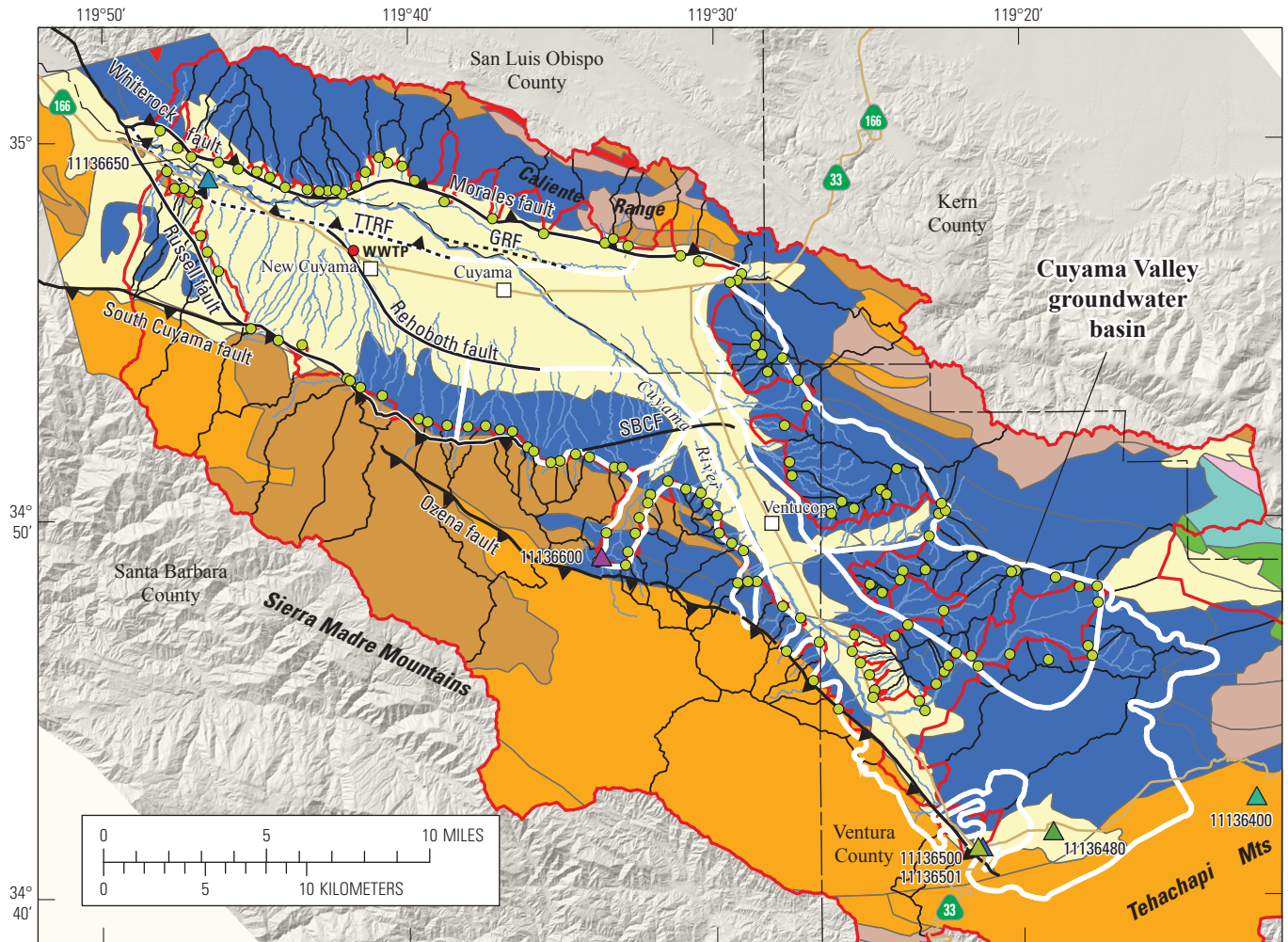


Figure 10. Estimated groundwater pumpage from municipal and domestic wells, Cuyama Valley, California.



Shaded relief base created from 30-m digital elevation model from USGS National Elevation Dataset (NED); North America Vertical Datum 1983 (NAVD83). Hydrology sourced from 1:24,000-scale National Hydrography Dataset, 1974-2009. Place names sourced from USGS Geographic Names Information System, 1974-2009. Albers Projection, NAD83.

Generalized Cuyama geology—
modified from Jennings, 1977

- Alluvium - valley fill, alluvium
- Conglomerate, limestone
- Conglomerate, sandstone
- Granite, granite
- Metasediments, metasediment
- Sandstone - shale, limestone
- Sandstone - shale, sandstone
- Sandstone, limestone
- Volcanics - lava flows, volcanics
- Water, water

 Watershed for Basin

Characterization Model analysis

 Subwatershed for Basin
Characterization Model analysis

— **Minor stream**

EXPLANATION

- Normal fault
- Thrust fault
- Thrust fault, concealed
- GRF, Graveyard fault;
SBCF, Santa Barbara Canyon fault;
TTRF, Turkey Trap Ridge fault

USGS stream gage and number

- ▲ Aliso Canyon Creek near New Cuyama—11136650
- ▲ Santa Barbara Canyon Creek near Ventucopa—11136600
- ▲ Cuyama River near Ventucopa—11136500
- ▲ Cuyama River near Ventucopa—11136501
- ▲ Reyes Creek near Ventucopa—11136480
- ▲ Wagon Road Creek near Stauffer—11136400

- **SFR_inflow points**
- **Wastewater treatment facility inflow**

Figure 11. The generalized distribution of bedrock, subwatersheds and related inflow points used with the Basin Characterization Model (BCM) recharge-runoff estimates for Cuyama Valley.

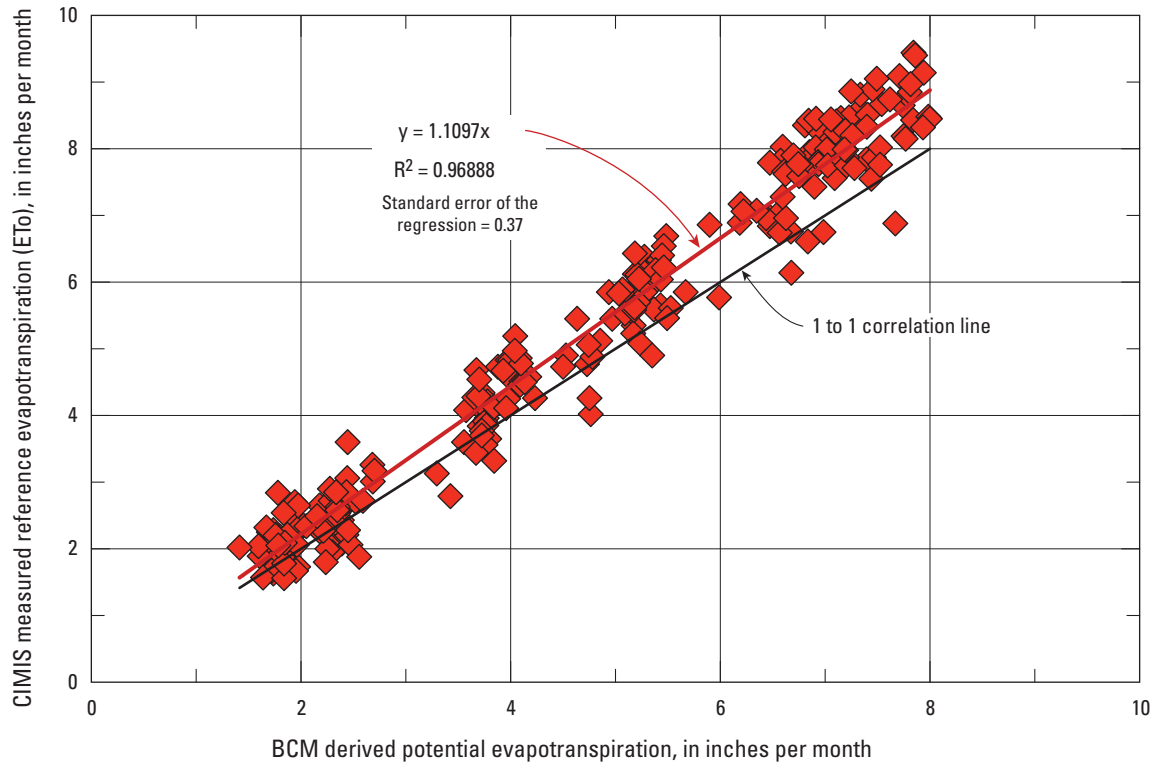


Figure 12. Comparison of Basic Characteristics Model (BCM) simulated potential evapotranspiration using the Priestley-Taylor approach with measured reference evapotranspiration (ET_o) from California Irrigation Management Information System (CIMIS) station in Cuyama Valley, California.

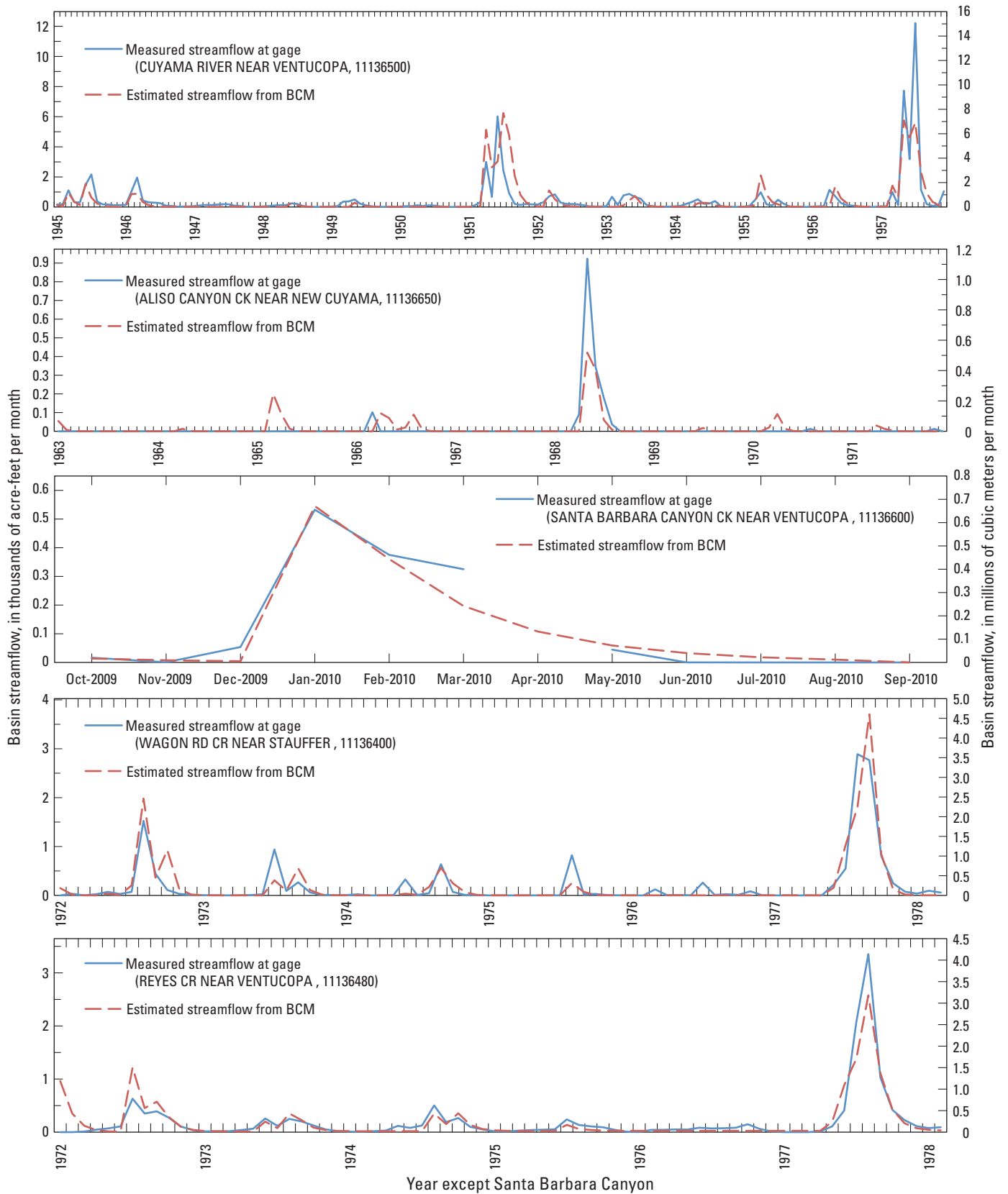


Figure 13. Comparisons of basin discharge, estimated by using the Basin Characterization Model (BCM), with measured streamflow for gaged basins in the Cuyama Valley model domain.

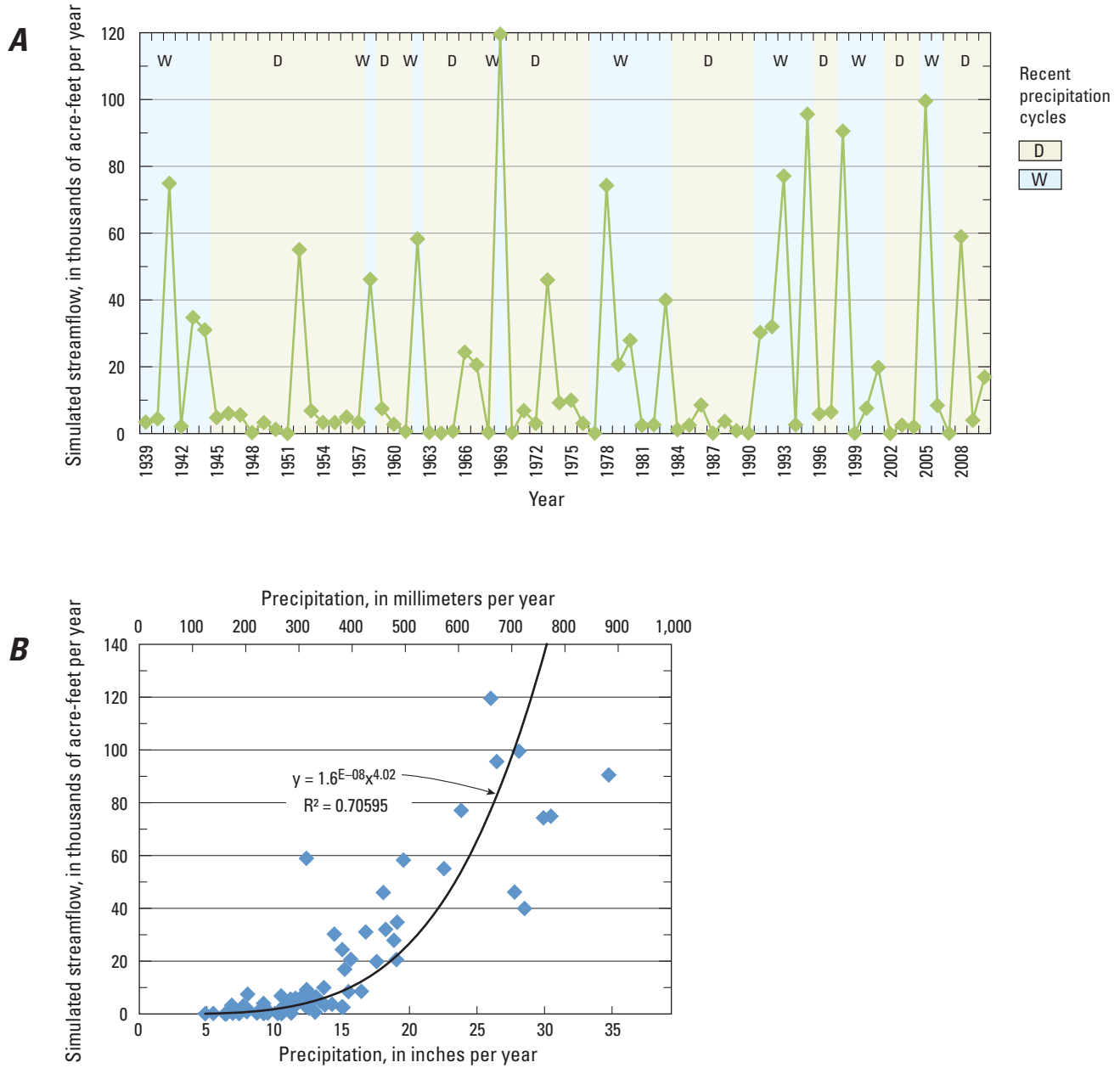
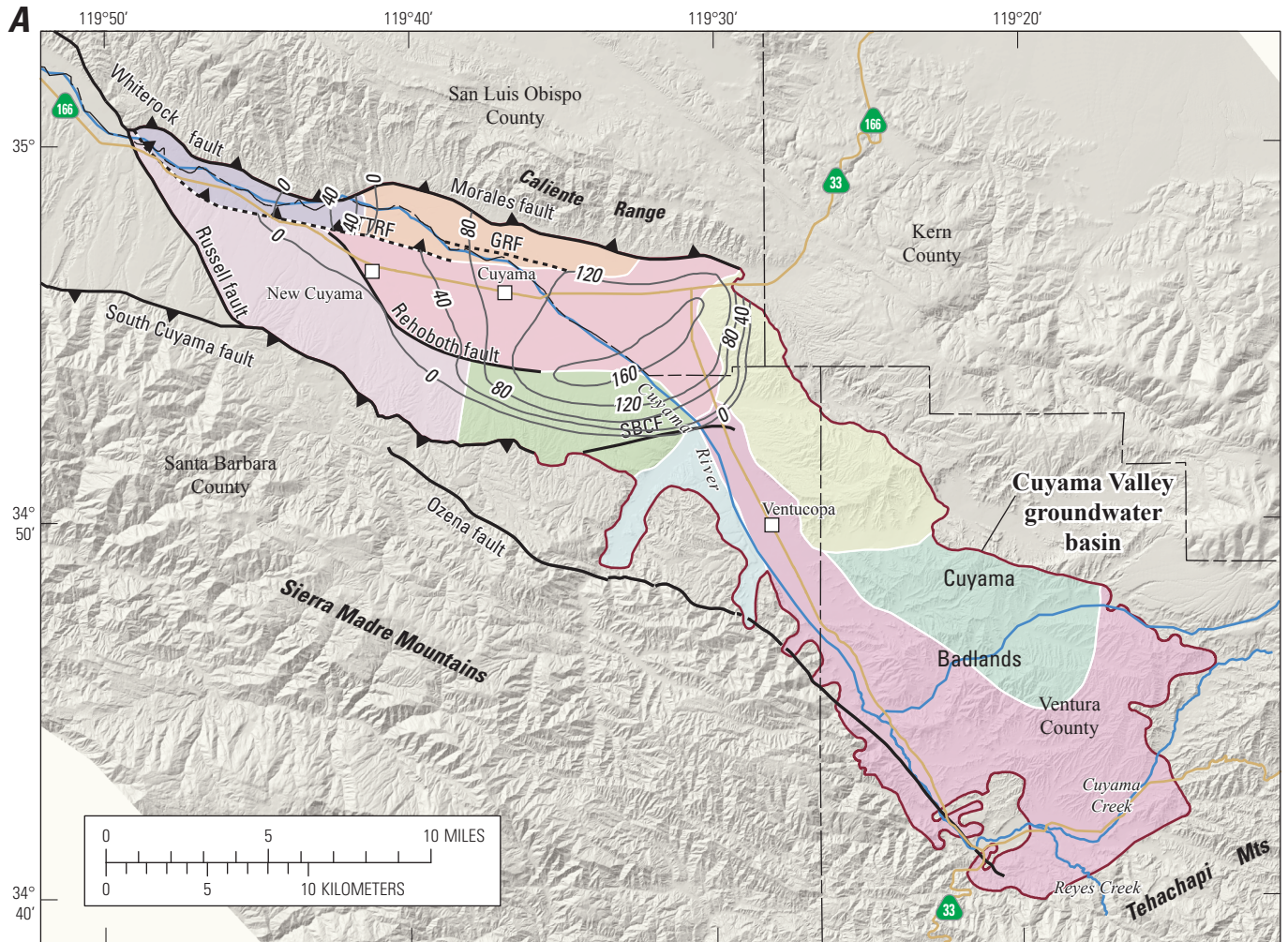


Figure 14. Annual streamflow for all Streamflow Routing (SFR) inflows in Cuyama Valley, California, *A*, for 1939–2009, and *B*, in comparison to precipitation.



Shaded relief base created from 30-m digital elevation model from USGS National Elevation Dataset (NED); North America Vertical Datum 1983 (NAVD83). Hydrology sourced from 1:24,000-scale National Hydrography Dataset, 1974-2009. Place names sourced from USGS Geographic Names Information System, 1974-2009. Albers Projection, NAD83.

Modified from Singer and Swarzenski, 1970

Cuyama groundwater basin subregion

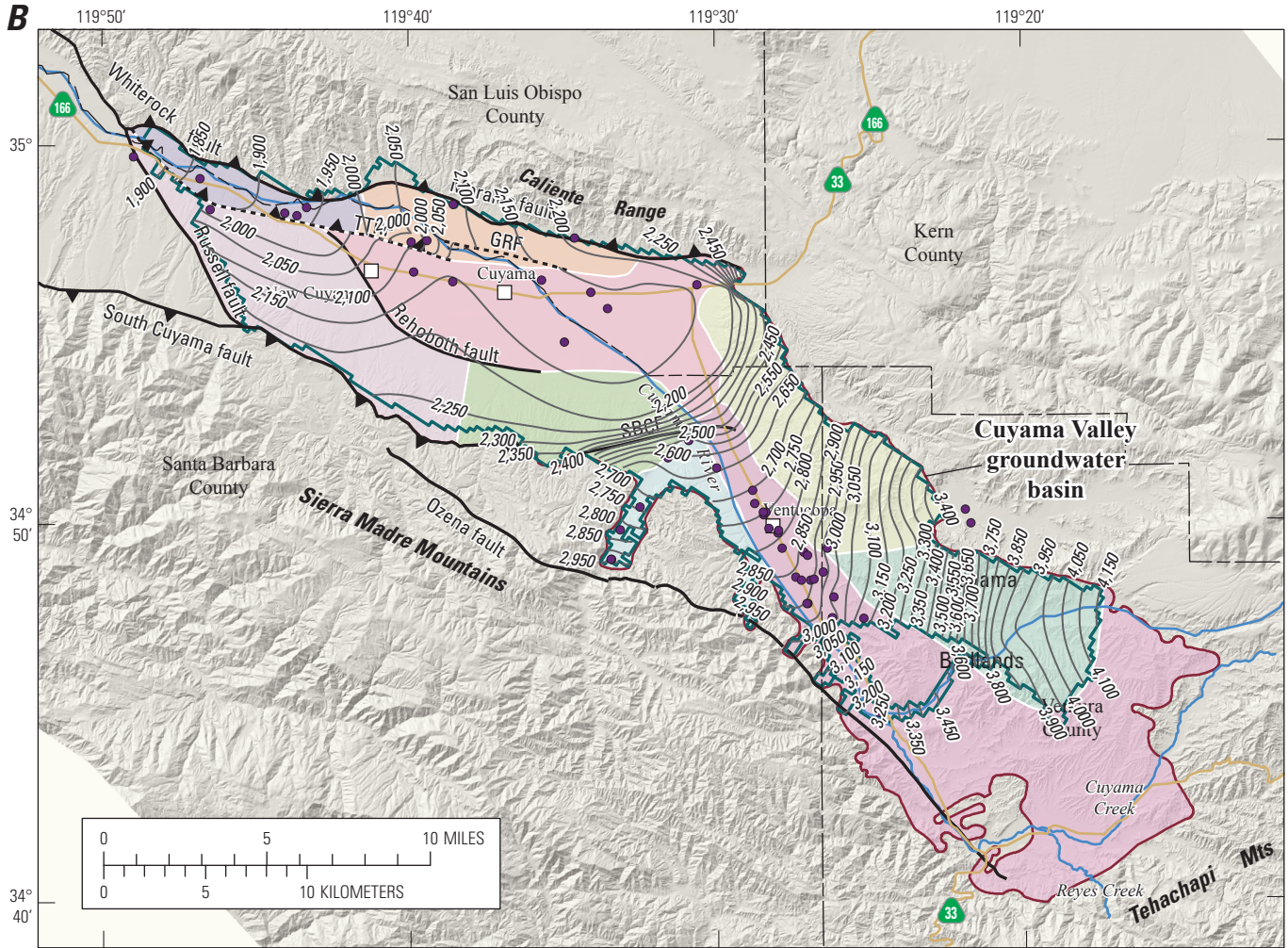
- Caliente Northern-Main
- Central Sierra Madre Foothills
- Northeast Ventucopa Uplands
- Northwestern Sierra Madre Foothills
- Northern Ventucopa Uplands
- Southern Sierra Madre Foothills
- Southern Ventucopa Uplands
- Southern-Main
- Western Basin

EXPLANATION

- Normal fault
- Thrust fault
- Thrust fault, concealed
- GRF, Graveyard fault; SBCF, Santa Barbara Canyon fault; TTRF, Turkey Trap Ridge fault

Estimated drawdown contour (1966-1947). Interval is 40 feet

Figure 15. A, drawdown contours for 1947-66; and groundwater-level contours for B, summer 1966, C, spring 2010, and D, summer 2010 for Cuyama Valley, California.



Shaded relief base created from 30-m digital elevation model from USGS National Elevation Dataset (NED); North America Vertical Datum 1983 (NAVD83). Hydrology sourced from 1:24,000-scale National Hydrography Dataset, 1974-2009. Place names sourced from USGS Geographic Names Information System, 1974-2009. Albers Projection, NAD83.

Modified from Singer and Swarzenski, 1970

EXPLANATION

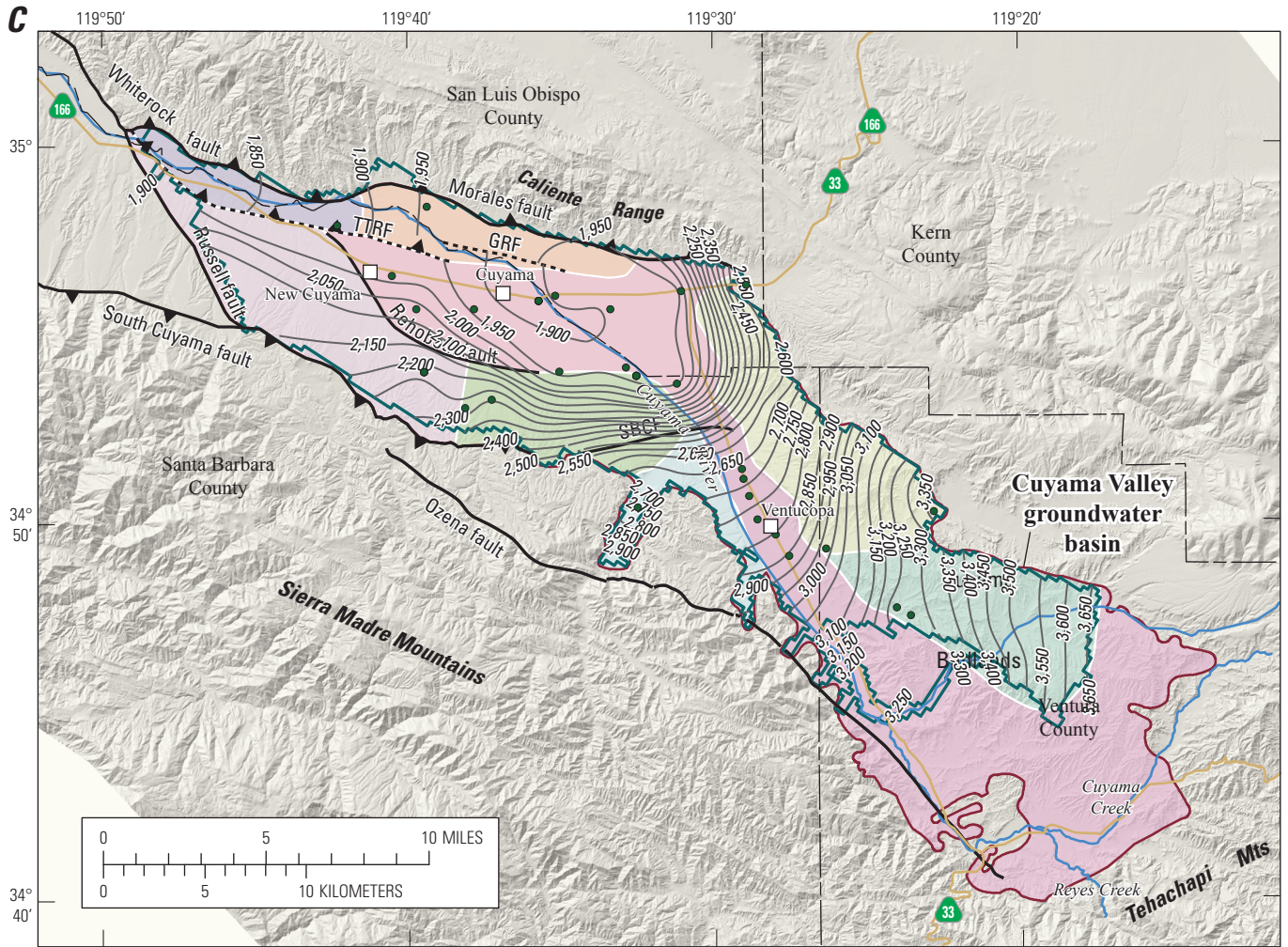
Cuyama groundwater basin subregion

- Caliente Northern-Main
- Central Sierra Madre Foothills
- Northeast Ventucopa Uplands
- Northwestern Sierra Madre Foothills
- Northern Ventucopa Uplands
- Southern Sierra Madre Foothills
- Southern Ventucopa Uplands
- Southern-Main
- Western Basin

- Normal fault
- Thrust fault
- Thrust fault, concealed
- GRF, Graveyard fault; SBCF, Santa Barbara Canyon fault; TTRF, Turkey Trap Ridge fault

- Active model-grid boundary
- Water-level altitude, summer 1966; interval is 50 feet
- Control point

Figure 15. —Continued



Shaded relief base created from 30-m digital elevation model from USGS National Elevation Dataset (NED); North America Vertical Datum 1983 (NAVD83). Hydrology sourced from 1:24,000-scale National Hydrography Dataset, 1974-2009. Place names sourced from USGS Geographic Names Information System, 1974-2009. Albers Projection, NAD83.

EXPLANATION

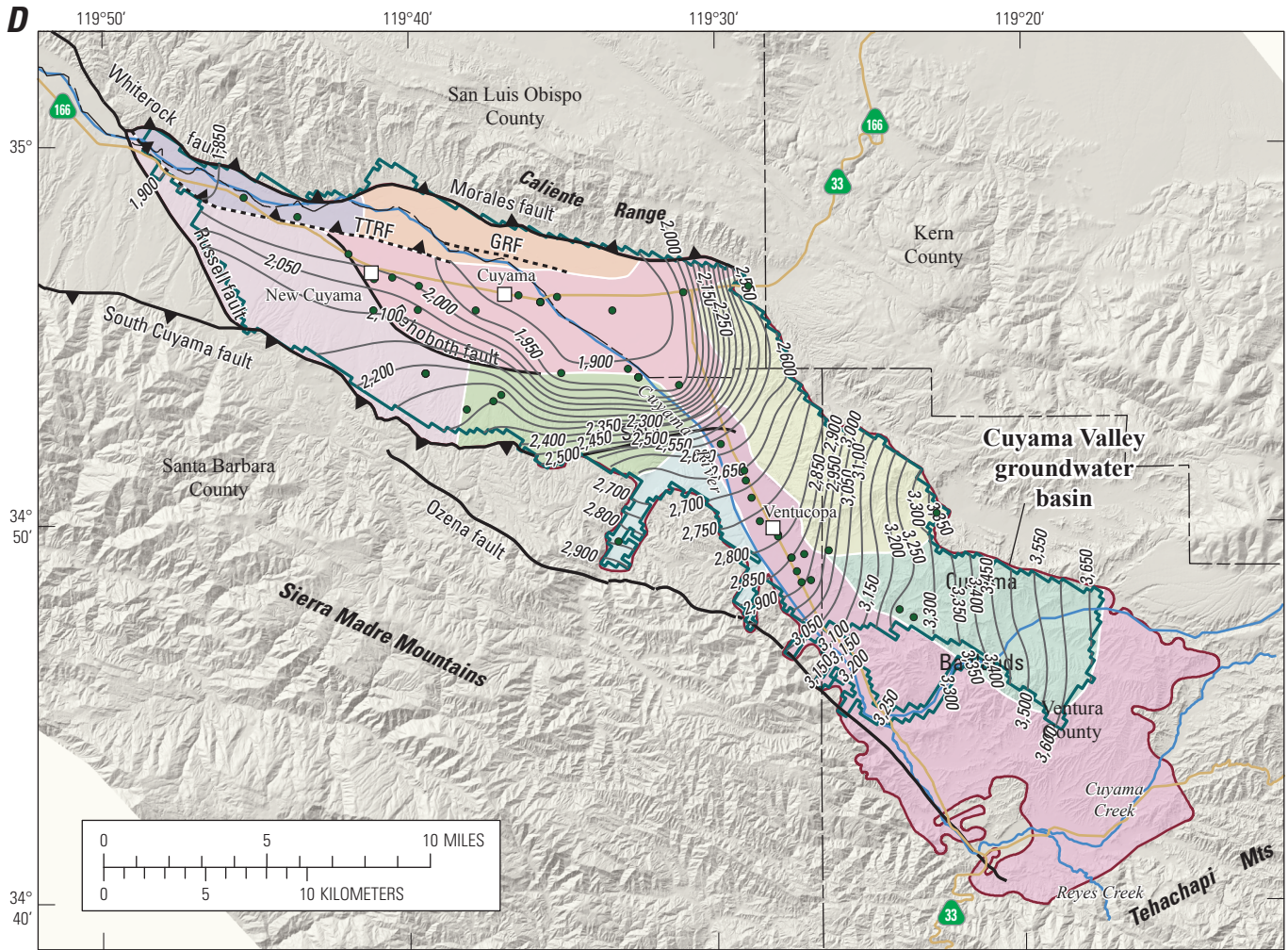
Cuyama groundwater basin subregion

- Caliente Northern-Main
- Central Sierra Madre Foothills
- Northeast Ventucopa Uplands
- Northwestern Sierra Madre Foothills
- Northern Ventucopa Uplands
- Southern Sierra Madre Foothills
- Southern Ventucopa Uplands
- Southern-Main
- Western Basin

- Normal fault
- Thrust fault
- Thrust fault, concealed
- GRF, Graveyard fault;
- SBCF, Santa Barbara Canyon fault;
- TTRF, Turkey Trap Ridge fault

- Active model-grid boundary
- Water-level altitude, spring 2010; interval is 50 feet
- Control point

Figure 15. —Continued



Shaded relief base created from 30-m digital elevation model from USGS National Elevation Dataset (NED); North America Vertical Datum 1983 (NAVD83). Hydrology sourced from 1:24,000-scale National Hydrography Dataset, 1974-2009. Place names sourced from USGS Geographic Names Information System, 1974-2009. Albers Projection, NAD83.

Cuyama groundwater basin subregion

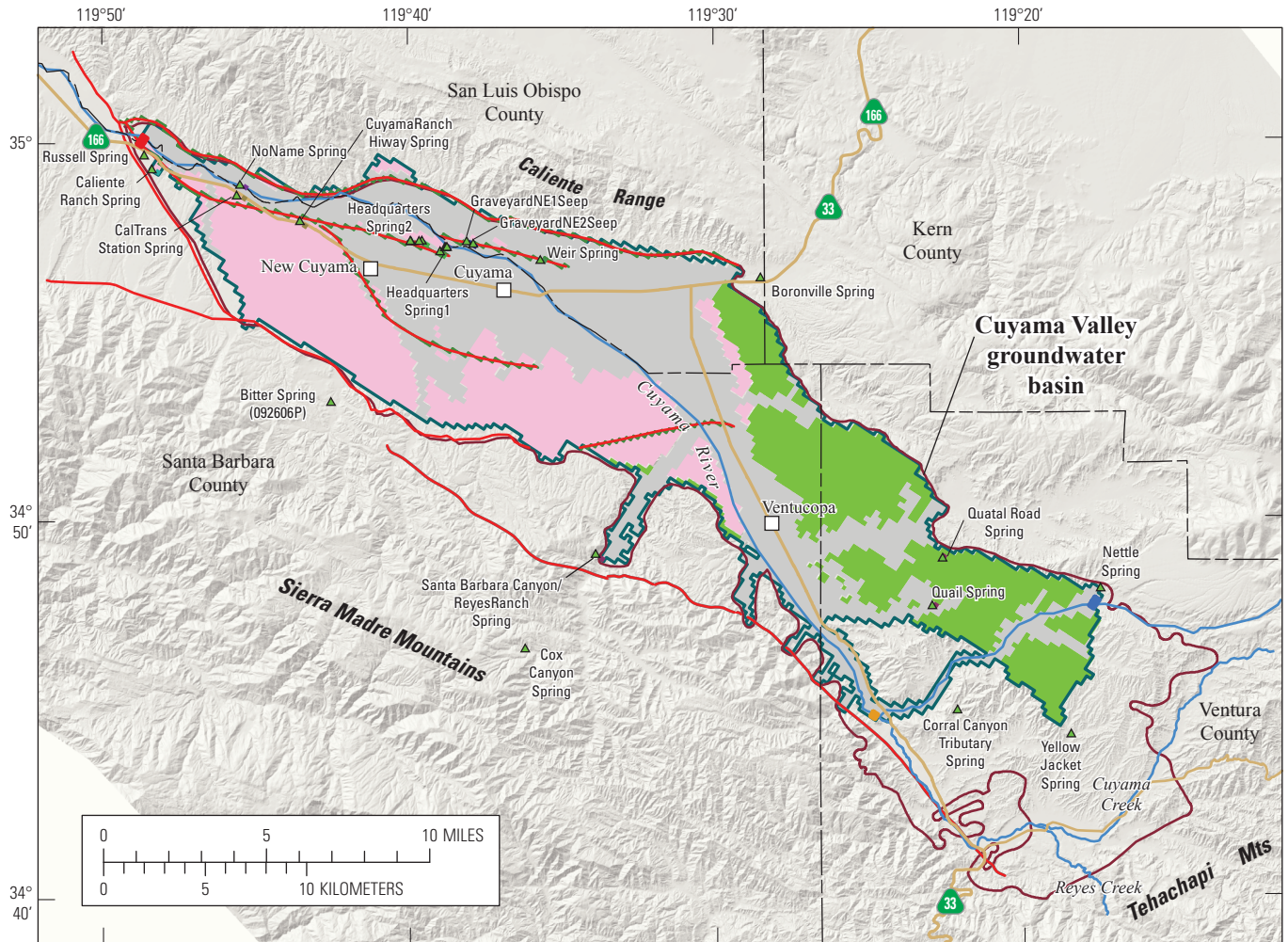
- Caliente Northern-Main
- Central Sierra Madre Foothills
- Northeast Ventucopa Uplands
- Northwestern Sierra Madre Foothills
- Northern Ventucopa Uplands
- Southern Sierra Madre Foothills
- Southern Ventucopa Uplands
- Southern-Main
- Western Basin

EXPLANATION

- Normal fault
- Thrust fault
- Thrust fault, concealed
- GRF, Graveyard fault; SBCF, Santa Barbara Canyon fault; TTRF, Turkey Trap Ridge fault

- Active model-grid boundary
- Water-level altitude, summer 2010; interval is 50 feet
- Control point

Figure 15. —Continued



Shaded relief base created from 30-m digital elevation model from USGS National Elevation Dataset (NED); North America Vertical Datum 1983 (NAVD83). Hydrology sourced from 1:24,000-scale National Hydrography Dataset, 1974-2009. Place names sourced from USGS Geographic Names Information System, 1974-2009. Albers Projection, NAD83.

EXPLANATION

- ▲ Spring or seep
- Hydraulic flow barrier
- Fault
- Active model-grid boundary (No-flow boundary except for underflow at general-head boundary cells)

Springs as drains

- Weir Seep
- Graveyard Seep
- Turkey Trap Fault Seeps
- Turkey Trap Hills Seeps
- Headquarters Spring
- CuyamaRanch_Hiway/CalTransStation
- No Name
- North Caliente Ranch
- St Barb Cyn-ReyesRch/QuatalRdSprBox/Quail

General-head boundary cells

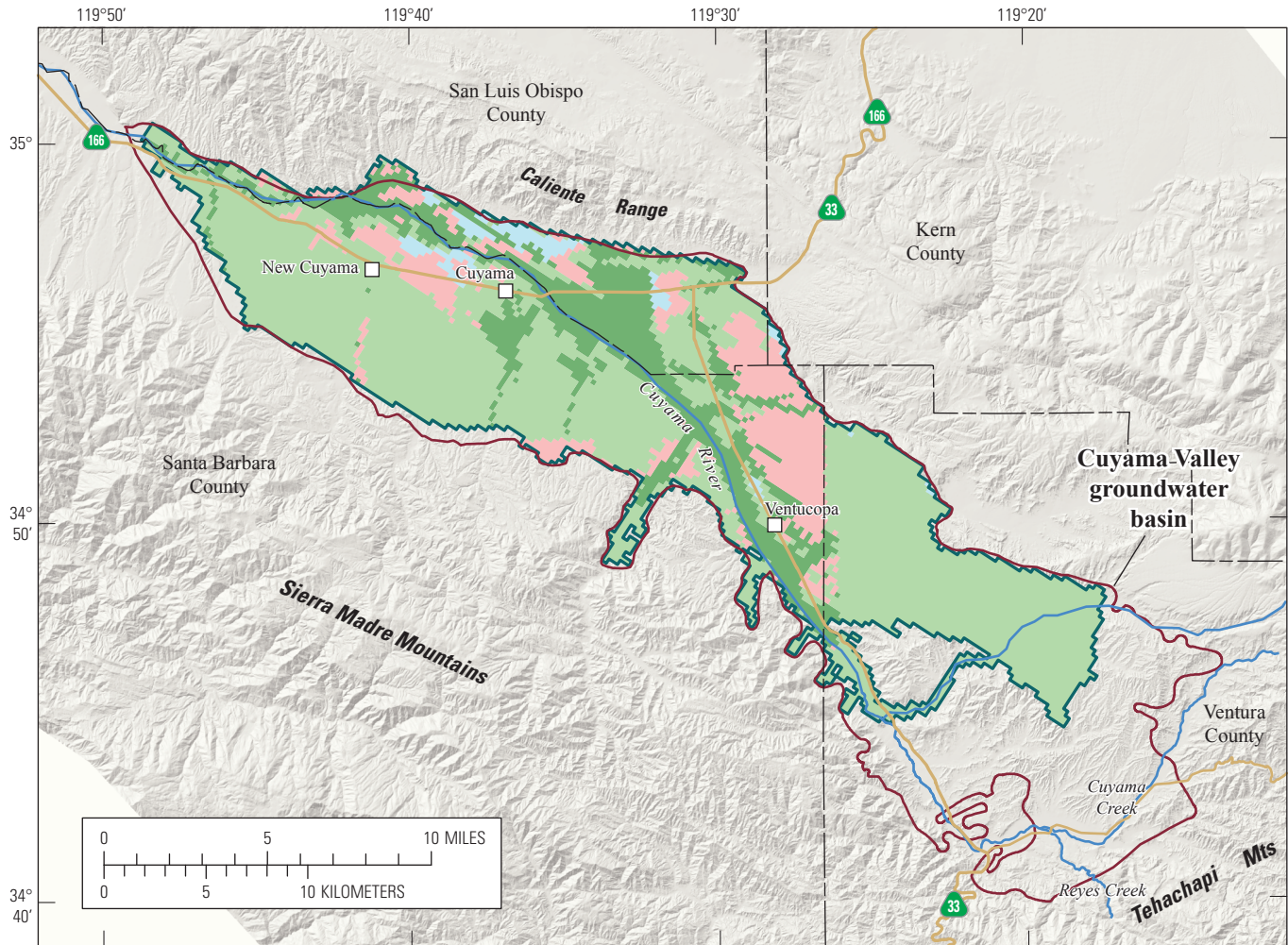
- Cuyama River below Greek Ranch
- Cuyama River above Ventucopa
- Reyes Creek above Ventucopa

Upper-most active layer

- Layer 1—Younger alluvium
- Layer 2—Older alluvium
- Layer 3—Morales Formation

Figure 16. Distribution of model cells representing no-flow, groundwater underflow, springs, streams, and horizontal groundwater flow barrier boundaries in the Cuyama Valley, California.

70 Hydrologic Models and Analysis of Water Availability in Cuyama Valley, California



Shaded relief base created from 30-m digital elevation model from USGS National Elevation Dataset (NED); North America Vertical Datum 1983 (NAVD83). Hydrology sourced from 1:24,000-scale National Hydrography Dataset, 1974-2009. Place names sourced from USGS Geographic Names Information System, 1974-2009. Albers Projection, NAD83.

EXPLANATION

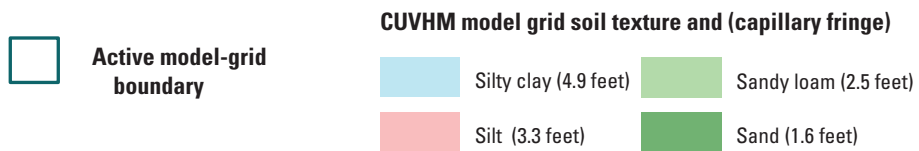
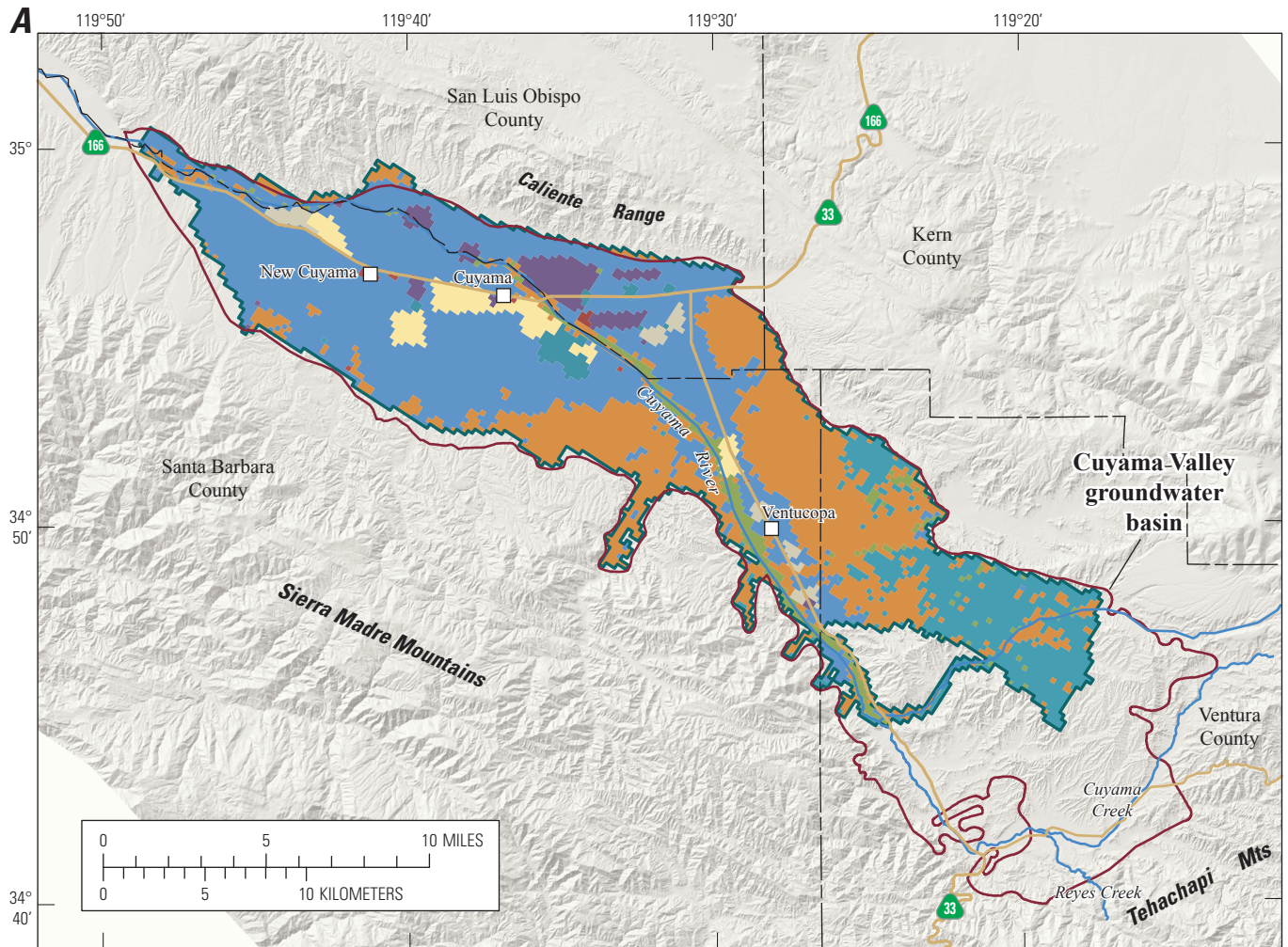


Figure 17. Agricultural soils for the Cuyama Valley simplified from Soil Survey Geographic Database (SSURGO) (U.S. Department of Agriculture Natural Resources Conservation Service, 2005).



Shaded relief base created from 30-m digital elevation model from USGS National Elevation Dataset (NED); North America Vertical Datum 1983 (NAVD83). Hydrology sourced from 1:24,000-scale National Hydrography Dataset, 1974-2009. Place names sourced from USGS Geographic Names Information System, 1974-2009. Albers Projection, NAD83.

EXPLANATION
 Active model-grid boundary

Values on pie charts are in list-order, clockwise from top center and may not equal 100 due to rounding of percentages.

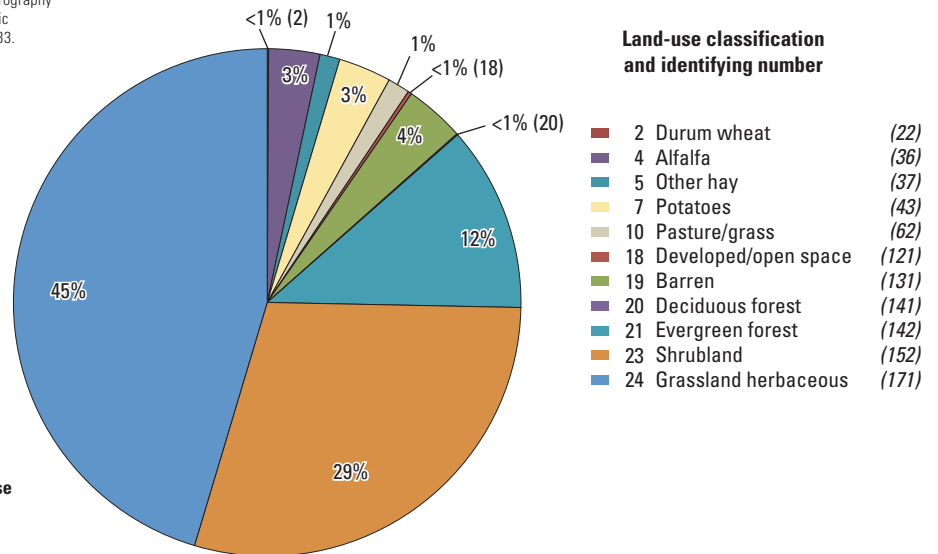
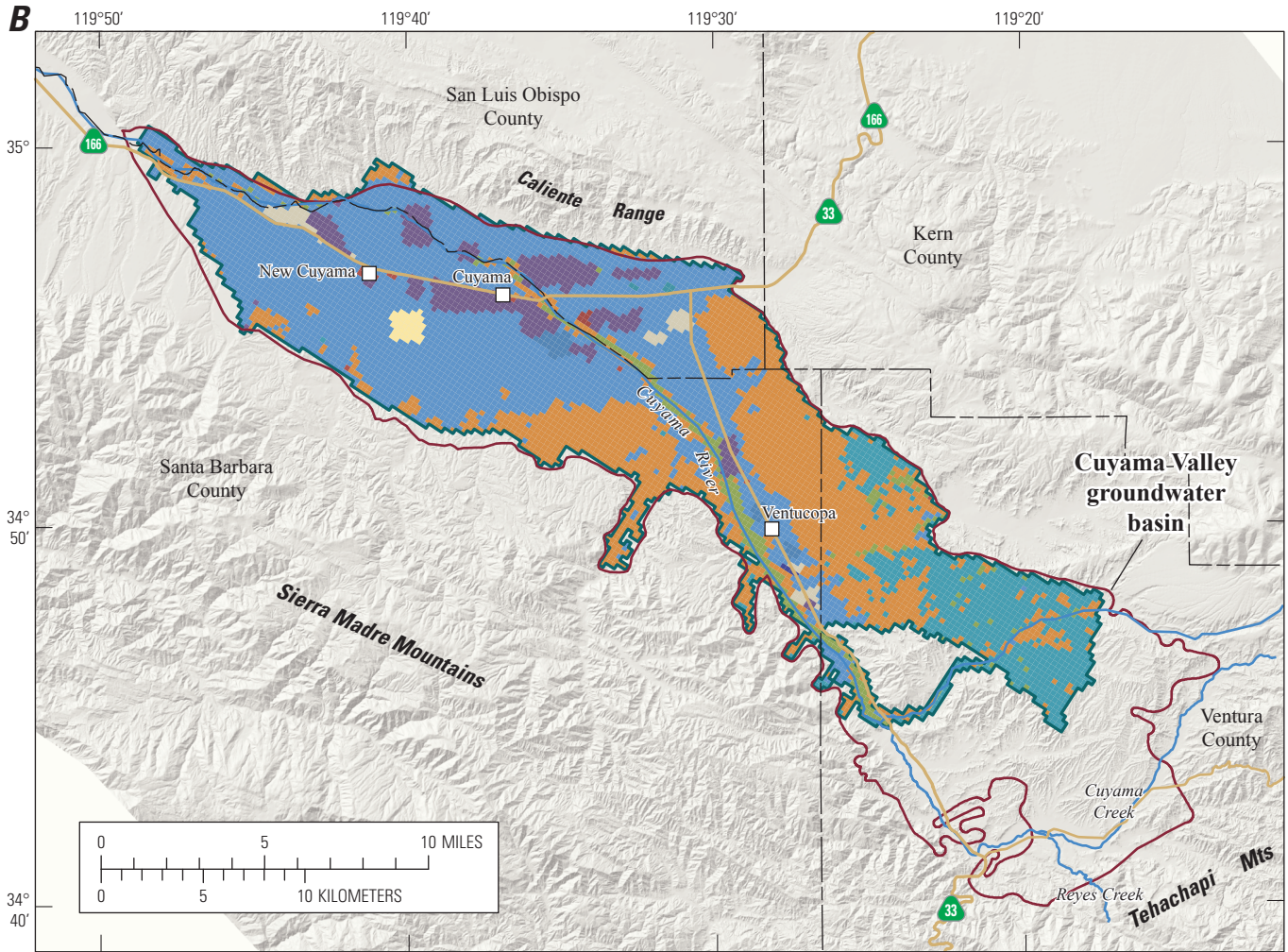
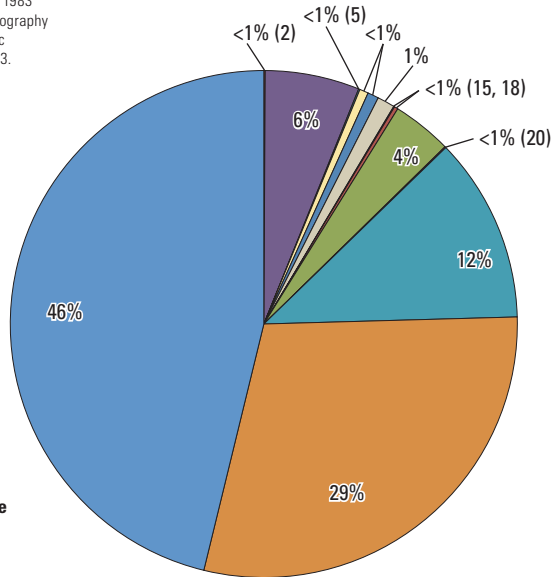


Figure 18. Early periods of land-use (virtual crop) groups discretized to the model grid, and pie chart of percentages of total land use over the modeled area for A, 1952; B, 1959; C, 1966; and D, 1977 for Cuyama Valley, California.



Shaded relief base created from 30-m digital elevation model from USGS National Elevation Dataset (NED); North America Vertical Datum 1983 (NAVD83). Hydrology sourced from 1:24,000-scale National Hydrography Dataset, 1974-2009. Place names sourced from USGS Geographic Names Information System, 1974-2009. Albers Projection, NAD83.

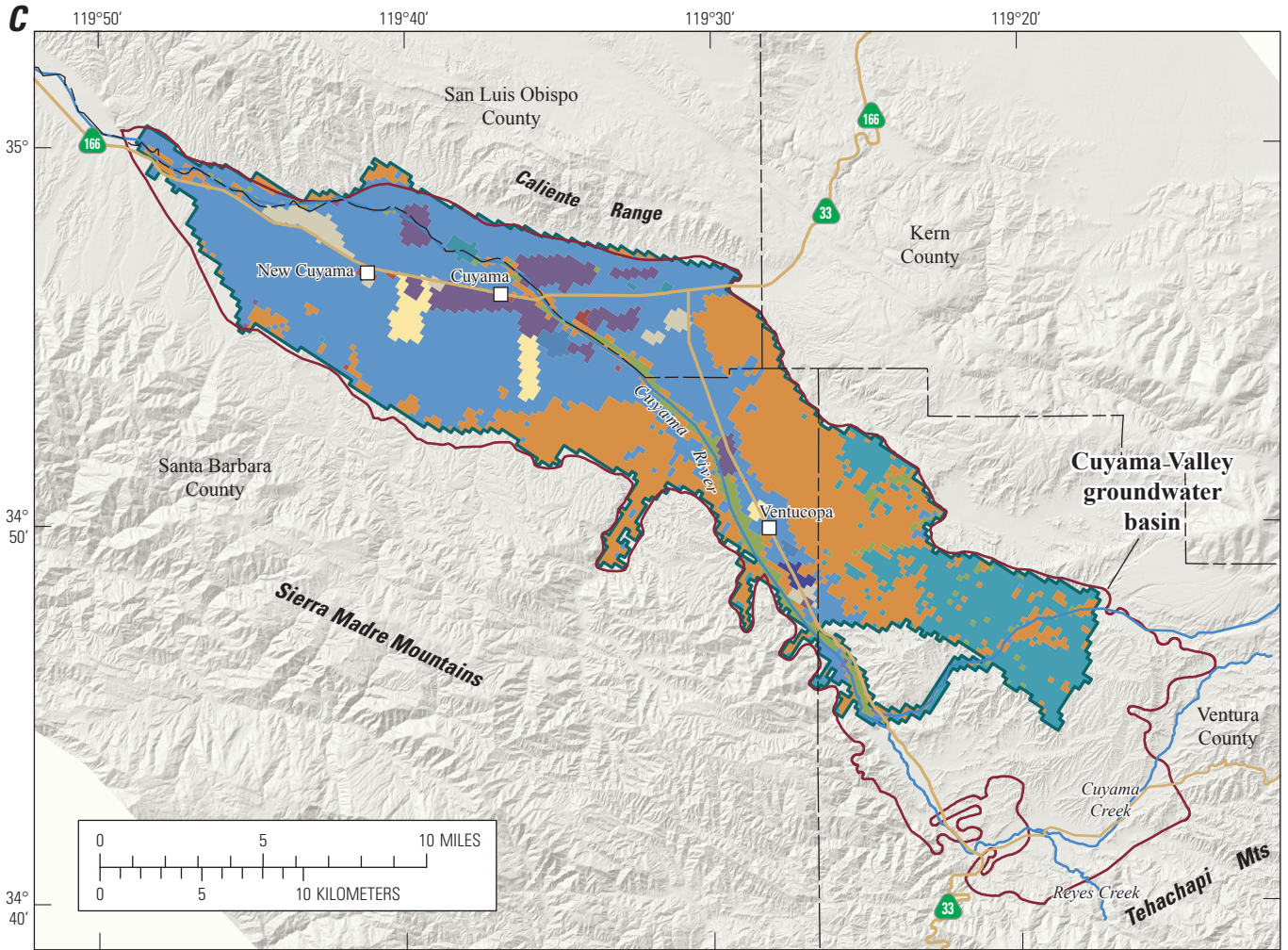
EXPLANATION
 Active model-grid boundary



- Land-use classification and identifying number**
- 2 Durum wheat (22)
 - 4 Alfalfa (36)
 - 5 Other hay (37)
 - 7 Potatoes (43)
 - 8 Onions (49)
 - 10 Pasture/grass (62)
 - 15 Other tree fruit (73)
 - 18 Developed/open space (121)
 - 19 Barren (131)
 - 20 Deciduous forest (141)
 - 21 Evergreen forest (142)
 - 23 Shrubland (152)
 - 24 Grassland herbaceous (171)

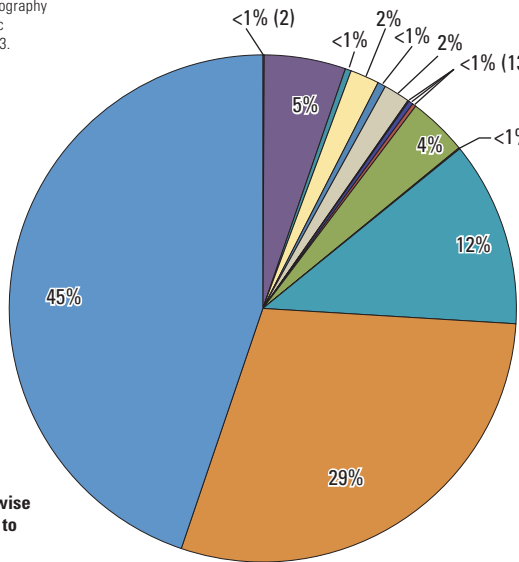
Values on pie charts are in list-order, clockwise from top center and may not equal 100 due to rounding of percentages.

Figure 18. —Continued



Shaded relief base created from 30-m digital elevation model from USGS National Elevation Dataset (NED); North America Vertical Datum 1983 (NAVD83). Hydrology sourced from 1:24,000-scale National Hydrography Dataset, 1974-2009. Place names sourced from USGS Geographic Names Information System, 1974-2009. Albers Projection, NAD83.

EXPLANATION
 Active model-grid boundary

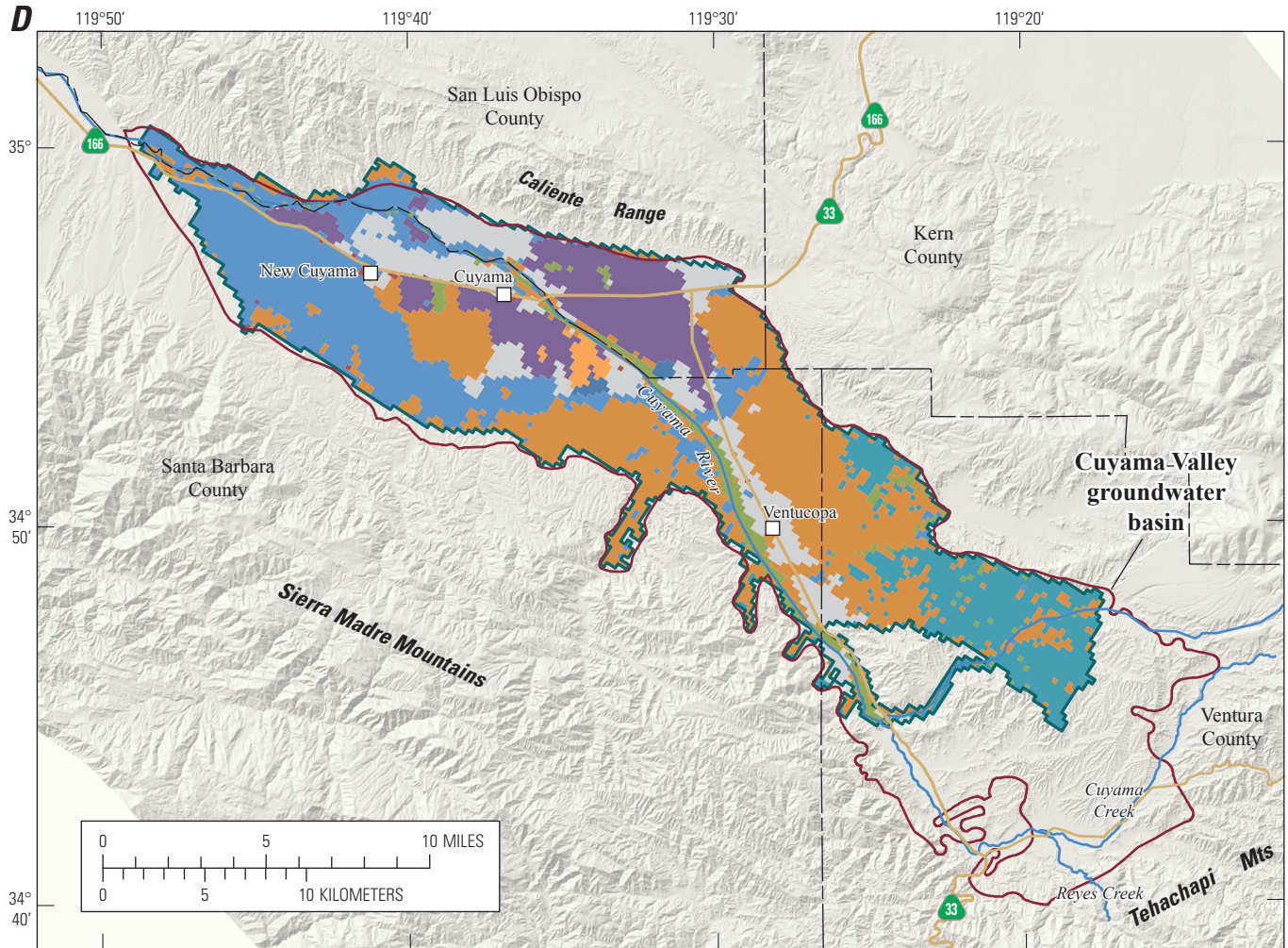


Land-use classification and identifying number

2	Durum wheat	(22)
4	Alfalfa	(36)
5	Other hay	(37)
7	Potatoes	(43)
8	Onions	(49)
10	Pasture/grass	(62)
13	Apples	(68)
15	Other tree fruit	(73)
18	Developed/open space	(121)
19	Barren	(131)
20	Deciduous forest	(141)
21	Evergreen forest	(142)
23	Shrubland	(152)
24	Grassland herbaceous	(171)

Values on pie charts are in list-order, clockwise from top center and may not equal 100 due to rounding of percentages.

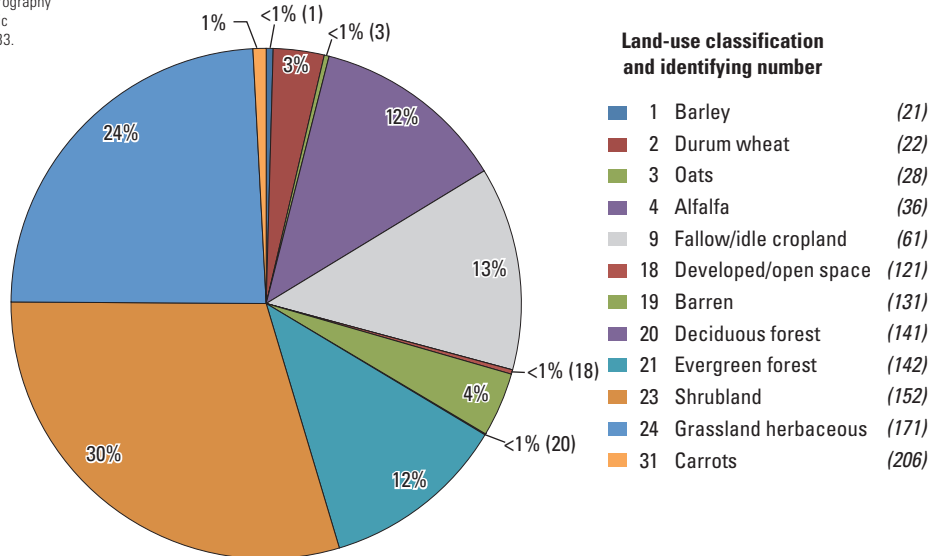
Figure 18. —Continued



Shaded relief base created from 30-m digital elevation model from USGS National Elevation Dataset (NED); North America Vertical Datum 1983 (NAVD83). Hydrology sourced from 1:24,000-scale National Hydrography Dataset, 1974-2009. Place names sourced from USGS Geographic Names Information System, 1974-2009. Albers Projection, NAD83.

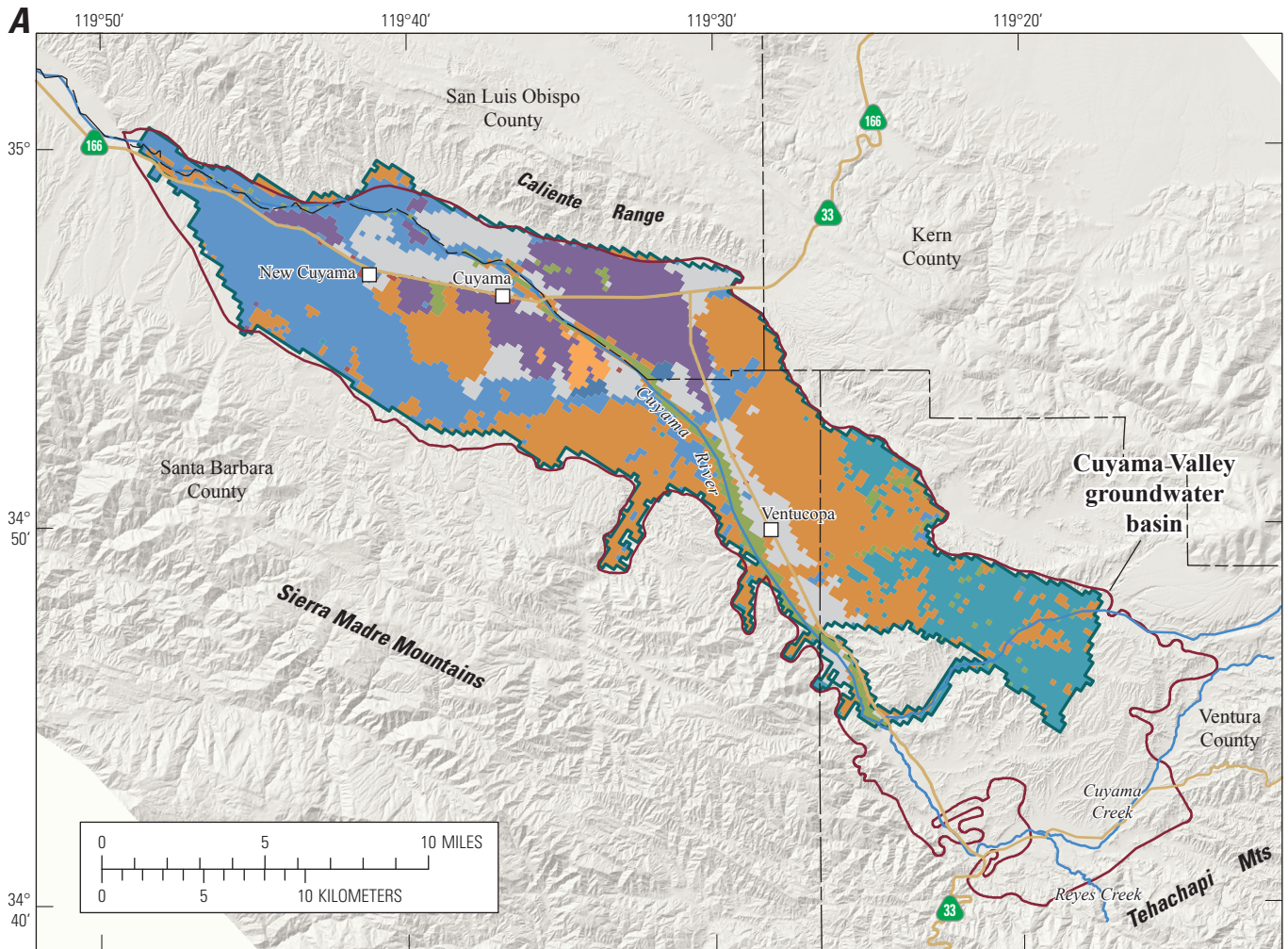
EXPLANATION

 Active model-grid boundary



Values on pie charts are in list-order, clockwise from top center and may not equal 100 due to rounding of percentages.

Figure 18. —Continued



Shaded relief base created from 30-m digital elevation model from USGS National Elevation Dataset (NED); North America Vertical Datum 1983 (NAVD83). Hydrology sourced from 1:24,000-scale National Hydrography Dataset, 1974-2009. Place names sourced from USGS Geographic Names Information System, 1974-2009. Albers Projection, NAD83.

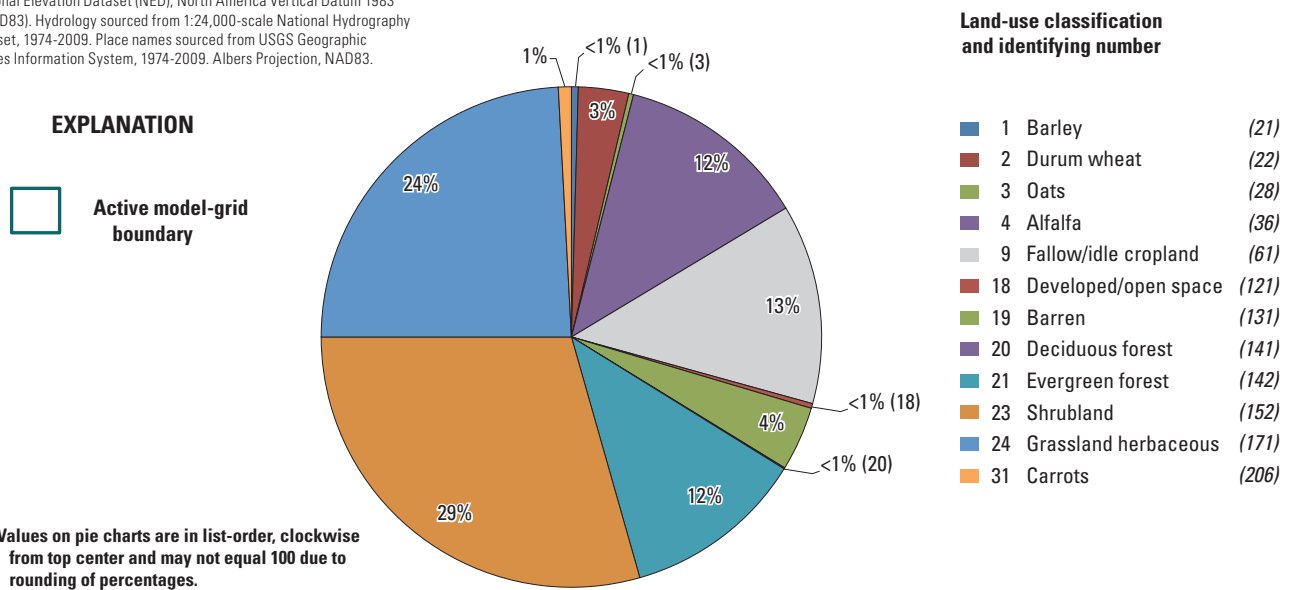
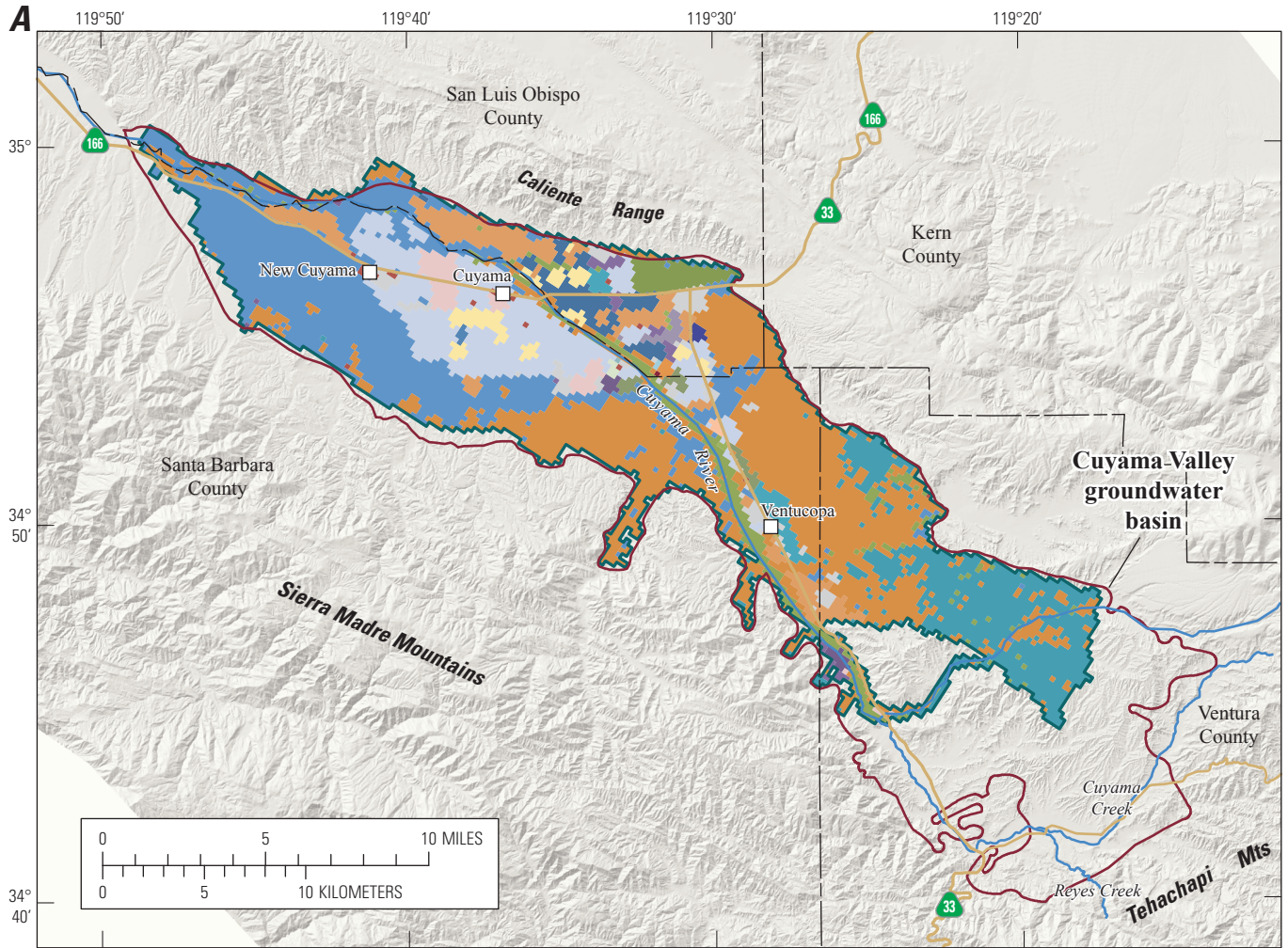


Figure 19. Land-use (virtual crop) groups discretized to the model grid, and pie chart of percentages of total land use over the modeled area for A, 1984; B, 2000; and C, 2002 for Cuyama Valley, California.



Shaded relief base created from 30-m digital elevation model from USGS National Elevation Dataset (NED); North America Vertical Datum 1983 (NAVD83). Hydrology sourced from 1:24,000-scale National Hydrography Dataset, 1974-2009. Place names sourced from USGS Geographic Names Information System, 1974-2009. Albers Projection, NAD83.

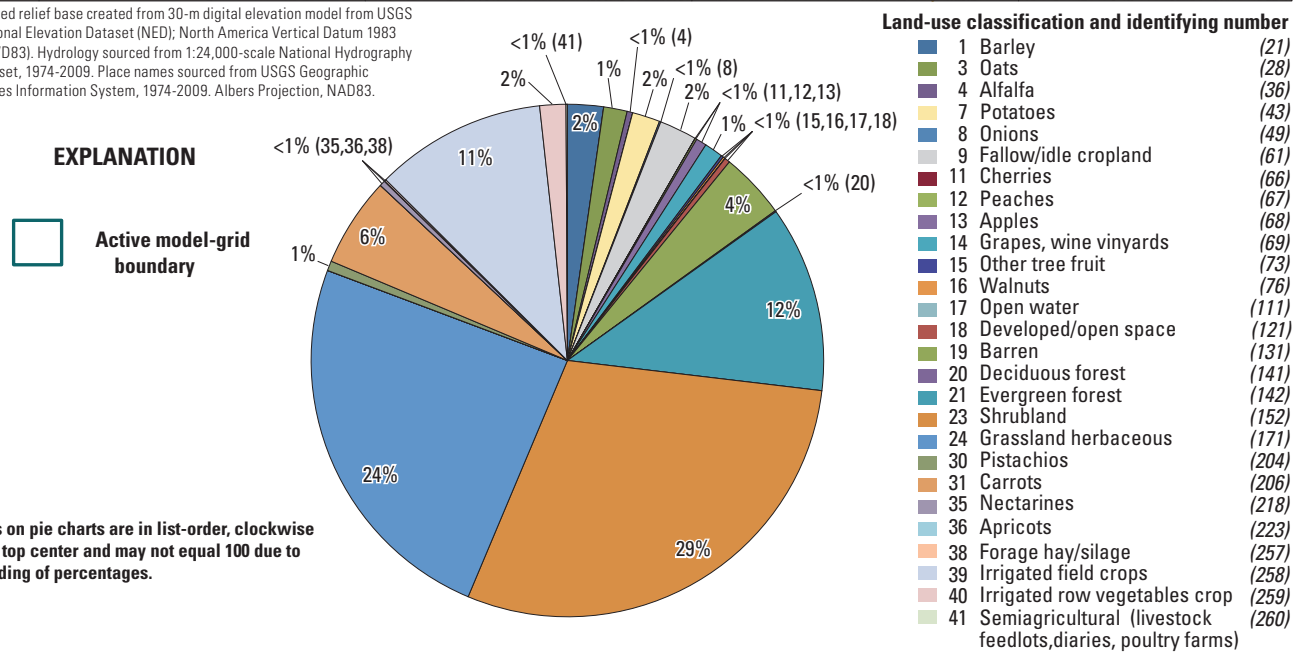
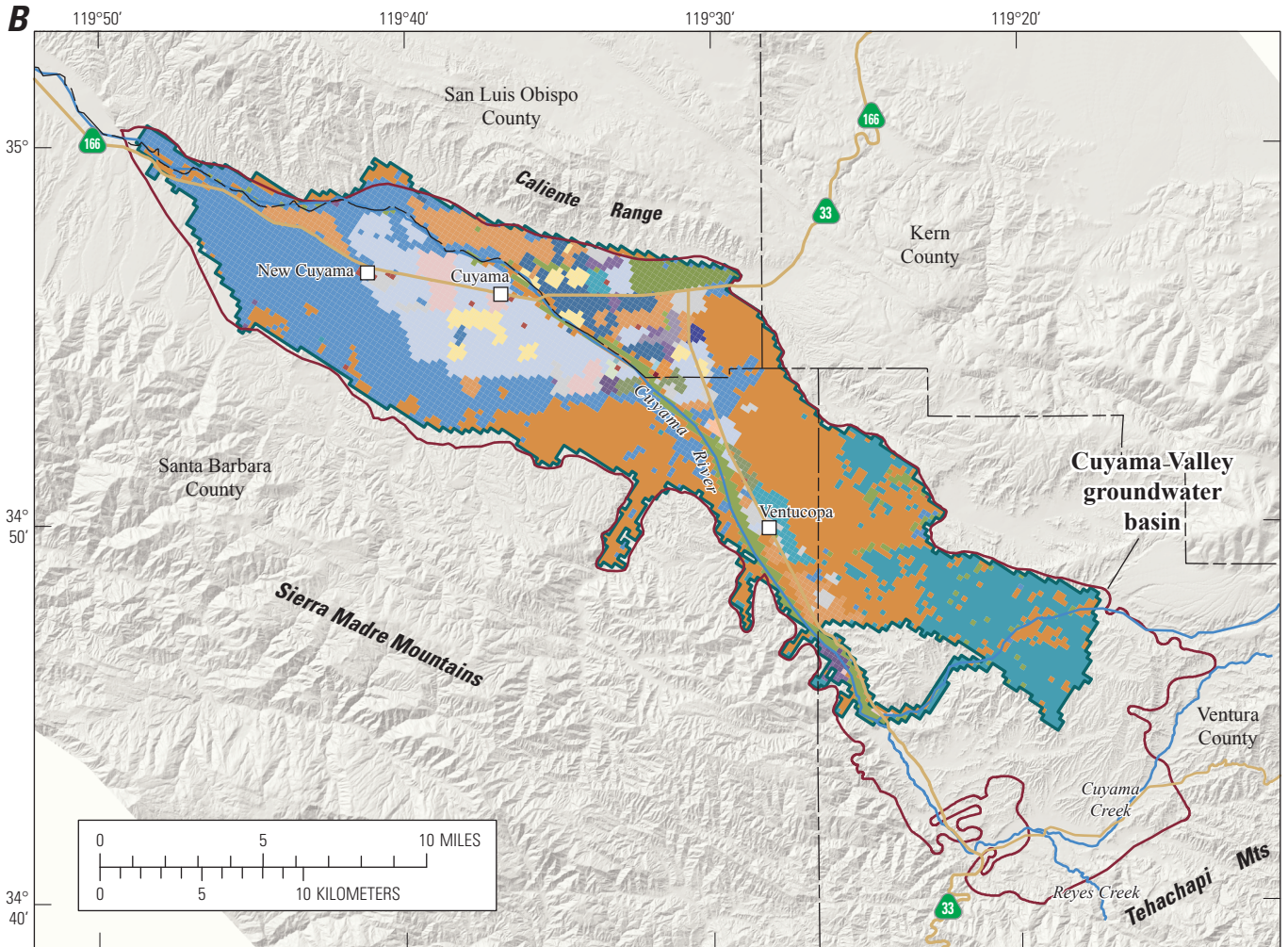


Figure 20. 2004–06 periods of land-use (virtual crop) groups discretized to the model grid, and pie chart of percentages of total land use over the modeled area for A, 2004; B, 2005; and C, 2006 for Cuyama Valley, California.



Shaded relief base created from 30-m digital elevation model from USGS National Elevation Dataset (NED); North America Vertical Datum 1983 (NAVD83). Hydrology sourced from 1:24,000-scale National Hydrography Dataset, 1974-2009. Place names sourced from USGS Geographic Names Information System, 1974-2009. Albers Projection, NAD83.

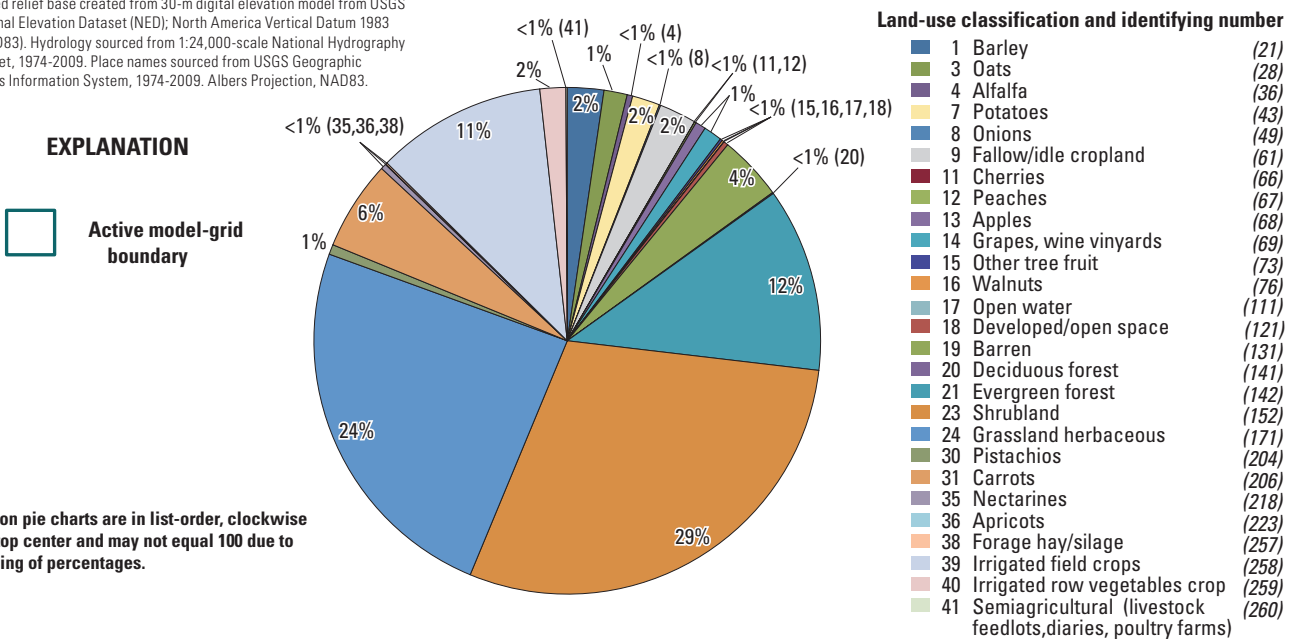
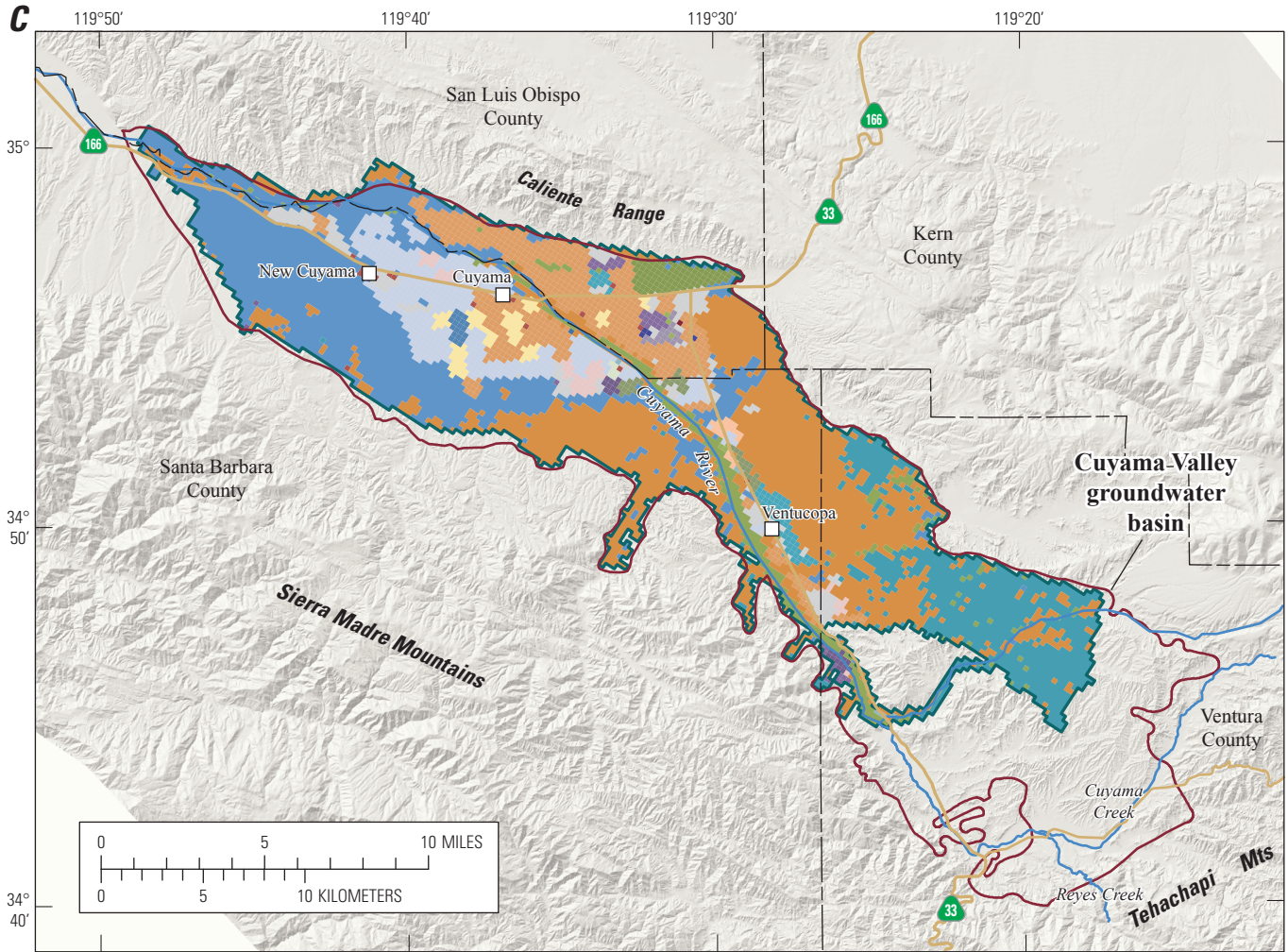


Figure 20. —Continued



Shaded relief base created from 30-m digital elevation model from USGS National Elevation Dataset (NED); North America Vertical Datum 1983 (NAVD83). Hydrology sourced from 1:24,000-scale National Hydrography Dataset, 1974-2009. Place names sourced from USGS Geographic Names Information System, 1974-2009. Albers Projection, NAD83.

EXPLANATION

□ Active model-grid boundary

Land-use classification and identifying number

- 1 Barley (21)
- 3 Oats (28)
- 4 Alfalfa (36)
- 7 Potatoes (43)
- 8 Onions (49)
- 9 Fallow/idle cropland (61)
- 11 Cherries (66)
- 12 Peaches (67)
- 13 Apples (68)
- 14 Grapes, wine vinyards (69)
- 15 Other tree fruit (73)
- 17 Open water (111)
- 18 Developed/open space (121)
- 19 Barren (131)
- 20 Deciduous forest (141)
- 21 Evergreen forest (142)
- 23 Shrubland (152)
- 24 Grassland herbaceous (171)
- 30 Pistachios (204)
- 31 Carrots (206)
- 35 Nectarines (218)
- 38 Forage hay/silage (257)
- 39 Irrigated field crops (258)
- 40 Irrigated row vegetables crop (259)
- 41 Semiagricultural (livestock feedlots,diaries, poultry farms) (260)

Values on pie charts are in list-order, clockwise from top center and may not equal 100 due to rounding of percentages.

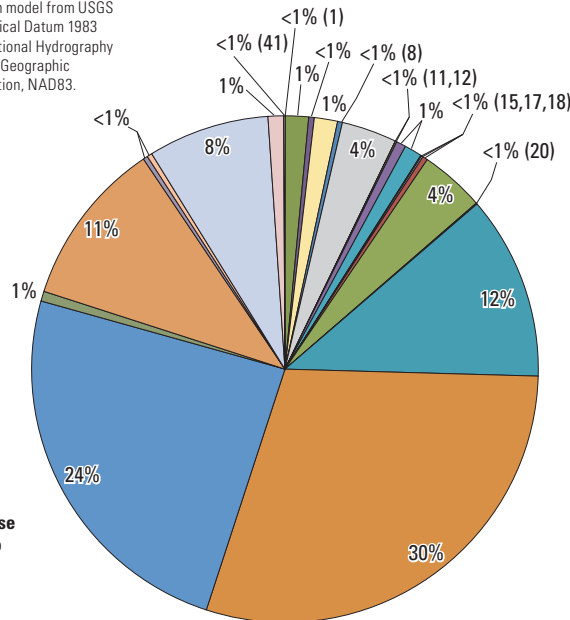
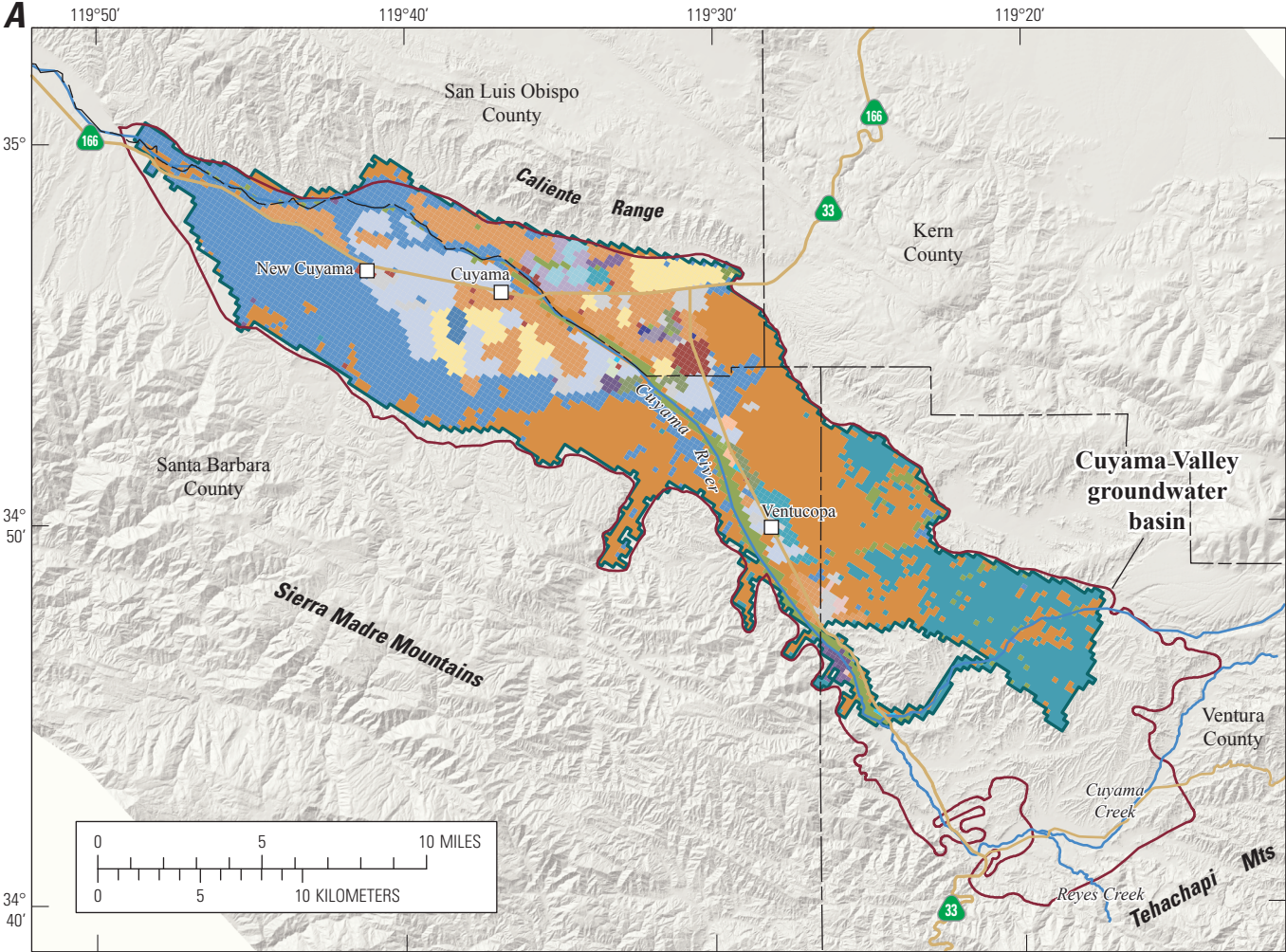


Figure 20. —Continued

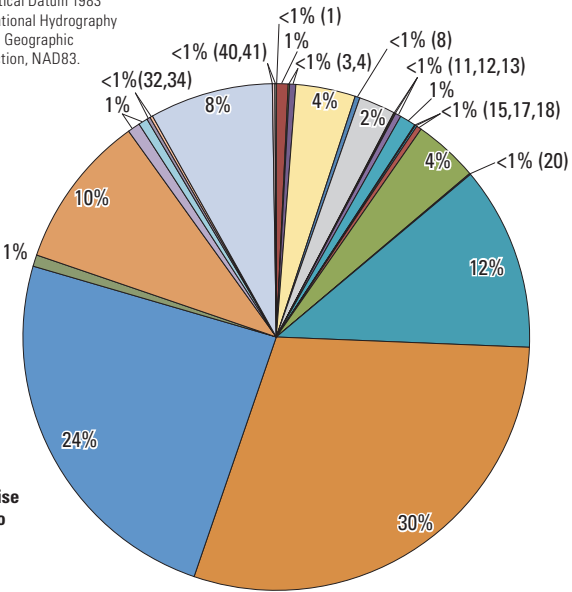


Shaded relief base created from 30-m digital elevation model from USGS National Elevation Dataset (NED); North America Vertical Datum 1983 (NAVD83). Hydrology sourced from 1:24,000-scale National Hydrography Dataset, 1974-2009. Place names sourced from USGS Geographic Names Information System, 1974-2009. Albers Projection, NAD83.

EXPLANATION

Active model-grid boundary

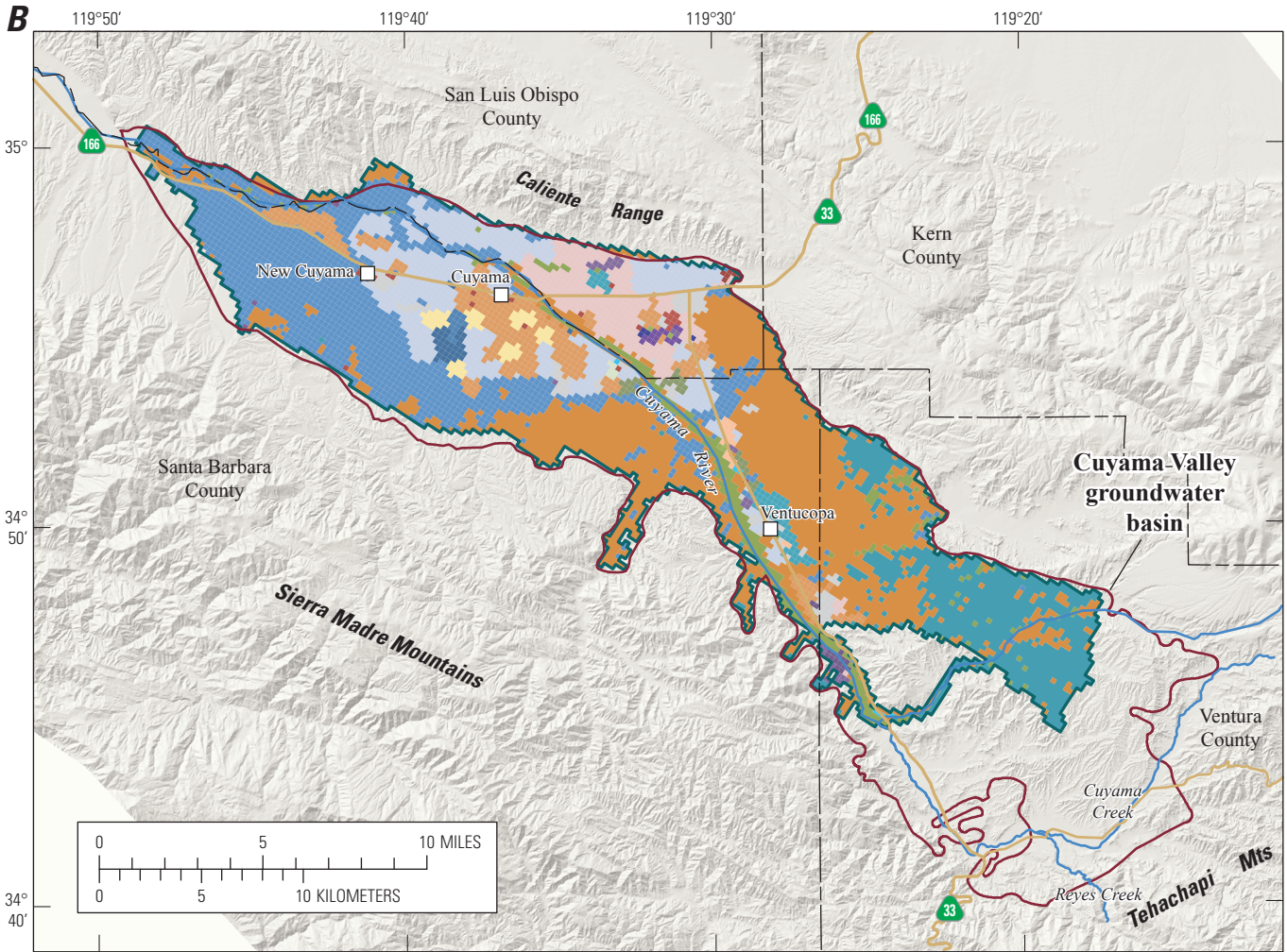
Values on pie charts are in list-order, clockwise from top center and may not equal 100 due to rounding of percentages.



Land-use classification and identifying number

- 1 Barley (21)
- 2 Durum wheat (22)
- 3 Oats (28)
- 4 Alfalfa (36)
- 7 Potatoes (43)
- 8 Onions (49)
- 9 Fallow/idle cropland (61)
- 11 Cherries (66)
- 12 Peaches (67)
- 13 Apples (68)
- 14 Grapes, wine vineyards (69)
- 15 Other tree fruit (73)
- 17 Open water (111)
- 18 Developed/open space (121)
- 19 Barren (131)
- 20 Deciduous forest (141)
- 21 Evergreen forest (142)
- 23 Shrubland (152)
- 24 Grassland herbaceous (171)
- 30 Pistachios (204)
- 31 Carrots (206)
- 32 Cantaloupes (209)
- 34 Broccoli (214)
- 35 Nectarines (218)
- 38 Forage hay/silage (257)
- 39 Irrigated field crops (258)
- 40 Irrigated row vegetables crop (259)
- 41 Semiagricultural (livestock feedlots, dairies, poultry farms) (260)

Figure 21. 2007–09 periods of land-use (virtual crop) groups discretized to the model grid, and pie chart of percentages of total land use over the modeled area for A, 2007; B, 2008; and C, 2009 for Cuyama Valley, California.



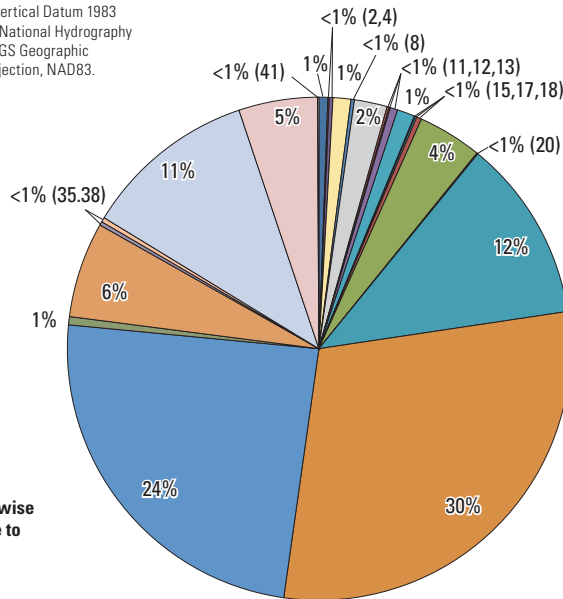
Shaded relief base created from 30-m digital elevation model from USGS National Elevation Dataset (NED); North America Vertical Datum 1983 (NAVD83). Hydrology sourced from 1:24,000-scale National Hydrography Dataset, 1974-2009. Place names sourced from USGS Geographic Names Information System, 1974-2009. Albers Projection, NAD83.

EXPLANATION

□ Active model-grid boundary

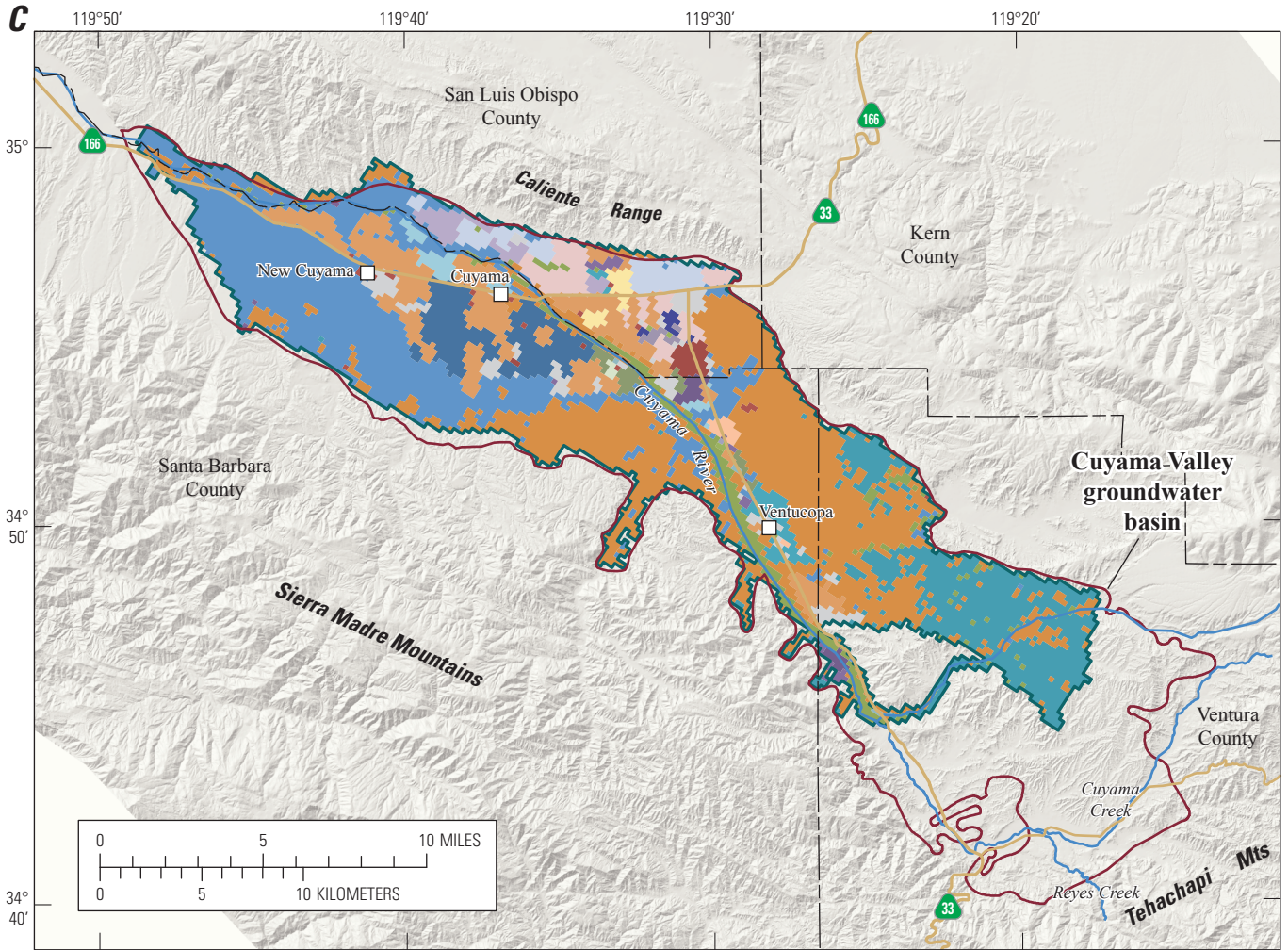
Land-use classification and identifying number

- 1 Barley (21)
- 2 Durum wheat (22)
- 4 Alfalfa (36)
- 7 Potatoes (43)
- 8 Onions (49)
- 9 Fallow/idle cropland (61)
- 11 Cherries (66)
- 12 Peaches (67)
- 13 Apples (68)
- 14 Grapes, wine vineyards (69)
- 15 Other tree fruit (73)
- 17 Open water (111)
- 18 Developed/open space (121)
- 19 Barren (131)
- 20 Deciduous forest (141)
- 21 Evergreen forest (142)
- 23 Shrubland (152)
- 24 Grassland herbaceous (171)
- 30 Pistachios (204)
- 31 Carrots (206)
- 35 Nectarines (218)
- 38 Forage hay/silage (257)
- 39 Irrigated field crops (258)
- 40 Irrigated row vegetables crop (259)
- 41 Semiagricultural (livestock feedlots, dairies, poultry farms) (260)



Values on pie charts are in list-order, clockwise from top center and may not equal 100 due to rounding of percentages.

Figure 21. —Continued



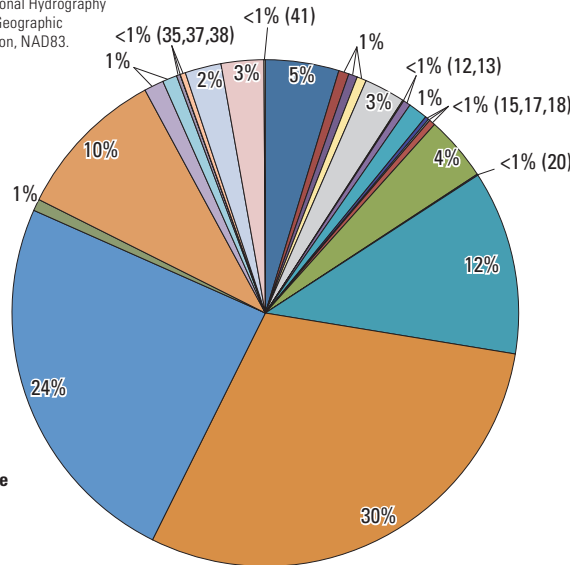
Shaded relief base created from 30-m digital elevation model from USGS National Elevation Dataset (NED); North America Vertical Datum 1983 (NAVD83). Hydrology sourced from 1:24,000-scale National Hydrography Dataset, 1974-2009. Place names sourced from USGS Geographic Names Information System, 1974-2009. Albers Projection, NAD83.

EXPLANATION

□ Active model-grid boundary

Land-use classification and identifying number

- 1 Barley (21)
- 2 Durum wheat (22)
- 4 Alfalfa (36)
- 7 Potatoes (43)
- 9 Fallow/idle cropland (61)
- 12 Peaches (67)
- 13 Apples (68)
- 14 Grapes, wine vineyards (69)
- 15 Other tree fruit (73)
- 17 Open water (111)
- 18 Developed/open space (121)
- 19 Barren (131)
- 20 Deciduous forest (141)
- 21 Evergreen forest (142)
- 23 Shrubland (152)
- 24 Grassland herbaceous (171)
- 30 Pistachios (204)
- 31 Carrots (206)
- 32 Cantaloupes (209)
- 34 Broccoli (214)
- 35 Nectarines (218)
- 37 Cauliflower (244)
- 38 Forage hay/silage (257)
- 39 Irrigated field crops (258)
- 40 Irrigated row vegetables crop (259)
- 41 Semiagricultural (livestock feedlots, dairies, poultry farms) (260)



Values on pie charts are in list-order, clockwise from top center and may not equal 100 due to rounding of percentages.

Figure 21. —Continued

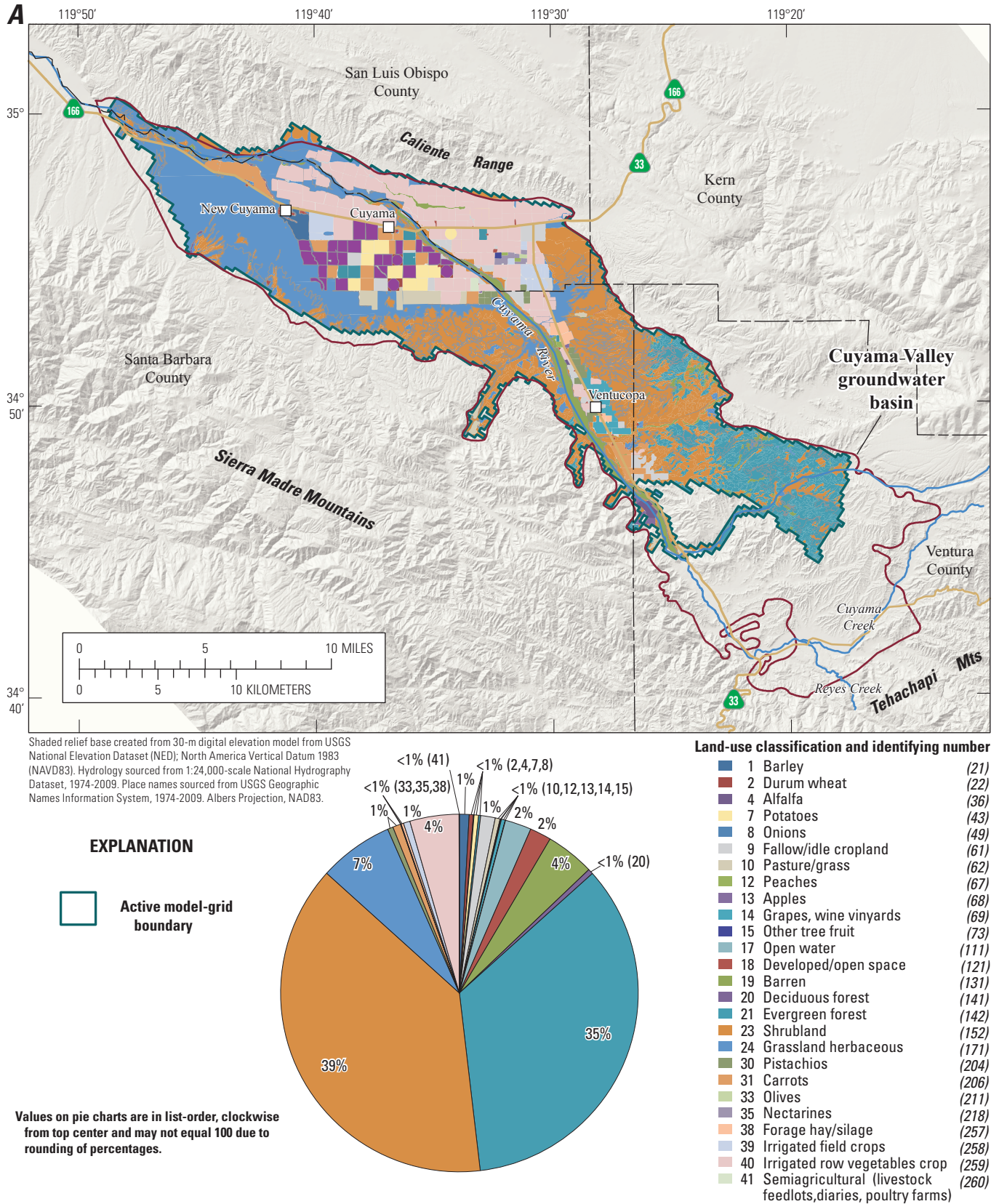
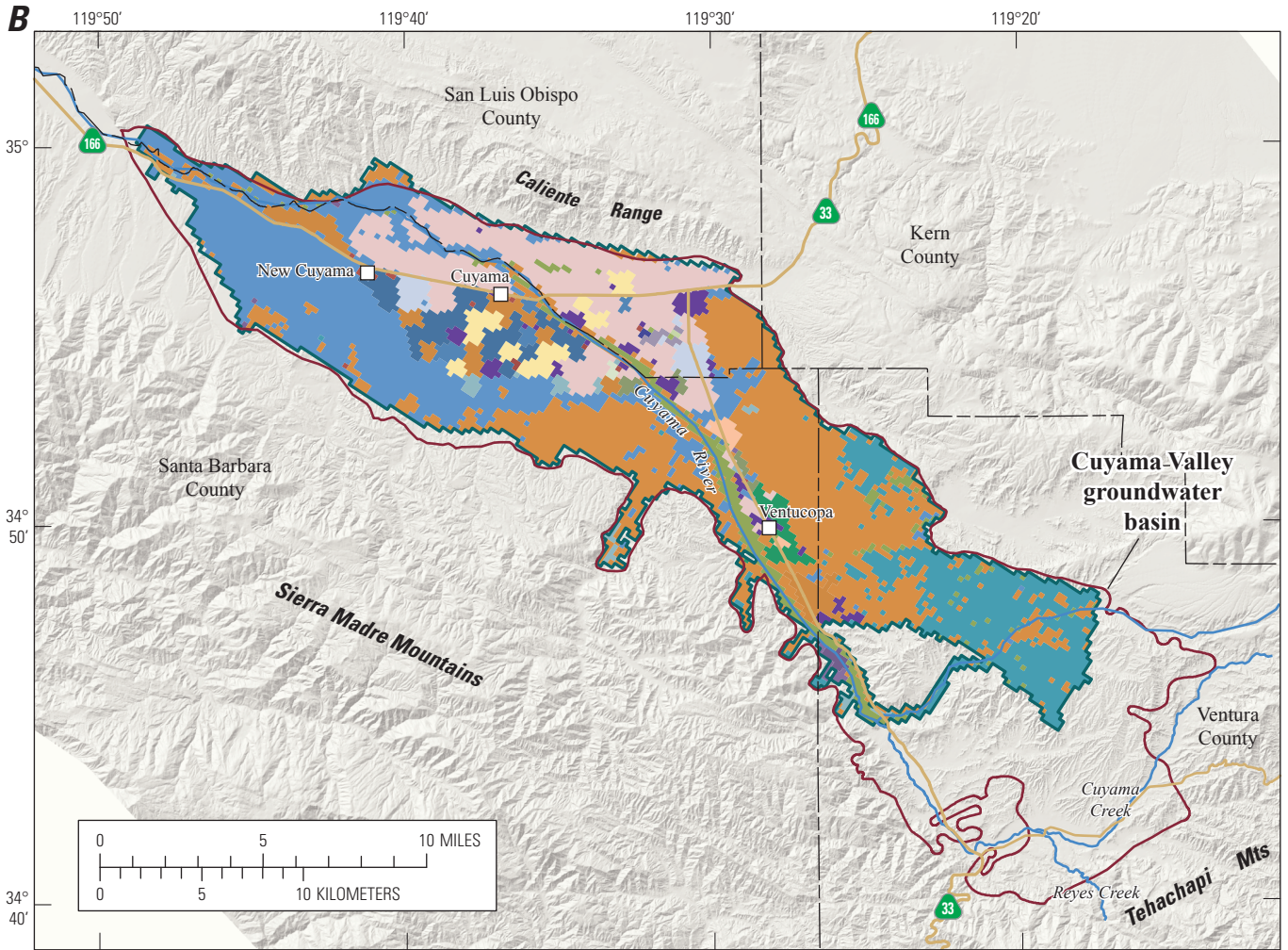


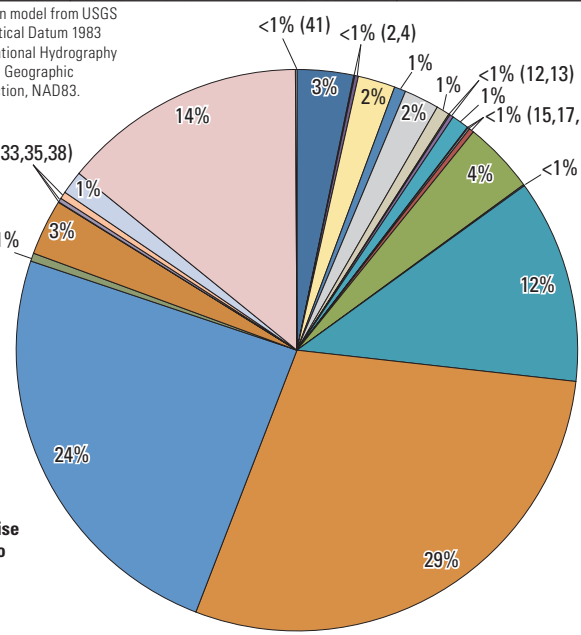
Figure 22. A, actual major categories of land-use for 2010; B, equivalent land-use (virtual crop) groups discretized to the model grid, and pie chart of percentage of total land use over the entire model area; and C, changes in percentages of selected land use through time, Cuyama Valley, California.



Shaded relief base created from 30-m digital elevation model from USGS National Elevation Dataset (NED); North America Vertical Datum 1983 (NAVD83). Hydrology sourced from 1:24,000-scale National Hydrography Dataset, 1974-2009. Place names sourced from USGS Geographic Names Information System, 1974-2009. Albers Projection, NAD83.

EXPLANATION
 Active model-grid boundary

Values on pie charts are in list-order, clockwise from top center and may not equal 100 due to rounding of percentages.



- Land-use classification and identifying number**
- 1 Barley (21)
 - 2 Durum wheat (22)
 - 4 Alfalfa (36)
 - 7 Potatoes (43)
 - 8 Onions (49)
 - 9 Fallow/idle cropland (61)
 - 10 Pasture/grass (62)
 - 12 Peaches (67)
 - 13 Apples (68)
 - 14 Grapes, wine vineyards (69)
 - 15 Other tree fruit (73)
 - 17 Open water (111)
 - 18 Developed/open space (121)
 - 19 Barren (131)
 - 20 Deciduous forest (141)
 - 21 Evergreen forest (142)
 - 23 Shrubland (152)
 - 24 Grassland herbaceous (171)
 - 30 Pistachios (204)
 - 31 Carrots (206)
 - 33 Olives (211)
 - 35 Nectarines (218)
 - 38 Forage hay/silage (257)
 - 39 Irrigated field crops (258)
 - 40 Irrigated row vegetables crop (259)
 - 41 Semiagricultural (livestock feedlots, dairies, poultry farms) (260)

Figure 22. —Continued

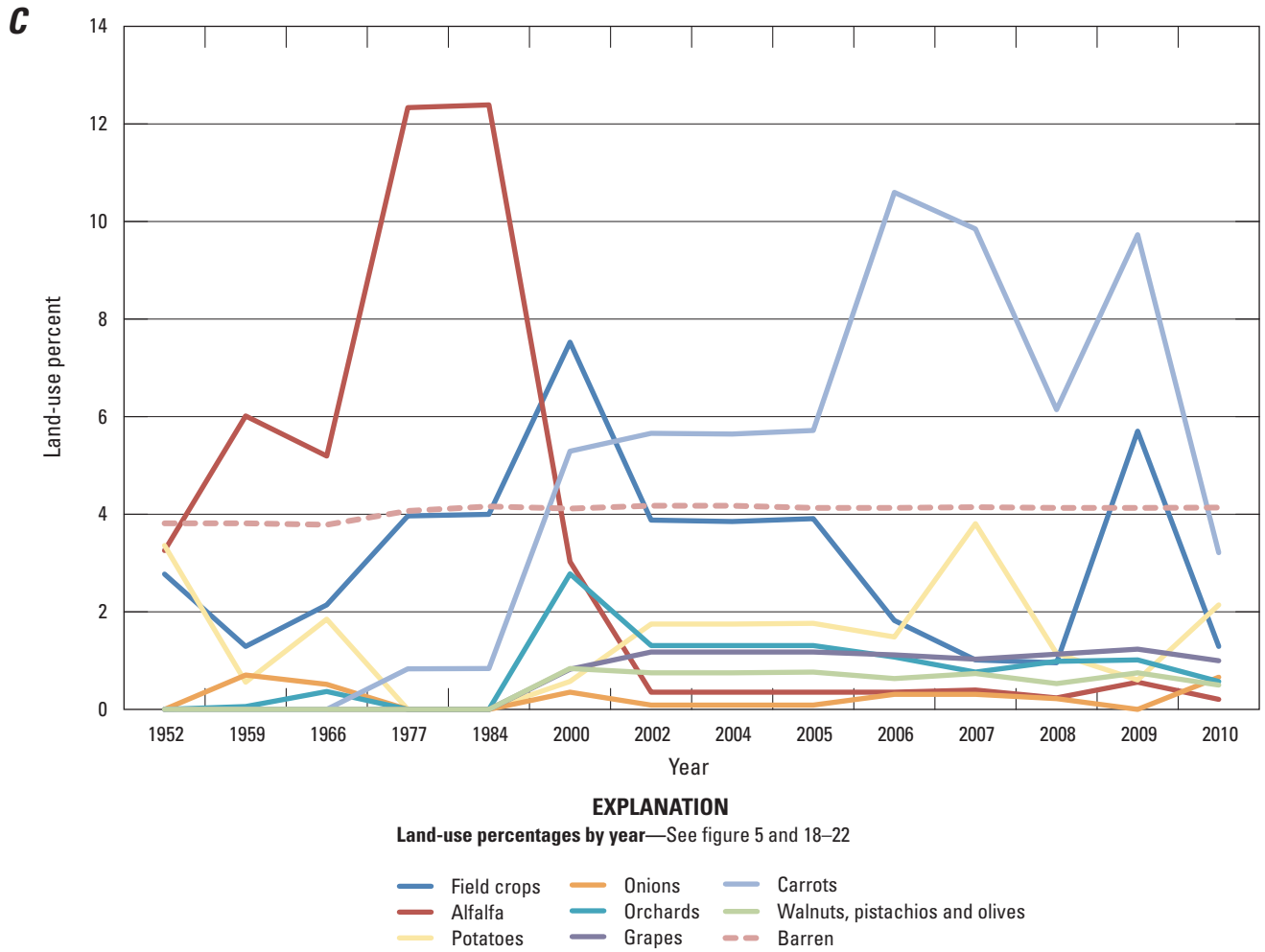


Figure 22. —Continued

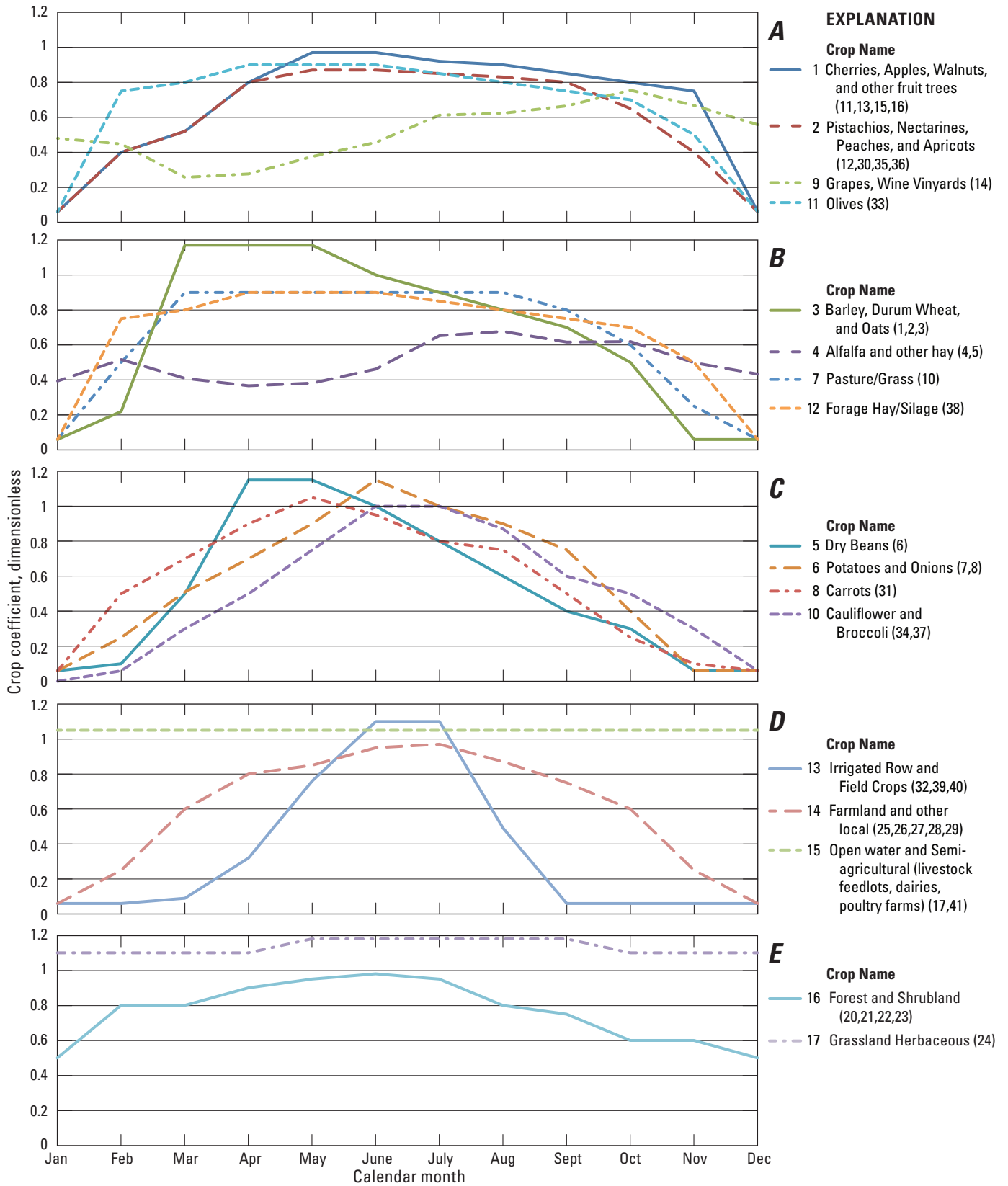
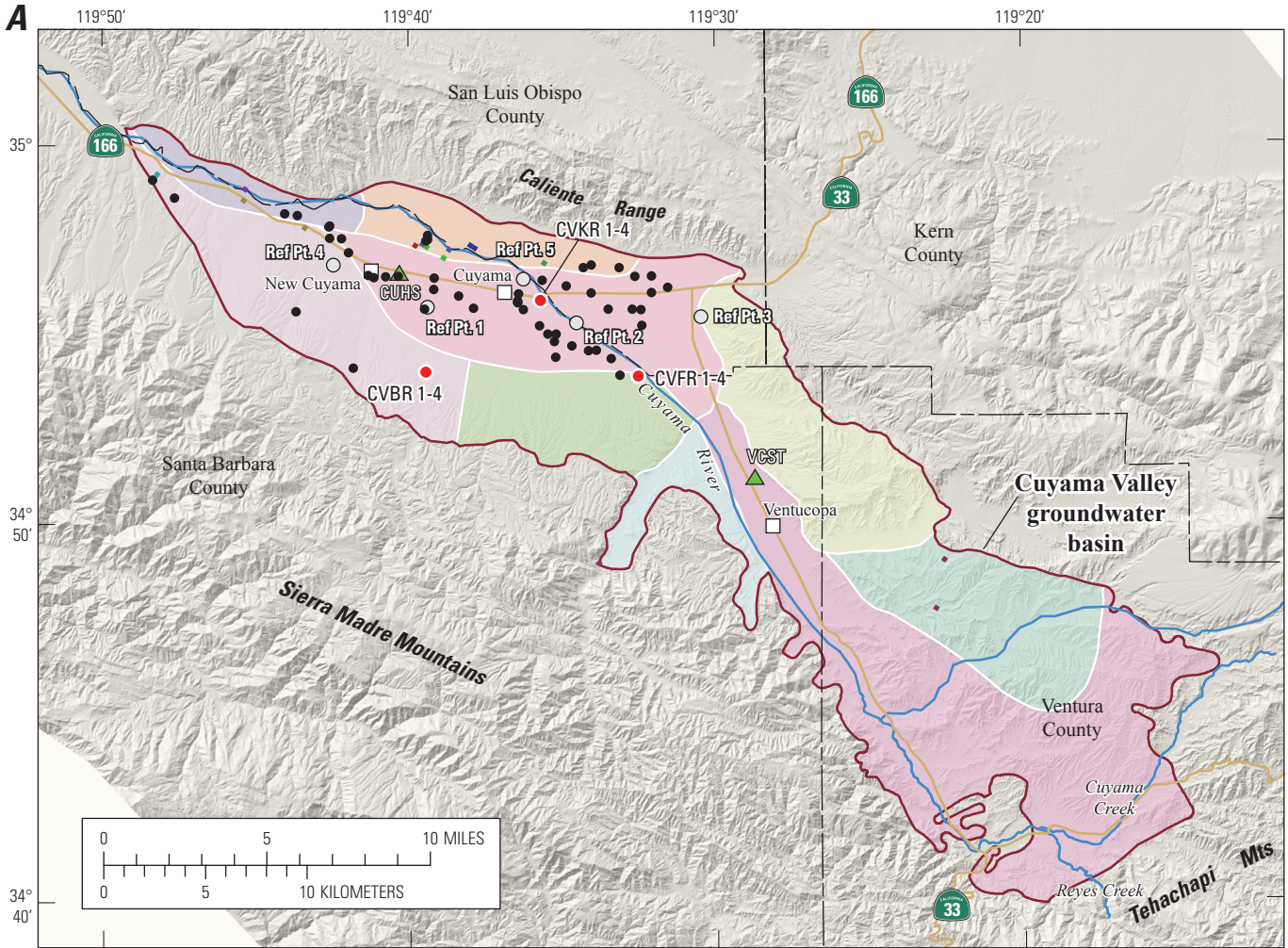


Figure 23. Monthly crop coefficients for *A*, orchards; *B*, grains and hay; *C* vegetables; *D*, general land use; and *E*, native vegetation in the Cuyama Valley, California.



Shaded relief base created from 30-m digital elevation model from USGS National Elevation Dataset (NED); North America Vertical Datum 1983 (NAVD83). Hydrology sourced from 1:24,000-scale National Hydrography Dataset, 1974-2009. Place names sourced from USGS Geographic Names Information System, 1974-2009. Albers Projection, NAD83.

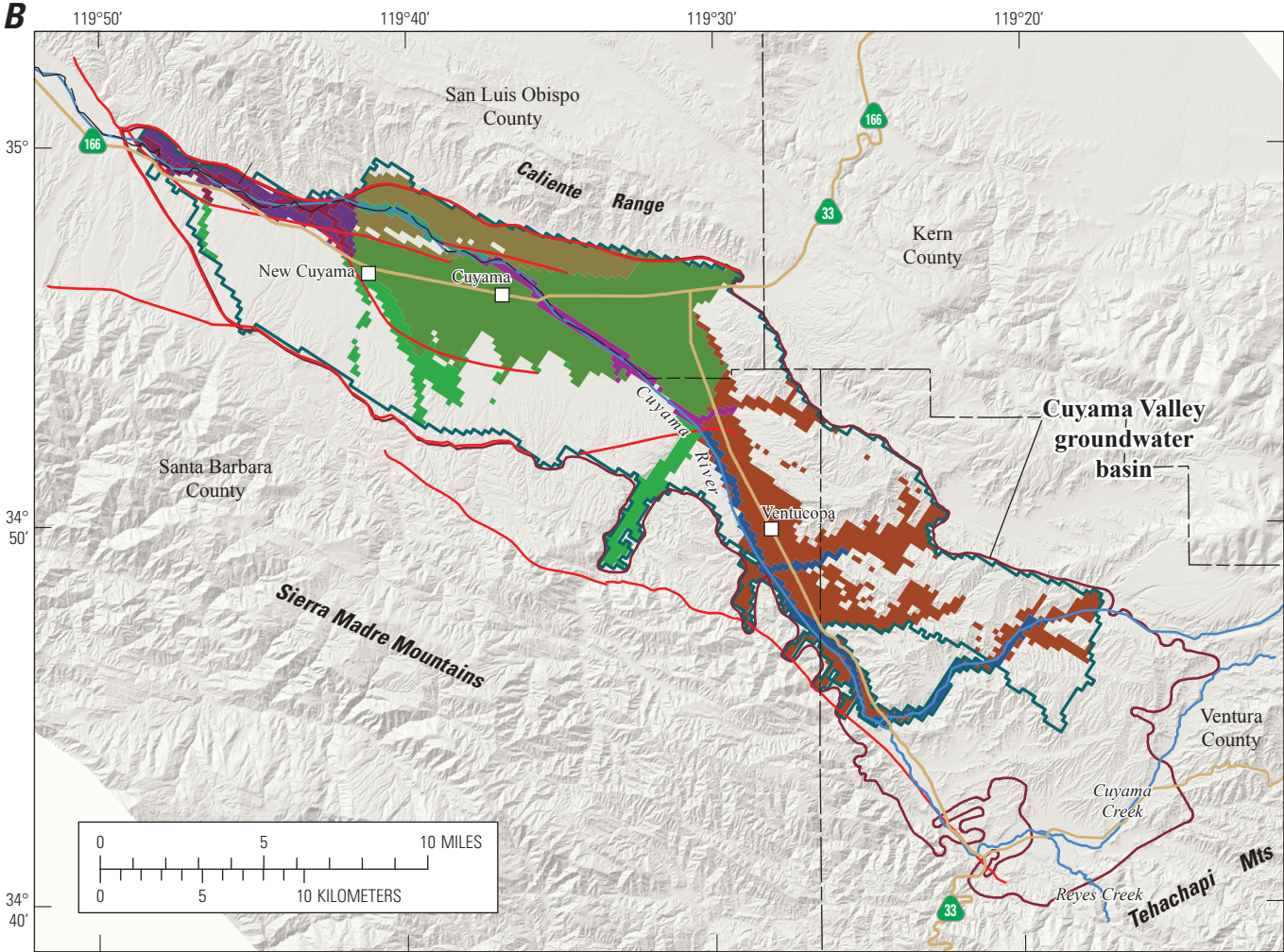
EXPLANATION

- Cuyama groundwater basin subregion**
- Caliente Northern-Main
 - Central Sierra Madre Foothills
 - Northeast Ventucopa Uplands
 - Northwestern Sierra Madre Foothills
 - Northern Ventucopa Uplands
 - Southern Sierra Madre Foothills
 - Southern Ventucopa Uplands
 - Southern-Main
 - Western Basin

- Drains**
- Weir Seep
 - Graveyard Seep
 - Turkey Trap Fault Seeps
 - Turkey Trap Hills Seeps
 - Headquarters Spring
 - CuyamaRanch_Hiway/CalTransStation
 - No Name
 - North Caliente Ranch
 - St Barb Cyn-ReyesRch/QuatalRdSprBox/Quail

- USGS-monitoring site
- Pump-test site
- InSAR reference point
- Continuous GPS station

Figure 24. A, locations of wells with pumping tests, and the distribution of parameter zones used for model calibration of hydraulic properties for B, model layer 1, C, model layer 2, and D, model layer 3 in the Cuyama Valley, California.



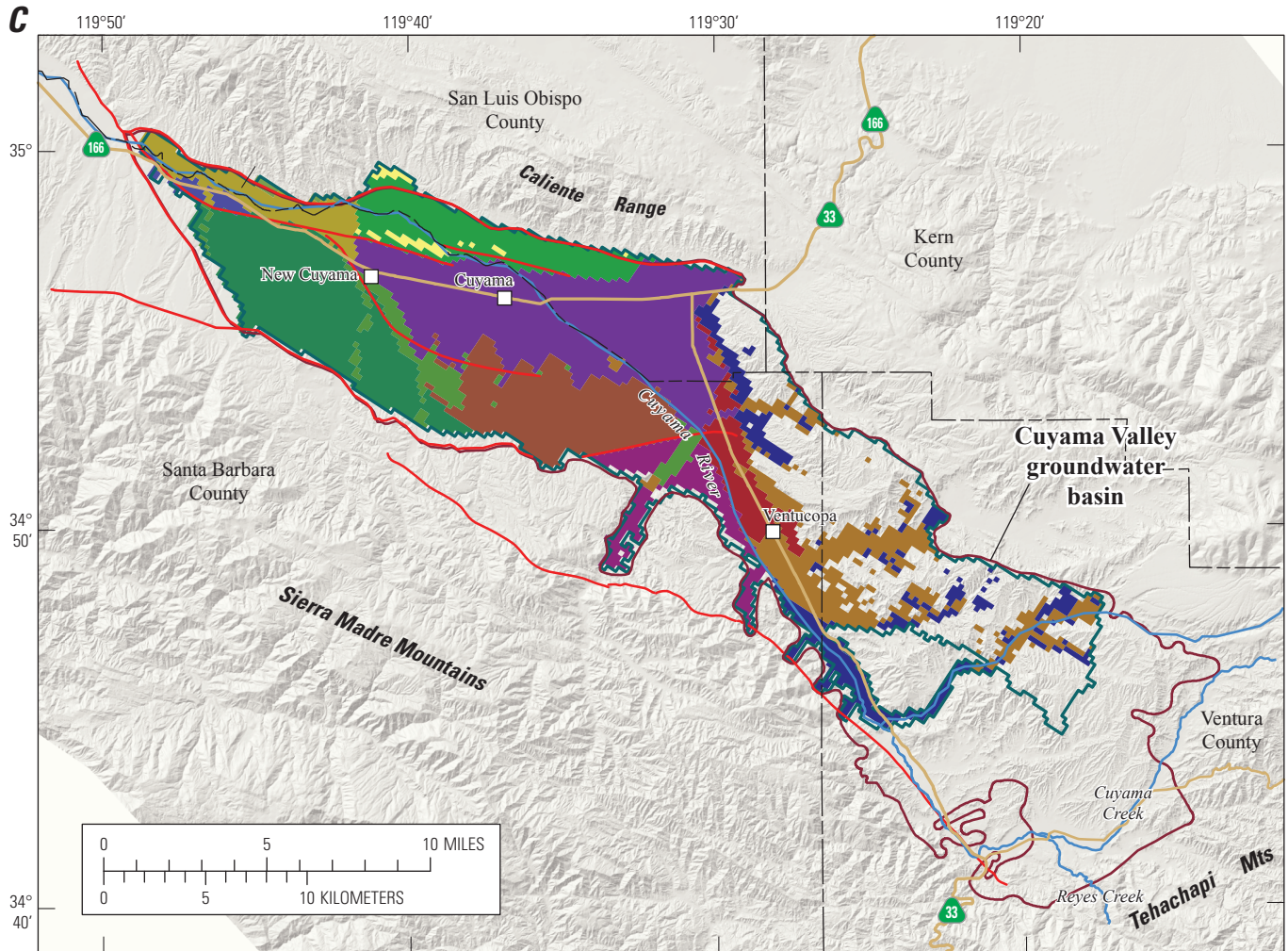
Shaded relief base created from 30-m digital elevation model from USGS National Elevation Dataset (NED); North America Vertical Datum 1983 (NAVD83). Hydrology sourced from 1:24,000-scale National Hydrography Dataset, 1974-2009. Place names sourced from USGS Geographic Names Information System, 1974-2009. Albers Projection, NAD83.

EXPLANATION

Layer 1 hydraulic property zone and (zone number)—
(See table 13 for description of acronyms)

Northern Main	Western	Sierra Madre Foothills	Ventucopa Uplands	 Active model-grid boundary  Fault
 NMZ_QYA (1)  NMZQYACC (2)	 WZ_QYA (8)  WZ_QYACC (9)	 SMFHQYA (3)	 VC_QYACC (6)  VC_QYAUC (7)	
Southern Main				
 SMZ_QYA (4)  SMZ_QYACC (5)				

Figure 24. —Continued



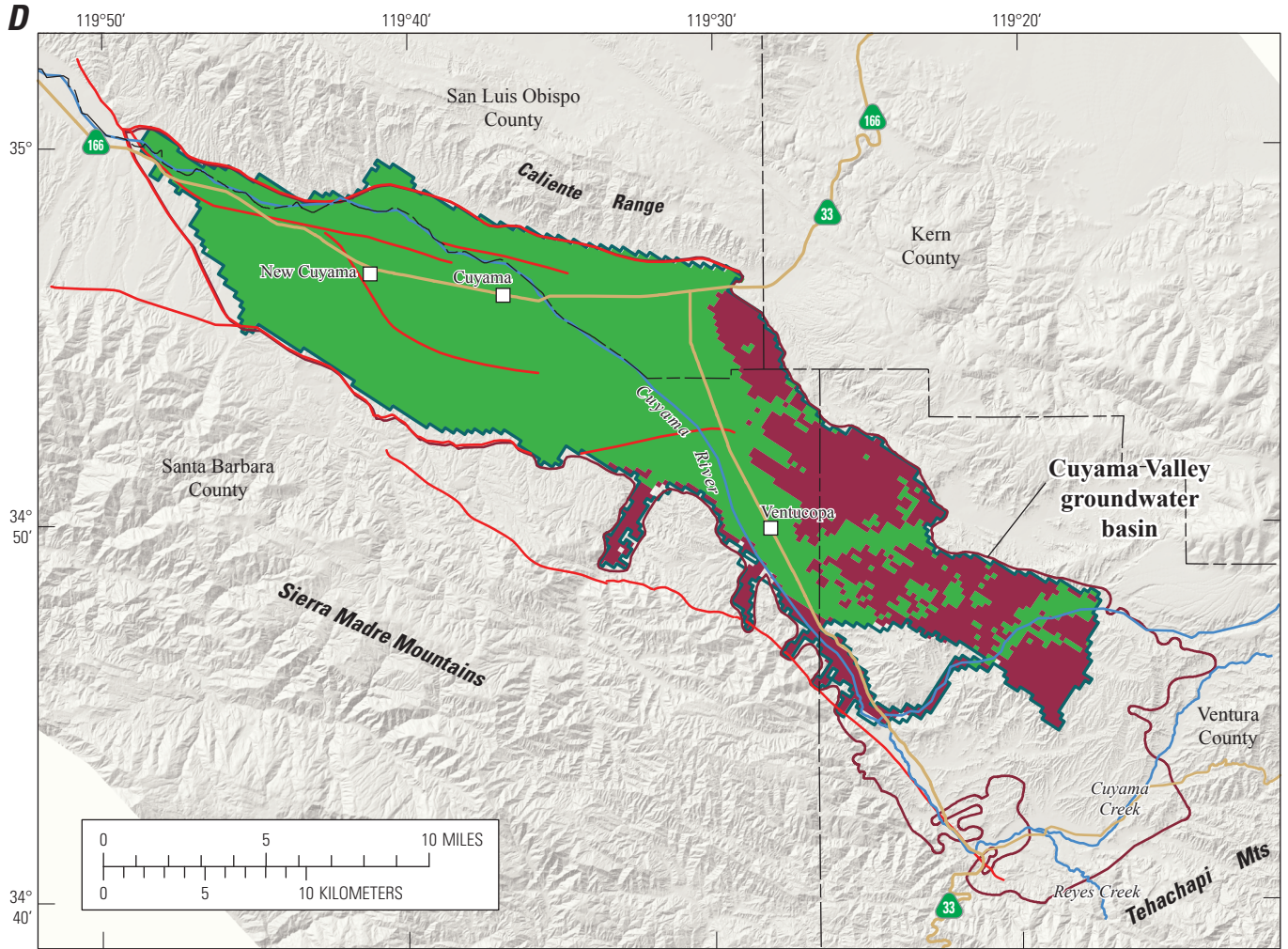
Shaded relief base created from 30-m digital elevation model from USGS National Elevation Dataset (NED); North America Vertical Datum 1983 (NAVD83). Hydrology sourced from 1:24,000-scale National Hydrography Dataset, 1974-2009. Place names sourced from USGS Geographic Names Information System, 1974-2009. Albers Projection, NAD83.

EXPLANATION

Layer 2 hydraulic property zone and (zone number)—
(See table 13 for description of acronyms)

North Main	Western	Sierra Madre Foothills	Ventucopa Uplands	
NMZ_QOA (10)	WZ_QOAC (22)	SMFH_QOAC (19)	VC_QOAN (14)	Active model-grid boundary
NMZ_QOAC (18)	WZ_QOA_N (15)	SMFH_QOAN (11)	VC_QOAC (21)	Fault
South Main	WZ_QOA_S (16)	SMFH_QOAM (12)	QOA_PHT (23)	
SMZ_QOAC (20)		SMFH_QOAS (13)		

Figure 24. —Continued



Shaded relief base created from 30-m digital elevation model from USGS National Elevation Dataset (NED); North America Vertical Datum 1983 (NAVD83). Hydrology sourced from 1:24,000-scale National Hydrography Dataset, 1974-2009. Place names sourced from USGS Geographic Names Information System, 1974-2009. Albers Projection, NAD83.

EXPLANATION

Layer 3 hydraulic property zone and (zone number)—
 (See table 13 for description of acronyms)

Morales Formation

MO_C (24)

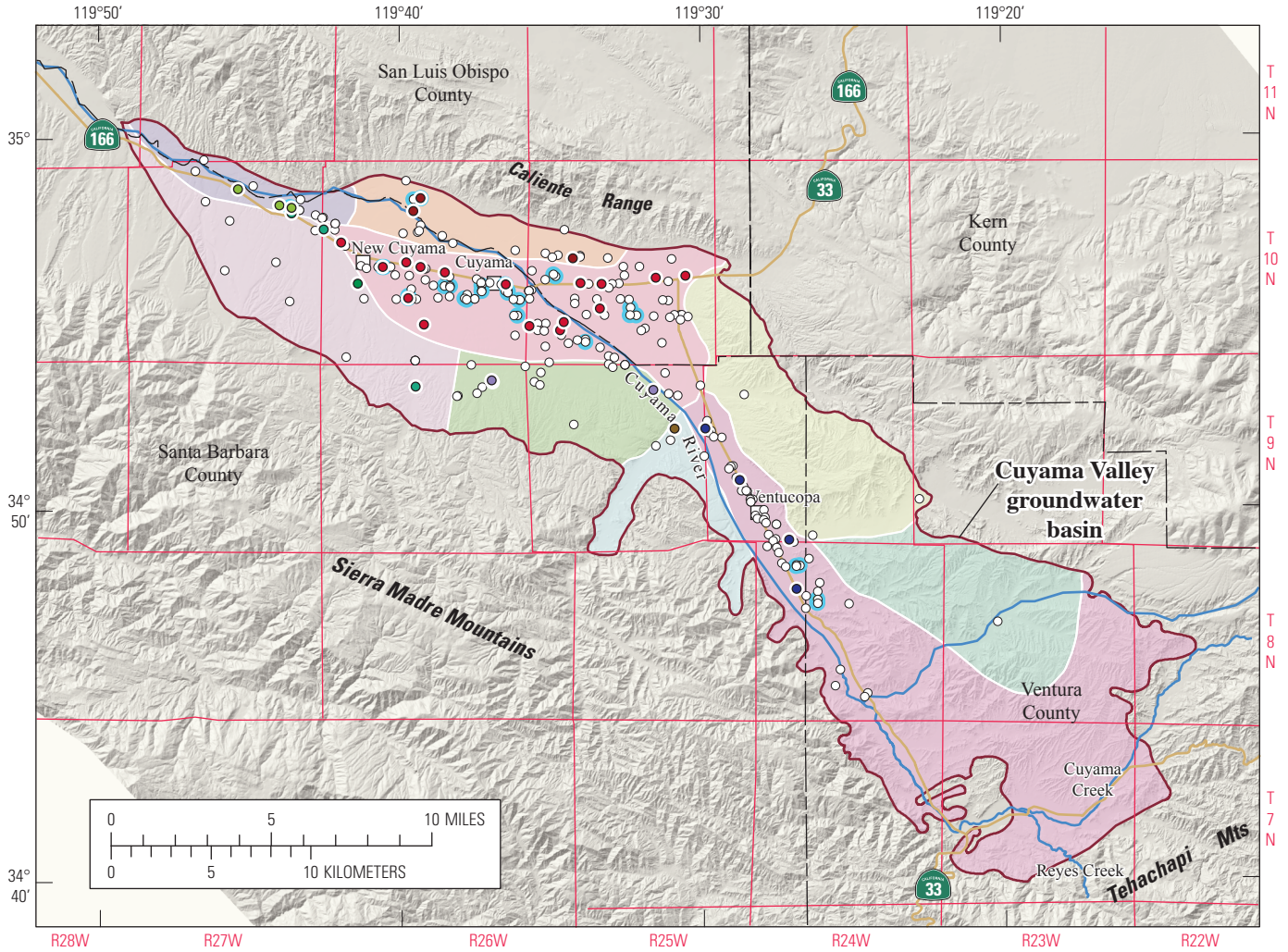
Ventucopa Uplands

VC_MOUC (17)

Active model-grid boundary

Fault

Figure 24. —Continued



Shaded relief base created from 30-m digital elevation model from USGS National Elevation Dataset (NED); North America Vertical Datum 1983 (NAVD83). Hydrology sourced from 1:24,000-scale National Hydrography Dataset, 1974-2009. Place names sourced from USGS Geographic Names Information System, 1974-2009. Albers Projection, NAD83.

EXPLANATION

- Cuyama groundwater basin subregions**
- Caliente Northern-Main
 - Central Sierra Madre Foothills
 - Northeast Ventucopa Uplands
 - Northwestern Sierra Madre Foothills
 - Northern Ventucopa Uplands
 - Southern Sierra Madre Foothills
 - Southern Ventucopa Uplands
 - Southern-Main
 - Western Basin

- Selected observation well shown on figure 26**
- Western Basin
 - Caliente Northern-Main
 - Southern Sierra Madre Foothills
 - Central Sierra Madre Foothills
 - Northern Sierra Madre Foothills
 - Southern Ventucopa Uplands
 - Southern-Main

- All wells used for model observations shown on figure 27a
- Well used for vertical water-level difference as shown on figure 27c

Figure 25. Calibration data sites of wells for groundwater levels and water-level differences for the Cuyama Valley Hydrologic Model, Cuyama Valley, California.

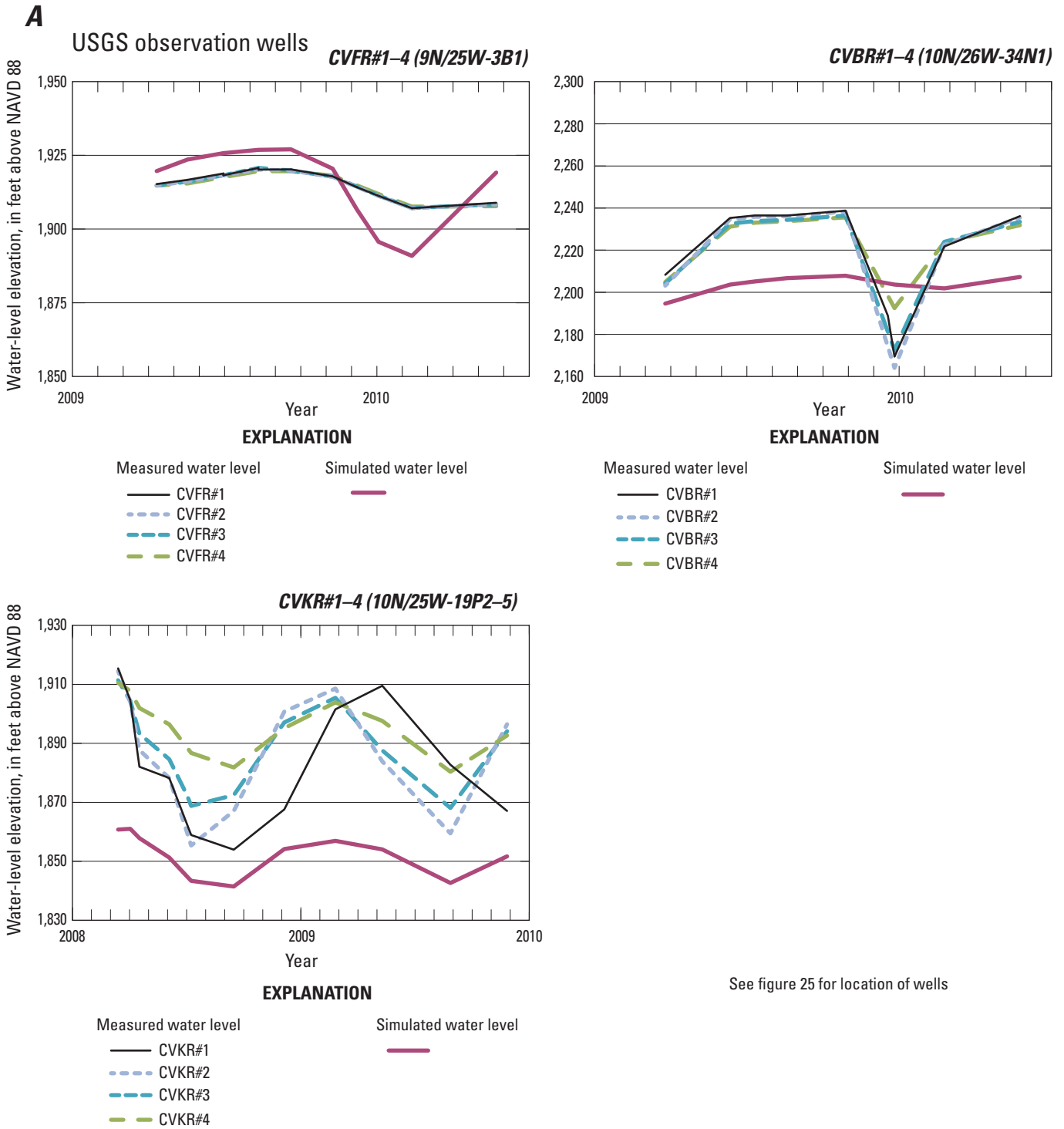


Figure 26. Simulated and measured hydrographs for selected wells in A, Main-zone, B, Ventucopa Upland, and C, Sierra Madre Foothills subregions, Cuyama Valley, California.

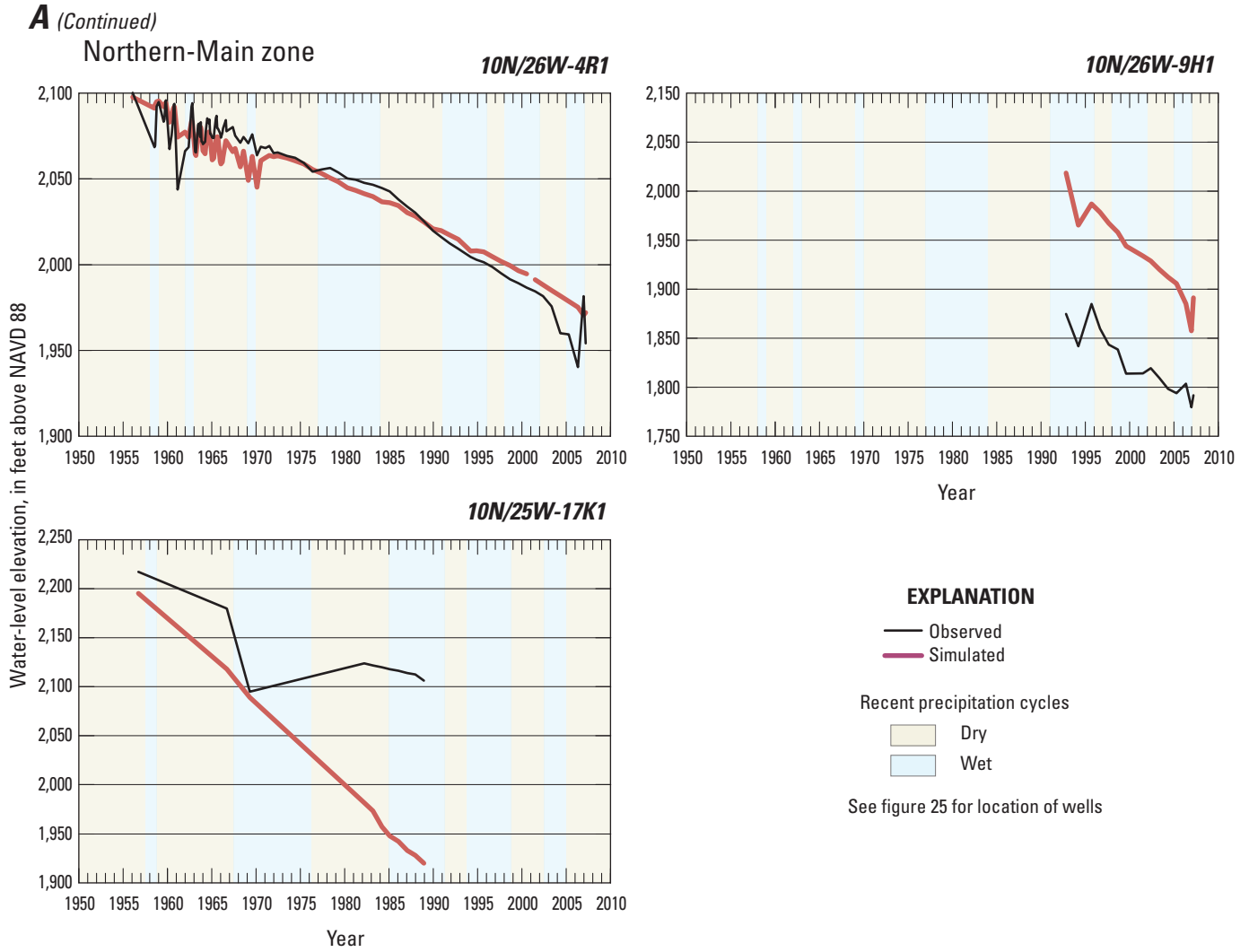


Figure 26. —Continued

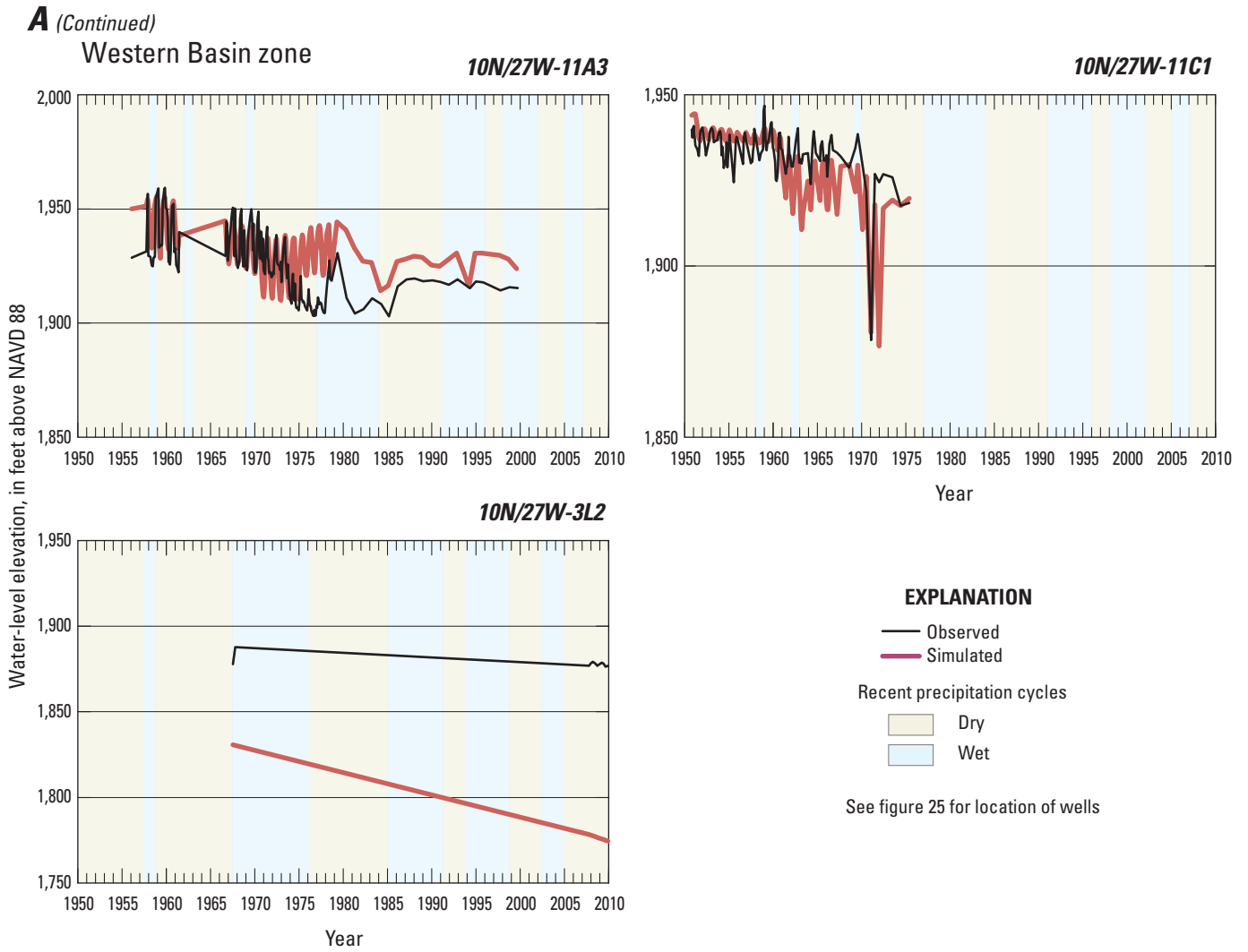


Figure 26. —Continued

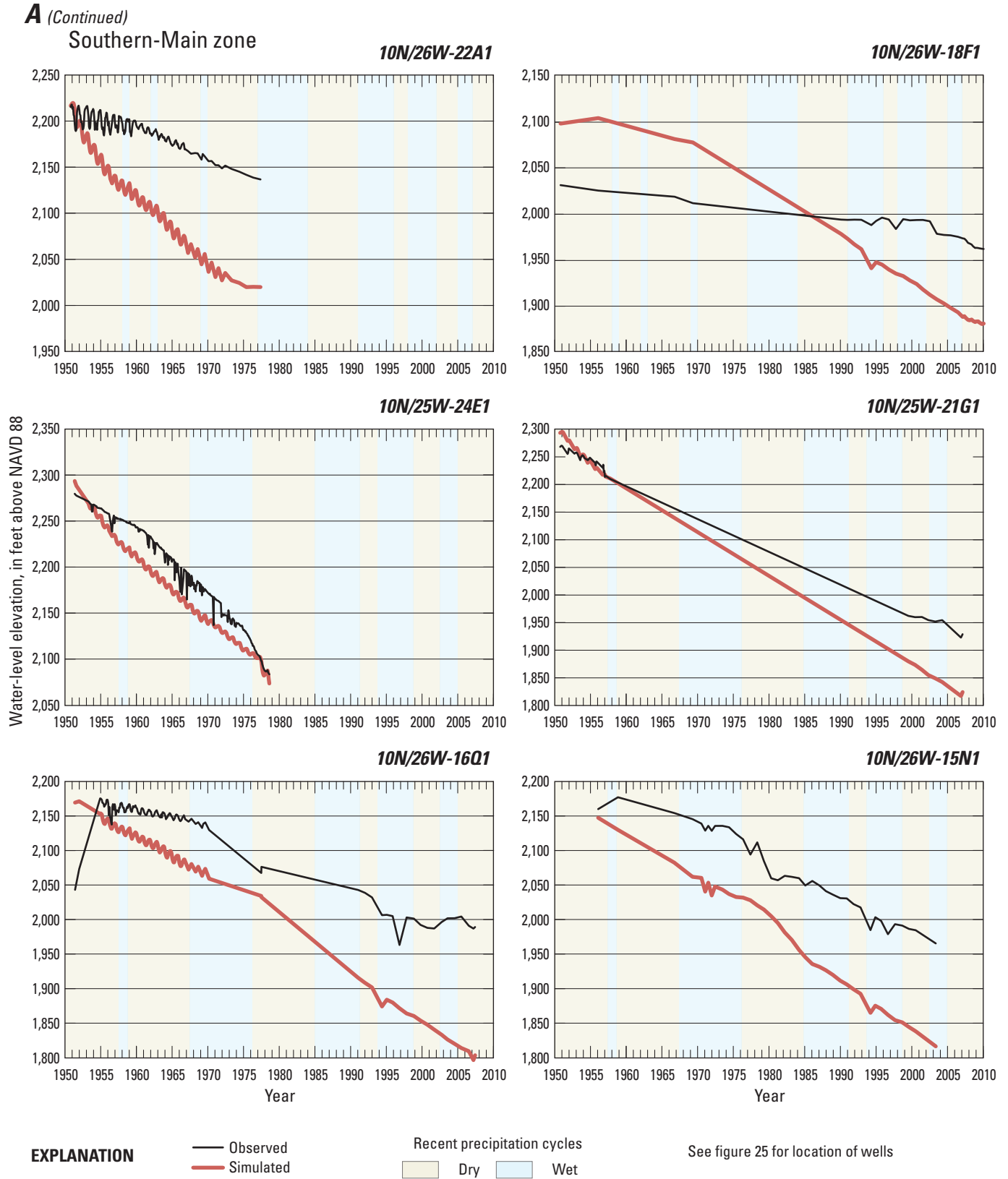


Figure 26. —Continued

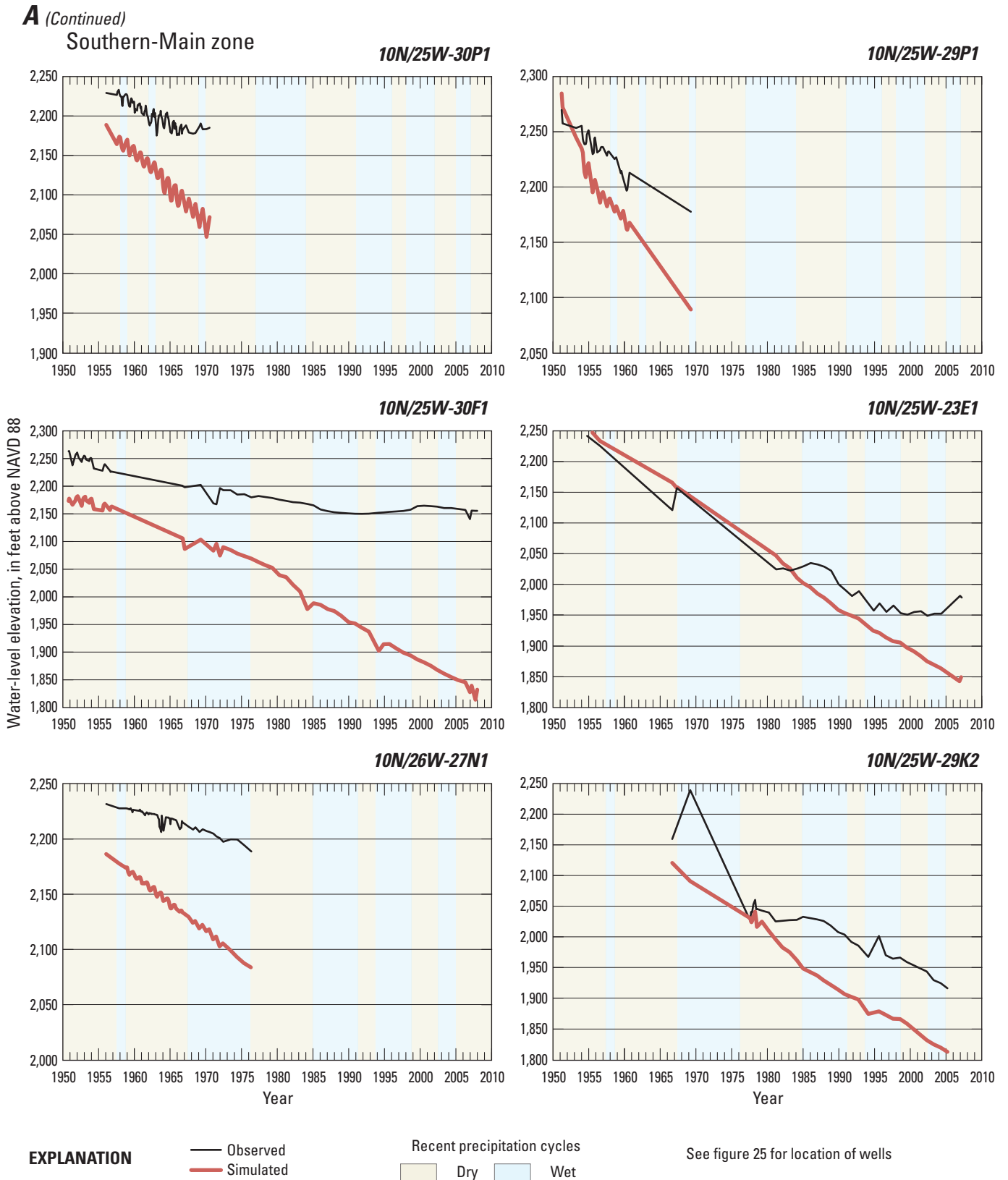
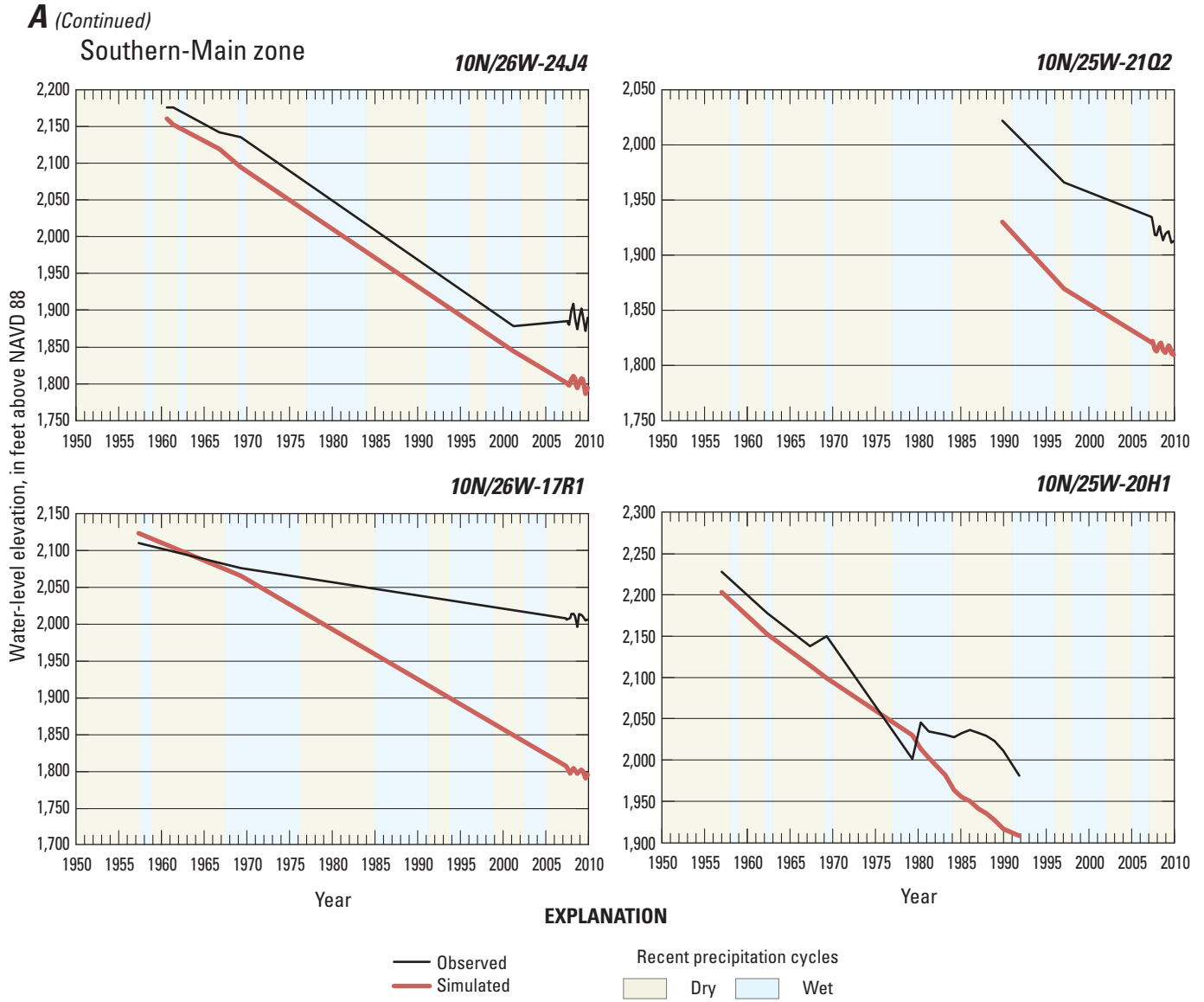


Figure 26. —Continued



See figure 25 for location of wells

Figure 26. —Continued

B Southern Ventucopa Uplands

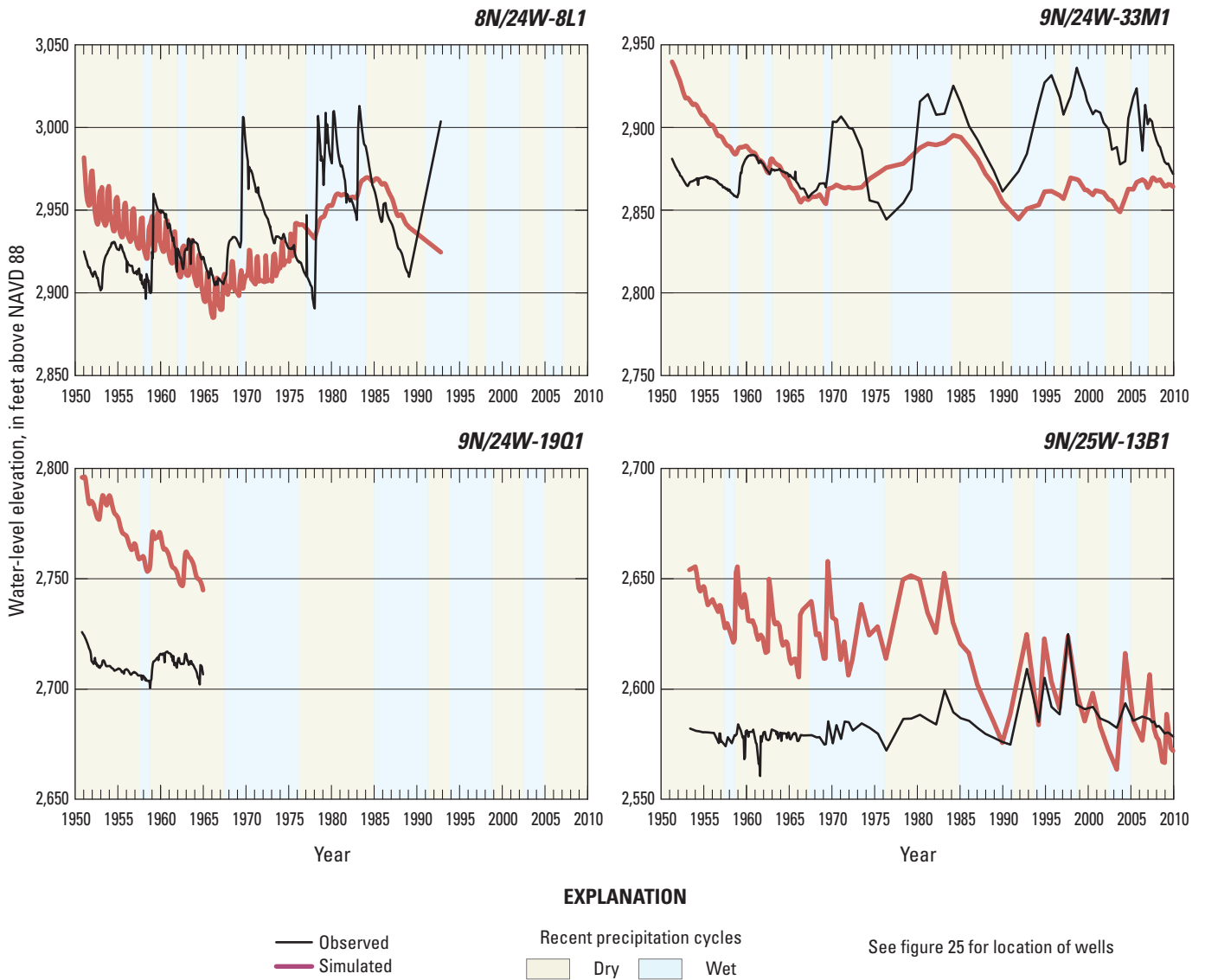


Figure 26. —Continued

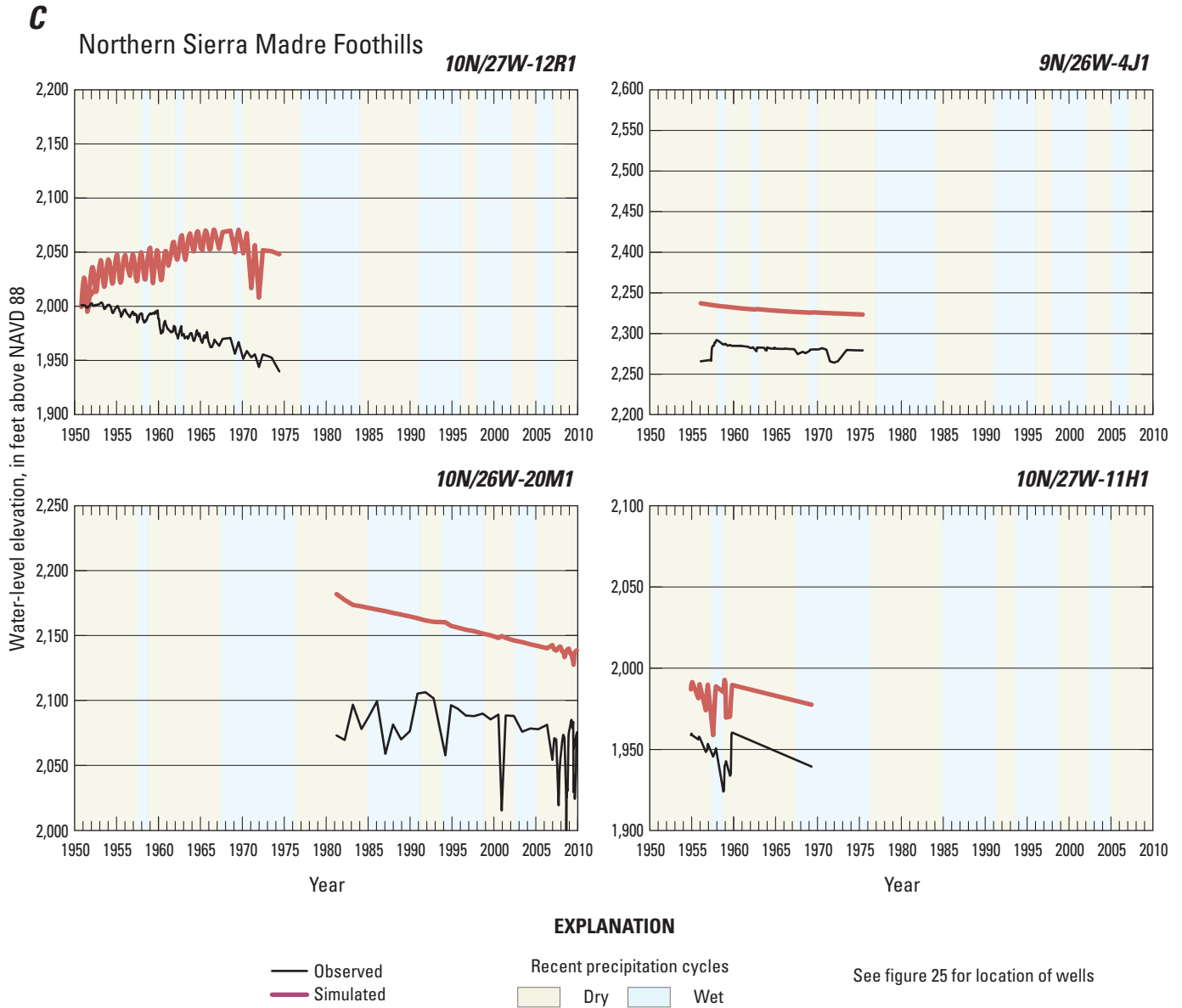


Figure 26. —Continued

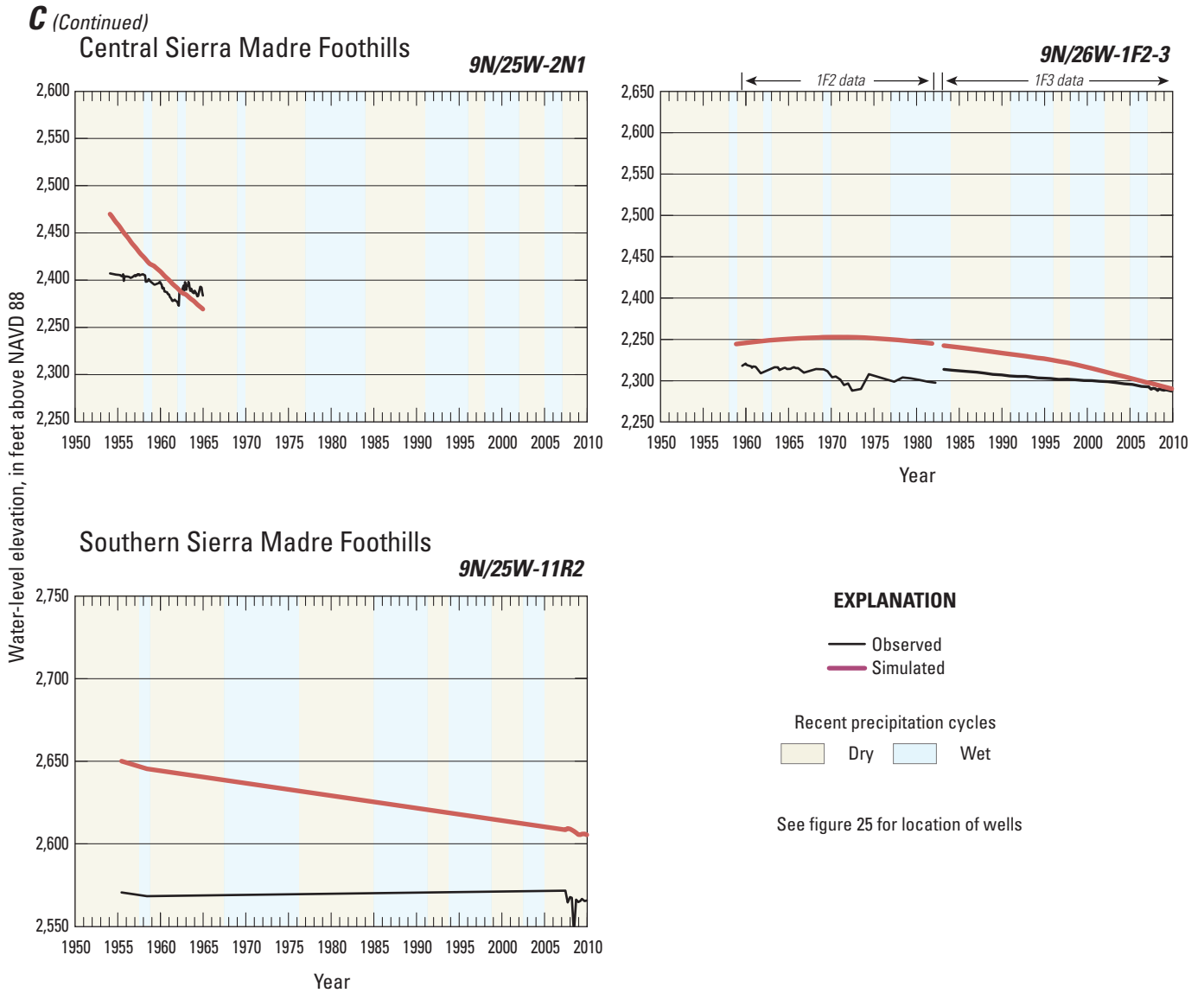


Figure 26. —Continued

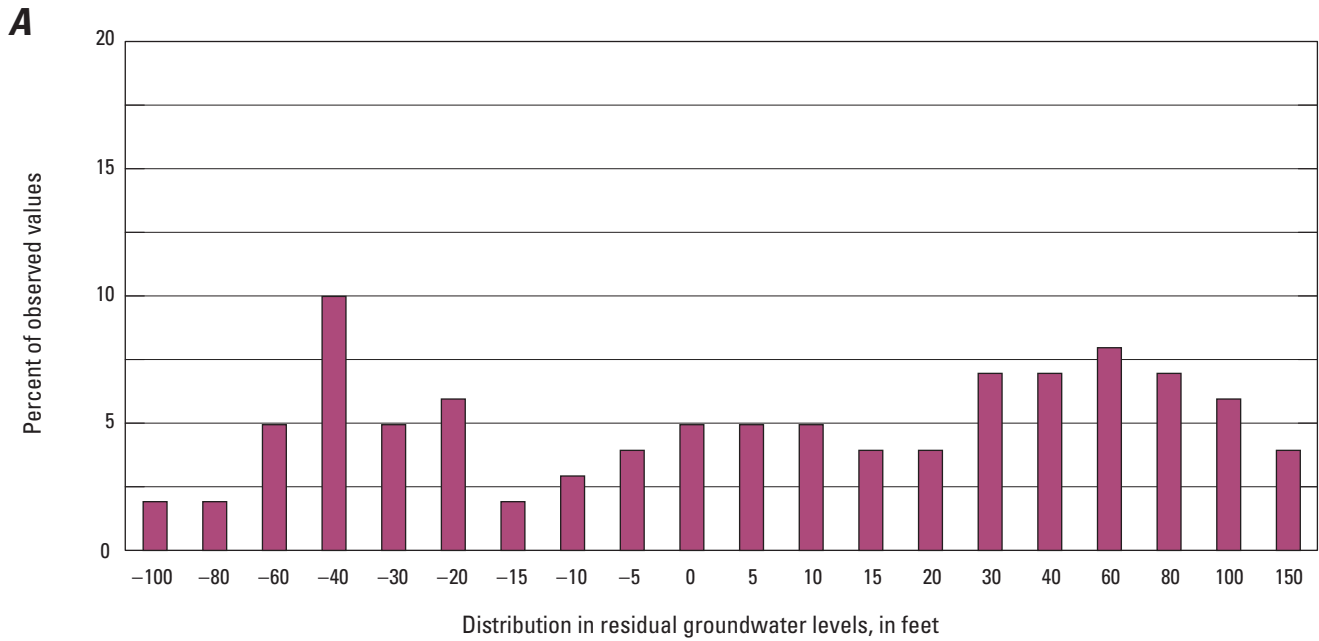


Figure 27. *A*, histogram of distribution of water-level residuals (observed minus simulated) for the Cuyama Valley hydrologic model (CUVHM) model, *B*, correlation graph by subregions of measured versus simulated water levels, and *C*, correlation between simulated and measured vertical water-level differences for selected wells, Cuyama Valley, California.

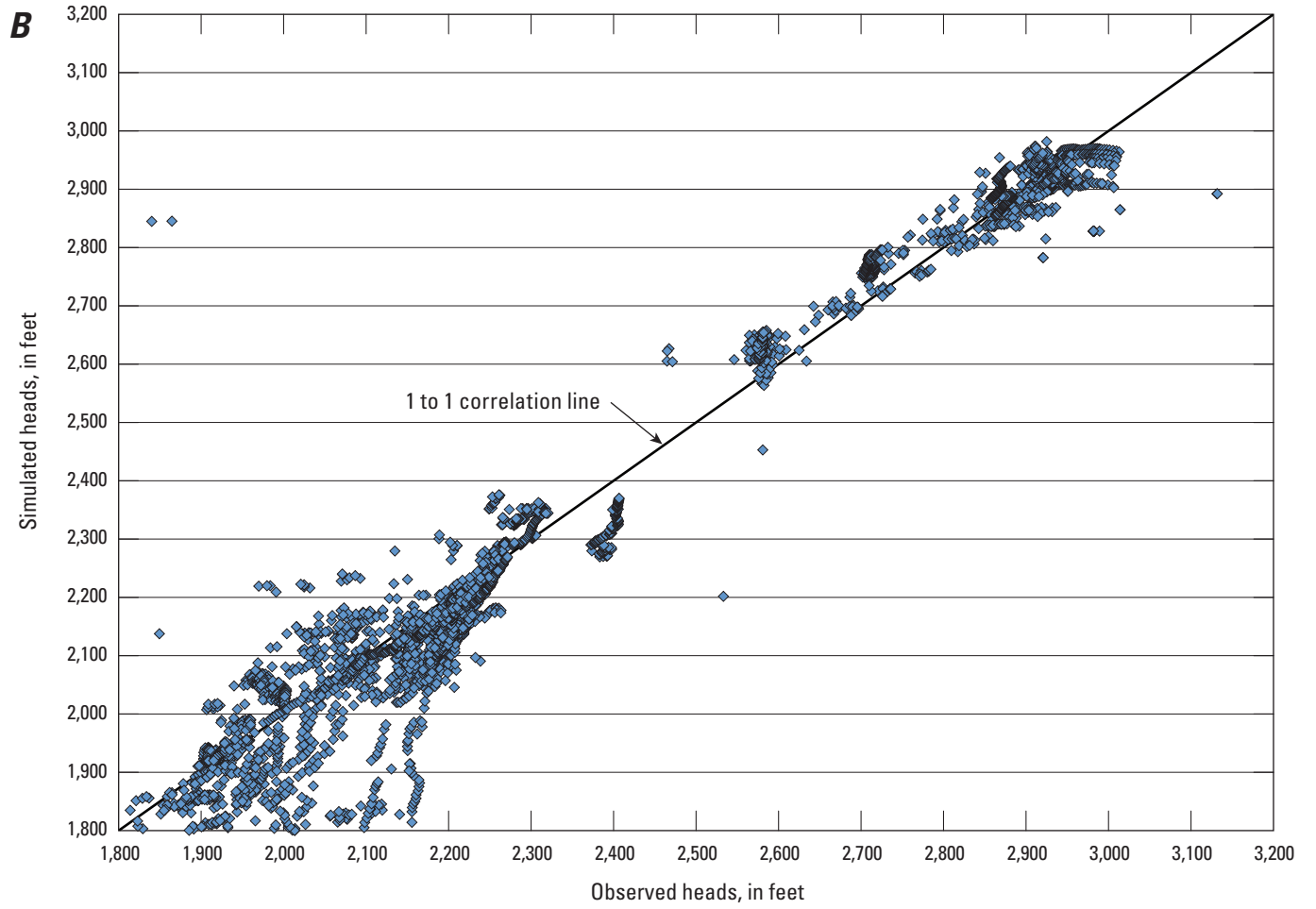


Figure 27. —Continued

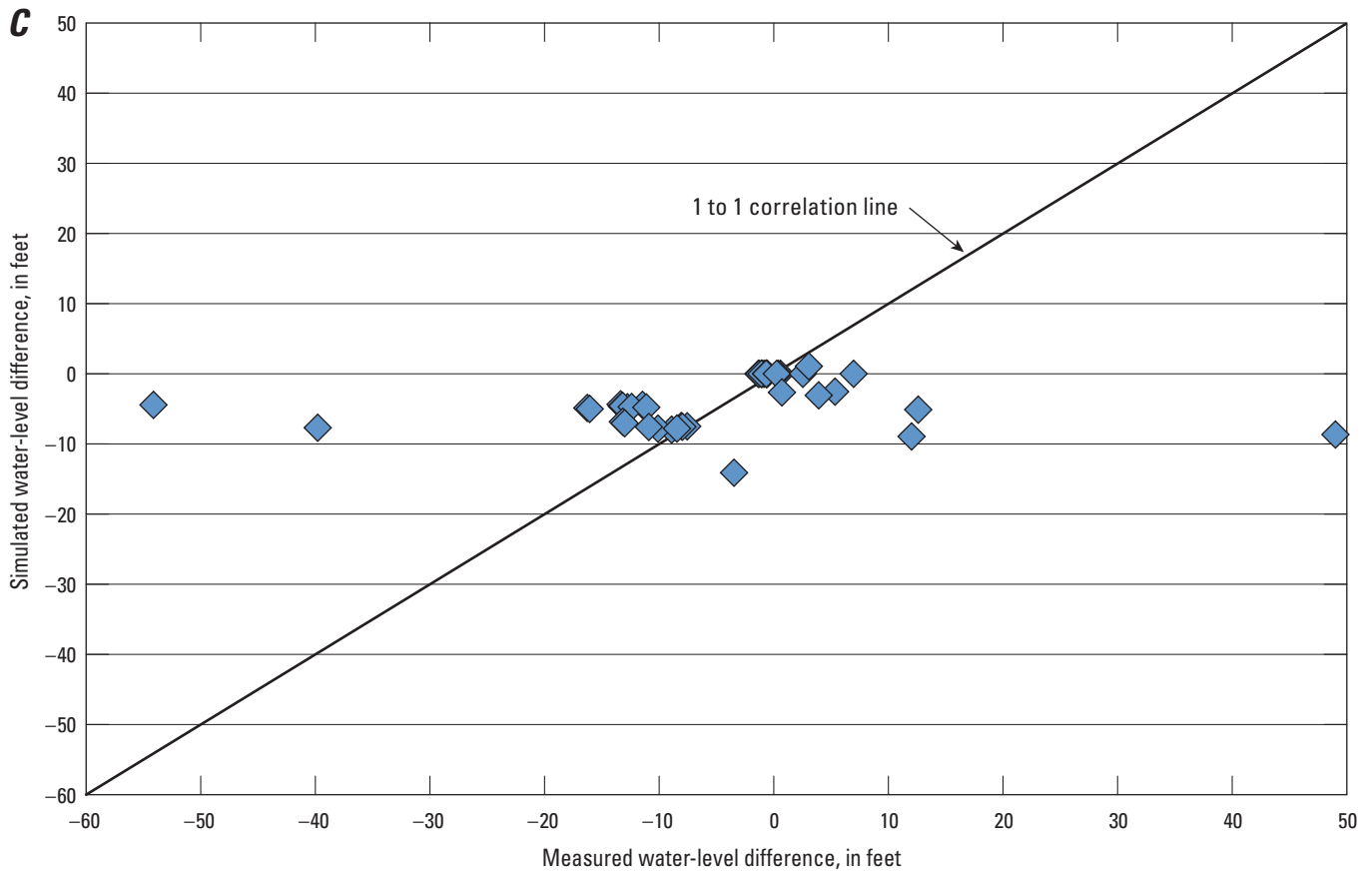
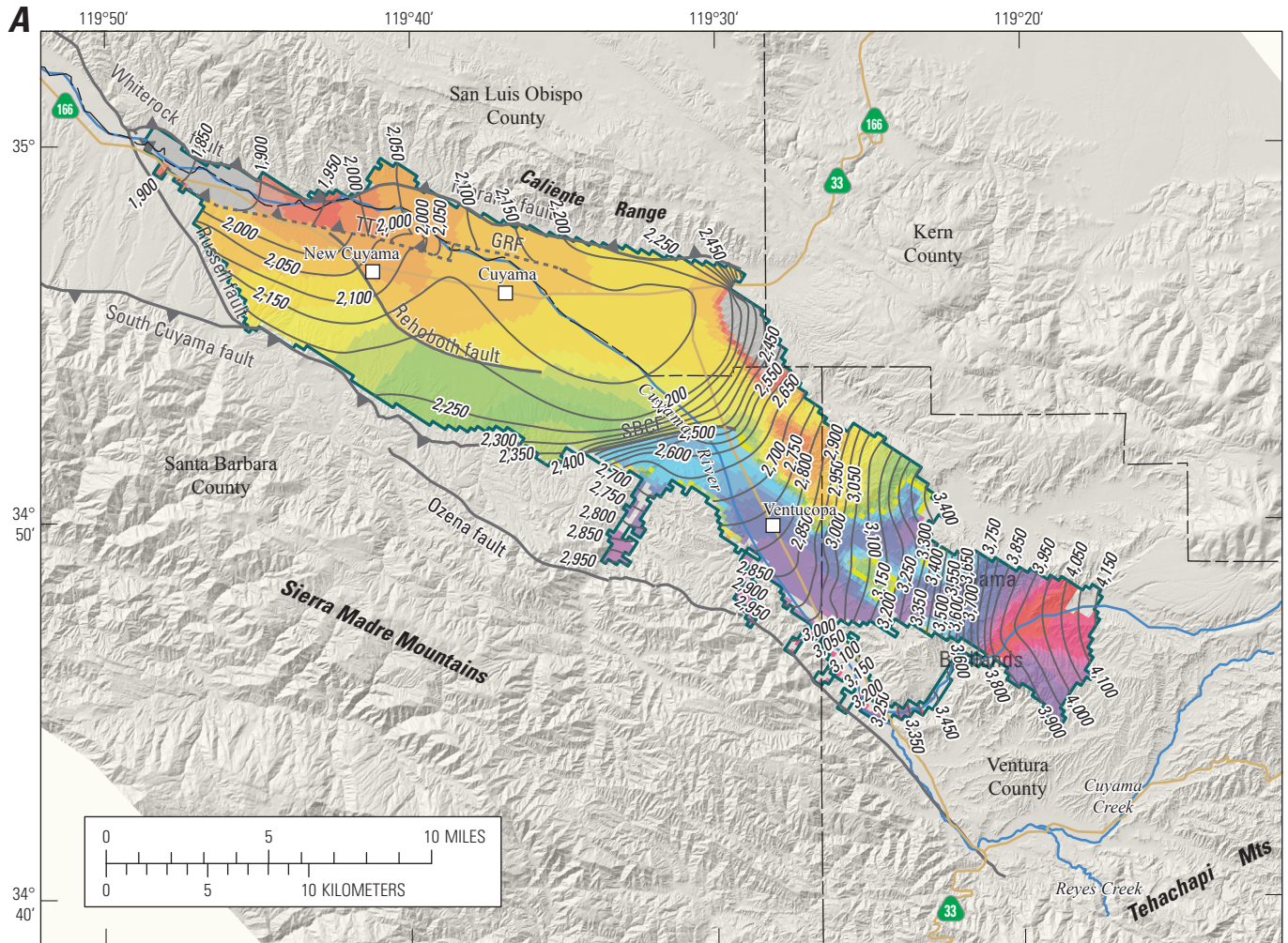


Figure 27. —Continued



Shaded relief base created from 30-m digital elevation model from USGS National Elevation Dataset (NED); North America Vertical Datum 1983 (NAVD83). Hydrology sourced from 1:24,000-scale National Hydrography Dataset, 1974-2009. Place names sourced from USGS Geographic Names Information System, 1974-2009. Albers Projection, NAD83.

EXPLANATION

Simulated water-level altitude, summer 1966; interval is 50 feet

<1,850	>2,450 to 2,500
>1,850 to 1,900	>2,500 to 2,550
>1,900 to 1,950	>2,550 to 2,600
>1,950 to 2,000	>2,600 to 2,650
>2,000 to 2,050	>2,650 to 2,700
>2,050 to 2,100	>2,700 to 2,750
>2,100 to 2,150	>2,750 to 2,800
>2,150 to 2,200	>2,800 to 2,850
>2,200 to 2,250	>2,850 to 2,900
>2,250 to 2,300	>2,900 to 3,000
>2,300 to 2,350	>3,000 to 3,100
>2,350 to 2,400	>3,100
>2,400 to 2,450	

— Active model-grid boundary

— Water-level altitude, summer 1966; interval is 50 feet

— Normal fault

▲ Thrust fault

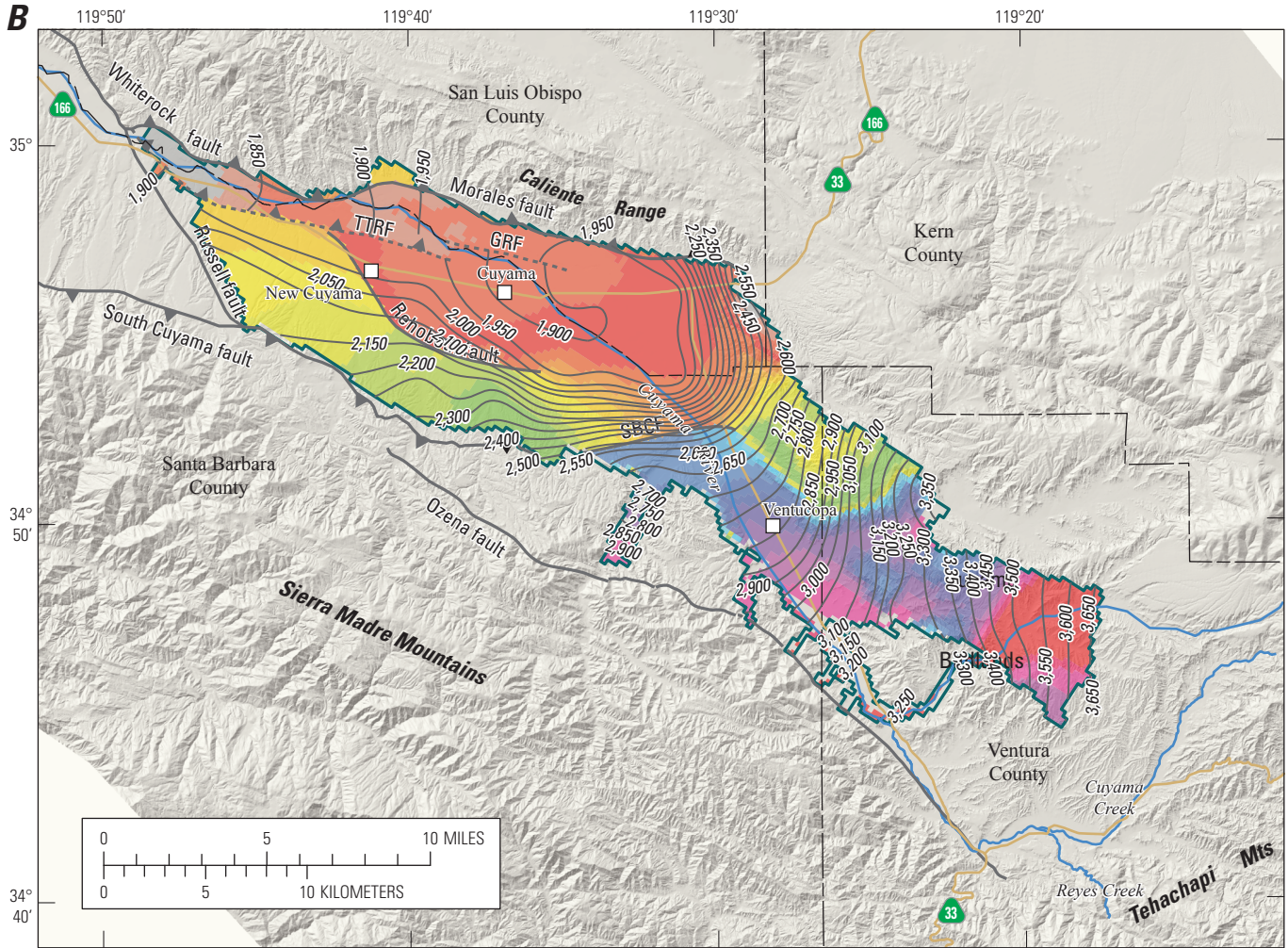
---▲ Thrust fault, concealed

GRF, Graveyard fault;

SBCF, Santa Barbara Canyon fault;

TTRF, Turkey Trap Ridge fault

Figure 28. Comparison of the contoured measured water levels with simulated water levels A, for fall 1966, B, for spring 2010, and C, for fall 2010, Cuyama Valley, California.



Shaded relief base created from 30-m digital elevation model from USGS National Elevation Dataset (NED); North America Vertical Datum 1983 (NAVD83). Hydrology sourced from 1:24,000-scale National Hydrography Dataset, 1974-2009. Place names sourced from USGS Geographic Names Information System, 1974-2009. Albers Projection, NAD83.

EXPLANATION

Simulated water-level altitude, spring 2010; interval is 50 feet

<1,750	>2,400 to 2,450
>1,750 to 1,800	>2,450 to 2,500
>1,800 to 1,850	>2,500 to 2,550
>1,850 to 1,900	>2,550 to 2,600
>1,900 to 1,950	>2,600 to 2,650
>1,950 to 2,000	>2,650 to 2,700
>2,000 to 2,050	>2,700 to 2,750
>2,050 to 2,100	>2,750 to 2,800
>2,100 to 2,150	>2,800 to 2,850
>2,150 to 2,200	>2,850 to 2,900
>2,200 to 2,250	>2,900 to 3,000
>2,250 to 2,300	>3,000 to 3,100
>2,300 to 2,350	>3,100
>2,350 to 2,400	

— Active model-grid boundary

— Water-level altitude, spring 2010; interval is 50 feet

— Normal fault

▲ Thrust fault

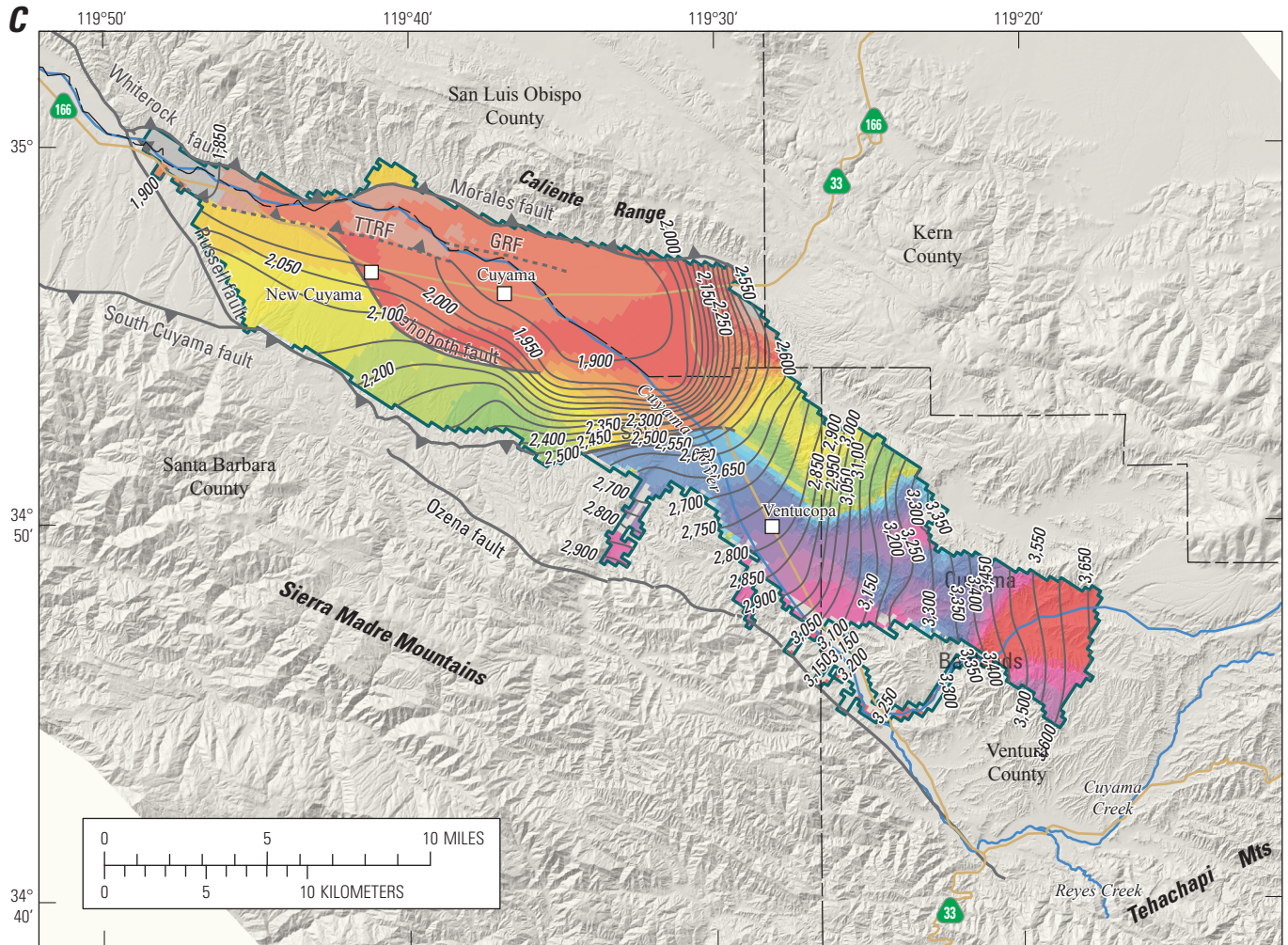
--- Thrust fault, concealed

GRF, Graveyard fault;

SBCF, Santa Barbara Canyon fault;

TTRF, Turkey Trap Ridge fault

Figure 28. —Continued



Shaded relief base created from 30-m digital elevation model from USGS National Elevation Dataset (NED); North America Vertical Datum 1983 (NAVD83). Hydrology sourced from 1:24,000-scale National Hydrography Dataset, 1974-2009. Place names sourced from USGS Geographic Names Information System, 1974-2009. Albers Projection, NAD83.

EXPLANATION

Simulated water-level altitude, summer 2010; interval is 50 feet

<1,750	>2,400 to 2,450
>1,750 to 1,800	>2,450 to 2,500
>1,850 to 1,850	>2,500 to 2,550
>1,850 to 1,900	>2,550 to 2,600
>1,900 to 1,950	>2,600 to 2,650
>1,950 to 2,000	>2,650 to 2,700
>2,000 to 2,050	>2,700 to 2,750
>2,050 to 2,100	>2,750 to 2,800
>2,100 to 2,150	>2,800 to 2,850
>2,150 to 2,200	>2,850 to 2,900
>2,200 to 2,250	>2,900 to 3,000
>2,250 to 2,300	>3,000 to 3,100
>2,300 to 2,350	>3,100
>2,350 to 2,400	

— Active model-grid boundary

— Water-level altitude, summer 2010; interval is 50 feet

— Normal fault

▲ Thrust fault

--- Thrust fault, concealed

GRF, Graveyard fault; SBCF, Santa Barbara Canyon fault; TTRF, Turkey Trap Ridge fault

Figure 28. —Continued

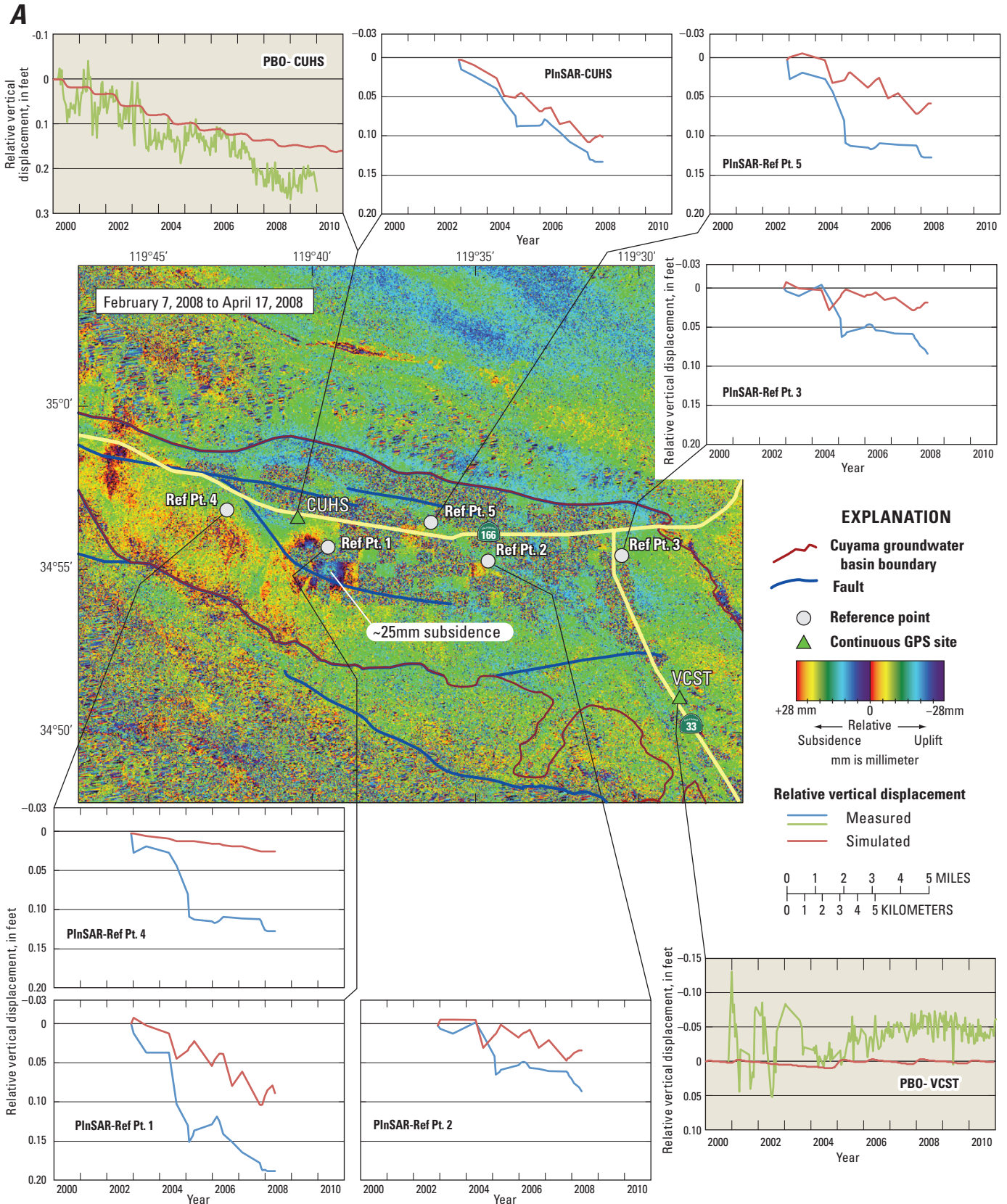
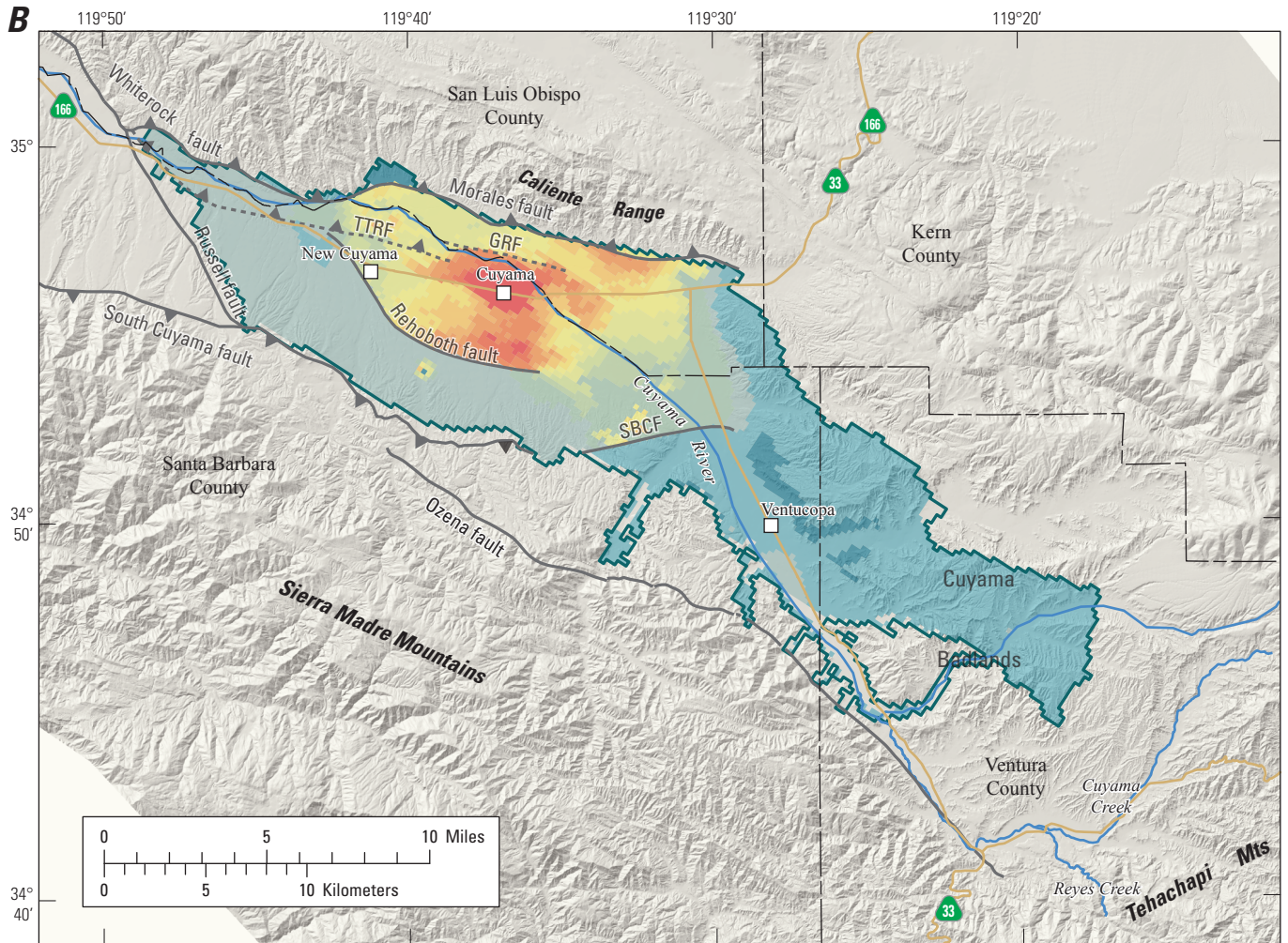


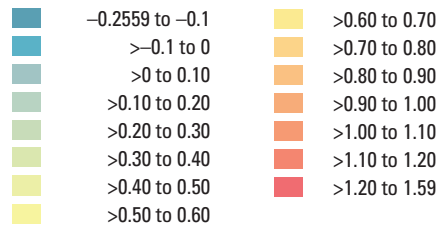
Figure 29. Historical subsidence as *A*, map of seasonal InSAR with graphs of simulated and measured time series for selected locations of relative land-surface deformation from Plate-Boundary Observation (PBO) sites and Point InSAR targets, and *B*, simulated total subsidence 1950–2010 for the calibrated hydrologic flow model, Cuyama Valley, California.



Shaded relief base created from 30-m digital elevation model from USGS National Elevation Dataset (NED); North America Vertical Datum 1983 (NAVD83). Hydrology sourced from 1:24,000-scale National Hydrography Dataset, 1974-2009. Place names sourced from USGS Geographic Names Information System, 1974-2009. Albers Projection, NAD83.

EXPLANATION

**Simulated subsidence, in feet
negative values are uplift**



Active model-grid boundary

Normal fault

▲
 Thrust fault
 Thrust fault, concealed
 GRF, Graveyard fault;
 SBCF, Santa Barbara Canyon fault;
 TTRF, Turkey Trap Ridge fault

Figure 29. —Continued

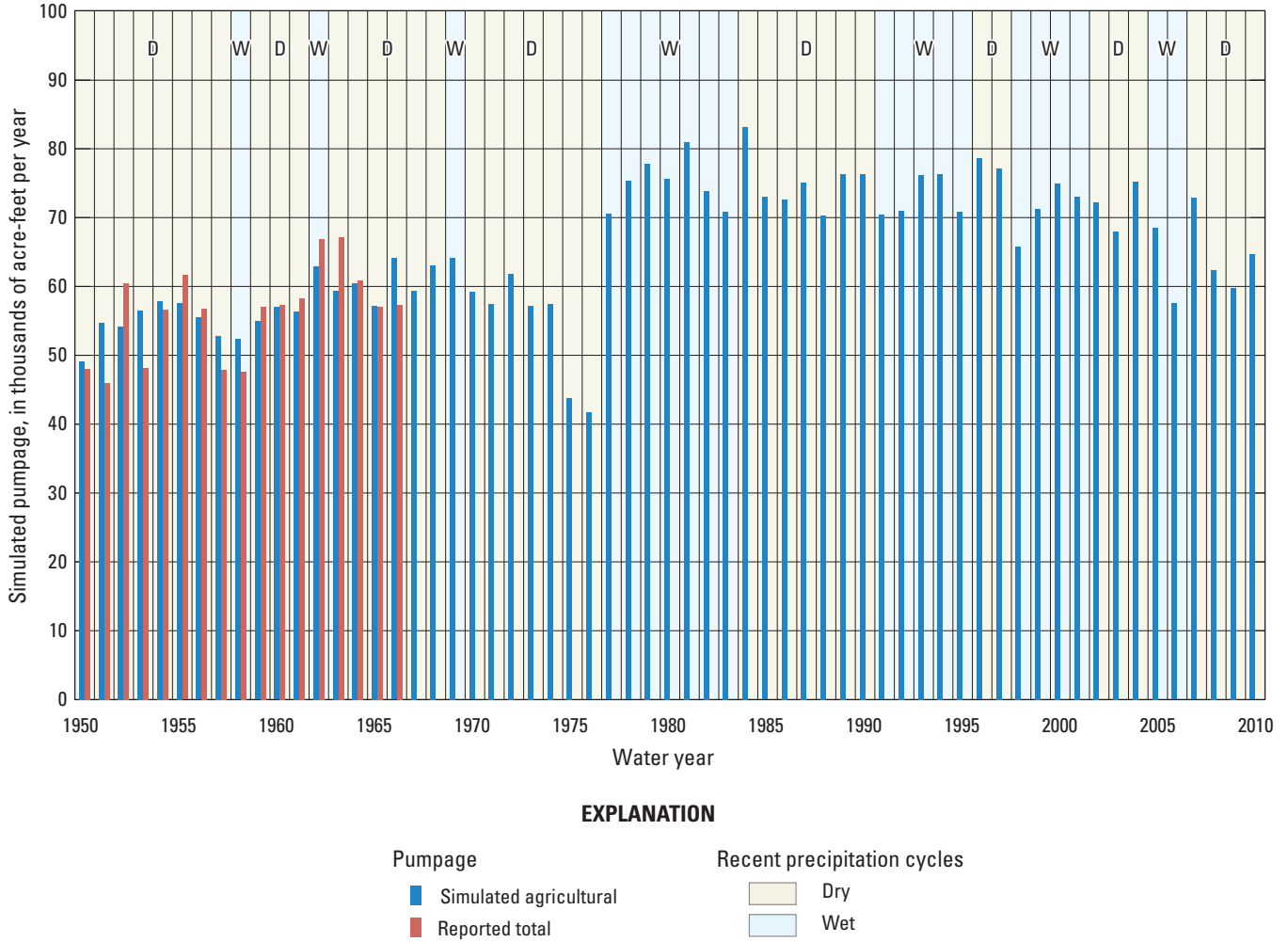
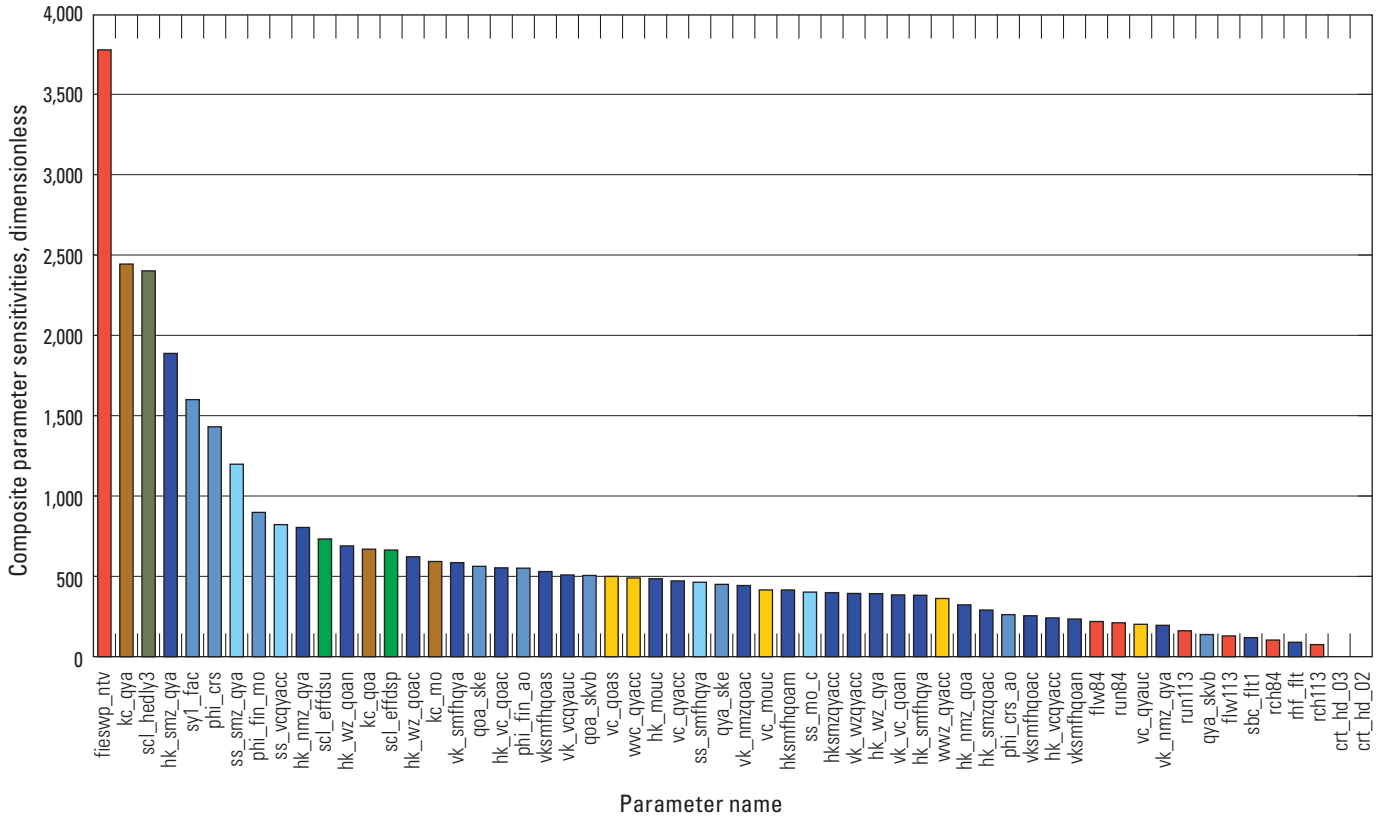


Figure 30. Reported and simulated agricultural pumpage for Cuyama Valley, California.



EXPLANATION

Parameter groups—

- Runoff
- Streambed conductivity
- Irrigation
- Hydraulic conductivity
- Storage property
- Hydraulic conductivity multipliers
- Storage property multiplier
- Initial water-level multiplier

See tables 14 and 15 for names and explanations of all parameter identifiers.

Figure 31. Relative composite sensitivity of computed observations at calibration points to changes in selected parameters from analysis with PEST.

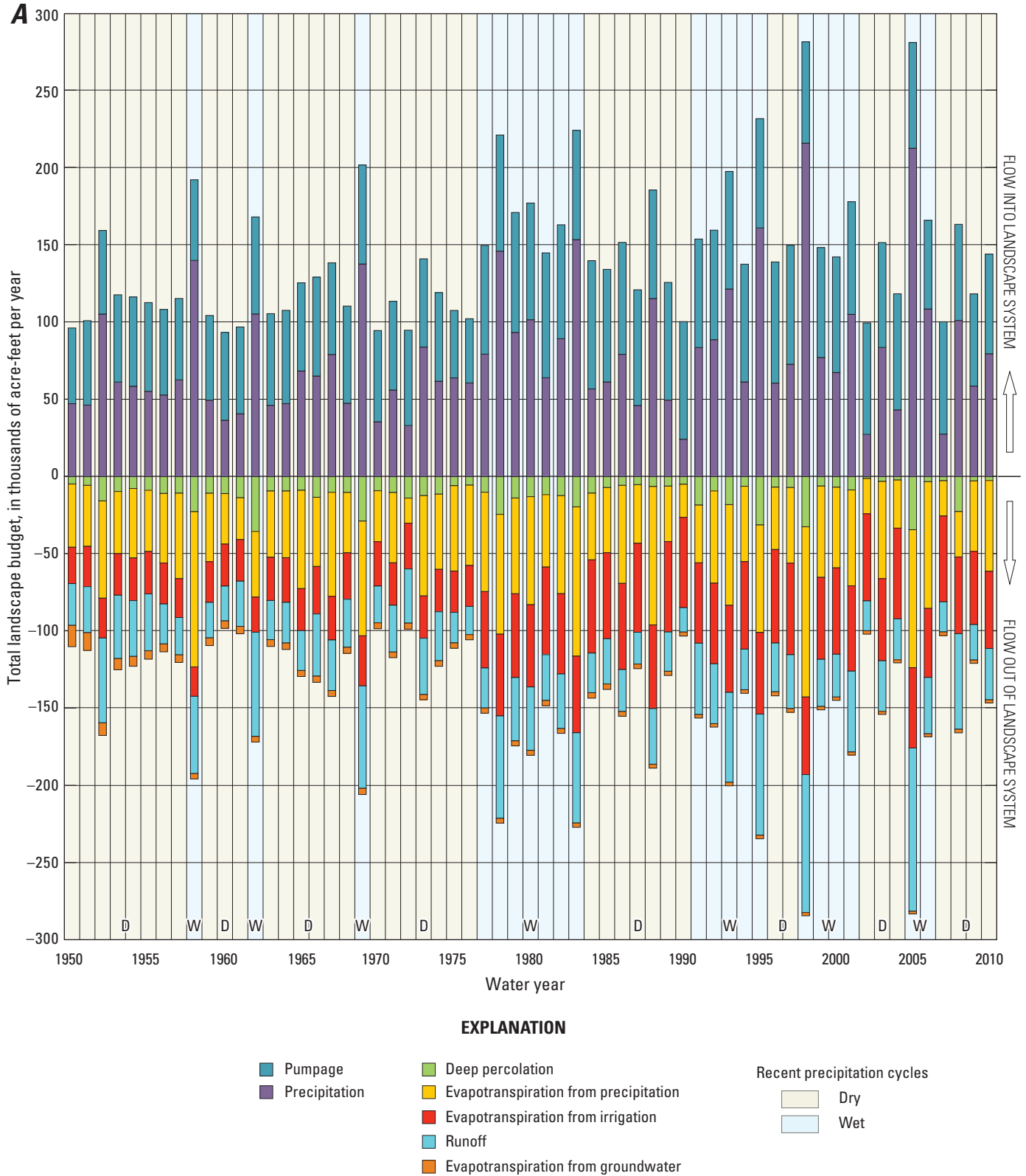
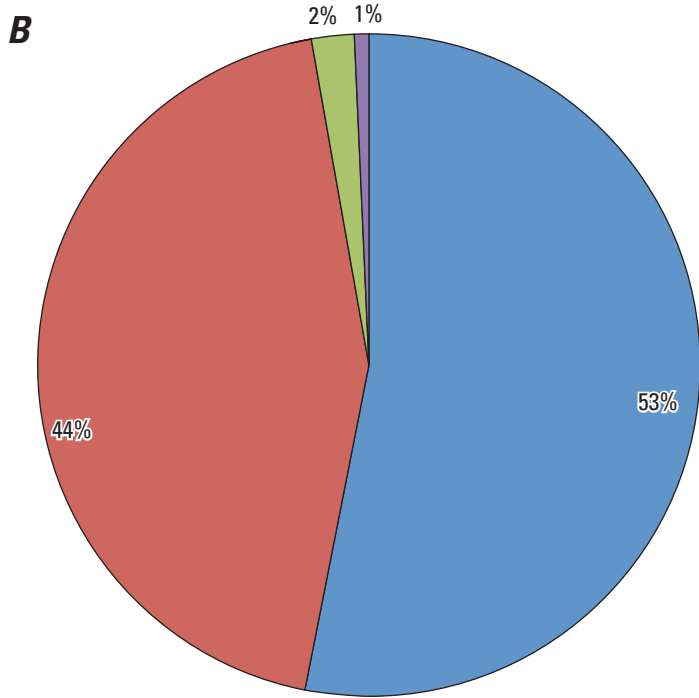
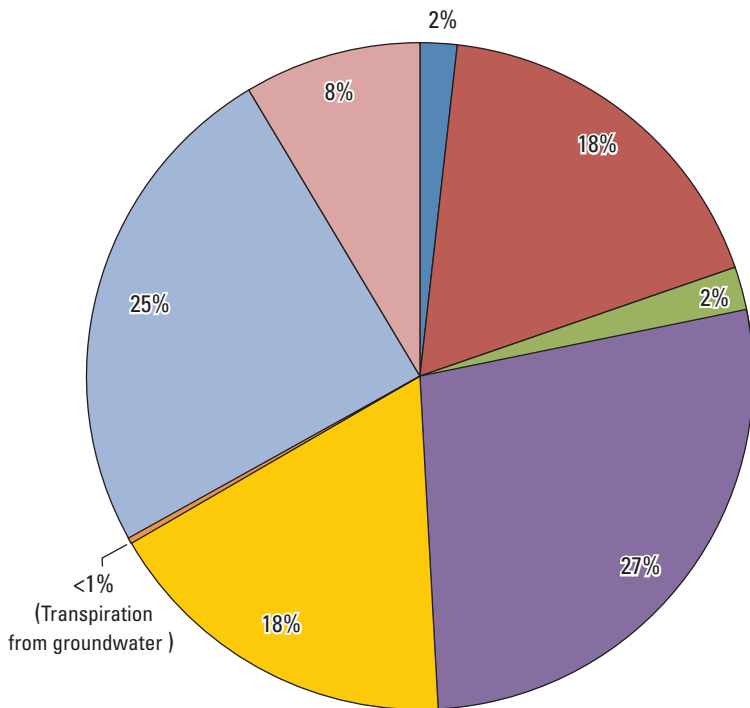


Figure 32. Hydrologic budget for the landscape with *A*, the temporal distribution of total landscape inflows and outflows, and *B*, average annual components of farm budget of the simulated landscape flow system within the Cuyama Valley Hydrologic Model (CUVHM), Cuyama Valley, California.



Average landscape inflows, in percent

- Precipitation
- Groundwater well pumping (irrigation) deliveries
- Evaporation uptake directly from groundwater
- Transpiration uptake directly from groundwater



Average landscape outflows, in percent

- Evaporation from irrigation
- Evaporation from precipitation
- Evaporation from groundwater
- Transpiration from irrigation
- Transpiration from precipitation
- Transpiration from groundwater
- Overland runoff
- Deep percolation

Values on pie charts are in list-order, clockwise from top center and may not equal 100 due to rounding of percentages.

Figure 32. —Continued

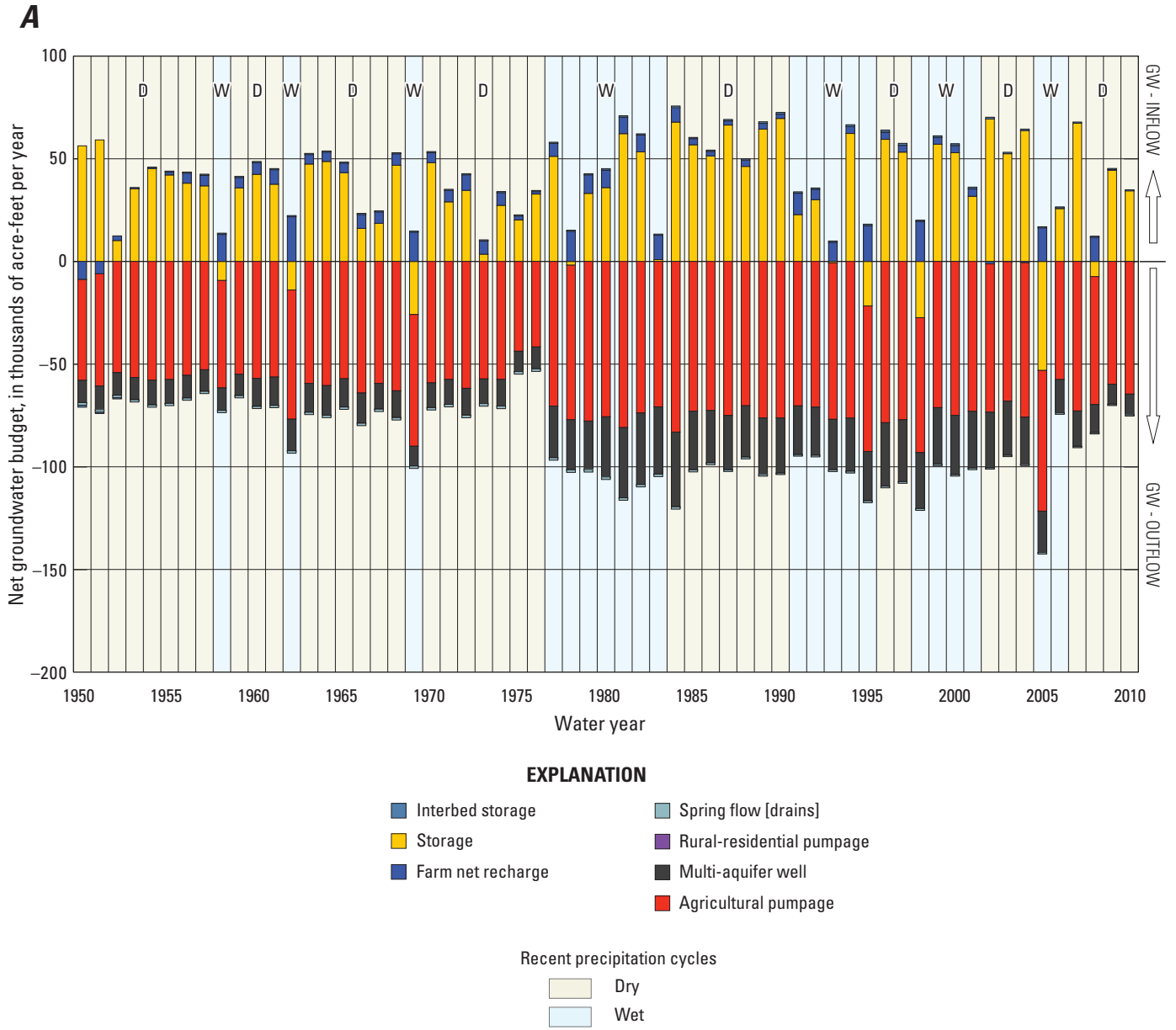
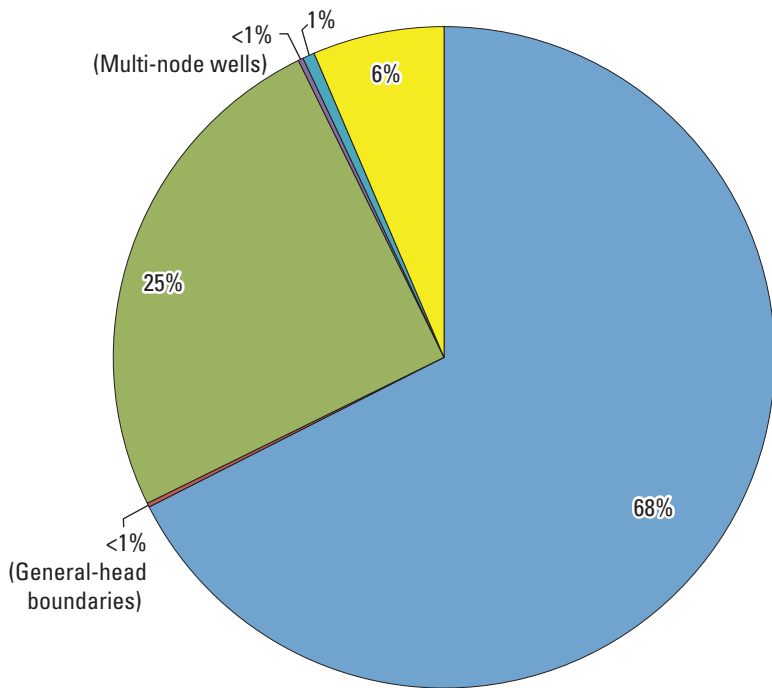


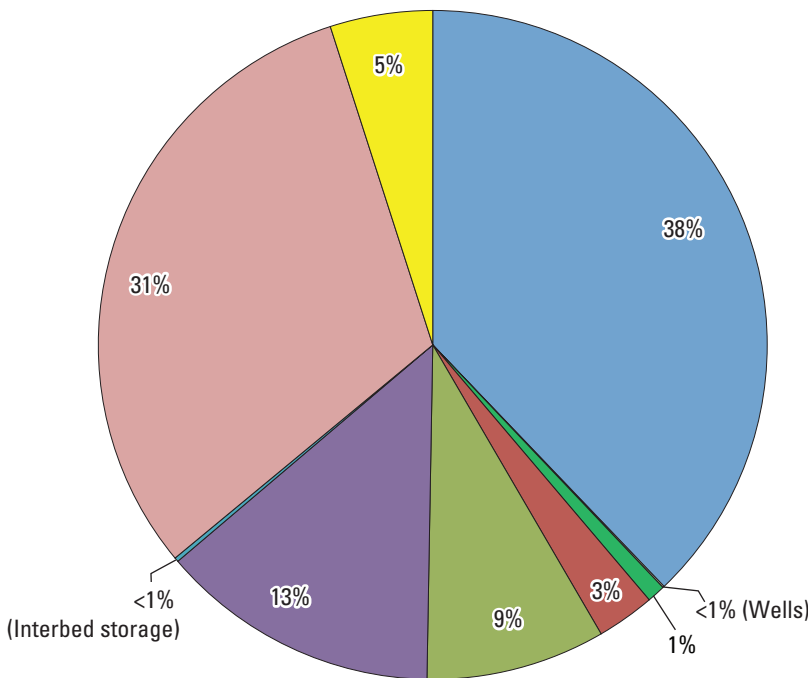
Figure 33. A, the simulated net flow of groundwater in the hydrologic cycle, B, average annual components of simulated groundwater flow, and C, the cumulative change in storage and D, changes in groundwater storage, Cuyama Valley, California.

B



Cumulative inflows, in percent

- Storage
- Groundwater underflow (general-head boundaries)
- Stream leakage
- Multi-node wells
- Interbed storage
- Farm net recharge



Cumulative outflows, in percent

- Storage
- Wells
- Spring discharges (drains)
- Groundwater underflow (general-head boundaries)
- Stream leakage
- Multi-node wells
- Interbed storage
- Farm wells
- Farm net recharge

Values on pie charts are in list-order, clockwise from top center and may not equal 100 due to rounding of percentages.

Figure 33. —Continued

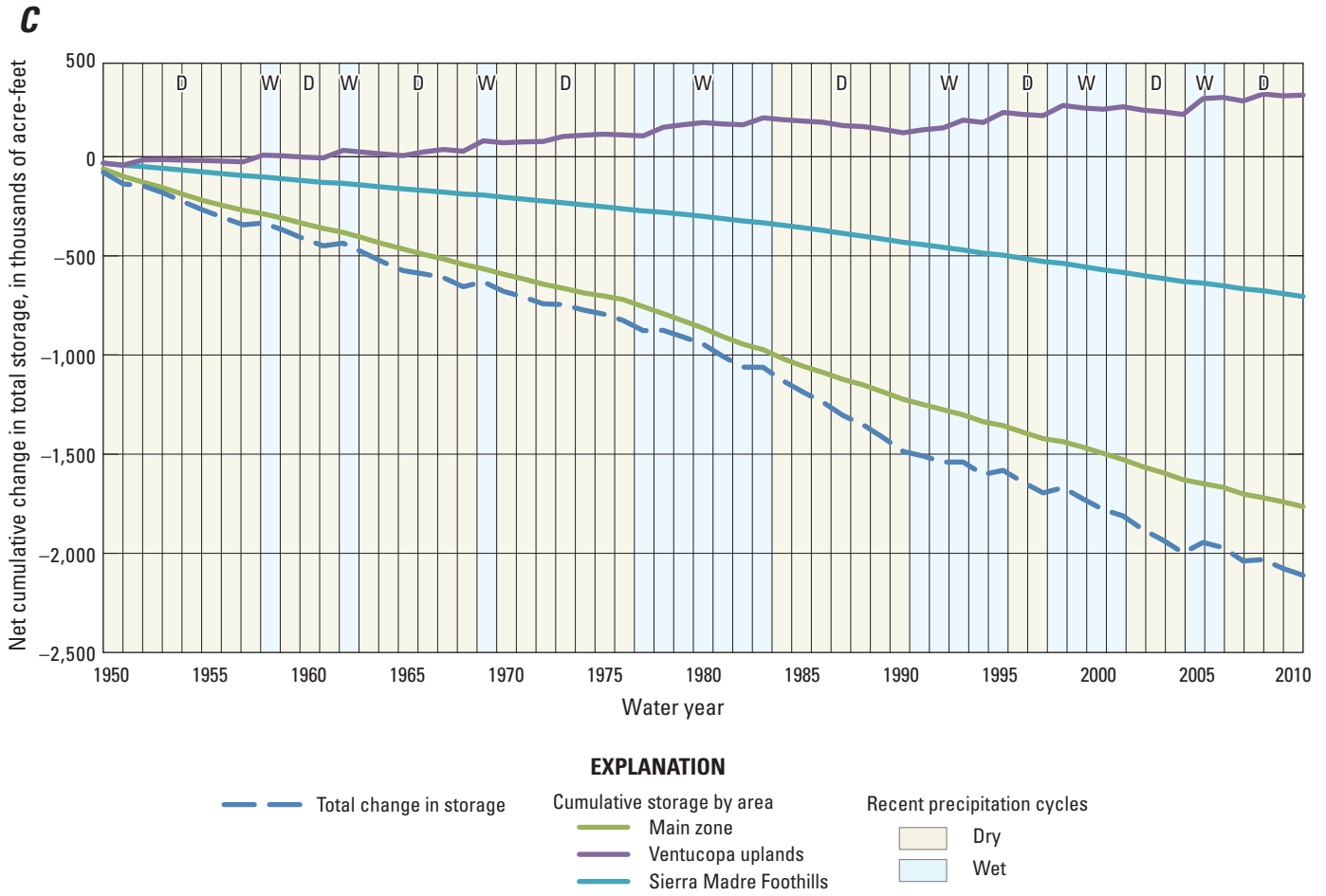
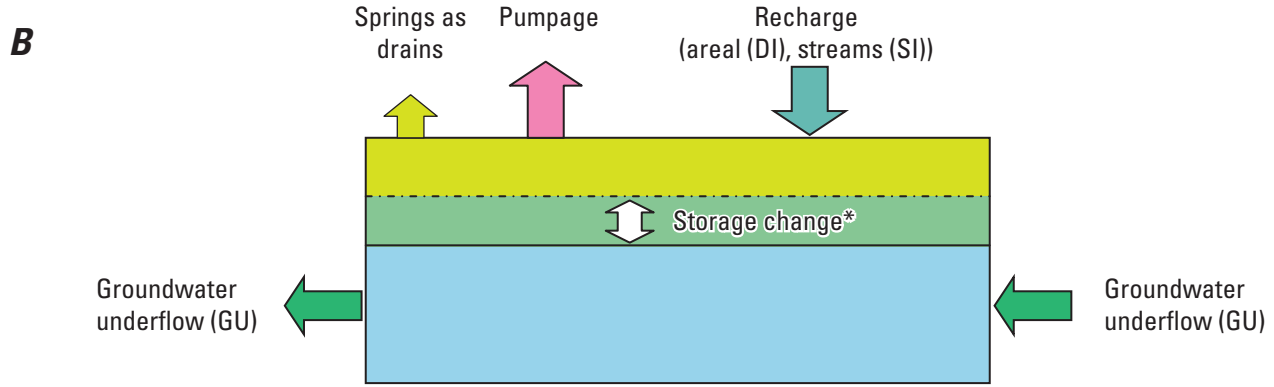


Figure 33. —Continued



GROUNDWATER-FLOW BUDGET SUMMARY

(Average-net flows in acre-feet per year)

Source	Valley wide				Main zone	Ventucopa Uplands	Sierra Madre Foothills	Base case ¹	Reduced supply ²	Reduced demand ³
Time period (Water years)	1950–2010 ⁴	2000–2010 ⁵	2005 (Wet)	2009 (Dry)	2000–2010	2000–2010	2000–2010	2011–2071 ⁶	2011–2071	2011–2071
Inflows:										
Storage depletion:	34,100	34,800	0	45,860	27,500	0	13,800	32,700	500	0
Direct infiltration (DI) ⁷	5,600	3,100	16,600	100	700	1,500	900	2,400	1,100	1,300
Streamflow infiltration (SI)	27,500	30,300	93,600	16,700	8,300	20,500	1,600	29,500	25,600	29,500
Total recharge (DI+SI):	33,100	33,400	110,200	16,800	9,000	22,000	2,500	31,900	26,700	30,800
Total inflows:	67,200	68,200	164,210	62,660	36,500	22,000	16,300	64,600	27,200	30,800
Outflows:										
Storage accretion:	0	0	54,010	0	0	6,000	0	0	0	11,900
Underflow (GU):	3,700	3,100	700	500	3,200	15	0	2,900	3,700	3,000
Springs as drains:	1,000	600	700	500	600	0	0	400	500	600
Domestic pumpage:	20	10	10	10	6	8	2	7	7	7
Water-supply pumpage:	90	190	180	1900	190	0	0	190	190	190
Agricultural pumpage:	65,300	68,100	68,100	61,000	56,700	10,000	1,400	63,700	32,800	15,800
Total pumpage:	65,400	68,300	68,290	61,200	56,900	10,000	1,400	63,900	33,000	16,000
Total outflows:	70,100	68,900	123,000	107,560	57,500	16,000	1,400	67,200	36,400	31,500
Inflows - Outflows =	-2,900⁸	-700⁸	41,210⁹	-44,900⁸	-21,000⁸	6,000⁹	-14,900⁸	-2,600⁸	-9,200⁸	-700⁹

¹ Base Case projection of current demand with historical climate
² Base Case projection with supply limited to recharge
³ Base Case projection with no agriculture in the Main-zone subregions
⁴ Historical period that represents two climate cycles
⁵ Historical period that represents recent climate and land use conditions

⁶ Projection of historical climate and 2010 land use
⁷ Includes water lost to evapotranspiration
⁸ Demand greater than replenishment (overdraft)
⁹ Replenishment is greater than demand

Figure 33. —Continued

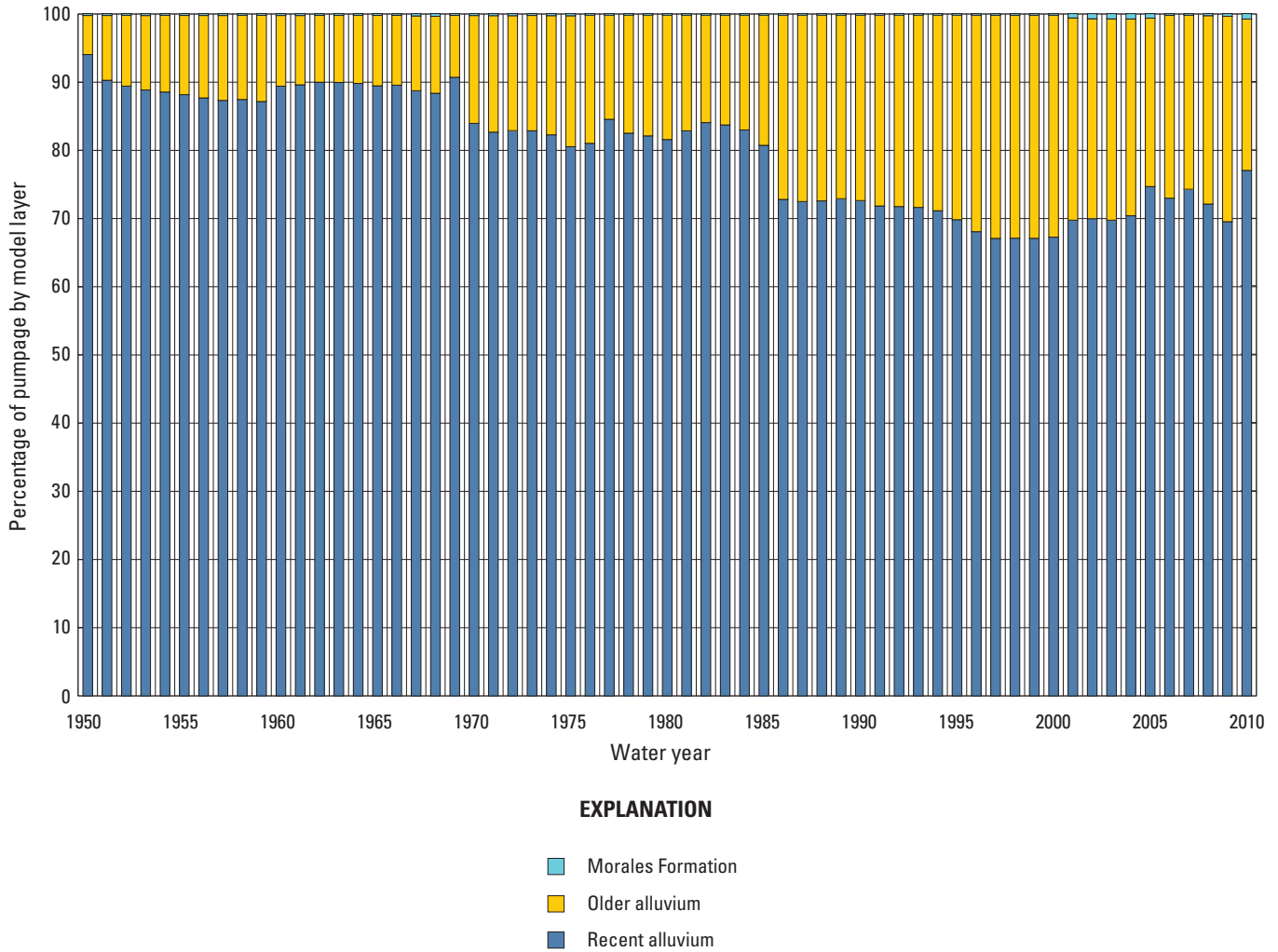


Figure 34. Percentage of simulated groundwater pumpage for the water years 1950–2010 for all three model layers, Cuyama Valley, California.

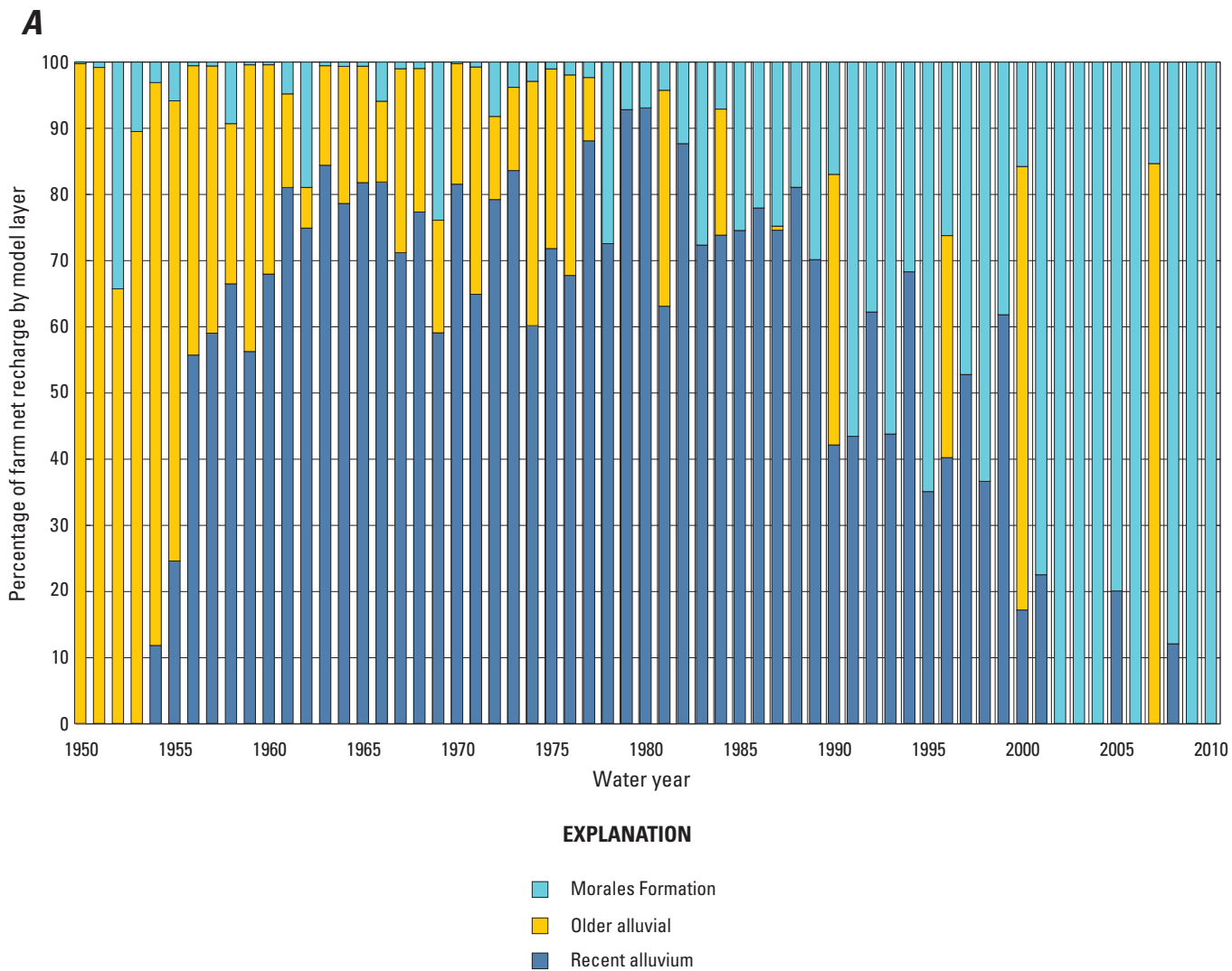
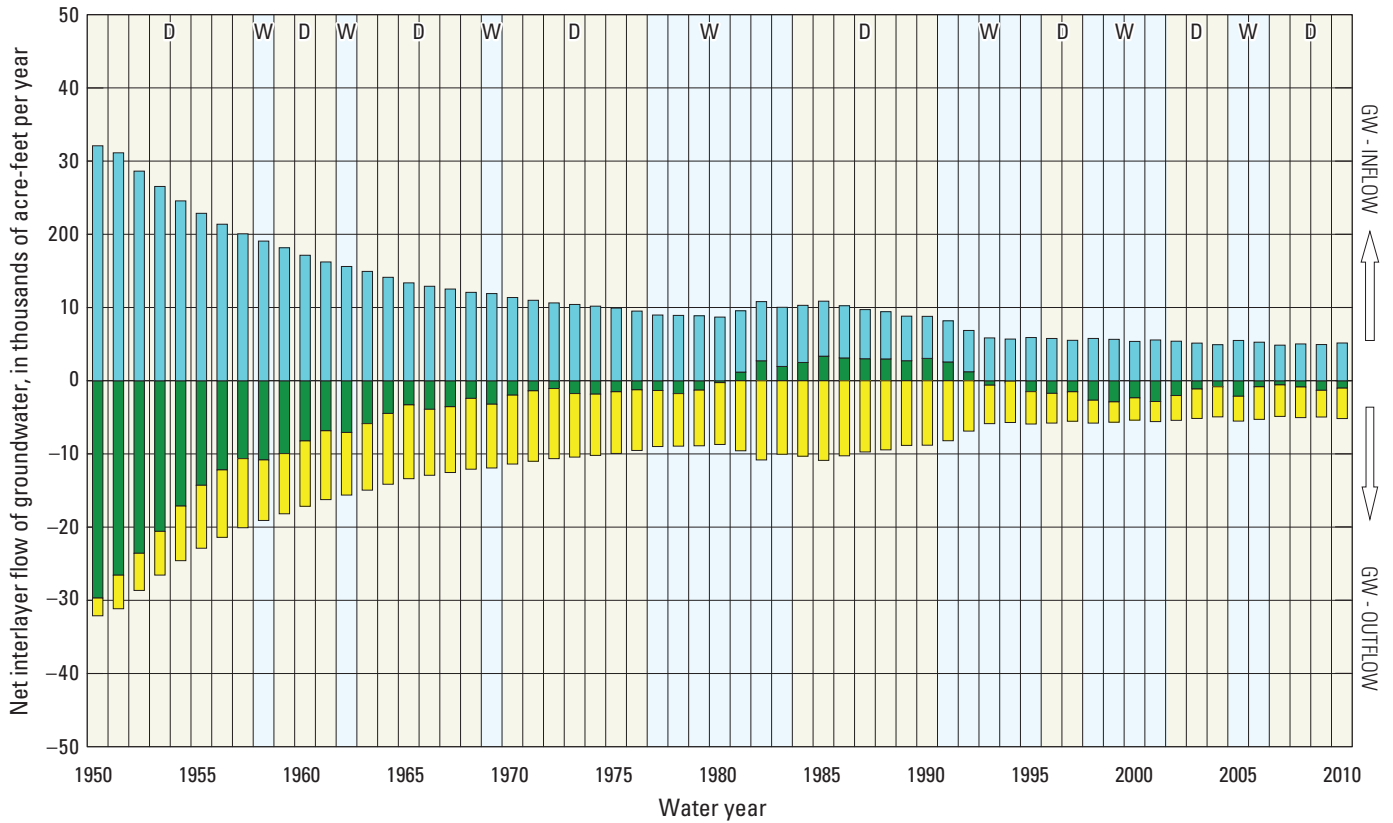


Figure 35. Stacked bar chart showing *A*, percentage of total recharge by aquifer model layers, and *B*, Net downward flow between model layers, Cuyama Valley, California.

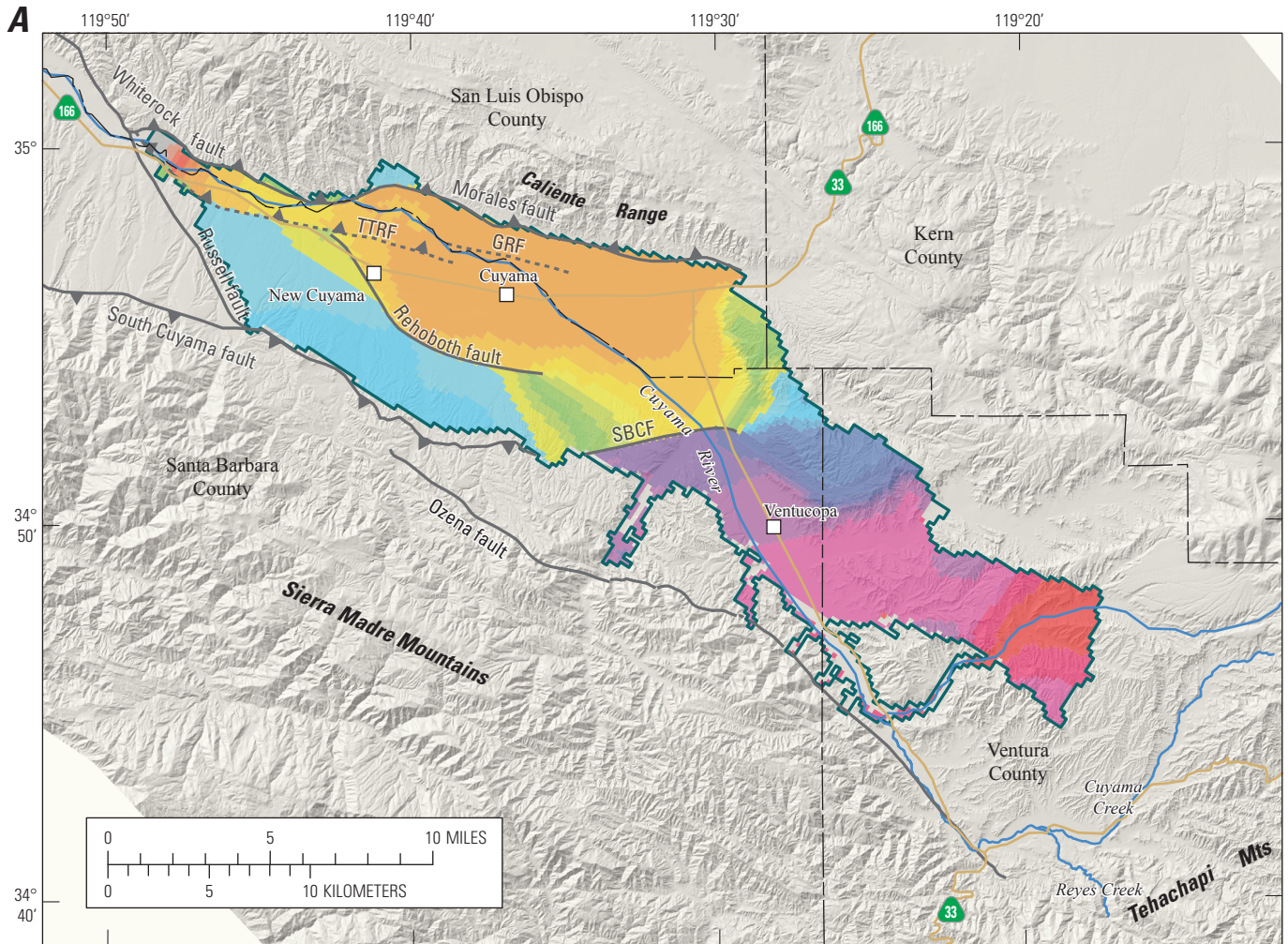
B



EXPLANATION

- | | |
|--|---|
| ■ Flow to recent alluvium | Recent precipitation cycles |
| ■ Flow to older alluvium | |
| ■ Flow to Morales Formation | Dry |
| | Wet |

Figure 35. —Continued



Shaded relief base created from 30-m digital elevation model from USGS National Elevation Dataset (NED); North America Vertical Datum 1983 (NAVD83). Hydrology sourced from 1:24,000-scale National Hydrography Dataset, 1974-2009. Place names sourced from USGS Geographic Names Information System, 1974-2009. Albers Projection, NAD83.

EXPLANATION

Simulated water-level altitude, in feet, summer 2071; contour interval varies

Grey	<1,400	Light Green	>2,000 to 2,050
Light Red	>1,400 to 1,450	Light Blue	>2,050 to 2,100
Red	>1,450 to 1,500	Blue	>2,100 to 2,150
Dark Red	>1,500 to 1,550	Dark Blue	>2,150 to 2,200
Orange	>1,550 to 1,600	Dark Purple	>2,200 to 2,300
Yellow-Orange	>1,600 to 1,650	Dark Blue-Black	>2,300 to 2,400
Yellow	>1,650 to 1,700	Black	>2,400 to 2,500
Light Green	>1,700 to 1,750	Black	>2,500 to 2,600
Green	>1,750 to 1,800	Black	>2,600 to 2,800
Dark Green	>1,800 to 1,850	Black	>2,800 to 3,000
Light Green	>1,850 to 1,900	Black	>3,000 to 3,400
Green	>1,900 to 1,950	Black	>3,400
Dark Green	>1,950 to 2,000		

— Active model-grid boundary

— Normal fault

▲ Thrust fault

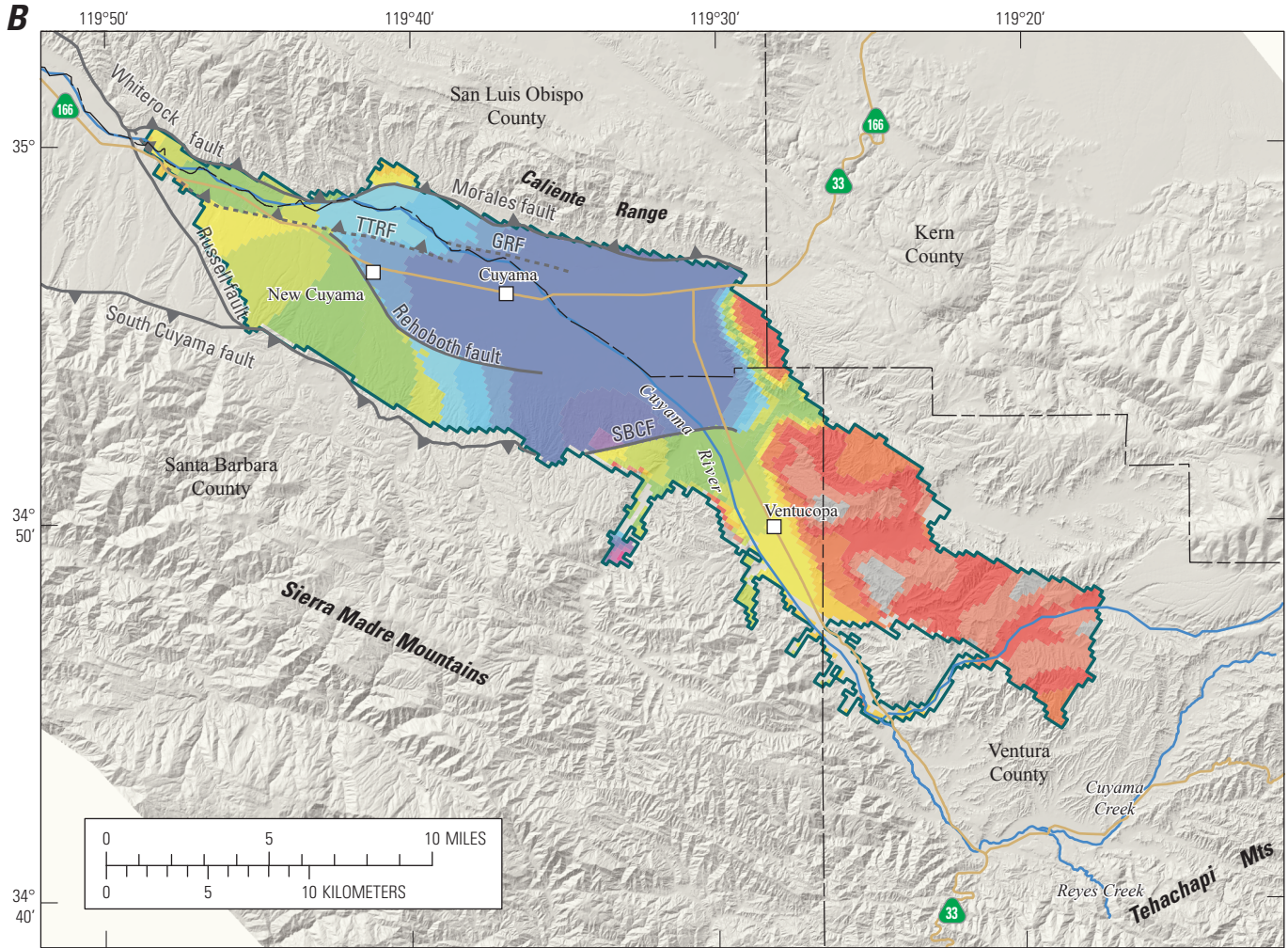
---▲ Thrust fault, concealed

GRF, Graveyard fault;

SBCF, Santa Barbara Canyon fault;

TTRF, Turkey Trap Ridge fault

Figure 36. A, projected simulated water levels and B, the difference in water levels between projection of simulated water levels in fall 2071 and simulated water levels in fall 2010 for the hydrologic flow model of Cuyama Valley, California.



Shaded relief base created from 30-m digital elevation model from USGS National Elevation Dataset (NED); North America Vertical Datum 1983 (NAVD83). Hydrology sourced from 1:24,000-scale National Hydrography Dataset, 1974-2009. Place names sourced from USGS Geographic Names Information System, 1974-2009. Albers Projection, NAD83.

EXPLANATION

Simulated difference in water-level altitude, in feet, summer 2010 minus summer 2071; interval varies

<ul style="list-style-type: none"> <-150 >-150 to -100 >-100 to -50 >-50 to 0 >0 to 1 >1 to 10 >10 to 25 >25 to 50 >50 to 75 >75 to 100 	<ul style="list-style-type: none"> >100 to 125 >125 to 150 >150 to 175 >175 to 200 >200 to 250 >250 to 275 >275 to 300 >300 to 350 >350 to 400
---	---

Active model-grid boundary

Normal fault

Thrust fault

Thrust fault, concealed

Figure 36. —Continued

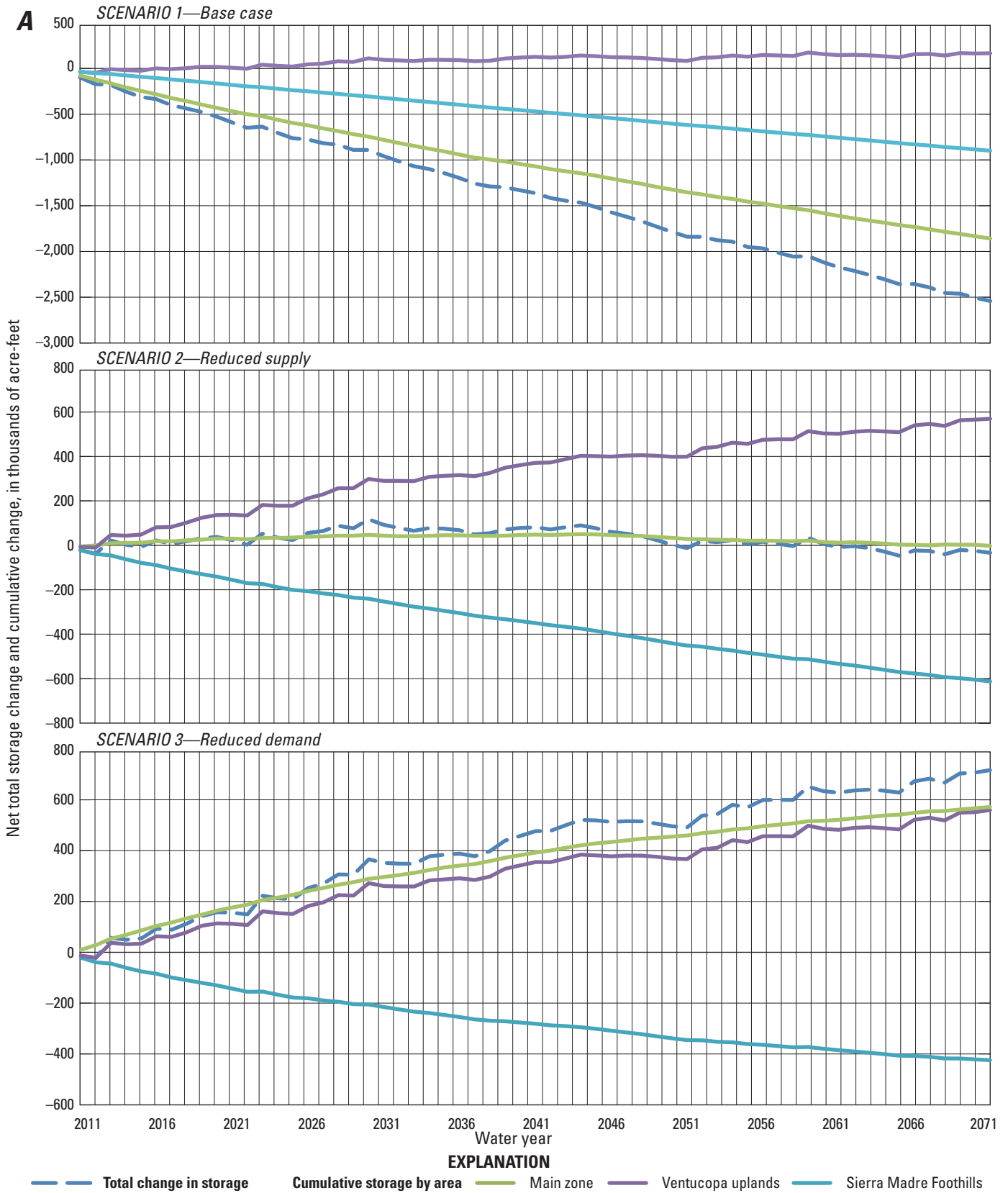


Figure 37. Three projected scenarios showing projected *A*, cumulative change in net groundwater storage, *B*, potential groundwater levels at CVKR and CVBR monitoring sites, and *C*, potential land subsidence near Cuyama, Cuyama Valley, California.

B

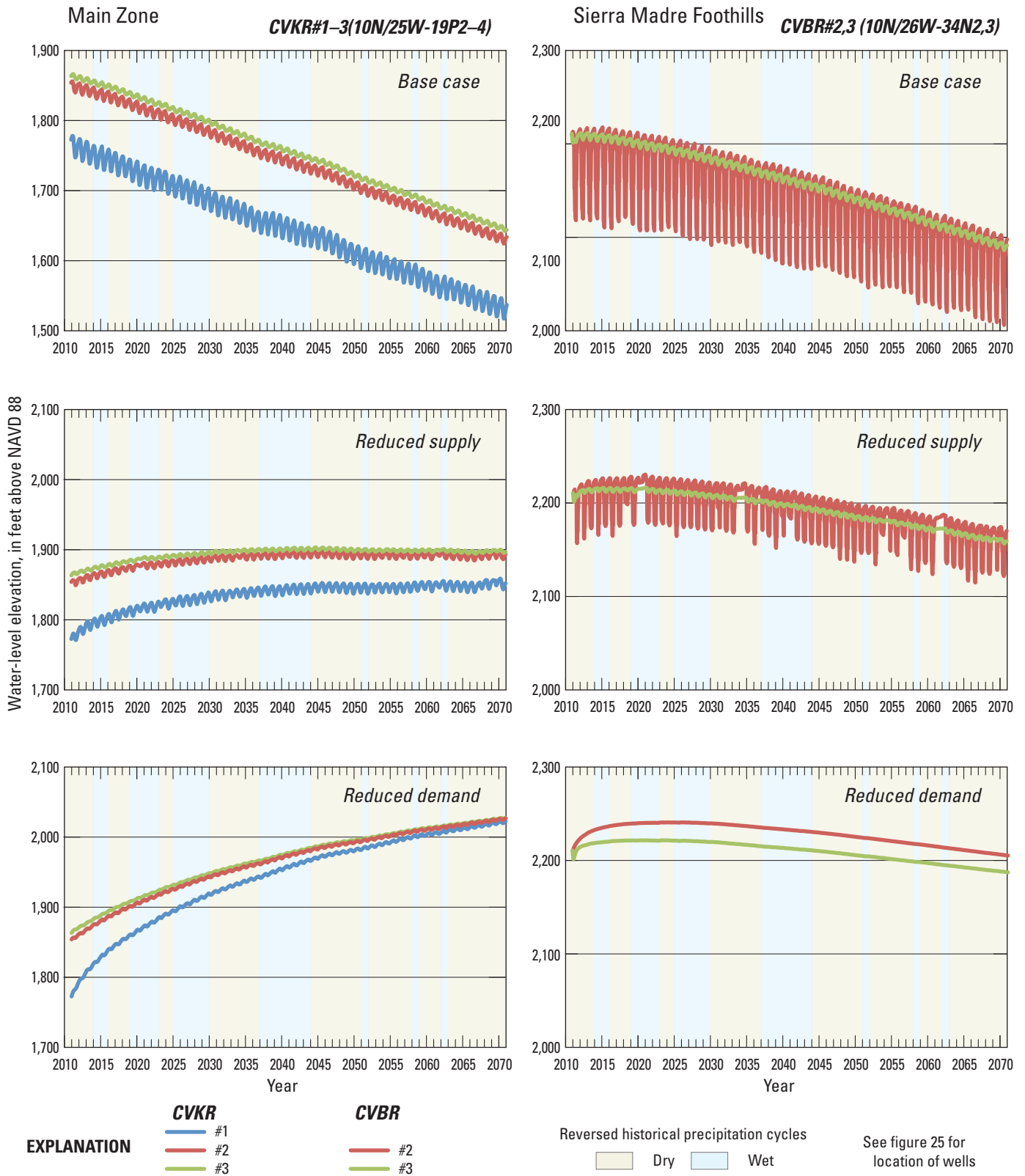


Figure 37. —Continued

C

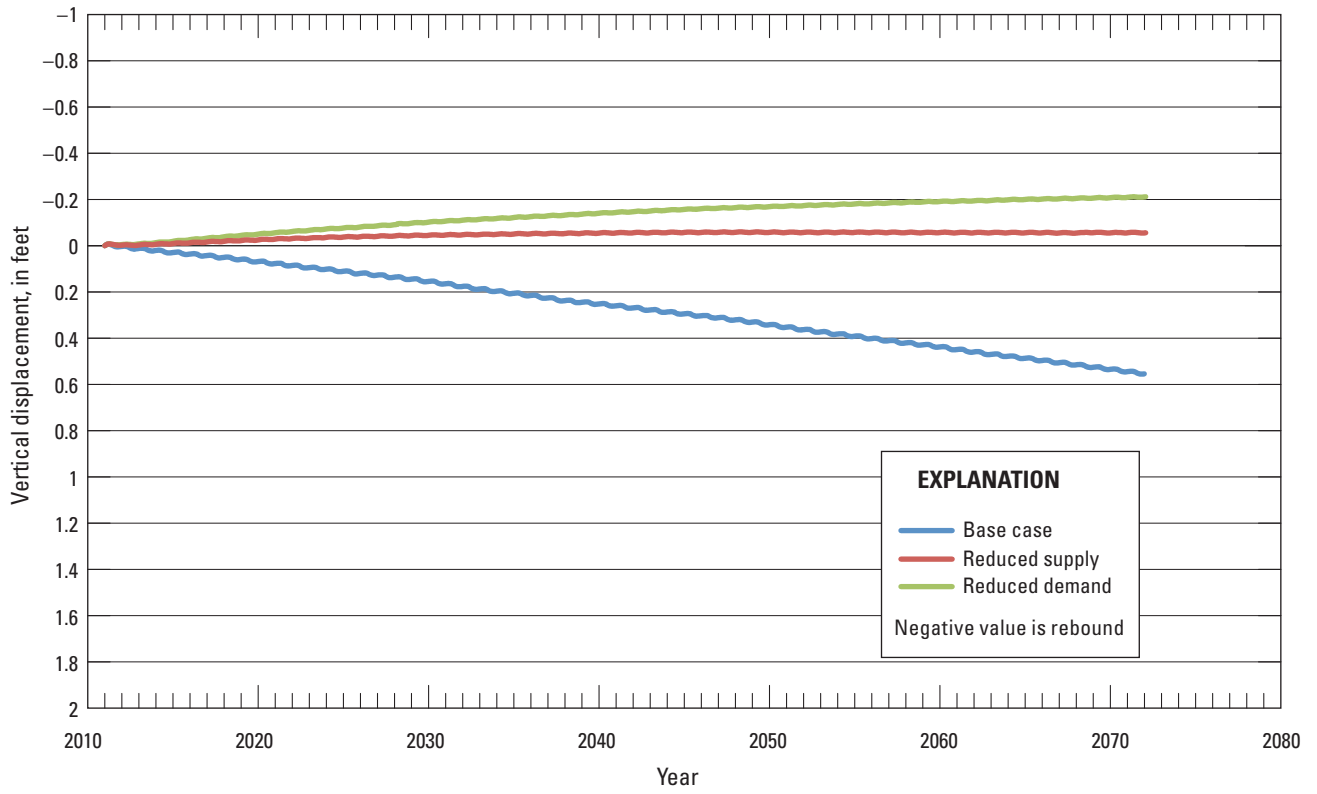


Figure 37. —Continued

Tables

Table 1. Summary of groundwater regional zones and subregions for the Cuyama Valley Hydrologic Model (CUVHM), Cuyama Valley, California.

CUVHM hydrologic subregion zone number	Groundwater subregions group name (fig. 2A)	Regional zone groups (fig. 2B)	Groundwater subregional zone description
1	Caliente northern main zone (CNMZ)	Main zone	Tributaries to Cuyama River draining the Caliente Foothills Badlands
2	Central Sierra Madre foothills (CSMFH)	Sierra Madre foothills	Central subregion of tributaries draining the Sierra Madre foothills between Salsbury Canyon and Santa Barbara Canyon
3	Northeast Ventucopa uplands (NEVU)	Ventucopa uplands	Northeastern Upper Cuyama Creek Drainage and related tributaries and Reyes Creek
4	Northwestern Sierra Madre foothills (NSMFH)	Sierra Madre foothills	Northwestern subregion of tributaries draining the Sierra Madre foothills north of Salsbury Canyon
5	Northern Ventucopa uplands (NVU)	Ventucopa uplands	Region surrounding Berringer Canyon and draining the Morales formation outcrop region
6	Southern Sierra Madre foothills (SSMFH)	Sierra Madre foothills	Southern subregion of tributaries draining the Sierra Madre foothills south of Santa Barbara Canyon
7	Southern Ventucopa uplands (SVU)	Ventucopa uplands	Southern Ventucopa adjacent to Cuyama River uplands corridor
8	Southern main zone (SMZ)	Main zone	South-Central Cuyama bounded by faults on north and south
9	Western main zone (WMZ)	Main zone	Western region surrounding Cuyama River at outflow of Cuyama groundwater basin

Table 2. Summary of climate periods for the Cuyama Valley Hydrologic Model, Cuyama Valley, California (as shown in figure 5).

Climate period ¹ (year)		Climate
1939	1944 ²	Wet
1945	1957 ²	Dry
1958	1958	Wet
1959	1961	Dry
1962	1962	Wet
1963	1968	Dry
1969	1969	Wet
1970	1976	Dry
1977	1983	Wet
1984	1990	Dry
1991	1995	Wet
1996	1997	Dry
1998	2001	Wet
2002	2004	Dry
2005	2006	Wet
2007	2010	Dry

¹Calendar years.

²Climate periods prior to model simulation period that begins in October, 1949.

Table 3. Scaling coefficients for estimation of streamflow for MODFLOW Streamflow Routing (SFR) from recharge and runoff maps developed by the Basin Characterization Model for ungaged basins in three geologic types in Cuyama Valley.

[Abbreviation: —, no estimate made]

Geologic type	Shallow subsurface flow from recharge that becomes baseflow (SFR recharge)	Runoff that becomes streamflow (SFR runoff)	Runoff that becomes deep recharge (subsurface recharge)
Alluvium	0.01	0.05	—
Sandstone	0.04	0.4	0.2
Conglomerate	0.01	0.2	0.3

Table 4. Streamgages used for Basin Characterization Model (BCM) calibration with calibration statistics for Cuyama Valley, California.

[Abbreviations: BL, below; CA, California; CK, creek; CR, creek; CYN, Canyon; ID, identification; NR, near; NSE, Nash-Sutcliffe Efficiency statistic; R, river; RD, road]

Gage ¹	Station ID	Period of record (year)	NSE	Calibration statistics		Recharge and runoff returning as baseflow (percent)	Recharge and runoff that is streamflow (percent)	Total stream-flow that is subsurface recharge to mountain block (percent)
				R ² monthly	R ² annual			
WAGON RD CR NEAR STAUFFER	11136400	1972–1978	0.81	0.81	0.9	0	15	36
REYES CR NEAR VENTUCOPA	11136480	1972–1987	0.76	0.82	0.87	5	53	1
CUYAMA RIVER NEAR VENTUCOPA	11136500	1945–1958	0.44	0.56	0.83	1	22	11
SANTA BARBARA CANYON CK NEAR VENTUCOPA	11136600	2009–2010	0.84	0.95	—	0	12	24
ALISO CANYON CK NEAR NEW CUYAMA	11136650	1963–1972		0.68	0.82	0	5	0
CUYAMA R BL BUCKHORN CYN NR SANTA MARIA CA ²	11136800	1963–2009		0.80	0.82	0	13	37
CUYAMA R NR SANTA MARIA CA ²	11137000	1939–1962		0.50	0.84	0	5	16

¹Locations are shown on figure 11.

²Outside of basin area and downstream of study area.

Table 5. Summary of One-Water Hydrologic Flow Model (OWHM) Packages and processes used with the hydrologic flow model of Cuyama Valley, California.

[Abbreviations: FMP, farm process; MF-FMP, MODFLOW with the farm process; OBS, Observation Package]

Computer program (packages, processes, parameter estimation)	Function	References cited
Processes and solver		
Groundwater flow (GWF) processes of MOD- FLOW-2005	Setup and solve equations simulating a basic groundwater flow model.	Harbaugh (2005), Harbaugh and others (2000), Hill and others (2000)
Preconditioned conjugate- gradient (PCG)	Solves groundwater flow equations; requires convergence of heads and (or) flow rates.	Hill (1990); Harbaugh (2005)
Farm process (FMP)	Setup and solve equations simulating use and movement of water on the landscape as irrigated agriculture, urban landscape, and natural vegetation.	Schmid and Hanson (2009), Schmid and others (2006a, b), Hanson and others (2014b)
Files		
Name file (Name)	Controls the capabilities of MF-FMP utilized during a simulation. Lists most of the files used by the OBS, and FMP processes.	Harbaugh (2005)
Output control option (OC)	Used in conjunction with flags in other packages to output head, drawdown, and budget information for specified time periods into separate files.	Harbaugh (2005)
List file (LIST)	Output file for allocation information, values used by the GWF process, and calculated results such as head, drawdown, and the water budget.	Harbaugh (2005)
Discretization		
Basic package (BAS6)	Defines the initial conditions and some of the boundary conditions of the model.	Harbaugh (2005)
Discretization package (DIS)	Space and time information.	Harbaugh (2005)
Multiplier package (MULT)	Defines multiplier arrays for calculation of model-layer characteristics from parameter values.	Harbaugh (2005), Schmid and Hanson (2009)
Zones (ZONE)	Defines arrays of different zones. Parameters may be composed of one or many zones.	Harbaugh (2005)
Aquifer parameters		
Layer property flow package (LPF)	Calculates the hydraulic conductance between cell centers.	Harbaugh (2005)
Hydrologic flow barriers (HFB6)	Simulates a groundwater barrier by defining a hydraulic conductance between two adjacent cells in the same layer.	Hsieh and Freckelton (1993)
Boundary conditions		
General head boundaries (GHB)	Head-dependent boundary condition used along the edge of the model to allow groundwater to flow into or out of the model under a regional gradient.	Harbaugh (2005)
Recharge and discharge		
Multi-node wells (MNW1)	Simulates pumpage from wells with screens that span multiple layers.	Halford and Hanson (2002)
Streamflow routing (SFR2)	Simulates the routed streamflow, infiltration, exfiltration, runoff, and returnflows from FMP.	Niswonger and Prudic (2005)
Output, observations and sensitivity		
Headobservation (HOB)	Defines the head observation and weight by layer(s), row, column, and time and generates simulated values for comparison with observed values.	Hill and others (2000), Harbaugh (2005)
Hydmod (HYD)	Generates simulated values for specified locations at each time-step for groundwater levels and streamflow attributes.	Hanson and Leake (1998)
Sensitivity (PVAL)	Specifies parameter values used in other packages.	Harbaugh (2005)

Table 6. Coordinates of the hydrologic flow model of Cuyama Valley, California.

[Model grid is rotated 33 degrees west of north; coordinates below are calculated at the outer corner of the model grid using the North American Datum of 1983 in the Universal Transverse Mercator (UTM) Projection of North America, Zone 11; each model cell is 250 meters by 250 meters. **Abbreviation:** DMS, degree, minute, second]

Corner of model grid	Model coordinates X (column)	Model coordinates Y (row)	Latitude (DMS)	Longitude (DMS)	UTM coordinates X (easting) (meters)	UTM coordinates Y (northing) (meters)
Northwest	1	1	34° 54' 57"	119° 56' 36"	-231,090	3,867,673
Northeast	135	1	35° 10' 07"	119° 44' 23"	-250,476	3,895,182
Southwest	1	300	34° 32' 54"	119° 15' 10"	-293,276	3,825,260
Southeast	135	300	34° 48' 00"	119° 02' 53"	-312,648	3,852,769

Table 7. Percentage of different virtual crop categories in Cuyama Valley Hydrologic Model for selected land-use periods.

[Abbreviations: FMP ID, farm process identification; no., number]

Description (FMP ID/cropsScape land-use no.)	Percentage of active model area													
	1952	1959	1966	1977	1984	2000	2002	2004	2005	2006	2007	2008	2009	2010
Field crops ¹	2.8	1.2	2.1	4	4	7.5	3.9	3.8	3.9	1.8	1	1	5.7	4.5
Alfalfa (4/36)	3.3	6.0	5.2	12.3	12.4	3.03	0.35	0.35	0.35	0.35	0.4	0.24	0.56	0.21
Dry beans (6/42)	0	0	0	0	0	0.32	0	0	0	0	0	0	0	0
Potatoes (7/43)	3.4	0.6	1.9	0	0	0.57	1.75	1.75	1.76	1.48	3.81	1.15	0.6	2.14
Onions (8/49)	0	0.7	0.5	0	0	0.35	0.09	0.09	0.09	0.31	0.31	0.22	0	0.66
Various orchards ²	0	0.1	0.4	0	0	2.78	1.28	1.28	1.28	1.07	2.15	0.98	3.19	0.6
Grapes (14/69)	0	0	0	0	0	0.8	1.2	1.2	1.2	1.1	1	1.1	1.2	1
Walnuts (16/76)	0	0	0	0	0	0.1	0.1	0.1	0.1	0	0	0	0	0
Native trees ³	12	11.9	11.9	11.8	11.8	11.8	11.8	11.8	11.8	11.8	11.8	11.8	11.8	11.9
Native shrubland (23/152) and grass- land (24/171)	74.7	75.4	74.1	53.8	53.6	53.9	53.8	53.8	53.7	53.9	53.9	53.9	54	53.4
Various farmland categories ⁴	4.1	0	3.8	4	4.2	4.1	4.2	4.2	4.1	4.1	4.1	4.1	4.1	4.1
Pistachios (30/204)	0	0	0	0	0	0.7	0.6	0.6	0.6	0.6	0.7	0.5	0.8	0.5
Carrots (31/206)	0	0	0	0.8	0.8	5.3	5.7	5.6	5.7	10.6	9.9	6	9.7	3.2
Cantaloupes (32/209)	0	0	0	0	0	0	0	0	0	0	0.8	0	1.3	0
Broccoli (34/214) and cauliflower (37/244)	0	0	0	0	0	0	0	0	0	0	0.6	0	0.9	0
Irrigated row and vegetable crops (40/259)	0	0	0	0	0	0.5	1.7	1.7	1.7	1	0.2	5	2.7	14
Fallow/idle cropland (9/61)	0	0	0	12.9	12.9	4.2	2.3	2.4	2.4	3.5	2.3	2.1	2.6	2

¹Field crops were simulated separately as they occurred historically. Summaries of areas and percentages represent collective area for this group of crops that includes barley (1/21), durham wheat (2/22), oats (3/28), other hay (5/37), pasture/grass (10/62), forage hay/silage (38/257), and irrigated field crops (39/258).

²Various fruit trees were simulated separately as they occurred historically. Summaries of areas and percentages represent collective area for this group of crops that includes cherries (11/66), peaches (12/67), apples (13/68), other fruit trees (15/73), nectarines (34/218), apricots (35/223), and olives (32/211).

³Native trees were simulated separately as they occurred historically. Summaries of areas and percentages represent collective area for this group of crops that includes deciduous (20/141), evergreen (21/142), and mixed forest (22/143) vegetation.

⁴Various farmland categories were simulated separately as they occurred historically. Summaries of areas and percentages represent collective area for this group of crops that includes prime farmland (25/183), statewide importance (26/184), unique farmland (27/185), local importance (28/186), and local potential (29/187), developed/open space (19/282).

Table 8. Summary of Cuyama Valley Farm process (FMP) virtual-crop crop category, crop-index number, and select properties for the Cuyama Valley Hydrologic Model (CUVHM), Cuyama Valley, California.

Farm process (FMP) crop index number and virtual-crop crop category ¹	Root depth (feet)	Root uptake pressure heads (feet)				Fraction of surface-water runoff (dimensionless)	
		Anoxia	Lower optimal range	Upper optimal range	Wilting	Precipitation	Irrigation
Field crops (1, 2, 3, 5, 10, 38)	4.4–12	-0.49 – -0.24	-0.98 – -0.66	-171 – -18	-525 – -262	0.8–0.99	0.24–0.97
Alfalfa (4)	12.0	-0.49	-0.98	-18	-262	0.9	0.6
Dry beans (6)	5.5	-0.43	-0.89	-23	-36	0.97	0.97
Potatoes (7)	4.7	-0.49	-0.98	-20	-262	0.97	0.97
Onions (8)	3.3	-0.49	-0.98	-24	-262	0.8	0.21
Various orchards (11, 12, 13, 15, 33, 35)	1.5–6.6	-0.49 – -0.43	-0.98 – -0.89	-37 – -0.18	-377 – -262	0.95–0.97	0.05–0.97
Grapes (14)	5.0	-0.49	-0.98	-18	-262	0.97	0.25
Walnuts (16)	6.0	-0.49	-0.98	-18	-262	0.95	0.04
Native trees (20, 21, 22)	6.6–10.8	-0.49	-0.98	-18	-262	0.92	0.05
Native shrubland and grassland (23, 24)	5.3–15.4	-0.49	-0.98	-18	-262	0–0.9	0.05
Various farmland categories (19, 25, 26, 27, 28, 29)	0.3–12	-0.49–0	-0.98–0	-98 – -20	-406 – -262	0.8–0.97	0.21–0.97
Pistachios (30)	1.6	-0.49	-0.98	-171	-525	0.97	0.97
Carrots (31)	1.5	-0.43	-0.92	-37	-262	0.97	0.97
Cantaloupes (32)	1.5	-0.49	0	-27	-377	0.95	0.05
Broccoli (34) and cauliflower (37)	2.5–6.5	-0.49 – -0.43	-0.98–0.33	-37 – -1.0	-262 – -1.31	0.97	0.97
Irrigated row and vegetable crops (40)	1.5	-0.49	-0.98	-18	-262	0.97	0.97
Fallow/idle cropland (9)	5.3	-0.49	-0.98	-18	-262	0.97	0.97

¹Refer to table 7 for explanation of crop and vegetation groupings. For groups of crops, the root uptake pressure heads represent the range in values for this grouping of crops.

Table 9. Summary of fractions of transpiration and evaporation by month, for Cuyama Valley crop categories (virtual crops).

[Abbreviations: FEI, fraction of evaporation from irrigation; FEP, fraction of evaporation from precipitation; FTR, fraction of transpiration]

Crop	January			February			March			April		
	FTR	FEP	FEI									
Field crops	0.05-0.58	0.43-0.95	0-0.5	0.05-0.78	0.23-0.95	0-0.5	0.05-0.88	0.13-0.95	0-0.5	0.15-0.97	0.03-0.85	0-0.1
Alfalfa	0.5-0.5	0.5-0.5	0.1-0.1	0.6-0.6	0.4-0.4	0.1-0.1	0.78-0.78	0.22-0.22	0.15-0.15	0.97-0.97	0.03-0.03	0.03-0.03
Dry beans	0.5-0.58	0.43-0.5	0.1-0.1	0.7-0.78	0.23-0.3	0.1-0.1	0.8-0.88	0.13-0.2	0.1-0.1	0.5-0.58	0.43-0.5	0.3-0.3
Potatoes	0.2-0.28	0.73-0.8	0.1-0.1	0.3-0.38	0.63-0.7	0.1-0.1	0.5-0.58	0.43-0.5	0.1-0.1	0.6-0.68	0.33-0.4	0.2-0.2
Onions	0.5-0.58	0.43-0.5	0.05-0.05	0.7-0.78	0.23-0.3	0.05-0.05	0.8-0.88	0.13-0.2	0.05-0.05	0.5-0.58	0.43-0.5	0.05-0.05
Various orchards	0.03-0.58	0.43-0.97	0-0.1	0.03-0.78	0.23-0.97	0-0.1	0.1-0.88	0.13-0.9	0-0.1	0.5-0.68	0.33-0.5	0-0.1
Grapes	0.05-0.13	0.88-0.95	0.1-0.1	0.05-0.13	0.88-0.95	0.1-0.1	0.28-0.36	0.65-0.72	0.1-0.1	0.4-0.48	0.53-0.6	0.1-0.1
Walnuts	0.03-0.11	0.9-0.97	0.05-0.05	0.03-0.11	0.9-0.97	0.05-0.05	0.1-0.18	0.83-0.9	0.05-0.05	0.5-0.58	0.43-0.5	0.05-0.05
Native trees	0.03-0.28	0.73-0.97	0-0.1	0.03-0.28	0.73-0.97	0-0.1	0.1-0.48	0.53-0.9	0-0.1	0.5-0.58	0.43-0.5	0-0.1
Native shrubland and grassland	0.23-0.36	0.65-0.77	0-0.1	0.23-0.36	0.65-0.77	0-0.1	0.61-0.74	0.27-0.39	0-0.15	0.61-0.74	0.27-0.39	0-0.15
Various farmland categories	0-0.5	0.5-1	0-0.1	0-0.5	0.5-1	0-0.1	0-0.5	0.5-1	0-0.2	0-0.97	0.03-1	0-0.03
Pistachios	0.03-0.11	0.9-0.97	0.1-0.1	0.03-0.11	0.9-0.97	0.1-0.1	0.1-0.18	0.83-0.9	0.2-0.2	0.5-0.58	0.43-0.5	0.2-0.2
Carrots	0.5-0.58	0.43-0.5	0-0	0.7-0.78	0.23-0.3	0-0	0.8-0.88	0.13-0.2	0-0	0.5-0.58	0.43-0.5	0-0
Cantaloupes	0.2-0.28	0.73-0.8	0-0	0.3-0.38	0.63-0.7	0-0	0.5-0.58	0.43-0.5	0-0	0.6-0.68	0.33-0.4	0-0
Broccoli and cauliflower	0.5-0.58	0.43-0.5	0.1-0.1	0.7-0.78	0.23-0.3	0.1-0.1	0.8-0.88	0.13-0.2	0.1-0.1	0.5-0.58	0.43-0.5	0.1-0.1
Irrigated row and vegetable crops	0.2-0.28	0.73-0.8	0-0	0.3-0.38	0.63-0.7	0-0	0.5-0.58	0.43-0.5	0-0	0.6-0.68	0.33-0.4	0-0
Fallow/idle cropland	0-0	1-1	0.1-0.1	0-0	1-1	0.1-0.1	0-0	1-1	0.1-0.1	0-0	1-1	0.03-0.03

Table 9. Summary of fractions of transpiration and evaporation by month for Cuyama Valley crop categories (virtual crops).—Continued

[Abbreviations: FEI, fraction of evaporation from irrigation; FEP, fraction of evaporation from precipitation; FTR, fraction of transpiration]

Crop	May			June			July			August		
	FTR	FEP	FEI									
Field crops	0.25–0.97	0.03–0.75	0–0.3	0.65–0.97	0.03–0.35	0.03–0.2	0.7–0.96	0.04–0.3	0.03–0.2	0.8–0.97	0.03–0.2	0.03–0.2
Alfalfa	0.97–0.97	0.03–0.03	0.02–0.02	0.97–0.97	0.03–0.03	0.02–0.02	0.96–0.96	0.04–0.04	0.02–0.02	0.97–0.97	0.03–0.03	0.02–0.02
Dry beans	0.6–0.68	0.33–0.4	0.3–0.3	0.65–0.73	0.28–0.35	0.03–0.03	0.7–0.78	0.23–0.3	0.03–0.03	0.8–0.88	0.13–0.2	0.03–0.03
Potatoes	0.7–0.78	0.23–0.3	0.2–0.2	0.8–0.88	0.13–0.2	0.1–0.2	0.8–0.88	0.13–0.2	0.1–0.2	0.8–0.88	0.13–0.2	0.1–0.2
Onions	0.6–0.68	0.33–0.4	0.05–0.05	0.65–0.73	0.28–0.35	0.05–0.05	0.7–0.78	0.23–0.3	0.05–0.05	0.8–0.88	0.13–0.2	0.05–0.05
Various orchards	0.6–0.78	0.23–0.4	0–0.1	0.65–0.88	0.13–0.35	0–0.1	0–0.1	0.7–0.88	0.13–0.3	0–0.1	0.8–0.98	0.03–0.2
Grapes	0.38–0.46	0.55–0.62	0.1–0.1	0.36–0.44	0.57–0.64	0.1–0.1	0.36–0.44	0.57–0.64	0.1–0.1	0.36–0.44	0.57–0.64	0.1–0.1
Walnuts	0.6–0.68	0.33–0.4	0.05–0.05	0.7–0.78	0.23–0.3	0.05–0.05	0.8–0.88	0.13–0.2	0.05–0.05	0.9–0.98	0.03–0.1	0.02–0.05
Native trees	0.6–0.68	0.33–0.4	0–0.3	0.7–0.78	0.23–0.3	0–0.2	0.8–0.88	0.13–0.2	0–0.2	0.9–0.98	0.03–0.1	0–0.1
Native shrubland and grassland	0.61–0.74	0.27–0.39	0–0.15	0.61–0.74	0.27–0.39	0.1–0.15	0.61–0.74	0.27–0.39	0.1–0.15	0.61–0.74	0.27–0.39	0.1–0.15
Various farmland categories	0–0.97	0.03–1	0–0.03	0–0.97	0.03–1	0–0.03	0–0.96	0.04–1	0–0.04	0–0.97	0.03–1	0–0.03
Pistachios	0.6–0.68	0.33–0.4	0.3–0.3	0.7–0.78	0.23–0.3	0.2–0.3	0.8–0.88	0.13–0.2	0.1–0.2	0.9–0.98	0.03–0.1	0.02–0.1
Carrots	0.6–0.68	0.33–0.4	0–0	0.65–0.73	0.28–0.35	0–0	0.7–0.78	0.23–0.3	0–0	0.8–0.88	0.13–0.2	0–0
Cantaloupes	0.7–0.78	0.23–0.3	0–0	0.8–0.88	0.13–0.2	0–0	0.8–0.88	0.13–0.2	0–0	0.8–0.88	0.13–0.2	0–0
Broccoli and cauliflower	0.6–0.68	0.33–0.4	0.1–0.3	0.65–0.73	0.28–0.35	0.1–0.2	0.1–0.2	0.7–0.78	0.23–0.3	0.1–0.2	0.8–0.88	0.13–0.2
Irrigated row and vegetable crops	0.7–0.78	0.23–0.3	0–0	0.8–0.88	0.13–0.2	0–0	0.8–0.88	0.13–0.2	0–0	0.8–0.88	0.13–0.2	0–0
Fallow/idle cropland	0–0	1–1	0.03–0.03	0–0	1–1	0.03–0.03	0–0	1–1	0.04–0.04	0–0	1–1	0.03–0.03

Table 9. Summary of fractions of transpiration and evaporation by month for Cuyama Valley crop categories (virtual crops).—Continued

[Abbreviations: FEI, fraction of evaporation from irrigation; FEP, fraction of evaporation from precipitation; FTR, fraction of transpiration]

Crop	September			October			November			December		
	FTR	FEP	FEI									
Field crops	0.7–0.97	0.03–0.3	0.03–0.2	0.33–0.83	0.18–0.67	0.01–0.5	0.05–0.88	0.13–0.95	0.1–0.5	0.05–0.88	0.13–0.95	0.1–0.5
Alfalfa	0.97–0.97	0.03–0.03	0.02–0.02	0.78–0.78	0.22–0.22	0.2–0.2	0.6–0.6	0.4–0.4	0.15–0.15	0.5–0.5	0.5–0.5	0.1–0.1
Dry beans	0.8–0.88	0.13–0.2	0.03–0.03	0.75–0.83	0.18–0.25	0.1–0.25	0.8–0.88	0.13–0.2	0.1–0.2	0.8–0.88	0.13–0.2	0.1–0.1
Potatoes	0.8–0.88	0.13–0.2	0.1–0.2	0.7–0.78	0.23–0.3	0.2–0.2	0.8–0.88	0.13–0.2	0.1–0.1	0.8–0.88	0.13–0.2	0.1–0.1
Onions	0.8–0.88	0.13–0.2	0.05–0.05	0.75–0.83	0.18–0.25	0.05–0.05	0.8–0.88	0.13–0.2	0.05–0.05	0.8–0.88	0.13–0.2	0.05–0.05
Various orchards	0–0.1	0.8–0.98	0.03–0.2	0–0.1	0.7–0.83	0.18–0.3	0–0.3	0.1–0.88	0.13–0.9	0–0.1	0.03–0.88	0.13–0.97
Grapes	0.36–0.44	0.57–0.64	0.1–0.1	0.36–0.44	0.57–0.64	0.1–0.1	0.2–0.28	0.73–0.8	0.1–0.1	0.05–0.13	0.88–0.95	0.1–0.1
Walnuts	0.9–0.98	0.03–0.1	0.02–0.05	0.7–0.78	0.23–0.3	0.05–0.05	0.1–0.18	0.83–0.9	0.05–0.05	0.03–0.11	0.9–0.97	0.05–0.05
Native trees	0.9–0.98	0.03–0.1	0–0.1	0.7–0.78	0.23–0.3	0–0.3	0.1–0.28	0.73–0.9	0–0.5	0.03–0.28	0.73–0.97	0–0.1
Native shrubland and grassland	0.61–0.74	0.27–0.39	0.1–0.2	0.61–0.74	0.27–0.39	0.1–0.2	0.61–0.74	0.27–0.39	0.1–0.15	0.23–0.36	0.65–0.77	0.1–0.1
Various farmland categories	0–0.97	0.03–1	0–0.03	0–0.5	0.5–1	0–0.3	0–0.5	0.5–1	0–0.25	0–0.5	0.5–1	0–0.1
Pistachios	0.9–0.98	0.03–0.1	0.02–0.1	0.7–0.78	0.23–0.3	0.2–0.2	0.1–0.18	0.83–0.9	0.1–0.1	0.03–0.11	0.9–0.97	0.1–0.1
Carrots	0.8–0.88	0.13–0.2	0–0	0.75–0.83	0.18–0.25	0–0	0.8–0.88	0.13–0.2	0–0	0.8–0.88	0.13–0.2	0–0
Cantaloupes	0.8–0.88	0.13–0.2	0–0	0.7–0.78	0.23–0.3	0–0	0.5–0.58	0.43–0.5	0–0	0.3–0.38	0.63–0.7	0–0
Broccoli and cauliflower	0.1–0.2	0.8–0.88	0.13–0.2	0.1–0.2	0.75–0.83	0.18–0.25	0.01–0.2	0.8–0.88	0.13–0.2	0.1–0.2	0.8–0.88	0.13–0.2
Irrigated row and vegetable crops	0.8–0.88	0.13–0.2	0–0	0.7–0.78	0.23–0.3	0–0	0.5–0.58	0.43–0.5	0–0	0.3–0.38	0.63–0.7	0–0
Fallow/idle cropland	0–0	1–1	0.03–0.03	0–0	1–1	0.3–0.3	0–0	1–1	0.1–0.1	0–0	1–1	0.1–0.1

¹Refer to table 7 for explanation of crop and vegetation groupings.

Table 10. Irrigation efficiency, by month, for each crop of the Cuyama Valley, California.^{1,2}

[Efficiencies are adjusted seasonally for wet and dry climatic periods with multipliers (see Model Calibration section). Refer to table 7 for explanation of crop and vegetation groupings.]

Crop categories	January	February	March	April	May	June	July	August	September	October	November	December
Field crops	0.5-0.75	0.5-0.75	0.5-0.75	0.5-0.75	0.5-0.75	0.5-0.75	0.5-0.75	0.5-0.75	0.5-0.75	0.5-0.75	0.5-0.75	0.5-0.75
Alfalfa	0.5-0.675	0.5-0.675	0.5-0.675	0.5-0.675	0.5-0.675	0.5-0.675	0.5-0.675	0.5-0.675	0.5-0.675	0.5-0.675	0.5-0.675	0.5-0.675
Dry beans	0.5-0.7	0.5-0.7	0.5-0.7	0.5-0.7	0.5-0.7	0.5-0.7	0.5-0.7	0.5-0.7	0.5-0.7	0.5-0.7	0.5-0.7	0.5-0.7
Potatoes	0.5-0.6	0.5-0.6	0.5-0.6	0.5-0.6	0.5-0.6	0.5-0.6	0.5-0.6	0.5-0.6	0.5-0.6	0.5-0.6	0.5-0.6	0.5-0.6
Onions	0.5-0.65	0.5-0.65	0.5-0.65	0.5-0.65	0.5-0.65	0.5-0.65	0.5-0.65	0.5-0.65	0.5-0.65	0.5-0.65	0.5-0.65	0.5-0.65
Various orchards	0.5-0.75	0.5-0.75	0.5-0.75	0.5-0.75	0.5-0.75	0.5-0.75	0.5-0.75	0.5-0.75	0.5-0.75	0.5-0.75	0.5-0.75	0.5-0.75
Grapes	0.5-0.875	0.5-0.875	0.5-0.875	0.5-0.875	0.5-0.875	0.5-0.875	0.5-0.875	0.5-0.875	0.5-0.875	0.5-0.875	0.5-0.875	0.5-0.875
Walnuts	0.5-0.75	0.5-0.75	0.5-0.75	0.5-0.75	0.5-0.75	0.5-0.75	0.5-0.75	0.5-0.75	0.5-0.75	0.5-0.75	0.5-0.75	0.5-0.75
Native trees	0.5-0.5	0.5-0.5	0.5-0.5	0.5-0.5	0.5-0.5	0.5-0.5	0.5-0.5	0.5-0.5	0.5-0.5	0.5-0.5	0.5-0.5	0.5-0.5
Native shrubland and grassland	0.5-0.5	0.5-0.5	0.5-0.5	0.5-0.5	0.5-0.5	0.5-0.5	0.5-0.5	0.5-0.5	0.5-0.5	0.5-0.5	0.5-0.5	0.5-0.5
Various farmland categories	0.5-0.75	0.5-0.75	0.5-0.75	0.5-0.75	0.5-0.75	0.5-0.75	0.5-0.75	0.5-0.75	0.5-0.75	0.5-0.75	0.5-0.75	0.5-0.75
Pistachios	0.5-0.7	0.5-0.7	0.5-0.7	0.5-0.7	0.5-0.7	0.5-0.7	0.5-0.7	0.5-0.7	0.5-0.7	0.5-0.7	0.5-0.7	0.5-0.7
Carrots	0.5-0.8	0.5-0.8	0.5-0.8	0.5-0.8	0.5-0.8	0.5-0.8	0.5-0.8	0.5-0.8	0.5-0.8	0.5-0.8	0.5-0.8	0.5-0.8
Cantaloupes	0.5-0.75	0.5-0.75	0.5-0.75	0.5-0.75	0.5-0.75	0.5-0.75	0.5-0.75	0.5-0.75	0.5-0.75	0.5-0.75	0.5-0.75	0.5-0.75
Broccoli and cauliflower	0.5-0.75	0.5-0.75	0.5-0.75	0.5-0.75	0.5-0.75	0.5-0.75	0.5-0.75	0.5-0.75	0.5-0.75	0.5-0.75	0.5-0.75	0.5-0.75
Irrigated row and vegetable crops	0.5-0.75	0.5-0.75	0.5-0.75	0.5-0.75	0.5-0.75	0.5-0.75	0.5-0.75	0.5-0.75	0.5-0.75	0.5-0.75	0.5-0.75	0.5-0.75
Fallow/idle cropland	0.5-0.8	0.5-0.8	0.5-0.8	0.5-0.8	0.5-0.8	0.5-0.8	0.5-0.8	0.5-0.8	0.5-0.8	0.5-0.8	0.5-0.8	0.5-0.8

¹Efficiencies are adjusted seasonally for wet and dry climatic periods with multipliers (see Model Calibration section)

²Refer to table 7 for explanation of crop and vegetation groupings.

Table 11. Summary of reference evapotranspiration (ET_h) comparisons between Penman-Montieth from California Irrigation Management Information System (CIMIS) stations and Priestley-Taylor estimates from regional climate data, Cuyama Valley, California.

[Abbreviations: Apr., April; Aug., August; Dec., December; Feb., February; Jan., January; Mar., March; Nov., November; Oct., October; Sept., September]

ET_h average monthly value (inches/month)	Jan.	Feb.	Mar.	Apr.	May	June	July	Aug.	Sept.	Oct.	Nov.	Dec.
¹ CIMIS station 88 (California Department of Water Resources, 2013)	2.10	2.43	3.97	5.33	7.07	8.06	8.55	7.84	6.01	4.39	2.58	1.94
Priestley-Taylor estimate	1.90	2.38	3.80	4.96	6.49	7.16	7.71	6.90	5.35	3.87	2.35	1.70
Adjusted fraction of CIMIS value of P-T estimate [dimensionless]	1.11	1.02	1.05	1.07	1.09	1.13	1.11	1.14	1.12	1.13	1.10	1.14

¹Average monthly values for 1989–2011.

Table 12. Summary of hydraulic properties estimated from the Cuyama Valley hydrologic model (CUVHM) calibration.

Aquifer (model layer)	Lateral hydraulic conductivity (feet/day)	Specific storage [1/foot]	Specific yield [dimensionless]	Vertical hydraulic conductivity [feet/day] (leakance, in feet/day/feet)	Skeletal elastic storage, coarse and fine- grained layers [dimensionless]	Skeletal inelastic storage, fine- grained layers [dimensionless]
Recent Alluvium (1)	5.2–85	2.2e-05–9.34e-03	0.02–0.14	0.0–12.3	5.9e-06–4.8e-04	6.37e-07–4.7e-03
Older Alluvium (2)	0.3–15.5	1.3e-06–8.0e-03	0.05–0.19	6.1e-04–0.34	7.4e-07–3.3e-04	1.5e-05–2.3e-02
Morales Formation (3)	0.02–0.4	1.3e-06–2.3e-02	0.06–0.25	3.4e-03–0.01	1.05e-05–4.5e-03	7.3e-05–9.2e-03

Table 13. Summary of parameter zones and related property parameter names used to calibrate horizontal hydraulic conductivity (K_h), vertical hydraulic conductivity (K_v), and aquifer specific storage and specific yield (S_s) in the Cuyama Valley hydrologic model (CUVHM), Cuyama Valley, California.

Feature/parameter zone	Root subregion model parameter names ¹ (zone number)	Description
Recent alluvial aquifer (layer 1)	<p><u>Unconfined Ventucopa</u> VC_QYAUC (7) <u>Unconfined main zones</u> NMZ_QYA (1) SMZ_QYA (4) WZ_QYA (8) <u>Sierra Madre foothills zones</u> SMFHQYA (3) <u>River channel</u> NMZQYACC (2) SMZ_QYACC (5) VC_QYACC (6) WZ_QYACC (9)</p>	<p><u>Unconfined Ventucopa</u> Ventucopa <u>Unconfined Main zones</u> Northern Main Southern Main Western <u>Sierra Madre foothills zones</u> Sierra Madre foothills <u>River channel</u> Northern Main Southern Main Ventucopa Western (includes selected tributary channels)</p>
Older alluvial aquifer (layer 2)	<p><u>Unconfined Ventucopa</u> VC_QOAN (14) VC_QOAC (21) <u>Unconfined main zones</u> NMZ_QOA (10) WZ_QOA_N (15) WZ_QOA_S (16) <u>Sierra Madre foothills zones</u> SMFH_QOAN (11) SMFH_QOAM (12) SMFH_QOAS (13) <u>River channel</u> None <u>Confined zone</u> NMZ_QOAC (18) SMFH_QOAC (19) SMZ_QOAC (20) WZ_QOAC (22) QOA_PHT (23)</p>	<p><u>Unconfined/confined Ventucopa</u> Northern Ventucopa foothills unconfined Ventucopa confined <u>Unconfined Main Zones</u> Northern Main Northern western—Badlands foothills Southern western <u>Sierra Madre foothills zones</u> Northern Middle Southern <u>River channel</u> None <u>Confined Ventucopa</u> None Confined Main zones Northern Main Sierra Madre foothills Southern Main Western Phantom layer cells</p>
Morales formation (layer 3)	<p><u>Unconfined Ventucopa</u> VC_MOUC (17) <u>Unconfined main zones</u> None <u>Sierra Madre foothills zones</u> None <u>River channel</u> None <u>Confined zone</u> MO_C (24)</p>	<p><u>Unconfined Ventucopa</u> Ventucopa foothills <u>Unconfined Main zones</u> None <u>Sierra Madre foothills zones</u> None <u>River channel</u> None <u>Confined Ventucopa and Main zones</u> Entire active model grid where Morales Formation is not uppermost model layer</p>

¹Root names have H_k , V_k , and SS added to the front of these names for parameter names used in PVAL and LPF input files.

Table 14. Summary of selected parameter values estimated for the Cuyama Valley hydrologic model (CUVHM), Cuyama Valley, California.

Parameter type [model layers]	Parameter name	Parameter description	Final values	Units	Estimated using automated methods ¹	Rank and composite scaled sensitivity	Package/process-parameter group
Crop properties							
Early years [1–3]	Dry seasons	Stress coefficient	0.85	Multiplier	No	16/54.9	FMP—K _c -value properties
	SCL_KCSDFL	for early (1963–92)	1.10		No	101/30.3	
	SCL_KCSDWN	agriculture crop	1.10		No	20/53.2	
	SCL_KCSDSP	coefficients	0.82		Yes	95/31.7	
	SCL_KCSDSU		=====		Yes	=====	
	Wet seasons		0.67		No	84/34.3	
	SCL_KCSWFL		0.71		No	102/29.8	
	SCL_KCSWWN		0.80		No	91/32.7	
	SCL_KCSWSP		0.80			44/46.7	
	SCL_KCSWSU						
Recent years [1–3]	Dry seasons	Stress coefficient	1.17	Multiplier	No	117/25.4	FMP—K _c -value properties
	SCL_KCSDFL2	for recent-	1.14		No	111/27.0	
	SCL_KCSDWN2	(1993–2006)	1.20		Yes	71/38.3	
	SCL_KCSDSP2	agriculture	1.03		Yes	126/18.4	
	SCL_KCSDSU2	crop coefficients	=====		No	=====	
	Wet seasons		1.03		No	115/26.2	
	SCL_KCSWFL2		1.15		No	112/26.7	
	SCL_KCSWWN2		0.87		No	94/31.8	
	SCL_KCSWSP2		1.11			99/30.7	
	SCL_KCSWSU2						
Runoff							
[1–3]	Fractions of inefficient losses to runoff from precipitation for truck-vegetable crops	Fraction runoff from precipitation for selected land use class	0.97	Fraction	No	7/7.40	FMP—runoff
	FIESWP_TVR		0.97		No	66/40.4	
	field crops FIESWP_FLD		0.97		No	70/38.5	
	orchards FIESWP_ORC		0.97		No	59/41.6	
	pasture FIESWP_PAS		0.92		Yes	48/45.4	
	native FIESWP_NTV						
[1–3]	Fractions of inefficient losses to runoff from irrigation for truck-vegetable crops	Fraction runoff from irrigation for selected land-use class	0.97	Fraction	No	127/17.2	FMP—runoff
	FIESWI_TVR		0.97		No	5/65.1	
	field crops FIESWI_FLD		0.97		No	86/33.9	
	orchards FIESWI_ORC		0.97		No	28/49.9	
	pasture FIESWI_PAS						
Irrigation efficiency							
Early years [1–3]	Dry seasons	Multiplier on	0.88	Multiplier	No	166/<0.1	FMP—irrigation
	SCL_EFFDFL	irrigation	0.89		No	167/<0.1	
	SCL_EFFDWN	efficiency for wet	1.06		Yes	168/<0.1	
	SCL_EFFDSP	and dry seasons	0.92		Yes	169/<0.1	
	SCL_EFFDSU		0.70		No	158/<0.1	
	Wet seasons		0.70		No	159/<0.1	
	SCL_EFFWFL		0.70		No	160/<0.1	
	SCL_EFFWWN		0.72		No	161/<0.1	
	SCL_EFFWSP						
SCL_EFFWSU							

Table 14. Summary of parameter values estimated for the Cuyama Valley hydrologic model (CUVHM), Cuyama Valley, California.—Continued

Parameter type [model layers]	Parameter name	Parameter description	Final values	Units	Estimated using automated methods ¹	Rank and composite scaled sensitivity	Package/process-parameter group
Irrigation efficiency—Continued							
Recent years [1–3]	Dry seasons	Multiplier on irrigation efficiency for wet and dry seasons	1.1	Multiplier	No	162/<0.1	FMP—irrigation
	SCL_EFFDFL2		1.1		No	163/<0.1	
	SCL_EFFDWN2		1.0		Yes	164/<0.1	
	SCL_EFFDSP2		1.1		Yes	165/<0.1	
	SCL_EFFDSU2		1.1		No	170/<0.1	
	Wet seasons		1.1		No	171/<0.1	
	SCL_EFFWFL2		0.8		Yes	172/<0.1	
	SCL_EFFWWN2		1.1		Yes	173/<0.1	
	SCL_EFFWSP2						
	SCL_EFFWSU2						
Lateral hydraulic conductivity							
[1–3]	KC_QYA	Hydraulic conductivity of coarse-grained deposits for each model layer	20.3	Feet/day	Yes	81/35.5	LPF/MULT—hydraulic conductivity
	KC_QOA		12.6		Yes	10/57.4	
	KC_MO		0.76		Yes	58/41.6	
[1–3]	KF_QYA	Hydraulic conductivity of fine-grained deposits for each model layer	0.004	Feet/day	No	12/57.2	LPF/MULT—hydraulic conductivity
	KF_QOA		0.004		No	80/35.6	
	KF_MO		0.003		No	122/21.6	
[1]	HK_NMZ_QYA	Hydraulic conductivity of the Recent Alluvium zones	1.95	Multiplier	Yes	109/27.1	LPF/PVAL—hydraulic conductivity multipliers
	HKNMZQYACC		2.61		No	113/26.6	
	HK_SMFHQYA		1.3		Yes	69/39.6	
	HK_SMZ_QYA		4.87		Yes	33/49.2	
	HKSMZQYACC		4.20		Yes	9/57.9	
	HK_VCQYACC		4.20		Yes	98/30.8	
	HK_VCQYAUC		1.58		No	55/42.3	
	HK_WZ_QYA		2.55		Yes	18/53.4	
	HK_WZQYACC		2.62		No	93/32.5	
[2]	HK_NMZ_QOA	Hydraulic conductivity of the older alluvial zones	2.3	Multiplier	Yes	34/49.1	LPF/PVAL—hydraulic conductivity multipliers
	HKSMFHQOAN		0.42		No	50/44.1	
	HKSMFHQOAM		0.38		Yes	82/35.4	
	HKSMFHQOAS		0.47		No	25/50.7	
	HK_VC_QOAN		1.47		No	83/34.7	
	HK_WZ_QOAN		1.36		Yes	85/34.1	
	HK_WZ_QOAS		2.16		No	21/52.9	
	HK_NMZQOAC		1.52		No	4/71.5	
	HKSMFHQOAC		0.52		No	32/49.3	
	HK_SMZQOAC		2.02		Yes	49/44.3	
	HK_VC_QOAC		0.48		Yes	110/27.1	
	HK_WZ_QOAC		0.94		Yes	65/40.6	
	HK_QOA_PHT		1.00		No	====	
	[3]		HK_MO_C		Hydraulic conductivity of the Morales formation zones	0.73	
HK_MOUC		0.10	Yes	6/64.3			

Table 14. Summary of parameter values estimated for the Cuyama Valley hydrologic model (CUVHM), Cuyama Valley, California.—Continued

Parameter type [model layers]	Parameter name	Parameter description	Final values	Units	Estimated using automated methods ¹	Rank and composite scaled sensitivity	Package/process-parameter group
Vertical hydraulic conductivity							
[1]	VK_NMZ_QYA	Vertical hydraulic conductivity of the Recent Alluvium zones	0.03	Multiplier	Yes	36/48.7	LPF/PVAL—hydraulic conductivity multipliers
	VKNMZQYACC		2.52		No	123/21.6	
	VK_SMFHQYA		1.00		Yes	72/37.8	
	VK_SMZ_QYA		0.09		No	31/49.3	
	VKSMZQYACC		4.75		No	96/31.6	
	VK_VCQYACC		3.56		No	13/56.3	
	VK_VCQYAUC		2.00		No	67/40.2	
	VK_WZ_QYA		2.64		No	114/26.3	
	VK_WZQYACC	1.72	Yes	23/52.1			
[2]	VK_NMZ_QOA	Vertical hydraulic conductivity of the older alluvial zones	0.94	Multiplier	No	42/46.9	LPF/PVAL—hydraulic conductivity multipliers
	VKSMFHQOAN		0.50		Yes	22/52.8	
	VKSMFHQOAM		1.10		No	119/25.1	
	VKSMFHQOAS		0.18		Yes	78/36.3	
	VK_VC_QOAN		0.80		Yes	90/33.5	
	VK_WZ_QOAN		0.80		No	37/48.7	
	VK_WZ_QOAS		1.02		No	76/36.4	
	VK_NMZQOAC		0.11		Yes	3/77.8	
	VKSMFHQOAC		0.45		Yes	108/28.1	
	VK_SMZQOAC		2.84		No	61/41.2	
	VK_VC_QOAC		2.16		No	17/54.8	
	VK_WZ_QOAC		2.25		No	2/80.6	
	VK_QOA_PHT		1.00		No	====	
[3]	VK_MO_C	Vertical hydraulic conductivity of the Morales formation zones	1.04	Multiplier	No	38/48.6	LPF/PVAL—hydraulic conductivity multipliers
	VK_MOUC		0.95		No	68/40.1	
Storage properties							
[1]	SY1_FAC	Specific yield of Recent Alluvium	0.13	Fraction	Yes	51/43.1	LPF/MULT—storage properties
[2]	SY2_FAC	Specific yield of Older Alluvium	0.10	Fraction	No	63/40.7	LPF/MULT—storage properties
[3]	SY3_FAC	Specific yield of Morales Formation	0.08	Fraction	No	87/33.8	LPF/MULT—storage properties
[1]	PHI_CRS	Porosity of Recent Alluvium	20	Percentage	Yes	57/42.1	LPF/MULT—storage properties
	PHI_FIN		37		No	46/46.3	

Table 14. Summary of parameter values estimated for the Cuyama Valley hydrologic model (CUVHM), Cuyama Valley, California.—Continued

Parameter type [model layers]	Parameter name	Parameter description	Final values	Units	Estimated using automated methods ¹	Rank and composite scaled sensitivity	Package/process-parameter group
Storage properties—Continued							
[2]	PHI_CRS_AO PHI_FIN_AO	Porosity of Older Alluvium	12 17	Percentage	Yes Yes	26/50.7 7/61.8	LPF/MULT— storage properties
[3]	PHI_CRS_MO PHI_FIN_MO	Porosity of Morales formation	10 29	Percentage	No Yes	104/29.1 45/46.7	LPF/MULT— storage properties
[1]	SS_NMZ_QYA SSNMZQYACC SS_SMFHQYA SS_SMZ_QYA SSSMZQYACC SS_VCQYACC SS_VCQYAUC SS_WZ_QYA SS_WZQYACC	Specific storage of Recent Alluvium zones	1.21 1.15 2.00 0.21 1.12 1.0 1.00 0.66 1.24	Multiplier	No No Yes Yes No Yes No No No	89/33.7 47/46.2 43/46.9 88/33.7 100/30.5 105/29.1 118/25.2 30/49.5 11/57.2	LPF/MULT— storage properties
[2]	SS_NMZ_QOA SSSMFHQOAN SSSMFHQOAM SSSMFHQOAS SS_VC_QOAN SS_WZ_QOAN SS_WZ_QOAS SS_NMZQOAC SSSMFHQOAC SS_SMZQOAC SS_VC_QOAC SS_WZ_QOAC SS_QOA_PHT	Specific storage of Older Alluvium zones	2.00 0.86 1.95 1.25 2.00 0.92 0.81 2.09 0.03 1.32 2.22 1.65 1.00	Multiplier	No No No No No No No No No No No No No	39/47.9 56/42.1 120/23.9 15/54.9 74/37.1 41/47.2 92/32.7 106/28.51 24/52.1 77/36.4 14/56.3 60/41.4 =====	LPF/PVAL— storage properties
[3]	SS_MO_C SS_MOUC	Specific storage of Morales formation zones	0.37 1.06	Multiplier	Yes No	79/36.0 19/53.3	LPF/PVAL— storage properties
Subsidence properties							
[1–3]	crt_hd_01 crt_hd_02 crt_hd_03	Critical heads for each layer	0.91 0.90 0.72	Multiplier as fraction of initial groundwater levels	No Yes No	1/97.7 64/40.6 52/42.9	SUB—storage properties
[1–3]	QYA_SKE QOA_SKE MO_SKE	Skeletal elastic storage coefficient for each layer	0.90 0.32 0.80	Multiplier	Yes Yes No	54/42.5 124/21.3 73/37.1	SUB—storage properties
[1–3]	QYA_SKVB QOA_SKVB MO_SKVBR	Skeletal inelastic storage coefficient for each layer	1.62e-05 2.30e-05 1.00e-05	1/Foot	Yes Yes No	97/31.6 75/36.5 103/29.6	SUB—storage properties

Table 14. Summary of parameter values estimated for the Cuyama Valley hydrologic model (CUVHM), Cuyama Valley, California.—Continued

Parameter type [model layers]	Parameter name	Parameter description	Final values	Units	Estimated using automated methods ¹	Rank and composite scaled sensitivity	Package/process-parameter group	
SKIN factor for multi-node wells								
[1–3]	SKIN_LY1	Skin factor for recent and Older Alluvium, and Morales formation layers	395	ft ² /day	No	27/50.6	MNW1 hydraulic property	
	SKIN_LY2		1,536		No	35/48.8		
	SKIN_LY3		1,622		No	8/60.7		
Horizontal flow-barrier conductance ²								
[1–3]	MO_FLT [2–3]	Conductance of internal faults	7.5e-12	ft ² /day	No	107/28.3	HFB—hydraulic conductance factor	
	GRV_FLT [1–3]		1.4e-10		No			40/47.7
	TTHL_FLT [1–3]		7.2e-10		No			62/40.9
	SBC_FLT [2–3]		1.9e-13		No			29/49.7
	SBC_FLT1 [1]		1.9e-13		No			121/23.8
	RHF_FLT [2–3]		4.0e-04		Yes			
Initial groundwater levels ³								
[1–3]	SCL_HEDLY1	Scale factor for adjusting initial groundwater levels	1.006	Multiplier	Yes	=====	Scale factor of initial groundwater levels	
	SCL_HEDLY2		1.00		Yes			
	SCL_HEDLY3		1.00		Yes			

¹Parameters used in calibration varies between calibration runs and indicators here reflect parameters that were generally estimated through the automated process. An additional 15 parameters for scaling precipitation and potential ET were included in the model but remained fixed at the standard values of units conversion.

²MO_FLT is the Morales Fault, GRV_FLT is the Graveyard Fault, TTHL_FLT is the Turkey Track Hill Fault, SBC_FLT is the Santa Barbara Canyon Fault, and RHF_FLT is the Rehobith Farm Fault. Numbers within brackets are layers where flow barriers are present.

³Scale factors for initial head not part of original sensitivity run. These parameters were added later and were then the most sensitive parameters.

Table 15. Summary of streambed conductivity parameters and current values, Cuyama Valley, California.

Segment categories	Segment conductance group name ¹	Stream segment conductivity (foot per day)	Estimated using automated methods ²	Rank and composite scaled sensitivity (=== not estimated)
Tributary channels and Cuyama River channel on Recent Alluvium	<u>Ventucopa</u>	52.5	Yes	148/1.65
	VC_QYAUC	1.91	No	146/1.74
	WVC_QYAUC	0.98	No	129/2.89
	<u>Main zones</u>	1.50	No	153/1.40
	NMZ_QYA	5.38	No	150/1.44
	SMZ_QYA	0.29	No	145/1.77
	WZ_QYA	0.23	No	152/1.44
	WNMZ_QYA	0.21	No	144/1.78
	WSMZ_QYA	==	None	==
	WWZ_QYA	2.23	No	134/2.28
	<u>Sierra Madre Foothills zones</u>	0.75	No	130/2.84
	None	2.11	No	141/1.85
	<u>Cuyama River channel</u>	52.5	Yes	128/3.34
	NMZ_QYACC	0.29	No	157/0.90
	SMZ_QYACC	1.06	No	139/1.89
	WZ_QYACC	4.95	Yes	143/1.80
	VC_QYACC	10.85	Yes	135/2.25
	WNMZ_QYACC			
	WSMZ_QYACC			
	WVC_QYACC			
WWZ_QYACC				
Tributary channels and Cuyama River channel on Older Alluvium	<u>Ventucopa</u>	2.16	Yes	156/1.09
	VC_QOAS	2.99	No	140/1.88
	WVC_QOAS	0.40	No	138/1.94
	<u>Main zones</u>	0.65	No	151/1.44
	NMZ_QOA	1.73	No	147/1.72
	WWZ_QOAS	0.11	No	155/1.39
	WNMZ_QOA	0.18	No	132/2.49
	WZ_QOAS	0.71	No	154/1.40
	<u>Sierra Madre Foothills zones</u>	0.27	No	131/2.75
	SMFH_QOAN	0.27	No	133/2.42
	SMFH_QOAM	6.87	No	137/1.94
	SMFH_QOAS	0.34	No	136/2.07
	WSMFH_QOAM		None	
	WSMFH_QOAN			
	WSMFH_QOAS			
	<u>Cuyama River channel</u>			
None				
Tributary channels and Cuyama River channel on Morales formation	<u>Ventucopa</u>	3.15	Yes	149/1.60
	VC_MOUC	3.40	No	142/1.81
	WVC_MOUC		None	
	<u>Main zones</u>		None	
	None		None	
	<u>Sierra Madre Foothills zones</u>			
	None			
	<u>Cuyama River channel</u>			
None				

Table 15. Summary of streambed conductivity parameters and current values, Cuyama Valley, California.—Continued

Segment categories	Segment conductance group name ¹	Stream segment conductivity (foot per day)	Estimated using automated methods ²	Rank and composite scaled sensitivity (=== not estimated)
Fraction of inflows as recharge plus runoff from basin characterization model				
	<u>Total inflow Cuyama River</u>	1.00	No	====
	Flw84	1.00	No	
	<u>Total Inflow Santa Barbara Canyon</u>			
	Flw113			
Fraction of inflows as recharge or runoff from basin characterization model				
	<u>Inflow Cuyama River as runoff or recharge</u>	1.00	No	====
	Run84	0.78	Yes	
	Run84	1.00	No	
	Rch84	0.76	Yes	
	<u>Inflow Santa Barbara as runoff or recharge Canyon</u>			
	Run113			
	Rch113			

¹Refer to figures 5 and 10 for distribution of stream segments and parameter distributions.

Table 16. Summary of groundwater-flow budgets for selected periods, Cuyama Valley, California.

[Average flows in acre-feet per year. Water Year is October through September of the following year. The precision of the numbers do not reflect the variabe accuracy of the estimates and round off. **Abbreviations:** CUVHM, Cuyama Valley hydrologic model; SMFH, Sierra Madre Foothills; +, plus]

Region/subregion and time period	Average-net inflows					Average-net outflows					Inflow – outflow ¹		
	Storage depletion	Direct infiltration (DI)	Stream flow infiltration (SI)	Total recharge (DI + SI)	Total inflows	Storage accretion	Net under flow	Outflow as springs	Domestic pumpage	Water-supply pumpage		Agricultural pumpage	Total pumpage discharge
CUVHM 1950–2010	234,500	5,600	27,500	33,100	67,600	0	3,700	1,000	16	90	65,300	70,100	-2,500
CUVHM 2000–10	235,300	3,100	30,400	33,500	68,800	0	3,200	600	10	190	68,100	72,100	-3,300
CUVHM 2005 (wet year)	28,100	16,600	93,200	109,800	190,800	80,900	3,200	700	17	180	68,500	153,600	37,200
CUVHM 2009 (dry year)	45,200	100	16,700	16,800	62,000	0	3,000	600	16	190	59,800	63,600	-1,600
Main zone 1950–2010	28,800	3,800	8,000	11,800	40,600	0	3,700	1,000	6	90	57,000	61,800	-21,200
Ventucopa uplands 1950–2010	0	1,200	17,700	18,900	18,900	5,500	-15	0	8	0	7,400	12,900	5,900
SMFH 1950–2010	11,200	600	1,800	2,400	13,600	0	0	0	2	0	900	900	12,800
Main zone 2000–10	27,479	700	8,300	9,000	36,500	0	3,200	600	6	190	56,700	60,700	-24,200
Ventucopa uplands 2000–10	0	1,500	20,500	22,000	22,000	6,000	-15	0	8	0	10,000	16,000	6,000
SMFH 2000–10	13,800	900	1,600	2,400	16,300	0	0	0	2	0	1,400	1,400	14,900
Base-case projection CUVHM 2011–71	32,700	2,400	29,500	31,900	64,600	0	2,900	400	7	190	63,700	67,200	-2,600
Reduced-supply projection 2011–71	500	1,100	25,600	26,700	27,200	0	2,900	500	7	190	32,800	36,400	-9,200
Reduced-demand projection 2011–71	0	1,300	29,500	30,800	30,800	11,900	3,000	600	7	190	15,800	31,500	-700

¹Negative difference is net depletion and positive difference is net accretion of groundwater flow.

²Valley wide storage depletion is net change in storage that also includes any storage accretion shown for individual zones.

This page intentionally left blank.

Prepared by the Sacramento Publishing Service Center.

For more information concerning this report, contact:

Director
U.S. Geological Survey
California Water Science Center
6000 J Street, Placer Hall
Sacramento, CA 95819
dc_ca@usgs.gov

or visit our Web site at:
<http://ca.water.usgs.gov>

